banner

Vapour transport across gas-filled enclosures

Thesis submitted by

Geordie Drummond McBAIN BE(Hons) *JCU*

for the degree of Doctor of Philosophy

in the School of Engineering

James Cook University

19 November 1999

STATEMENT OF ACCESS

I, the undersigned, the author of this thesis, understand that James Cook University will make it available for use within the University Library and, by microfilm or other means, allow access to users in other approved libraries.

All users consulting this thesis will have to sign the following statement:

> In consulting this thesis, I agree not to copy or closely paraphrase it in whole or in part without the written consent of the author; and to make proper public written acknowledgement for any assistance which I have obtained from it.

Beyond this, I do not wish to place any restriction on access to this thesis.

Signature

Date

Abstract

A mathematical model is developed for stationary nonisothermal unsaturated vapour transport. It incorporates the Boussinesq approximation, but includes the finite mass transfer rate effects of nonzero interfacial velocity and the enthalpy carried by diffusive fluxes. It is proved that (under conditions more general than those assumed in the model) strong local extrema of temperature or vapour mass fraction are impossible. The model is used to investigate the effect of finite mass transfer rates and bounding solid surfaces on vapour transport.

A solution is presented for the space bounded only by two parallel plane vertical walls held at different uniform temperatures and vapour mass fractions. This is used to demonstrate many of the basic features of vapour transport. In particular, it shows that the total energy transfer across a cavity may be greatly affected by the enthalpy carried by vapour.

Numerical solutions are obtained using the *Fastflo* finite element package. These demonstrate the existence of a fully developed region in plane vertical rectangular cavities with vertical aspect ratios as low as 5. The criterion for this is shown to depend on both the vertical aspect ratio and the combined Grashof number, $Gr(1+N)$.

In many applications, such as those involving humid air at ordinary temperatures, the mass transfer rates are low. A simplified but rational approximation to the model is derived that is valid under these conditions. The contribution of vapour gradients to buoyancy forces and particularly the effect of evaporative cooling must be retained in this limit.

The infinite vertical plane cavity solution is extended to horizontally bounded cavities with rectangular or elliptic sections for low mass transfer rates. It is found that the flow in the vertical midplane of a tall narrow cuboid is only effectively two-dimensional if the span of the cavity is at least 1.7 times its breadth.

An asymptotic solution, to first order in $Gr(1+N)$ and zeroth order in Φ, the mass transfer rate factor, is presented for spherical cavities. This follows from a new general solution of the inhomogeneous Stokes problem in the sphere. In addition to the primary buoyancy-driven circulation, the solution shows two secondary flows. These correspond to the 'convective' and 'inertial' mechanisms for three-dimensional flow in a side-heated cuboid identified by Mallinson and de Vahl Davis (1973, 1977). The analytical form of the solution clarifies the nature of these mechanisms. In particular, it is shown that the inertial mechanism vanishes quadratically as the primary flow tends to zero and also vanishes if the streamlines are straight.

Contents

List of figures viii

Preface x

Nomenclature xii

1 Introduction **1**

1.1 General description of the problem 1

1.2 Aims and significance 2

1.3 Methodology and scope 4

1.4 Summary 11

2 Basic Equations of Vapour Transport **12**

2.1 Field equations 13

2.1.1 The equations of continuity 13

Omissions in the species equation 14

2.1.2 The equation of motion 16

2.1.3 The energy equation 18

Possible difficulties with the energy equation 20

2.2 Boundary conditions 21

2.2.1 Velocity boundary conditions 22

2.2.2 Heat and mass transfer boundary conditions 23

2.3 Nondimensionalization 24

2.3.1 Mass and energy fluxes 25

2.3.2 Dimensionless field equations 27

2.3.3 Dimensionless transpiration condition 30
2.3.4 Wall fluxes 30
2.4 The single fluid heat transfer problem 32
2.5 Geometry 33
2.6 Some properties of the equations 35
2.6.1 Extrema of advected scalars 35
2.6.2 The nonexistence of hydrostatic solutions 39
2.6.3 An invariance property 42

3 Literature Review **46**
3.1 Free convection vapour transport 47
3.2 The Stefan diffusion tube 48
3.2.1 The no-slip condition 49
3.2.2 Meyer and Kostin (1975) 50
3.2.3 Markham and Rosenberger (1980) 52
3.2.4 Greenwell, Markham and Rosenberger (1981) 53
3.2.5 Buoyancy effects 53
3.2.6 Conclusions 54
3.3 Gas-filled enclosures 55
3.3.1 Klosse and Ullersma (1973) 55
3.3.2 Hu and El-Wakil (1974) 55
3.3.3 Jhaveri, Markham and Rosenberger (1981) 56
3.3.4 Jhaveri and Rosenberger (1982) 57
3.3.5 Bejan (1985) 57
3.3.6 Keey and Wee (1985) 58
3.3.7 Trevisan and Bejan (1987) 59
3.3.8 Ranganathan and Viskanta (1988) 60
3.3.9 Nelson and Wood (1989) 61
3.3.10 Wee, Keey and Cunningham (1989) 61
3.3.11 Lin, Huang and Chang (1990) 63

3.3.12 Weaver and Viskanta (1991*a*) 66
3.3.13 Weaver and Viskanta (1991*b*) 67
3.3.14 Weaver and Viskanta (1991*c*) 68
3.3.15 Béghein, Haghighat and Allard (1992) 68
3.3.16 McBain (1995, 1997*b*) 69
3.3.17 Costa (1997) 72
3.3.18 Rosenberger et al. (1997) 73
3.3.19 Conclusions 75

4 The Narrow Cavity Limit **77**
4.1 Introduction 77
4.2 The two-dimensional equations 79
4.3 The narrow cavity limit 81
4.4 The fully developed solution 82
4.4.1 Mass and energy fluxes at the vertical walls 88
4.4.2 The vertical pressure gradient 89
4.5 A numerical example 90
4.6 Limitations of the narrow cavity limit 91
4.6.1 The ceiling and floor regions 91
4.6.2 Stability 91
4.7 Conclusions 92

5 The Floor and the Ceiling **93**
5.1 Vapour transport in *Fastflo* 94
5.1.1 Continuum model 95
5.1.2 The interfacial velocity 96
5.1.3 Augmented Lagrangian algorithm 96
5.1.4 Implementation of unusual terms 98
5.1.5 The finite element mesh 99
5.2 Results 101

5.2.1 Grid independence 101
5.2.2 Postprocessing 102
5.2.3 Overall transfer rates 105
5.3 Conclusions on the use of *Fastflo* 107
5.4 The floor and ceiling problems 108
5.4.1 The fully developed solution 111
5.4.2 Numerical solutions 112
5.5 The conduction–diffusion regime 114
5.6 A possible analytical approach 117
5.7 Conclusions 119

6 Low Mass Transfer Rates 120
6.1 Implications of the narrow cavity limit 121
6.1.1 Utility of the narrow cavity limit 122
6.1.2 The narrow cavity and 'film theory' 123
6.1.3 Transport rate dependence on Φ 124
6.2 A rational approximation for low mass transfer rates 127
6.2.1 The low mass transfer rate equations 128
6.2.2 Other low mass transfer rate limits 130
6.3 Conclusions 132

7 Cavities with Bounded Sections 134
7.1 Introduction 134
7.1.1 Boundaries of the conduction regime 137
7.2 General model 138
7.3 Narrow cavities with bounded sections 140
7.3.1 Forced flow 142
7.3.2 Natural flow 142
7.3.3 Completely enclosed flows 144
7.3.4 Numerical evaluation of the solution 144

7.3.5 Results for rectangular sections 145
7.4 Extreme spanwise aspect ratios 146
7.4.1 Small spanwise aspect ratios 147
7.4.2 Large spanwise aspect ratios 150
7.4.3 Extent of the effect of the end-walls 151
7.5 Sections other than rectangular 152
7.5.1 Circular section 153
7.5.2 Elliptic section 154
7.6 Flow in the spanwise symmetry plane 156
7.6.1 Vorticity at the section centre 157
7.6.2 Velocity in the plane of spanwise symmetry 159
7.7 Finite mass transfer rates 163
7.8 Conclusions 163
7.9 Two theorems on fully developed flow 164

8 Bounded Cavities **167**
8.1 The spanwise component of velocity 167
8.1.1 Inertial generation of spanwise flow 168
8.2 Spherical enclosures 171
8.2.1 Previous work 171
8.2.2 Geometry and boundary conditions 172
8.2.3 The low Grashof number expansion 173
8.2.4 Conduction–diffusion 176
8.2.5 Creeping flow 176
8.2.6 First order mass fraction and temperature 180
8.2.7 First order flow correction for inertia 183
8.2.8 First order flow correction for buoyancy 186
8.2.9 Flow structure to first order 188
8.2.10 Overall vapour and energy transfer rates 194
8.3 Conclusions 194

9 Conclusions **197**

References **199**

A Sample *Fasttalk* Code **224**

B Vector Fields in a Sphere **237**

B.1 Solenoidal fields 237

B.2 Nonsolenoidal fields 239

B.3 Boundary conditions 241

B.4 The Stokes problem in the sphere 241

B.5 Axisymmetric poloidal fields 244

List of Figures

2.1 Cuboid domain geometry 34

3.1 Vapour transfer in a plane vertical square cavity 64
3.2 Energy transfer in a plane vertical square cavity 65

4.1 Profiles of m and T in the narrow cavity limit 84
4.2 Profiles of v in the narrow cavity limit 85
4.3 Variation of v with N in the narrow cavity limit 86
4.4 Variation of v with c in the narrow cavity limit 87

5.1 Geometry and boundary conditions for *Fastflo* solutions 94
5.2 Vinokur's (1983) symmetric stretching function 100
5.3 A typical mesh for the *Fastflo* solutions 100
5.4 A sample *Fastflo* solution 101
5.5 Processed solution variables in *Fastflo* 103
5.6 Energy flux components 104
5.7 Energy transfer in the cavity: vectors and 'heat-lines' 106
5.8 Contour plots from two *Fastflo* runs 112
5.9 Discrepancies between the *Fastflo* and analytic solutions 115
5.10 The effect of $\mathcal{A}$ on the conduction–diffusion regime 116
5.11 Penetration of convective effects into the core 118

7.1 Geometry for cavities of rectangular section 139
7.2 Fully developed buoyancy-induced flow 146

7.3 Stretched coordinates for regions near walls 148
7.4 The effect of the end-walls 153
7.5 Geometry for elliptic sections. 154
7.6 Fully developed buoyancy-induced flow in elliptic sections 155
7.7 Vorticity due to buoyancy at the section centre 158
7.8 Buoyancy-induced flow in the spanwise symmetry plane 159
7.9 Velocity maximum in rectangular sections 162

8.1 Cartesian axes for the spherical cavity 172
8.2 Temperature in the surrounding solid 174
8.3 Decomposition of a vector field 178
8.4 Zeroth order pressure 180
8.5 First order vapour mass fraction or temperature 181
8.6 Mass fraction or temperature to first order 182
8.7 First order stream-lines due to inertia 185
8.8 First order pressure due to inertia 185
8.9 First order stream-lines due to buoyancy 187
8.10 First order pressure due to buoyancy 188
8.11 Three-dimensional stream-lines in a spherical cavity 191
8.12 Three-dimensional stream-lines in a spherical cavity (cont.) 192

STATEMENT OF SOURCES

DECLARATION

I declare that this thesis is my own work and has not been submitted in any form for another degree or diploma at any university or other institution of tertiary education. Information derived from the published or unpublished work of others has been acknowledged in the text and a list of references is given.

Signature

Date

Preface

Several intermediate reports on the progress in this project have already been published (Suehrcke, Harris & McBain 1996; McBain 1997*a*, 1998; McBain, Close, Suehrcke, Harris & Brandemuehl 1998; McBain & Harris 1998; McBain, Harris, Close & Suehrcke 1998; Suehrcke & McBain 1998). It is a pleasure to acknowledge the assistance of my coauthors in preparing these papers; their direct contributions are noted where utilized.

I would also like to express my gratitude to Prof. Don Close for pointing out the relevance of the physics of rainclouds to the question of interior condensation (§ 2.1.1); Prof. Bob Street for pointing out the connection between Theorem 1 and Hopf's Maximum Principle; Dr Jonathan Harris for informing me of the work of Daniels (1985; Daniels & Wang 1994) on the destruction of the conduction regime (ch. 5); Dr Wolfgang Schöpf for indicating the importance of hydrodynamic stability and providing several of the relevant references, as discussed in § 4.6.2; Dr Harris for making available accurate finite element solutions of the creeping buoyant flow in a cuboid which proved very illuminating in the development of the material on the narrow cavity limit for bounded sections (ch. 7); Dr Harry Suehrcke for thorough checking of my derivations; and Dr Eric Peterson for interesting discussions on the inertial generation of axial flow by circulation in aquaculture tanks and provision of some of the references cited in § 8.1.1. Thanks also to Roger Hosking, John Patterson, Lance Bode, Patrick Le Quéré and Andrew Schultz for enlightening conversations on applied mathematics and fluid mechanics.

I would also like to thank Drs Nick Stokes and Zili Zhu for prompt and thorough technical support with the *Fastflo* finite element package, used in chapter 5; Dr Harris and Mr Darrin Stephens for general and generous assistance with computers; and Drs Harris and Schöpf, and Mr Schultz for help with LaTeX.

I am indebted to my supervisors (Prof. Close and Drs Suehrcke and Harris) and Ms Arian McVeigh for proofreading and helpful suggestions. I need hardly add that the remaining faults are entirely my own.

Finally I would like to thank Ms Kathleen Sharp for uncommonly painless administration of the financial assistance which enabled me to write this thesis.

Nomenclature

$\mathcal{A}$	vertical aspect ratio (reduced height) of cavity
A	arbitrary diffusivity tensor
B	Spalding's driving force for mass transfer, $\exp(-\Phi) - 1$
b	characteristic length, dimensional width of cavity
C	coefficient of Dirichlet term in Robin boundary condition
c	constant of integration
c_p	isobaric specific heat capacity
D	binary diffusivity
d	characteristic length of V in § 2.6.1
E_K	truncation error
$\hat{\boldsymbol{e}}$	arbitrary unit vector
$\mathbf{f}$	body force term in Stokes equation
$\mathbf{g}$	gravitational acceleration, $-g\hat{\boldsymbol{\jmath}}$
Gr	(thermal) Grashof number, $g\beta\Delta T_* b^3/\nu^2$
h	specific enthalpy
h_{fg}	specific heat of vaporization
h.o.t.	higher order terms
$\hat{\boldsymbol{\imath}}$	unit transverse vector

I coefficient of Neumann term in Robin boundary condition

i index for species in a multicomponent mixture

$\hat{\boldsymbol{\jmath}}$ unit vertical vector

$\mathbf{j}_*$ mass flux of vapour relative to $\mathbf{u}_*$

K number of evaluated terms in a truncated series

$\hat{\boldsymbol{k}}$ unit spanwise vector

k index for terms in a series

Le_A vapour Lewis number, $\lambda/\rho c_{pA}\delta$

M molar mass

m reduced vapour mass fraction, $(m_* - m_{*r})/\Delta m_*$

N buoyancy ratio, $\zeta\Delta m_*/\beta\Delta T_*$ number of species in a mixture in § 2.6.1

$\hat{\boldsymbol{n}}$ unit normal vector, positive outward from fluid phase

$\mathbf{n}_*$ absolute mass flux of vapour

Nu Nusselt number, $-\hat{\boldsymbol{\imath}} \cdot \mathbf{e}_* b[1 - \exp(-\Phi_T)]/\lambda\Delta T_*\Phi_T$

$\mathcal{P}[\mathbf{v}]$ scalar defining the poloidal part of $\mathbf{v}$

P_n^m function defined by (B.6)

p reduced pressure,

$(p_* + \rho g y_*)/\rho g(\beta\Delta T_* + \zeta\Delta m_*)b\mathcal{A}$

Pr Prandtl number, $\nu\rho c_p/\lambda$

Pr_r reference Prandtl number, $\nu\rho c_{pr}/\lambda$

Pr_I interdiffusion Prandtl number, $\nu\rho(c_{pA} - c_{pB})(1 - m_{*r})/\lambda$

$\mathbf{r}$ reduced position vector, $\mathbf{r}_*/b$

r reduced spherical coordinate, $|\mathbf{r}|$

Ra (thermal) Rayleigh number, $GrPr$

Re Reynolds number

$\mathcal{S}$ spanwise aspect ratio (reduced span) of cavity

$\mathcal{S}[\mathbf{v}]$ scalar defining the scaloidal part of $\mathbf{v}$

S level surface of arbitrary scalar field

s mesh stretching factor in § 5.1.5

arbitrary scalar field in § 2.6.1

Sc Schmidt number, ν/D

Sh Sherwood number, $-\hat{\boldsymbol{\imath}} \cdot \mathbf{n}_* b/\rho D \Phi$

$\mathcal{T}[\mathbf{v}]$ scalar defining the toroidal part of $\mathbf{v}$

T reduced temperature, $(T_* - T_{*r})/\Delta T_*$

$\mathbf{u}$ reduced velocity, $\mathbf{u}_* \nu / g(\beta \Delta T_* + \zeta \Delta m_*) b^2$

u reduced transverse component of velocity, $\hat{\boldsymbol{\imath}} \cdot \mathbf{u}$

$\mathcal{V}$ term of an inner matched asymptotic expansion

V volume enclosed by level surface, S

$\mathbf{v}$ arbitrary vector field

v reduced vertical component of velocity, $\hat{\boldsymbol{\jmath}} \cdot \mathbf{u}$

w reduced spanwise component of velocity, $\hat{\boldsymbol{k}} \cdot \mathbf{u}$

x reduced transverse coordinate, $\hat{\boldsymbol{\imath}} \cdot \mathbf{r}$

y reduced vertical coordinate, $\hat{\boldsymbol{\jmath}} \cdot \mathbf{r}$

z reduced spanwise coordinate, $\hat{\boldsymbol{k}} \cdot \mathbf{r}$

Greek symbols

β thermal coefficient of cubic expansion

γ_{ij} component of metric tensor

Δ inner gauge function in a matched asymptotic expansion

Δ characteristic difference

δ outer gauge function in a matched asymptotic expansion

ζ vapour coefficient of cubic expansion

stretched coordinate for region near front wall in §7.4.2

η spherical coordinate: colatitude, $\arctan(\sqrt{x^2+z^2}/y)$

θ spherical coordinate: colatitude, $\arctan(\sqrt{x^2+y^2}/z)$

λ thermal conductivity

Λ latent heat factor, $h_{fg}/c_{pA}\Delta T_*$

μ (dynamic) viscosity

ν kinematic viscosity

ξ stretched coordinate for region near hot wall

ρ density

σ function defined by (4.29), appearing in (4.27)

υ spherical coordinate: azimuth, $\arctan(y/z)$

Φ mass transfer rate factor, $\ln[(1-m_{*r})/(1-m_{*r}-\Delta m_*)]$

Φ_T thermal mass transfer rate factor, $\Phi(Pr_r+Pr_I)/Sc$

ϕ spherical coordinate: azimuth, $\arctan(x/y)$

φ test function for variational form of Navier-Stokes equation

ψ vertical component of solenoidal vector potential for $\mathbf{u}_\perp$

Stokes's stream-function in § 8.2

Ω rotational speed

Ω domain, with boundary $\partial\Omega$

Superscripts

$\hat{}$	unit magnitude
$\bar{}$	mean
$\tilde{}$	transformed
$\|$	in a domain with $\mathcal{S} \to \infty$
$=$	in a domain with $\mathcal{S} \to 0$
$\square$	in a domain with rectangular horizontal section
$\circ$	in a domain with circular horizontal section
$\circ\!\!-$	in a domain with elliptic horizontal section
i	contravariant component
j	contravariant component
(P)	poloidal part
(S)	scaloidal part
(T)	toroidal part

Subscripts

$,ij\ldots$	covariant derivative with respect to $x^i, x^j, \ldots$
$*$	dimensional
∞	fully developed
$\perp$	restricted to a horizontal plane
$\odot$	restricted to a plane of constant z
0	at the wall $x = 0$
1	at the wall $x = 1$
A	species A, the vapour
B	species B, the gas

f	forced
i	Cartesian tensor component
(i)	species index in a multicomponent mixture
j	Cartesian tensor component
m	pertaining to mass transfer or composition
n	natural
r	at the reference state
T	thermal

Chapter 1

Introduction

1.1 General description of the problem

The problem pursued in this project is how fast a vapour will cross a vertical space filled with a nonreacting gas. A simple example is water vapour transmission across an air-gap in a building wall. There are also several technological applications such as partial pressure distillation and solar desalination (Hu & El Wakil 1974), and crystal growth by physical vapour transport (PVT) (Jhaveri, Markham & Rosenberger 1981) and chemical vapour deposition (CVD) (Klosse & Ullersma 1973). The enclosures considered consist of a simply connected space for the gas–vapour mixture bounded by more or less solid walls which may be sources or sinks for the vapour or impermeable to it. The gas is typically completely confined.

Locally, there is a net migration of vapour due to diffusion, down gradients in its mass fraction with respect to the mixture, and advection with any bulk flow of the fluid. There is always a bulk flow in such problems due to the interfacial mass fluxes at the vapour source and sink. Additionally, the density of the mixture will vary, depending on the relative composition, and so the resulting buoyancy forces lead to natural circulation. In all practically occurring cases, such a system will be far from isothermal, either because the vapour source is a source because it is

heated or because of the energy absorbed and released by the vapour on evaporation/sublimation/desorption and condensation/incorporation/sorption. These temperature variations must, in general, be taken into account when calculating the buoyancy forces for the convective flow. The energy transfer is often a quantity of interest in itself, for example in assessing the thermal performance of air-spaces as part of a building envelope. Like the vapour, energy is transported through the fluid mixture by advection and diffusion (conduction). Since vapours typically have significantly higher specific heat capacities than gases (e.g. that of water vapour is about double than of air under normal conditions), the thermal energy transported with the diffusive flux of the vapour—the 'interdiffusion flux'—can be important.

In modelling vapour transport through gas-filled enclosures, then, attention must be paid to the strong coupling between the concentration, temperature and velocity fields.

1.2 Aims and significance

The basic aim of this project is to predict the heat and mass transfer rates given the temperature and humidity of the cavity walls. A complete attainment of this aim is still some way off, however, since convective transport is highly nonlinear and under many commonly occurring sets of boundary conditions the fluid will be turbulent. More specifically, then, the first aim of this project is to develop a consistent mathematical model of the transport processes and identify the key dimensionless parameters and possible regimes of behaviour of the system.

The second aim is to focus on some of these regimes, to model the behaviour within them, and to determine their approximate boundaries in the parameter space. The purpose of these simplified models is to provide the functional form for correlations of results from experiments and numerical solutions. This is necessary as the large number of governing dimensionless parameters (nine in the current model) makes an exhaustive set of either experiments or numerical

solutions prohibitively expensive.

As well as the fundamental significance of natural convection in the sciences of heat and mass transfer and fluid mechanics, and the practical and economic importance of understanding and predicting vapour transmission rates in the technological applications listed above, the findings of this study have environmental implications in the context of the thermal design of building envelopes, particularly in warm humid climates. Environmental implications are possible on the individual, regional and global levels. For example, if there is a high vapour transmission rate through a building wall cavity, this may well lead to moisture content related deterioration of other parts of the structure (TenWolde 1989; White 1989) while the attendant large energy transfer rate could significantly affect the comfort of the occupant individuals who, in turn, may go out and buy a large air-conditioning unit. This, of course, increases demand for and dependence on electricity which is supplied either by the damming of natural watercourses (regional environmental degradation) or the carbon dioxide-producing combustion of fossil fuels, both of which have been associated with global warming. On the other hand, a better understanding of the physics of vapour transport could lead to the design of more energy efficient housing in the tropics. As such advances are some way in off in the future, this project is more about uncovering the basic mechanisms of vapour transport and describing them in a simple but hopefully illuminating manner.

Considering the building wall cavity problem in more detail, the reason for horizontal vapour transfer can be explained as follows. Many common wall materials, such as brick, concrete, wood and plaster are porous and can both hold and transmit large amounts of moisture (Close, Suehrcke & Masatto 1995). The outside of an external wall may be exposed to sun and rain. The vapour pressure exerted by a porous material increases with both temperature and moisture content, so that the air in the cavity in contact with the surface of the outer leaf may well be more humid than that on the inner side. Given this information, the

task is to investigate how quickly the vapour crosses the cavity and how much thermal energy it takes with it.

This project is a fundamental study, and the conclusions to be presented are of sufficient generality to be relevant to all the applications listed. The building wall cavity problem, however, will be kept constantly in mind as an example and as a guide for selecting, when necessary, which parts of the parameter space to investigate.

1.3 Methodology and scope

Several investigators have approached the problem of vapour transport across gas-filled enclosures over the last three decades, including Klosse and Ullersma (1973), Hu and El-Wakil (1974), Meyer and Kostin (1975), Jhaveri et al. (1981), Greenwell, Markham & Rosenberger (1981), Jhaveri and Rosenberger (1982), Bejan (1985), Keey and Wee (1985), Trevisan and Bejan (1987), Ranganathan and Viskanta (1988), Nelson and Wood (1989), Wee, Keey and Cunningham (1989), Lin, Huang and Chang (1990), Weaver and Viskanta (1991*a*–*c*), Béghein, Haghighat and Allard (1992), Costa (1997) and Rosenberger et al. (1997). Their contributions are summarized in § 3.3.

One of the most obvious things to emerge from this body of work is that no one model has been adopted. This is in spite of the fact that with a very few exceptions, such as the question of diffusive slip at solid boundaries (§ 3.2; Sparrow, Nunez & Prata 1985; Ranganathan & Viskanta 1988), the fundamental governing partial differential equations and boundary conditions are very well established (e.g. Bird, Stewart & Lightfoot 1960). These equations are extremely complex: apart from their essentially nonlinear and coupled nature, each of the coefficients (representing thermophysical properties, such as diffusivity or viscosity) depends on the local temperature, vapour concentration and pressure. Moreover, the property variation is different for every combination of gas and vapour and is usually unknown.

There are three main reasons for the simplification of these equations:

1. The first is simply solvability. This was an unavoidable constraint in the past, but is becoming less so with modern advances in computing power and numerical methods.

2. The second is that the variation of thermodynamic and transport properties with temperature and composition is not known for most mixtures. Even if it were, the problem would then depend on a practically infinite number of parameters and the equations would have to be solved separately for each case.

3. The third is something of a combination of the preceding two. By careful and strategic simplification, hopefully one is able to produce a model which embodies the essential features of the real problem, is general enough to apply to a large number of real cases and yet is simple enough to allow solution by approximate, and especially where possible exact, analytical techniques.

Of course, it is with the third point in mind that this problem is here persued. The reason for the emphasis on analytical methods is that it is believed that these are most suitable for obtaining insight into physical behaviour and are indispensable for suggesting the functional form for correlating the results of experiments and more detailed simulations.

As mentioned above, the models have tended to increase in complexity over time, and although this has occasionally led to better agreement with experiment (e.g. Rosenberger et al. 1997), it does not necessarily improve general understanding of the physics. An example of this is that by including property variation in the numerical model (e.g. Rosenberger et al. 1997; Weaver & Viskanta 1991*a*) the results become limited to the particular gas–vapour pair considered. If, as in the case of Rosenberger et al. (1997), this is octofluorocyclobutane–iodine, this is limiting indeed. Such detailed modelling has its place of course, especially in the

refinement of designs for industrial processes, and can only be expected to proliferate in the future, but it cannot substitute for a general theoretical framework; indeed, it was admitted in one such study that 'the large number of parameters in the present study... result in an analysis which is hard to generalize' (Weaver & Viskanta 1991*a*).

Another reason that no one model has yet emerged into general acceptance is, paradoxically, due to the single greatest simplifying feature of the problem—the analogy between heat and mass transfer. The advection of thermal energy and the advection of species are in many ways analogous, as are the processes of conduction and diffusion, but there are fundamental differences. For example, interfacial mass transfer of a vapour from a mixture with a noncondensable gas to a condensed phase implies a net normal velocity. This has no parallel in the problem of heat transfer between a fluid and a solid. Treating mass transfer like heat transfer, then, must be done with caution. It is acceptable in the limit of vanishingly dilute transferred species, and so was quite appropriate in the study of Wee et al. (1989) of humid air in cold climates (New Zealand), where the mass fraction of water vapour rarely exceeds 1%, but all too often the analogy's 'indiscriminate application... has lead to some rather amusing conclusions' (Rosenberger & Müller 1983). This point has been made many times in the past, most demonstratively by Spalding (1963), but unfortunately confusion continues. One of the foci of the present work is to identify and clarify these similarities and differences and to find quantitative criteria for how dilute the vapour must be before the finite mass transfer rate effects of transpiration and species interdiffusion of enthalpy become insignificant. This is dealt with in chapter 6. In short, the analogy between heat and mass transfer is best used as a preamble to the catalogue of its exceptions.

The first task of this project is the development of a general model. To a large extent this has already been accomplished (McBain 1998), though it was later refined (McBain & Harris 1998; Suehrcke & McBain 1998). The latest version,

derived in chapter 2, is general enough to include all the essential phenomena considered by the investigators listed in the first paragraph of this section, while containing the minimum number of parameters. Its form is a set of dimensionless partial differential equations. The field equations of the model include six dimensionless parameters: Gr, N, Sc, Φ, Pr_r and Pr_I. These are described in § 2.3.2.

The second task is to select various configurations and situations in which to solve the equations of the model. Having developed a model capable of representing a great variety of flows, it is necessary to restrict the scope of the project. My selection is guided by the building wall cavity problem, as well as the available solution techniques. The cavity problem suggests that the most important geometry is the vertical cuboid.* One opposing pair of the vertical faces is taken to be the vapour source and sink while the other pair, along with the floor and ceiling, is taken to be solid, i.e. nonslip and impermeable. Such a geometry is described by one characteristic length, b, the distance between the source and sink, and two dimensionless parameters, $\mathcal{A}$ and $\mathcal{S}$, the vertical and spanwise aspect ratios.

The physics of the problem specifies two principal directions—that of the gravitational force and that of the normal to the source and sink walls—and two directions define a parallel family of planes (parallel to the bounding walls in the spanwise direction). Consequently, much of the research into vapour transport through gas-filled enclosures, including all of the studies cited in the first paragraph except that of Rosenberger et al. (1997), have assumed the flow to be planar. That is, all quantities are assumed to be independent of the location in the third dimension. In making this two-dimensional assumption, these investigators were in large part following in the tradition of those who study the analogous single fluid heat transfer problem:

> In the remaining direction, at right angles to the plane of the sketch, the air space is regarded as extending to infinity. All boundary con-

*'The need of some short word in the place of the polysyllabic "rectangular parallelepiped" has long been felt. I have coined the word "cuboid" ' (Hayward 1890).

> ditions will be assumed uniform in this latter direction, and the convective motion generated by buoyancy forces can then be assumed to be two-dimensional, lying in the plane of Fig. 1. (Batchelor 1954)
>
> If $B \gg L$ and H, the motion will be nearly everywhere two-dimensional, being confined to planes y=const. (Elder 1966)

This assumption was dramatically disproved by the numerical solutions of Mallinson and de Vahl Davis (1973, 1977) which clearly showed spanwise flow throughout the entire cavity. This phenomena will also occur in the vapour transport problem, and will be returned to later. More recent work on the pure fluid heat transfer problem has suggested that three-dimensional flow may also occur by instability of the two-dimensional flow, even if the cavity were unbounded in the third dimension (Chait & Korpela 1989).

So, while the reality of three-dimensional fluid motion should be kept firmly in mind, it is nevertheless profitable to first consider one- and two-dimensional problems. This may be done by restricting attention to flows for which the characteristic length in any direction is more or less equivalent to the extent of the cavity in the same direction, i.e. laminar unicellular flows, and then examining the limit as one or two of these dimensions tend to infinity or zero. In terms of the governing parameters, the restriction to laminar unicellular flows implies a small combined Grashof number, $Gr(1+N)$. Physically, it means that the cavity and the buoyancy forces must be small. A guide to how small can be obtained from the analogous pure fluid heat transfer problem: for a cavity large in the vertical and spanwise directions, it means a temperature difference between (heat) source and sink of less than 40 K for a 10 mm gap, or less than 5 K for a 20 mm gap (Gill & Davey 1969).

Also, attention here is restricted to steady-state problems. The rationale for this is that, considering the building wall cavity, while the wall as a whole would be subjected to variable thermal and hydrological conditions according to changes in the weather and the diurnal and seasonal cycles, the effect of these on the

fluid in the cavity will be attenuated to a large degree by the capacitance of the solid and porous solid parts of the building envelope. Further, in order to solve evolution problems, initial conditions must be stipulated, and there is no obvious choice of these for the building wall cavity; the step change in wall temperature contemplated by Patterson and Imberger (1980; see also Kwak & Hyun 1998) must be rejected as inappropriate and unphysical, particularly in view of the extreme sensitivity of the results to the initial conditions: compare the studies of Ivey (1984) and Schladow, Patterson and Street (1989). Unsteady fluid flow is of course possible even with steady boundary conditions, however this is probably best understood from the coign of vantage of the stationary flow (Gadoin & Le Quéré 1998). In restricting the scope in this manner, I am also adhering to the Cartesian principle of tackling the simplest problems first (Descartes 1911, p. 14).

Bearing this now rather lengthy list of restrictions in mind, let us return to the problem.

The geometry of building wall cavities is in general characterized by a large vertical aspect ratio, $\mathcal{A}$; i.e. they are much taller than they are wide. This suggests the first problem for the study—the limiting behaviour as $\mathcal{A}, \mathcal{S} \to \infty$. This is essentially a one-dimensional problem: the velocity, temperature and concentration varying in space only as a function of the position relative to the source and sink wall planes. The solution is obtained in closed form in § 4.4. It shows some similarities with the analogous pure fluid heat transfer problem (Jones & Furry 1946) but also noticeable effects peculiar to mass transfer: transpirational interfacial velocity and interdiffusive enthalpy flux. The contribution of the 'latent heat' to the total energy flux is also staggering—consider the numerical example from Yan, Tsay and Lin (1989), which is used in § 4.5 for validation: the total energy transfer rate, including mass transfer effects is 8.849 (Yan et al. 1989) or 8.851 (McBain 1998; § 4.5) times that which would be predicted on the basis of simple heat transfer. This example shows the potential importance of mass transfer in the thermal performance of building wall cavities.

The infinite plane layer solution, just discussed, is incompatible with a solid floor and ceiling. To see whether or not it could still describe a finitely tall cavity, at least sufficiently far from the ends, numerical solutions to the two-dimensional problem were obtained using the augmented Lagrangian algorithm with the finite element package *Fastflo* (CSIRO 1997; McBain 1997*a*; § 5.1). The results (McBain & Harris 1998; § 5.2) show that even if the vertical aspect ratio is as low as 5, the two-dimensional numerical solution agrees with the analytic one-dimensional solution to better than 1% in all the solution variables (velocity components, temperature, vapour mass fraction and pressure).

The next extension is again suggested by building wall cavities. Unlike the geometries imagined by Batchelor (1954) and Elder (1966), these do not extend indefinitely in the third-dimension. For example, the cavities in one locally popular variety of hollow concrete block have a span less than 20% longer than their breadth (Cement and Concrete Association of Australia 1976, p. 2.7). In chapter 7, the same asymptotic procedure as used for the infinite plane fluid layer problem is applied to the limit $\mathcal{A} \to \infty$ with $\mathcal{S}$ held fixed. It turns out that an effectively two-dimensional region does exist midway between the end-walls if the spanwise aspect ratio is greater than about 1.7. For smaller spans, their effect is felt throughout.

One of the interesting features of the bounded sections solution is that there is no component of velocity in the spanwise direction. This calls into question the universality of the conclusion of de Vahl Davis (1998; quoted in full on p. 195). This conclusion, however, was only based on a finite number of numerical solutions. The contradiction can be resolved by shifting from the cuboid to a topologically equivalent geometry for which closed-form solutions can be found—the sphere. This problem has been treated before by Lewis (1950) and Ostoumov (1958), who both, however, wrongly concluded that the flow would be limited to planes containing the directions of gravity and heating. The asymptotic expansion for small Grashof numbers replicates and explains many of the flow features observed

numerically by Mallinson and de Vahl Davis (1973, 1977) and experimentally by Morrison and Tran (1978). In particular, it can explain why no spanwise flow need be expected in a tall but bounded cavity, and strongly suggests that de Vahl Davis's (1998) conclusion that the spanwise flow tends to a constant fraction of the primary flow as the Grashof number tends to zero is false.

1.4 Summary

In this investigation into vapour transport across gas-filled enclosures, I first consider the various models used by earlier researchers and then construct one general enough to include all the essential physics but simple enough to be tractable. Solutions are found for simple geometries and limiting cases in order to quantify the effects of various phenomena. Here three phenomena are selected for particular attention: the interfacial velocity due to mass transfer, the interdiffusion enthalpy flux, and the role of the impermeable bounding walls connecting the source and the sink.

Chapter 2

The Basic Equations of Vapour Transport

In spite of the large number of previous studies of similar systems, it is necessary here to rederive the governing equations.

The species equation so obtained (2.7) is quite conventional, but in the derivation it is emphasized that it expresses the physical principle that the divergence of the absolute vapour flux vanishes. This flux is used later in the derivation of the velocity condition at mass transfer interfaces and in the selection of an appropriate normalization for the mass transfer rate. The latter is unconventional and has some interesting and useful properties.

The present momentum equation (2.10) is also fairly standard; it is included here because it differs in a simple but important way from that proposed by the principal reference for this section: Bird, Stewart and Lightfoot's *Transport Phenomena* (1960).

The energy equation (2.16) is derived here in some detail, since its form is not so well agreed upon as those of the previous two. In particular, the handling of the interdiffusion term has been a repeated source of error.

The equations are derived in dimensional form. The independent variables; $\mathbf{r}_*$ and its components and their operator, $\boldsymbol{\nabla}_*$; and the dependent variables;

$m_*, T_*, \mathbf{u}_*$ and p_*; are subscripted with asterisks. The dimensional coefficients appearing in the equations; other fluid mixture properties, e.g. ρ, D; are not, as they will eventually (§ 2.3) be combined into dimensionless groups such as the Schmidt number, Sc. All symbols are defined in the Nomenclature, page xii.

2.1 Field equations

2.1.1 The equations of continuity

For steady-state laminar flow, the equation for the continuity of the mixture is (Bird et al. 1960, p. 556):

$$\boldsymbol{\nabla}_* \cdot (\rho \mathbf{u}_*) = 0. \tag{2.1}$$

The mass flux of vapour with respect to a frame of reference fixed in space is (Bird et al. 1960, p. 561):

$$\mathbf{n}_* = \rho m_* \mathbf{u}_* + \mathbf{j}_* \tag{2.2}$$

where ρ is the mixture density, m_* is the mass fraction of the vapour in the gas–vapour mixture, $\mathbf{u}_*$ is the mass average velocity and $\mathbf{j}_*$ is the mass flux of the vapour relative to the mass average velocity.

Considering only Fickian diffusion (Bird et al. 1960, p. 502; see also 'Omissions', below),

$$\mathbf{j}_* = -\rho D \boldsymbol{\nabla}_* m_*, \tag{2.3}$$

where D is the binary diffusivity, so that

$$\mathbf{n}_* = \rho \left(m_* \mathbf{u}_* - D \boldsymbol{\nabla}_* m_* \right). \tag{2.4}$$

For steady-state vapour transport in a laminar flow, with no destruction or creation of vapour (see 'Omissions', below), conservation of vapour requires that its flux (2.4) is solenoidal (Bird et al. 1960, p. 561); i.e.

$$\boldsymbol{\nabla}_* \cdot \mathbf{n}_* = 0. \tag{2.5}$$

If the spatial variations of ρ and D are neglected in the mass fluxes ($\rho\mathbf{u}_*$) and $\mathbf{n}_*$, the equations of continuity reduce to

$$\boldsymbol{\nabla}_* \cdot \mathbf{u}_* = 0 \tag{2.6}$$

$$\mathbf{u}_* \cdot \boldsymbol{\nabla}_* m_* = D\nabla_*^2 m_* \tag{2.7}$$

It is obvious from (2.7) that the velocity field, $\mathbf{u}_*$, must be known for the distribution of vapour to be calculable. To this end, an equation of motion is obtained in § 2.1.2.

Omissions in the species equation

Other contributions to the diffusion flux, $\mathbf{j}_*$, are (Bird et al. 1960, p. 567):

- pressure diffusion, which is only important for tremendous pressure gradients, as in centrifuges;
- forced diffusion, which is only relevant when the net external force per unit mass differs from species to species, as in electrochemical systems; and
- the Soret effect, which is only important for very steep temperature gradients, as in Clusius–Dickel columns (Jones & Furry 1946), or for gas–vapour mixtures with very different molecular weights (Abernathy & Rosenberger 1981).

Although large temperature differences and vapour mixtures including some very heavy species are occasionally employed in crystal growth systems (see, for example, Evans & Greif 1998), neither the temperature nor pressure gradients can be very large in a building wall cavity. Further, the ratio of the molecular weights of water vapour and atmospheric air (considered as a single gas), 0.62, is almost unity compared to those encountered by Abernathy and Rosenberger (1981), 32.8 and 3.28, or Evans and Greif (1998), 11.0.

With the temperature and mass fraction varying through the cavity, supersaturation of the vapour is possible. Whether or not this leads to condensation

in the body of the cavity, and, if so, at what rate droplet formation and growth proceed, depends on the presence, nature and distribution of nucleating aerosols. An analysis of these molecular kinetics lies outside the scope of continuum fluid mechanics and this project. The physics is described in the meteorological treatises of Fletcher (1962, ch. 3) and Rogers and Yau (1989, ch. 6) and summarized in chapter 3 of my B.E. thesis (McBain 1995).

If condensation takes place only at the boundaries, the steady-state species equation can be written in divergence form with no source or sink terms, as above (2.5).

A simple way of investigating the effect of the condensation within the gas–vapour phase on the overall energy transfer rate is to solve the system of equations assuming each of two extreme possibilities:

i. No aerosols are available for heterogeneous nucleation, in which case the species and energy equations are as above—homogeneous nucleation occurring only at very high supersaturations; e.g. relative humidity in excess of 400% for water vapour at normal temperatures (McBain 1995).

ii. Aerosols perfectly suitable for heterogeneous nucleation are abundant, so that the mixture cannot sustain any degree of supersaturation.

In the latter case, provided the gas–vapour mixture is saturated at its boundaries, the analogy developed by Close and Sheridan (1989) and verified by Close et al. (1991) becomes available, and the overall energy transfer rate can be predicted from single fluid heat transfer correlations, with modified properties. I carried out such an investigation as part of my B.E. thesis (McBain 1995). The results, reported therein and by McBain, Harris, Close and Suehrcke (1998), indicated that condensation within the gas–vapour phase led to higher overall energy transfer rates, particularly at higher mean temperatures. The greatest increase, 8%, was found at the highest mean temperature, 50°C.

The problem of condensation of the vapour away from the boundaries is very important in the growth of crystals by PVT, where saturated boundary conditions

are the norm, as it can lead to 'morphological instability' of the growth face (Faktor & Garrett 1974, pp. 216–7; Rosenberger et al. 1997).

The present work is restricted to the case where the vapour only condenses at the boundaries, a case which will certainly prevail if the gas–vapour mixture is everywhere unsaturated. The basic equations presented in this chapter ignore the degree of saturation (relative humidity for air–water vapour systems). The solutions of these equations will be valid if, for a particular dimensional set of values of the boundary conditions, the predicted degree of saturation is everywhere less than unity. Since the most likely cause for this not being the case in practice is that the vapour is saturated at the boundaries (so that the Close–Sheridan analogy is applicable), this is not a very serious restriction. I have no recommendations on how to treat cases of mixed saturation and unsaturation, except to say that, based on the study cited above, the present methods neglecting vapour-phase condensation should give a reasonable approximation of the overall mass and energy transfer rates.

2.1.2 The equation of motion

The equation of motion used here is not that derived by Bird et al. (1960, pp. 320, 563) for free convection. Neglecting the variation of pressure due to motion leads to an overconstrained system so that the equation for continuity of the mixture, (2.1) or (2.6), could not be enforced (see Gresho 1988).

The basic steady-state Navier–Stokes equation (Bird et al. 1960, p. 80) is:

$$\rho \mathbf{u}_* \cdot \boldsymbol{\nabla}_* \mathbf{u}_* = -\boldsymbol{\nabla}_* p_* + \rho \mathbf{g} + \mu \boldsymbol{\nabla}_*^2 \mathbf{u}_* \tag{2.8}$$

where p and μ are the pressure and viscosity, and $\mathbf{g}$ is the body force per unit mass, assumed hereafter to be uniform and downward. The density and viscosity are assumed uniform in (2.8), except in the body force term, $\rho\mathbf{g}$, where ρ is replaced by its linear Taylor series expansion as a function of the temperature

and vapour mass fraction about some reference state (Bird et al. 1960, p. 563):

$$\rho\left[1-\beta(T_*-T_{*r})-\zeta(m_*-m_{*r})\right], \tag{2.9}$$

where β and ζ are the thermal and vapour mass fraction coefficients of volumetric expansion. This Boussinesq approximation forms the basis of the vast majority of studies in natural convection. Its consistency and limitations are discussed by Spiegel and Veronis (1960), Ostrach (1964), Chenoweth and Paolucci (1986), Gebhart et al. (1988, ch. 2) and Perez-Cordon and Mengual (1997), amongst others. Few of the works reviewed in § 3.3 did not use the approximation, and, as noted there, no qualitatively different features were found nor were any quantitative effects on the overall vapour or energy transport rates reported. Particular attention is drawn to my earlier non-Boussinesq numerical simulations, which gave results quite consistent with Boussinesq models (McBain 1995, 1997*b*). Boyadjiev and Halatchev (1998) came to the same conclusion for vapour transport from a vertical semi-infinite plate. Apart from the obvious simplification of the governing equations, the principal advantage in using the approximation is the increase in generality of the results, that is, the differences between various species are reduced to their essentials.

On rearranging the simple potential part of the body force and the pressure term,

$$\mathbf{u}_*\cdot\boldsymbol{\nabla}_*\mathbf{u}_*=-\boldsymbol{\nabla}_*\left(\frac{p_*}{\rho}+gy_*\right)+g\left[\beta(T_*-T_{*r})+\zeta(m_*-m_{*r})\right]\hat{\boldsymbol{\jmath}}+\nu\boldsymbol{\nabla}_*^2\mathbf{u}_*, \tag{2.10}$$

where y_* and $\hat{\boldsymbol{\jmath}}$ are the vertical coordinate and unit vector, and $\nu=\mu/\rho$ is the kinematic viscosity.

It is obvious from (2.10) that the temperature field must be known for the distribution of velocity, and therefore vapour, to be calculable. To this end, the equation of (thermal) energy is obtained in § 2.1.3.

2.1.3 The energy equation

Neglecting the gravitational potential energy (since the cavities of interest are of limited vertical extent, see Spiegel & Veronis 1960), the steady-state energy equation is (Bird et al. 1960, p. 561):

$$\boldsymbol{\nabla}_* \cdot \mathbf{e}_* = 0, \tag{2.11}$$

where $\mathbf{e}_*$ is the energy flux with respect to a fixed frame of reference.

If the gas–vapour mixture is diathermanous (so that the radiant energy flux can be handled separately), and the Dufour effect, viscous stresses and the advection of kinetic energy are negligible, the energy flux is (Bird et al. 1960, p. 566):

$$\mathbf{e}_* = -\lambda \boldsymbol{\nabla}_* T_* + (h_A - h_B)\mathbf{j}_* + \rho h \mathbf{u}_* \tag{2.12}$$

where λ is the thermal conductivity and h_A and h_B are the partial specific enthalpies of the gas and vapour and $h = h_B + m_*(h_A - h_B)$ is the specific enthalpy of the mixture (Guggenheim 1959, pp. 213–4).

If the gas and vapour form a 'perfect gaseous mixture', so that the partial specific heat capacities, defined by (Guggenheim 1959, p. 212)

$$c_{pi} = \left(\frac{\partial h_i}{\partial T_*}\right)_{p_*} \qquad i = A, B, \tag{2.13}$$

are equal to the specific heat capacities of the pure components and independent of pressure (Guggenheim 1959, pp. 225, 118) and if the gas and vapour are calorically perfect, so that their specific heat capacities are independent of temperature, then the partial specific enthalpies appearing in the energy flux (2.12) can be expressed in terms of the temperature:

$$h_i = h_{ir} + c_{pi}(T_* - T_{*r}), \ i = A, B. \tag{2.14}$$

Whence,

$$\begin{aligned} \mathbf{e}_* &= -\lambda \boldsymbol{\nabla}_* T_* \\ &+ \rho(T_* - T_{*r})[c_{pB} + m_*(c_{pA} - c_{pB})]\mathbf{u}_* \\ &- \rho(T_* - T_{*r})(c_{pA} - c_{pB}) D \boldsymbol{\nabla}_* m_* \\ &+ \rho h_{Br} \mathbf{u}_* + (h_{Ar} - h_{Br})\mathbf{n}_* \end{aligned} \tag{2.15}$$

where (2.3) and (2.2) have been used for the definitions of $\mathbf{n}_*$ and $\mathbf{j}_*$.

In (2.15):

- $-\lambda \boldsymbol{\nabla}_* T_*$ is the Fourier conduction flux;
- $\rho(T_* - T_{*r})[c_{pB} + m_*(c_{pA} - c_{pB})]\mathbf{u}_*$ is the advection of thermal energy by the mean flow; and
- $-\rho(T_* - T_{*r})(c_{pA} - c_{pB}) D \boldsymbol{\nabla}_* m_*$ is the advection of thermal energy by the vapour diffusion flux (the 'interdiffusion' term).

The last two terms in (2.15) are divergence-free, by (2.6) and (2.5), and so have no effect on the energy equation (2.11). They must be included, however, in the energy flux at the boundary. Both terms are also of arbitrary magnitude, since enthalpies are only defined by their changes, rather than absolutely (Guggenheim 1959, pp. 11, 32). The reference enthalpy of the noncondensable gas, h_{Br}, may be set to zero, since all the cavities considered in this project are impermeable to the gas. The reference enthalpy of the vapour on the other hand must include the heat of vaporization or sublimation, since it is the term $h_{Ar}\mathbf{n}_*$ that accounts for the latent heat.

Substituting (2.15) into (2.11), with λ assumed constant, the primitive thermal energy equation is:

$$\rho[c_{pB} + m_*(c_{pA} - c_{pB})]\mathbf{u}_* \cdot \boldsymbol{\nabla}_* T_* = \lambda \nabla_*^2 T_* + \rho D(c_{pA} - c_{pB})(\boldsymbol{\nabla}_* m_*) \cdot (\boldsymbol{\nabla}_* T_*). \tag{2.16}$$

Multiples of the equations of continuity of the mixture (2.6) and the vapour (2.5) were subtracted to eliminate the terms proportional to $(T_* - T_{*r})$, which is important, as pointed out in the following paragraphs.

Possible difficulties with the energy equation

It does not make sense to treat the mixture specific heat capacity,

$$c_p = c_{pB} + m_*(c_{pA} - c_{pB}), \tag{2.17}$$

as a constant in the bulk advection term if the interdiffusion term is included. Two different difficulties would thereby arise, depending on whether it were treated as constant before or after the divergence of the energy flux was taken.

In the first case, constant c_p in (2.15), it is not possible to use the species equation (2.5) to simplify the energy equation and an additional term appears on the right hand side of (2.16):

$$\rho D(c_{pA} - c_{pB})(T_* - T_{*r})\nabla_*^2 m_*. \tag{2.18}$$

This would mean that the reference temperature, T_{*r}, the datum for the enthalpies, would appear in the energy equation, so that the temperature field would depend on a completely arbitrary quantity, which is obviously unphysical and unacceptable.

In the second case, constant c_p in (2.16), if one attempts to write the energy equation (2.16) in the form of a divergence (2.11), a spurious source term appears:

$$\begin{aligned} \boldsymbol{\nabla}_* \cdot \mathbf{e}_* &= -\rho D(c_{pA} - c_{pB}) T \nabla_*^2 m_* \\ &= (c_{pA} - c_{pB}) T (\boldsymbol{\nabla}_* \cdot \mathbf{j}_*) \end{aligned} \tag{2.19}$$

This would mean that energy was not conserved. While the degree to which the conservation of energy (2.11) was violated might be small and within the limits of accuracy of the Boussinesq approximation, it is inconvenient for a number of reasons. For example, a global energy balance is often a useful check on the accuracy of an analytic or numerical solution (e.g. Incropera & DeWitt 1990, p. 198; de Vahl Davis 1983). Further, it would be necessary to specify the method by which the overall energy transfer rate was calculated.

Most importantly, however, the order of approximation involved in a constant mixture specific heat is inconsistent with the inclusion of interdiffusion. It should

be clear by now—if not from the fundamental expression for the energy flux (2.12) then at least from the two possible errors exposed here—that the bulk advection of thermal energy and the interdiffusion of enthalpy are closely related. Indeed, they are an often convenient but somewhat artificial way of repartitioning the thermal energy transported by each of the species present when they move.

Another error was committed by myself (McBain 1995, 1997*b*) and Weaver and Viskanta (1991*a*): allowing the mixture specific heat to vary, but excluding the interdiffusion term. In the case of Weaver and Viskanta (1991*a*; discussed in § 3.3.12), this may have caused their prediction of a spatial minimum in the gas–vapour phase temperature; an impossibility (as proven in § 2.6.1) strongly suggestive of a spurious sink in the energy equation.

In conclusion, the interdiffusion term should be included in the energy equation if, and only if, the mixture specific heat is treated as a function of the vapour mass fraction. The question of when these should be included is taken up once the equations are nondimensionalized and some examples examined (ch. 6).

2.2 Boundary conditions

The principal concern of this project is the transport of vapour across gas-filled cavities. For this to occur, there must be some gradient or difference in thermodynamic potential imposed by the boundary conditions. In any physical situation this is determined dynamically by the state of the surrounding media and the conditions at the interface are that certain quantities, such as the thermodynamic potential (Guggenheim 1959, p. 230) and flux of the vapour species, should be continuous. The vapour transport in the surrounding media depends in turn on the conditions imposed at its external boundaries, and so on *ad infinitum*. Thus, it is necessary to terminate the domain somewhere: the simplest choice is the boundary of the gas–vapour phase.

2.2.1 Velocity boundary conditions

The two types of velocity boundary conditions are those at solid and semipermeable walls.

At a solid wall, no fluid (gas or vapour) can pass through the boundary, therefore

$$\hat{\boldsymbol{n}} \cdot \mathbf{u}_* = 0 \tag{2.20}$$

where $\hat{\boldsymbol{n}}$ is the unit outward normal.

At an ideally semipermeable mass transfer interface, the vapour alone can pass; i.e. the surface is impermeable to the gas. In this case, the normal component of the total mass flux must equal that of the vapour mass flux (2.4):

$$\hat{\boldsymbol{n}} \cdot \rho \mathbf{u}_* = \hat{\boldsymbol{n}} \cdot \mathbf{n}_* \tag{2.21}$$

$$\hat{\boldsymbol{n}} \cdot \rho \mathbf{u}_* = \hat{\boldsymbol{n}} \cdot \rho(m_* \mathbf{u}_* - D \boldsymbol{\nabla}_* m_*) \tag{2.22}$$

$$\hat{\boldsymbol{n}} \cdot \mathbf{u}_* = \frac{-D}{1 - m_*} \hat{\boldsymbol{n}} \cdot \boldsymbol{\nabla}_* m_*. \tag{2.23}$$

This 'transpiration' boundary condition was used by, for example, Hu and El-Wakil (1974), and Rosenberger and Müller (1983).

The no-slip condition is uncontroversial for the semipermeable walls, except for situations like the experiments of Hu and El-Wakil (1974; § 3.3.2) or Weaver and Viskanta (1991*c*; § 3.3.14), where liquefied vapour streamed down the walls. For the solid walls, however, there is a deep division of opinion on the validity of the no-slip condition, dating back at least to 1954 (Lee, C. Y. & Wilke), and continuing up to the present (§ 3.2).

Though the issue may have been obscured by several simultaneous phenomena, I am persuaded by the agreement between experiment and model (including nonslip solid walls) in the recent detailed study of Rosenberger et al. (1997), and so accept the validity of the boundary condition. Another test of the no-slip condition could be provided by the agreement between theory, numerical solutions and experiment on the criterion for the onset of convective flow in a Stefan diffusion tube with a light vapour (McBain, Suehrcke & Harris, in press; § 3.2.5),

although to date measurements are only available for very low mass transfer rates ($0 < \Phi < 0.012$).

Further verification, in the form of a more specific experiment or 'a rigorous statistical mechanical treatment', as suggested by Markham and Rosenberger (1980) and Jhaveri et al. (1981), may be required before this question is finally settled.

2.2.2 Heat and mass transfer boundary conditions

For simplicity, either Dirichlet (fixed value), Neumann (fixed normal derivative) or Robin (a linear combination of the previous two) boundary conditions will be specified for the vapour mass fraction and temperature, depending on the particular problem. Ideas for how these idealizations might be implemented have been presented elsewhere (McBain, Close, Suehrcke, Harris & Brandemuehl 1998).

Appropriate thermal boundary conditions for the analogous single fluid heat transfer problem (§ 2.4) have been discussed by many authors, including Batchelor (1954), Mallinson (1987) and Leong, Hollands and Brunger (1998), but comparatively little attention has been paid to the mass transfer boundary conditions. The only investigation I am aware of is the simple parametric study of Costa (1997). This is probably because the nonisothermal transport of moisture (or other condensed vapour) through porous media is in itself an extremely difficult problem, indeed, the fundamentals seem to be less well understood than in the present problem (see, for example, Dahl et al. 1996; Hens 1996; Künzel & Kiessl 1997). At some stage, once the transport of vapour through gaseous and porous phases is better understood, it will be possible to properly consider the conjugate heat and mass transfer problem.

No vapour passes an impermeable wall so that, on eliminating the normal component of velocity by (2.20) from (2.4),

$$\begin{aligned} \hat{\boldsymbol{n}} \cdot \mathbf{n}_* &= 0 \\ \hat{\boldsymbol{n}} \cdot \boldsymbol{\nabla}_* m_* &= 0. \end{aligned} \tag{2.24}$$

Possibly the simplest thermal boundary condition for these walls is the adiabatic, which results from setting the normal component of the absolute energy flux (2.15) to zero, and eliminating the mass fluxes by (2.20) and (2.24):

$$\begin{aligned} \hat{\boldsymbol{n}} \cdot \mathbf{e}_* &= 0 \\ \hat{\boldsymbol{n}} \cdot \boldsymbol{\nabla}_* T_* &= 0. \end{aligned} \tag{2.25}$$

The adiabatic condition is not meaningful at a mass transfer interface, since the enthalpy carried by the mass fluxes is arbitrary. Its relevance for any wall bounding a gas–vapour phase is questionable (see studies cited above) since the thermal conductivity of any solid is higher than that of most gas–vapour mixtures. A better idealization, first suggested by Batchelor (1954), is to treat the solid wall as a perfect conductor. This uncouples the heat conduction in the solid, which sees the boundary with the gas–vapour phase as adiabatic, and leads to a Dirichlet condition for the gas–vapour phase temperature. An example is described in § 7.5.2.

2.3 Nondimensionalization

The primitive dependent variables are reduced to dimensionless form by:

$$m_* = m_{*r} + m\Delta m_*; \tag{2.26}$$

$$\mathbf{u}_* = \frac{g(\beta\Delta T_* + \zeta\Delta m_*)b^2}{\nu}\mathbf{u}; \tag{2.27}$$

$$p_* = \rho g(\beta\Delta T_* + \zeta\Delta m_*)b\mathcal{A}p - \rho g y_*; \quad \text{and} \tag{2.28}$$

$$T_* = T_{*r} + T\Delta T_*; \tag{2.29}$$

where b is a characteristic length of the domain and Δm_* and ΔT_* are characteristic differences of vapour mass fraction and temperature, to be introduced by the boundary conditions, respectively. Also,

$$\boldsymbol{\nabla}_* = \frac{1}{b}\boldsymbol{\nabla} \quad \text{and} \tag{2.30}$$

$$\mathbf{r}_* = b\mathbf{r}, \tag{2.31}$$

where $\mathbf{r}_*$ is the position vector.

The scales in this scheme were chosen to ensure that the variables have values of order unity in the solutions later obtained (ch. 4, 7, 8). In general, these are characterized by a dominance of the diffusive (including conduction and viscous diffusion of momentum) as opposed to the advective terms in the field equations.

2.3.1 Mass and energy fluxes

Define the reduced vapour mass flux by:

$$\mathbf{n} \equiv \frac{b}{\rho D \Phi} \mathbf{n}_*, \tag{2.32}$$

where

$$\Phi \equiv \ln\left(\frac{1 - m_{*r}}{1 - m_{*r} - \Delta m_*}\right) \tag{2.33}$$

is the mass transfer rate factor. This apparently complicated choice of a driving force arises naturally in one-dimensional problems (ch. 4) and will be much discussed, particularly in chapter 6.

The vapour flux is the sum of advective and diffusive fluxes:

$$\mathbf{n} = \mathbf{n}_{adv} + \mathbf{n}_{diff} \tag{2.34}$$

$$\mathbf{n}_{adv} = \left[m_{*r} + m(1 - m_{*r})\left(1 - \mathrm{e}^{-\Phi}\right)\right] \frac{Gr(1+N)Sc}{\Phi}\, \mathbf{u} \tag{2.35}$$

$$\mathbf{n}_{diff} \equiv \mathbf{j} = -(1 - m_{*r}) \frac{1 - \mathrm{e}^{-\Phi}}{\Phi} \boldsymbol{\nabla} m \tag{2.36}$$

where

$$Gr \equiv \frac{g\beta \Delta T_* b^3}{\nu^2}, \tag{2.37}$$

$$N \equiv \frac{\zeta \Delta m_*}{\beta \Delta T_*}, \quad \text{and} \tag{2.38}$$

$$Sc \equiv \frac{\nu}{D} \tag{2.39}$$

are dimensionless parameters (see § 1.3). Note that the reference vapour mass fraction m_{*r} appearing here is not covered by the set of governing dimensionless

parameters. This is unimportant, though, as it cancels out of the field equations, the boundary conditions and the expressions for the wall fluxes.

Define the reduced energy flux by

$$\mathbf{e} \equiv \frac{b[1-\exp(-\Phi_T)]}{\lambda \Delta T_* \Phi_T}\mathbf{e}_*, \tag{2.40}$$

where

$$\Phi_T \equiv \frac{\Phi(Pr_r + Pr_I)}{Sc} \tag{2.41}$$

is the thermal mass transfer rate factor, and

$$Pr_r \equiv \frac{\rho[c_{pB} + m_{*r}(c_{pA} - c_{pB})]\nu}{\lambda}, \quad \text{and} \tag{2.42}$$

$$Pr_I \equiv \frac{\rho(c_{pA} - c_{pB})(1 - m_{*r})\nu}{\lambda} \tag{2.43}$$

are the reference and interdiffusion Prandtl numbers, respectively.

The arbitrary reference enthalpy of the gas may be set to zero,

$$h_{Br} = 0, \tag{2.44}$$

for the reasons stated above (§ 2.1.3), and the reference enthalpy of the vapour equated to its heat of vaporization at the reference temperature,

$$h_{Ar} = h_{fg}. \tag{2.45}$$

The reduced heat of vaporization of the vapour, or the latent heat factor, is defined:

$$\Lambda \equiv \frac{h_{fg}}{c_{pA}\Delta T_*}. \tag{2.46}$$

The energy flux has components due to advection and conduction. The advective fluxes are split into a bulk advective flux, the interdiffusion flux and the latent heat flux:

$$\mathbf{e} = \mathbf{e}_{cond} + \mathbf{e}_{adv} + \mathbf{e}_{int} + \mathbf{e}_{lat} \tag{2.47}$$

$$\mathbf{e}_{cond} = -\frac{1-\exp(-\Phi_T)}{\Phi_T}\boldsymbol{\nabla} T \tag{2.48}$$

$$\mathbf{e}_{adv} = \frac{1-\exp(-\Phi_T)}{\Phi_T} Gr(1+N)\left[Pr_r + Pr_I\left(1-\mathrm{e}^{-\Phi}\right)m\right]T\mathbf{u} \tag{2.49}$$

$$\mathbf{e}_{int} = -\frac{1-\exp(-\Phi_T)}{\Phi_T}\frac{Pr_I}{Sc}\left(1-\mathrm{e}^{-\Phi}\right)T\boldsymbol{\nabla}m \tag{2.50}$$

$$\mathbf{e}_{lat} = \frac{1-\exp(-\Phi_T)}{\Phi_T}\Phi_T\Lambda\mathbf{n} \tag{2.51}$$

The conservation of species (2.5) and energy (2.11) then requires simply that $\mathbf{n}$ and $\mathbf{e}$ are solenoidal. These equations may be obtained thus or by nondimensionalizing equations (2.7) and (2.16); the result is given in § 2.3.2. The latent heat flux, $\mathbf{e}_{lat}$, is solenoidal, being proportional to $\mathbf{n}$, and so makes no contribution to the energy equation. It must be retained, however, for calculation of the total flux at the boundaries.

The intrinsic link between the variability of the mixture specific heat and the interdiffusion term in the energy equation is made even more obvious by the above reduction: both depend on the same dimensionless parameter, the interdiffusion Prandtl number, Pr_I.

2.3.2 Dimensionless field equations

The dimensionless equations of continuity (2.6, 2.7), motion (2.10), and energy (2.16) are:

$$\boldsymbol{\nabla}\cdot\mathbf{u} = 0 \tag{2.52}$$

$$Gr(1+N)Sc\ \mathbf{u}\cdot\boldsymbol{\nabla}m = \nabla^2 m \tag{2.53}$$

$$Gr(1+N)\mathbf{u}\cdot\boldsymbol{\nabla}\mathbf{u} + \mathcal{A}\boldsymbol{\nabla}p - \frac{T+Nm}{1+N}\hat{\boldsymbol{j}} = \boldsymbol{\nabla}^2\mathbf{u} \tag{2.54}$$

$$\begin{aligned} Gr(1+N)\left[Pr_r + Pr_I\left(1-\mathrm{e}^{-\Phi}\right)m\right]\mathbf{u}\cdot\boldsymbol{\nabla}T \\ -\frac{Pr_I}{Sc}\left(1-\mathrm{e}^{-\Phi}\right)(\boldsymbol{\nabla}m)\cdot(\boldsymbol{\nabla}T) = \nabla^2 T. \end{aligned} \tag{2.55}$$

The dimensionless parameters appearing here are not all independent, since the interdiffusion Prandtl number, Pr_I, and the mass transfer rate factor, Φ, only appear in the group $Pr_I[1-\exp(-\Phi)]$. The mass transfer rate factor, however, enters separately in the transpiration boundary condition (2.59), below.

The general roles of the various dimensionless parameters are as follows.

i. Gr, the thermal Grashof number, indicates the strength of buoyancy forces due to temperature variations. It is a measure of the nonlinearity of the system. It has the same sign as the temperature difference (for fluids expanding on heating), which is usually taken as positive.

ii. N, the buoyancy ratio, indicates the strength of buoyancy forces due to vapour concentration variations relative to the thermal effects. Since buoyancy is usually the main driving force for the flow (rather than the interfacial velocity), the combined Grashof number, $Gr(1+N)$, is a measure of the relative importance of advective and diffusive (viscous) processes. Thus, fluid motion instabilities are more likely at higher combined Grashof numbers. N can range over $(-\infty, \infty)$.

iii. Sc, the Schmidt number, is the ratio of the diffusivities of momentum and species, a necessarily positive quantity. Its product with the combined Grashof number indicates the relative importance of advection and diffusion for species transport. Its numerical value for air–water vapour under normal conditions is about 0.61 (Gebhart et al. 1988, p. 943).

iv. Φ, the mass transfer rate factor, is central to all aspects of mass transfer. It is the driving force for vapour transport, and enters into the boundary conditions on velocity at the interfaces, as well as the interdiffusion term in the energy equation.

v. Pr_r, the reference Prandtl number, is the ratio of the diffusivities of momentum and heat, based on the (isobaric) specific heat capacity of the mixture at the reference composition. When mass transfer rate effects are small, this approaches the usual single fluid Prandtl number, and as such is proportional to the bulk advection term in the energy equation. When the diffusion flux is comparable to the mean mass flux, this interpretation must be modified. This quantity is necessarily positive. Its numerical value for dry air at 275–310 K is 0.71 (Gebhart et al. 1988, p. 935).

vi. Pr_I, the interdiffusion Prandtl number, has the form of a Prandtl number, except that in the usual place of a specific heat it has the difference of the specific heats of the vapour and gas. While this quantity is not necessarily positive (although $Pr_r + Pr_I > 0$), it will often be so in practice since vapours are typically distinguishable from gases by a greater molecular complexity—this being related to the causes of the intermolecular attractions responsible for their relatively high boiling point. More complex molecules have more kinds of energy (e.g. rotational and vibrational) and so higher specific heats (Jeans 1940, pp. 33–6, 275 f.). This trend is somewhat offset by the fact that specific heat capacities are, all else being equal, inversely proportional to molar mass (Jeans 1940, pp. 35, 276). The alkanes form a counterexample: the boiling points (at 1 atm) and specific heat capacities (at 298 K and low pressure) of methane, ethane and propane are 112, 185 and 231 K and 2219, 1746 and 1669 $\mathrm{J.K^{-1}.kg^{-1}}$, respectively (Dean, J. A. 1992, pp. 1.199 – 1.286, 6.19 – 6.33). In our principal example, however, the rule is true: the specific heat capacities of air and water vapour at 300 K being 1003.5 and 1872.3 $\mathrm{J.kg^{-1}.K^{-1}}$. At infinite dilution, 300 K and 1 atm, the value of the interdiffusion Prandtl number for air–water vapour is:

$$Pr_I \equiv \frac{\rho D(c_{pA} - c_{pB})(1 - m_{*r})}{\lambda} \tag{2.56}$$

$$= \frac{(1.1768)(2.58 \times 10^{-5})(1872.3 - 1003.5)(1 - 0)}{0.0263} \tag{2.57}$$

$$= 1.004. \tag{2.58}$$

The interdiffusion Prandtl number occurs twice in the energy equation: in the interdiffusion term; and in the bulk advection term, where it is proportional to the variation in the mixture specific heat. As explained in § 2.1.3, the variation of the mixture specific heat and the interdiffusion effect are two aspects of the same phenomenon. It is inconsistent to include one without the other. Including interdiffusion without variable mixture specific heat in

the bulk advection term introduces a term into the energy flux divergence (the steady energy equation) which is dependent on the temperature datum for enthalpy, which must be arbitrary. If the mixture specific heat is treated as a constant in the flux divergence, a spurious source term occurs. This has not always been recognized in the literature, and is one of the important features of the present model.

2.3.3 Dimensionless transpiration condition

The dimensionless form of the transpiration boundary condition (2.23) is:

$$\hat{\boldsymbol{n}} \cdot \mathbf{u} = \frac{1 - \mathrm{e}^{-\Phi}}{Gr(1+N)Sc\left[(1-\mathrm{e}^{-\Phi})\, m - 1\right]} \hat{\boldsymbol{n}} \cdot \boldsymbol{\nabla} m. \tag{2.59}$$

It may be seen that the mass transfer rate factor, Φ, enters into both the transpiration boundary condition (2.59) and the variable mixture specific heat and interdiffusion parts of the energy equation (2.55). The relationship between these effects will become evident once solutions of the above system are presented in chapter 4.

2.3.4 Wall fluxes

In this project, the primary interest is in vapour transport between parallel vertical walls. Denoting their common unit normal by $\hat{\boldsymbol{\imath}}$ (see § 2.5), the reduced vapour flux at these walls, the (local) Sherwood number, is

$$Sh \equiv -\hat{\boldsymbol{\imath}} \cdot \mathbf{n}. \tag{2.60}$$

Since the walls are impermeable to the gas, (2.21) holds. In dimensionless form this is

$$\frac{Gr(1+N)Sc}{\Phi} \hat{\boldsymbol{n}} \cdot \mathbf{u} = \hat{\boldsymbol{n}} \cdot \mathbf{n}, \tag{2.61}$$

so that the Sherwood number can be calculated from the transverse component of velocity:

$$Sh = -\frac{Gr(1+N)Sc}{\Phi}\, \hat{\boldsymbol{\imath}} \cdot \mathbf{u}; \tag{2.62}$$

or, because of the transpiration boundary condition (2.59), from the mass fraction field:

$$Sh = \frac{1 - \mathrm{e}^{-\Phi}}{\Phi \left[1 - m\left(1 - \mathrm{e}^{-\Phi}\right)\right]} \, \hat{\boldsymbol{\imath}} \cdot \boldsymbol{\nabla} m. \tag{2.63}$$

This definition of the Sherwood number (2.60, see also equation 2.32), using the mass transfer rate factor, Φ, instead of the mass fraction difference, Δm_*, for the driving force, is unconventional, though it was used by Jhaveri and Rosenberger (1982). Spalding (1960, 1963) has explained in detail the disadvantages of using the mass fraction difference as a driving force, but instead proposed the use of a quantity equivalent to $[\exp(-\Phi) - 1]$. The superiority of the present choice will become apparent once solutions of the system of equations are found and examined (ch. 4), especially when a rational approximation for the system at low mass transfer rates is considered (ch. 6).

The (local) Nusselt number, Nu, is defined at the parallel vertical walls by:

$$\begin{aligned} Nu &\equiv -\hat{\boldsymbol{\imath}} \cdot \mathbf{e} && (2.64) \\ &= \frac{1 - \exp(-\Phi_T)}{\Phi_T} \Big\{ \hat{\boldsymbol{\imath}} \cdot \boldsymbol{\nabla} T \\ &\quad - Gr(1+N)\left[Pr_r + Pr_I\left(1 - \mathrm{e}^{-\Phi}\right) m\right] T \hat{\boldsymbol{\imath}} \cdot \mathbf{u} \\ &\quad + \frac{Pr_I}{Sc}(1 - \mathrm{e}^{-\Phi}) T \hat{\boldsymbol{\imath}} \cdot \boldsymbol{\nabla} m + \Phi_T \Lambda Sh \Big\}. && (2.65) \end{aligned}$$

The interfacial velocity and the mass fraction gradient can be eliminated from this expression by the equations for the Sherwood number (2.62) and (2.63):

$$Nu = \frac{1 - \exp(-\Phi_T)}{\Phi_T} \left[\hat{\boldsymbol{\imath}} \cdot \boldsymbol{\nabla} T + (T + \Lambda)\Phi_T Sh\right] \tag{2.66}$$

Since the latent heat factor, Λ, does not appear in the field equations (2.52)–(2.55), it will occasionally be convenient to consider that part of the energy transfer rate independent of it—the sensible Nusselt number:

$$Nu_{sen} = \frac{1 - \exp(-\Phi_T)}{\Phi_T} \left(\hat{\boldsymbol{\imath}} \cdot \boldsymbol{\nabla} T + T \Phi_T Sh\right). \tag{2.67}$$

The remainder,

$$Nu_{lat} \equiv Nu - Nu_{sen} = [1 - \exp(-\Phi_T)] \Lambda Sh, \tag{2.68}$$

is the latent Nusselt number.

The above comments on the unconventionality of the definition of the Sherwood number apply equally to the Nusselt number. As will be seen in § 2.4, the present Nusselt number reverts to the conventional definition (e.g. Incropera & DeWitt 1990, p. 347) in the absence of mass transfer ($\Phi = 0$).

2.4 The single fluid heat transfer problem

In discussing various hydrodynamic features of the present problem, I shall often have cause to refer to the 'analogous single fluid heat transfer problem', for which there exists an extremely extensive body of literature; see Gebhart et al. (1988, pp. 737–52), Ostrach (1988) or Bejan (1995, ch. 5) for a review.

To facilitate this, its equations are derived here; this being briefly accomplished since they are merely a limiting case of the present set, formed by setting the vapour mass fraction difference, Δm_*, to zero (i.e. $\Phi = N = 0$) in the equations of motion (2.54) and energy (2.55):

$$Gr\,\mathbf{u}\cdot\boldsymbol{\nabla}\mathbf{u} = -\boldsymbol{\nabla}p + T\hat{\boldsymbol{\jmath}} + \boldsymbol{\nabla}^2\mathbf{u}; \tag{2.69}$$

$$GrPr_r\,\mathbf{u}\cdot\boldsymbol{\nabla}T = \nabla^2 T. \tag{2.70}$$

It is clear that these equations are uncoupled from the equation of continuity of the diffusing species (2.53), which may therefore be dropped. The equation of continuity of the 'mixture' (2.52) is unchanged. The Nusselt number (2.66) becomes

$$Nu = \hat{\boldsymbol{\imath}}\cdot\boldsymbol{\nabla}T, \tag{2.71}$$

since

$$\lim_{\Phi\to 0}\frac{1-\exp(-\Phi_T)}{\Phi_T} = 1. \tag{2.72}$$

The product $GrPr_r$ is frequently called the Rayleigh number, Ra.

2.5 Geometry

In order to solve the system of equations developed above, a domain and boundary conditions must be specified. Various limiting cases of the vertical cuboid are considered in chapters 4–7.

One opposing vertical pair of walls are taken to be the source and sink of vapour, while the other four walls, the front, back, floor and ceiling, serve mainly to bound the domain. Let uniform temperatures and vapour mass fractions be specified on the hot ($T = m = 1$) and cold ($T = m = 0$) walls, and take the others to be impermeable, postponing the question of their thermal boundary conditions. The cuboid is defined by one length scale, b, which is taken to be the distance separating the hot and cold walls, and two aspect ratios: $\mathcal{A}$, vertical; and $\mathcal{S}$, spanwise. As illustrated in figure 2.1, the cold and hot walls lie in the planes $x = 0$ and 1, respectively; the y-axis is vertical and the z-axis is chosen so as to form a right-handed system with x and y. Since solutions of (2.52)–(2.55) are symmetrical about the central spanwise plane—the corresponding result for the analogous single fluid heat transfer problem was stated and used by Mallinson and de Vahl Davis (1977)—the origin of the coordinate system is located halfway along the base of the cold wall. Note that the centrosymmetry properties of the analogous single fluid heat transfer problem (see § 2.4) described by Gill (1966) do not hold for the solutions of the present system.

In addition to the simply nondimensionalized coordinates:

$$x = x_*/b, y = y_*/b \quad \text{and} \quad z = z_*/b; \tag{2.73}$$

the a normalized set

$$X = x_*/b, Y = y_*/b\mathcal{A} \quad \text{and} \quad Z = z_*/b\mathcal{S} \tag{2.74}$$

is also useful. The transformation from primitive to normalized coordinates, in which the cuboid becomes a unit cube, is illustrated in figure 2.1. The normalized coordinates have the advantage of having a unit range. The apparent disadvan-

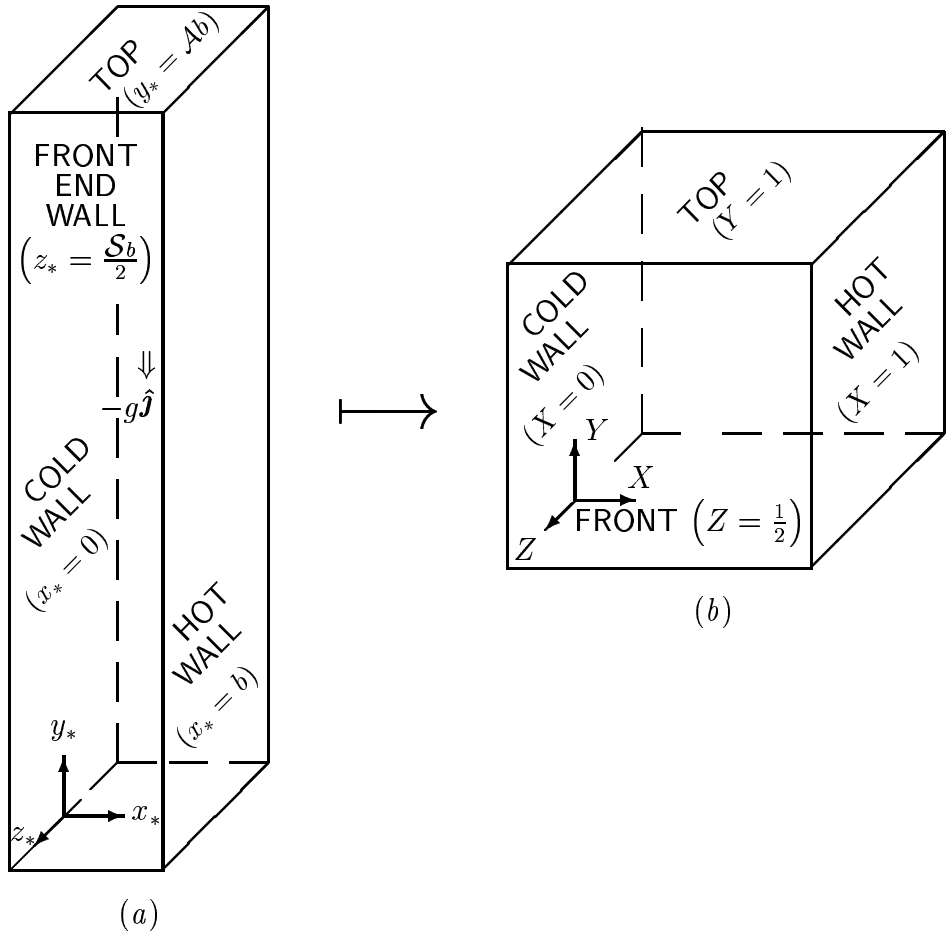

Figure 2.1: Cuboid domain geometry, in (a) primitive and (b) normalized coordinates. The gravitational field strength is also shown in (a).

tage that the expression for nabla in terms of them is more cumbersome;

$$\boldsymbol{\nabla} = \frac{\partial}{\partial x}\hat{\boldsymbol{\imath}} + \frac{\partial}{\partial y}\hat{\boldsymbol{\jmath}} + \frac{\partial}{\partial z}\hat{\boldsymbol{k}} = \frac{\partial}{\partial X}\hat{\boldsymbol{\imath}} + \frac{1}{\mathcal{A}}\frac{\partial}{\partial Y}\hat{\boldsymbol{\jmath}} + \frac{1}{\mathcal{S}}\frac{\partial}{\partial Z}\hat{\boldsymbol{k}}; \tag{2.75}$$

is in fact also an advantage, since it moves the parameters $\mathcal{A}$ and $\mathcal{S}$ from the boundary conditions to the field equations. Great use will be made of this in examining limiting forms of the cuboid in chapters 4 and 7.

2.6 Some properties of the equations

2.6.1 Extrema of advected scalars

That no temperature field, being a solution of the steady-state energy equation (2.55), can possess a strong relative maximum or minimum at an interior point of its domain of existence follows from the essential elliptic nature of the equation and the absence of sources or sinks.

Theorem 1 (Nonexistence of extrema of advected scalars) *If a scalar field, s, is a regular solution of the steady-state advection–diffusion equation*

$$\boldsymbol{\nabla} \cdot [-\mathsf{A} \cdot \boldsymbol{\nabla} s + \sum_{i=1}^{N} h_{(i)}(s)\mathbf{v}_{(i)}] = 0 \tag{2.76}$$

in some domain for some scalar functions $h_{(i)}$, solendoidal vector fields, $\mathbf{v}_{(i)}$, and symmetric, positive definite tensor field, A; all continuously differentiable; then there are no interior strong relative extrema of s.

Proof: The idea for this proof, suggested by Prof. Bob Street (1999, pers. comm., 4 Feb.), is to recast the equation in quasilinear elliptic form, for which the result is known.

Carrying out the divergence,

$$\mathsf{A}\!:\!\boldsymbol{\nabla}(\boldsymbol{\nabla} s) + (\boldsymbol{\nabla} \cdot \mathsf{A}) \cdot \boldsymbol{\nabla} s - \sum_{i=1}^{N} \mathbf{v}_{(i)} \cdot h'_{(i)}(s)\boldsymbol{\nabla} s = 0 \tag{2.77}$$

or

$$\mathsf{A}\!:\!\boldsymbol{\nabla}(\boldsymbol{\nabla} s) + \mathbf{v} \cdot \boldsymbol{\nabla} s = 0 \tag{2.78}$$

where

$$\mathbf{v} \equiv \boldsymbol{\nabla} \cdot \mathsf{A} - \sum_{i=1}^{N} h'_{(i)}(s)\mathbf{v}_{(i)}. \tag{2.79}$$

In Cartesian tensor notation with the summation convention in force, this is

$$A_{jk}s_{,jk} + v_j s_{,j} = 0, \tag{2.80}$$

which is of the form for which Hopf's Maximum Principle is shown to hold in treatises on partial differential equations (Courant & Hilbert 1962, pp. 320–8; Garabedian 1964, pp. 227–38). □

Alternative Proof: I offer here an original and quite different proof which I hope, by avoiding the artifice of a comparison function and using vectorial concepts rather than a general calculus of several variables, is more conducive to physical intuition. The use of vectors also ensures that the result is not tied to any particular coordinate system. The reader uncomfortable with a tensorial diffusivity may replace $\mathsf{A} \cdot \boldsymbol{\nabla} s$ by $A\boldsymbol{\nabla} s$ wherever it appears; this is the special case of isotropy.

The proof is by contradiction: assume that there does exist an interior relative extremum. For definiteness, and without loss of generality, take this to be a minimum.

Construct a family of rays originating at the minimum and terminating when they encounter either:

(i) a boundary point of the domain; or

(ii) a stationary point, with respect to the ray, of s; i.e. $\hat{\boldsymbol{r}} \cdot \boldsymbol{\nabla} s = 0$, where $\hat{\boldsymbol{r}}$ is the unit radial vector from the minimum.

Except at the origin, and possibly the rays' termini, s is strictly increasing along the rays:

$$\hat{\boldsymbol{r}} \cdot \boldsymbol{\nabla} s > 0, \tag{2.81}$$

by the definitions of a minimum and the rays (ii). Choose a value s_1 of s between that at the minimum and the least of those at the rays' termini. Let S be the set of points with $s = s_1$ passed through by the rays.

Each ray intersects S exactly once, and, since s possesses at least two continuous spatial derivatives (Gresho 1988), S is closed and smooth enough to have a well-defined unit outward normal, $\hat{\boldsymbol{n}}$. No ray is tangent to S, since then the ray should have terminated, by (ii); thus,

$$\hat{\boldsymbol{r}} \cdot \hat{\boldsymbol{n}} > 0. \tag{2.82}$$

Now, by definition of the vector triple product,

$$\hat{\boldsymbol{r}} \times (\hat{\boldsymbol{n}} \times \boldsymbol{\nabla} s) = (\hat{\boldsymbol{r}} \cdot \boldsymbol{\nabla} s)\hat{\boldsymbol{n}} - (\hat{\boldsymbol{r}} \cdot \hat{\boldsymbol{n}})\boldsymbol{\nabla} s, \tag{2.83}$$

but $\hat{\boldsymbol{n}} \times \boldsymbol{\nabla} s = 0$, since the normal of a level surface is parallel to the gradient; therefore,

$$\hat{\boldsymbol{n}} \cdot (\mathsf{A} \cdot \boldsymbol{\nabla} s) = \frac{(\hat{\boldsymbol{r}} \cdot \hat{\boldsymbol{n}})}{(\hat{\boldsymbol{r}} \cdot \boldsymbol{\nabla} s)} \boldsymbol{\nabla} s \cdot (\mathsf{A} \cdot \boldsymbol{\nabla} s) > 0 \tag{2.84}$$

by (2.81), (2.82) and since A is positive definite.

Integrate the steady-state advection–diffusion equation (2.76) over the volume V enclosed by S:

$$\iiint_V \boldsymbol{\nabla} \cdot \left[-\mathsf{A} \cdot \boldsymbol{\nabla} s + \sum_{i=1}^{N} h_{(i)}(s) \mathbf{v}_{(i)} \right] \mathrm{d}V. \tag{2.85}$$

Applying the divergence theorem gives:

$$\sum_{i=1}^{N} \iint_S \hat{\boldsymbol{n}} \cdot h_{(i)}(s) \mathbf{v}_{(i)} \, \mathrm{d}S = \iint_S \hat{\boldsymbol{n}} \cdot \mathsf{A} \cdot \boldsymbol{\nabla} s \, \mathrm{d}S, \tag{2.86}$$

of which the right hand side is positive by (2.84). The left hand side, however, vanishes;

$$\begin{aligned} \iint_S \hat{\boldsymbol{n}} \cdot h_{(i)}(s) \mathbf{v}_{(i)} \, \mathrm{d}S &= h_{(i)}(s_1) \iint_S \hat{\boldsymbol{n}} \cdot \mathbf{v}_{(i)} \, \mathrm{d}S & (2.87) \\ &= h_{(i)}(s_1) \iiint_V \boldsymbol{\nabla} \cdot \mathbf{v}_{(i)} \, \mathrm{d}V = 0; & (2.88) \end{aligned}$$

by virtue of the hypotheses on the $\mathbf{v}_{(i)}$.

This is a contradiction, so that the theorem is proved. □

Notes:

- There would always be a net diffusion through a closed level surface surrounding a strong relative extremum, but the net advection would vanish.

- The application to the multicomponent energy equation is clear (cf. Bird et al. 1960, pp. 561–6). The variables s, A, $h_{(i)}$ and $\mathbf{v}_{(i)}$ are the temperature, (tensor) conductivity, partial specific enthalpies and absolute species fluxes, respectively. The required assumption is that the partial specific enthalpies are independent of pressure and composition.

- Often, as in this project, the diffusivity is isotropic; i.e. a product of a (positive) scalar field and the Kronecker delta; and so is symmetric and positive definite, as required.

- The diffusivity and velocities can depend on s, so that the equation is only quasilinear. In the proof, s is assumed given, so that A and the $\mathbf{v}_{(i)}$ can be re-expressed as functions of position.

- Completely analogous theorems hold in one and two dimensions.

- In the special case $\mathbf{v}_{(i)} = \mathbf{0}$ and $A_{ij} = A\delta_{ij}$, where A is a constant, the steady-state advection–diffusion equation (2.76) reduces to Laplace's equation, for which the corresponding result is classical (Lamb 1932, p. 39).

- The species (2.53) and energy (2.55) equations both fall under the hypotheses of the theorem.

  - For (2.53), take $s = m$, $A_{ij} = \delta_{ij}$, $N = 1$, $h_{(1)}(m) = Sc\ m$ and $\mathbf{v}_{(1)} = Gr(1+N)\ \mathbf{u}$. The hypothesis on $\mathbf{v}_{(1)}$ follows from (2.52).
  - For (2.55), take $s = T$, $A_{ij} = \delta_{ij}$, $N = 2$ and

$$h_{(1)}(T) = Pr_r T, \tag{2.89}$$

$$\mathbf{v}_{(1)} = Gr(1+N)\ \mathbf{u}, \tag{2.90}$$

$$h_{(2)}(T) = \frac{Pr_r}{Sc}\left(1 - \mathrm{e}^{-\Phi}\right) T, \quad \text{and} \tag{2.91}$$

$$\mathbf{v}_{(2)} = Gr(1+N)Sc\; m\; \mathbf{u} - \boldsymbol{\nabla} m. \tag{2.92}$$

The hypotheses on the $\mathbf{v}_{(i)}$ follow from the equations of continuity of the mixture (2.52) and the vapour (2.53).

- Thus, no extrema of vapour mass fraction or temperature are expected in the solutions of our system of equations (2.52)–(2.55), and one can conclude that the temperature minimum discovered by Weaver & Viskanta (1991*a*; referred to in § 2.1.3) was erroneous.

- Extrema might occur if there were source or sink terms in the equations, such as if the vapour condensed in the domain; the Dufour effect were appreciable; or there were viscous heating.

- Extrema are of course possible in transient advection–diffusion, as for example they may be specified as part of the initial conditions. I leave unanswered the question of whether strong local extrema can arise in the evolution of a scalar field; this was predicted in the two-dimensional numerical solutions of Bergman and Hyun (1996) for the mass fraction of tin in a nonisothermal amalgam with lead.

2.6.2 The nonexistence of hydrostatic solutions

One of the most interesting problems in natural convection is whether or not buoyancy forces lead to flow. In addition to much work on the analogous single fluid heat transfer problem (see, for example, Busse 1978; Chandrasekhar 1981, ch. 2), there have been studies on isothermal (Sparrow et al. 1985; Suehrcke & Harris 1995; Suehrcke et al. 1996) and heated (Olson & Rosenberger 1979; Abernathy & Rosenberger 1981) gas–vapour mixtures. A still greater variety of phenomena is displayed by liquid mixtures, for which the Schmidt number is

typically much larger than the Prandtl number (Turner 1973, pp. 251–9; 1974, 1985; Griffiths, R. W. 1979).

In contrast to these studies, where the imposed density gradient is typically parallel or antiparallel to the gravitational field, the above (§ 2.5) compositional and thermal boundary conditions mean that they are perpendicular. This always leads to flow; i.e. $\mathbf{u} \not\equiv \mathbf{0}$.

Taking the curl of the equation of motion (2.54) and setting the velocity to zero gives:

$$\mathbf{0} = -\hat{\boldsymbol{\jmath}} \times \frac{\boldsymbol{\nabla}(T + Nm)}{1 + N}, \tag{2.93}$$

which implies that $(T + Nm)$ depends only on y (Gershuni & Zhukhovitskii 1976, p. 6). This is only consistent with the boundary conditions described in § 2.5 if $N = -1$ and $T \equiv m$. The scheme of nondimensionalization (2.27) breaks down in this case, as $\mathbf{u}$ must be unbounded if $\mathbf{u}_*$ is nonzero. The possibility of hydrostatic solutions is a mathematically correct deduction from $N = -1$ and the equation of motion, but not a physical possibility. Flows at $N = -1$ were numerically calculated by Mahajan and Angirasa (1993) for free convection from a semi-infinite vertical plate.

To see how there can be a flow at $N = -1$, consider the vapour transport analog of Patterson and Imberger's (1980) cavity suddenly heated from the side. The fluid is initially isothermal and uniform, and then the temperature and vapour mass fraction at one vertical wall are suddenly raised and lowered, respectively. The different diffusivities of temperature and species, inversely proportional to the Prandtl and Schmidt numbers, respectively, mean that the thermal and solutal disturbances propagate at different rates (conduction and diffusion must precede convection). Assume, for definiteness, properties appropriate for air–water vapour: $Pr > Sc$ and $\zeta > 0$. After a short time, the layer of desiccated air will be thicker than the layer of heated air, and the concentration gradients less than the temperature gradients. The outer isothermal desiccated air will be heavier than the still uniform air, further out, and so it will begin to fall. The inner

heated desiccated air will be somewhat buoyed up by the thermal expansion and so fall less slowly (or even rise if the Prandtl number is sufficiently greater than the Schmidt number). There is, therefore, a nonzero flow, even though $N = -1$. The establishment of a nonzero steady flow from this initial condition is probably not impossible. Numerical solutions of this problem were obtained by Lin et al. (1990; reviewed in § 3.3.11), but not for $N = -1$. The stability of the hydrostatic solution at $N = -1$ was considered by Gobin and Bennacer (1994) for zero mass transfer rate factor; though their problem seems rather artificial, since surely non-Boussinesq effects (property variations) or imperfections in the boundary conditions would prevent the required perfect balancing of the opposing buoyancy forces.

Hydrostatic solutions can be completely ruled out when the mass transfer rate factor, Φ, is finite. The transpiration boundary condition (2.59) would require the normal derivative of m to vanish at the mass transfer interfaces. If the domain's boundary consists of mass transfer interfaces and impermeable surfaces, then a hydrostatic solution would require that $\hat{\boldsymbol{n}} \cdot \boldsymbol{\nabla} m = 0$ everywhere on the boundary. Further, when $\mathbf{u} \equiv \mathbf{0}$, the species equation (2.53) reduces to Laplace's equation. It is well known that the only harmonic functions whose normal derivatives vanish over the entire boundary of a domain are constants (Lamb 1932, p. 41). This is clearly inconsistent with the imposed mass fraction difference, $\Delta m_* \neq 0$, so that hydrostatic solutions are indeed impossible.

This is to be contrasted with the situation for infinite horizontal layers (Pellew & Southwell 1940), or closed cylinders (Charlson & Sani 1970, 1971) filled with single fluids, or impermeable enclosures filled with gas–vapour mixtures (Olson & Rosenberger 1979; Abernathy & Rosenberger 1981) where there do exist hydrostatic solutions for all values of $Gr(1 + N)$, if the imposed temperature gradient is vertical.

2.6.3 An invariance property

It should be expected on physical grounds that the system is invariant in some sense if the 'cold' and 'hot' walls are renamed; i.e. if one looks at the same cuboid from behind.

This is most easily seen if the governing equations are expressed in tensor form. For definiteness, consider uniform vapour mass fraction and temperature on the cold and hot walls and let the other four walls of the cuboid be perfectly conducting and impermeable. As usual, all walls are assumed to be non-slip. With the contravariant coordinates $(x^1, x^2, x^3) = (x, y, z)$, (2.52)–(2.55) can be rewritten:

$$u^i_{,i} = 0; \tag{2.94}$$

$$Gr(1+N)Sc\ u^i m_{,i} = \gamma^{ij} m_{,ij} \tag{2.95}$$

$$Gr(1+N)\ u^j u^i_{,j} + \mathcal{A}\gamma^{ij} p_{,j} - \frac{T+Nm}{1+N}\gamma^{ij} x^2_{,j} = \gamma^{jk} u^i_{,jk}; \tag{2.96}$$

$$Gr(1+N)\left[Pr_r + Pr_I\left(1-\mathrm{e}^{-\Phi}\right)m\right] u^i T_{,i} - \frac{Pr_I}{Sc}\left(1-\mathrm{e}^{-\Phi}\right)\gamma^{ij} T_{,i} m_{,j} = \gamma^{ij} T_{,ij}; \tag{2.97}$$

where subscripts and superscripts refer to covariant and contravariant components, respectively, and subscripts following a comma indicate covariant differentiation. Summation over indices appearing in both upper and lower positions in a term is understood. (See, for example, Aris 1989, ch. 7, for a summary of tensor calculus).

The inhomogeneous boundary conditions are:

$$m = T = x^1 \tag{2.98}$$

$$x^1_{,i} u^i = \frac{1-\mathrm{e}^{-\Phi}}{Gr(1+N)Sc\left[\left(1-\mathrm{e}^{-\Phi}\right)m - 1\right]}\gamma^{ij} x^1_{,i} m_{,j} \tag{2.99}$$

at $x^1 = 0, 1$ and

$$T = x^1 \tag{2.100}$$

on the other four walls.

The components of the metric tensor, γ_{ij}, are unity on the diagonal and zero otherwise for this coordinate system; therefore, since γ^{ij} denotes the ij^{th} element of the inverse of the matrix of γ_{ij},

$$\gamma^{11} = \gamma^{22} = \gamma^{33} = 1 \tag{2.101}$$

and

$$\gamma^{ij} = 0 \qquad (i \neq j). \tag{2.102}$$

The transformation discussed above is:

$$(\tilde{x}^1, \tilde{x}^2, \tilde{x}^3) = (1 - x^1, x^2, -x^3), \tag{2.103}$$

which leaves the metric tensor unchanged, since it is only a rigid rotation and translation of the coordinate axes.

The solution to the new system in terms of the solution of the old system is

$$\tilde{u}^i = -u^i \tag{2.104}$$

$$\tilde{p} = x^2/\mathcal{A} - p \tag{2.105}$$

$$\tilde{T} = 1 - T \tag{2.106}$$

$$\tilde{m} = 1 - m \tag{2.107}$$

if

$$\tilde{Gr} = -Gr \tag{2.108}$$

$$\tilde{N} = N \tag{2.109}$$

$$\tilde{Sc} = Sc \tag{2.110}$$

$$\tilde{\Phi} = -\Phi \tag{2.111}$$

$$\tilde{Pr}_r = Pr_r + Pr_I \left(1 - \mathrm{e}^{-\Phi}\right) \tag{2.112}$$

$$\tilde{Pr}_I = -Pr_I \frac{1 - \mathrm{e}^{-\Phi}}{1 - \mathrm{e}^{\Phi}} \tag{2.113}$$

$$\tilde{\Lambda} = -1 - \Lambda, \tag{2.114}$$

which agrees with the result that would be deduced by transforming the parameters according to their definitions in terms of the physical properties and boundary conditions.

The Sherwood and Nusselt numbers are given by

$$Sh = -\frac{Gr(1+N)}{\Phi}x^1_{,j}u^j = \frac{1-\mathrm{e}^{-\Phi}}{\Phi\left[1-m\left(1-\mathrm{e}^{-\Phi}\right)\right]}\gamma^{ij}x^1_{,j}m_{,i} \tag{2.115}$$

$$Nu = \frac{1-\mathrm{e}^{-\Phi_T}}{\Phi_T}\left[\gamma^{ij}x^1_{,j}T_{,i} + (T+\Lambda)\Phi_T Sh\right] \tag{2.116}$$

so that

$$\tilde{Sh} = Sh \tag{2.117}$$

$$\tilde{Nu} = \mathrm{e}^{-\Phi_T}Nu. \tag{2.118}$$

The Nusselt number does not transform as simply as the Sherwood number as the driving force for energy transfer, unlike that for mass transfer, cannot be written in terms of a function of a single property at the boundaries; energy transfer is driven by both the temperature difference and the mass transfer. If ΔT_* had been taken as the driving force for energy, then the 'Nusselt number'

$$\left.\frac{-\hat{\boldsymbol{\imath}}\cdot\mathbf{e}_* b}{\lambda\Delta T_*}\right|_{x^1=0,1} \tag{2.119}$$

would be an invariant of the transformation, like the Sherwood number. As will be seen in chapters 4–6, however, this would lead to the value of the Nusselt number depending more strongly on the thermal mass transfer rate factor, Φ_T.

When $\Phi = 0$, the transformation of the parameters simplifies to

$$\tilde{\Phi} = -\Phi = 0 \tag{2.120}$$

$$\tilde{Pr}_r = Pr_r \tag{2.121}$$

and $\tilde{Pr}_I = -Pr_I$, although the interdiffusion Prandtl number is then irrelevant. In this case, both the Sherwood and Nusselt numbers are invariants of the transformation.

The significance of the present findings lies in what they reveal about the symmetry of the Sherwood and Nusselt numbers with respect to the parameters of the problem. This should be exploited when constructing the functional form of correlations, for example. An instance of this will be found in § 8.2.10, when the

behaviour of the system at low Grashof number is examined. Also, the simplicity of the symmetry of Sh with respect to Φ is one advantage of using Φ as the parameter representing finite mass transfer effects; this becomes important when considering a rational approximation for the system at low mass transfer rates (ch. 6, see especially §,6.2.2).

Chapter 3

Literature Review

The present work is deeply indebted to the fundamental expositions of mass transfer by Colburn and Drew (1937), Bird et al. (1960), and Spalding (1960, 1963). Their influences will be noticed throughout. More recent fundamental research into vapour transport has been conducted by Rosenberger and coworkers (Olson & Rosenberger 1979*b*; Markham & Rosenberger 1980; Abernathy & Rosenberger 1981; Greenwell et al. 1981; Jhaveri et al. 1981; Jhaveri & Rosenberger 1982; Rosenberger & Müller 1983; Rosenberger et al. 1997), which will be examined more closely in §§ 3.2.3, 3.2.4, 3.3.3, 3.3.4 and 3.3.18.

The numerous parallels between the present problem and the analogous single fluid heat transfer problem (§ 2.4) mean that the large body of literature surrounding the latter has had great bearing, but it is too extensive to review here. Three recent reviews were listed in § 2.4. The work of Jones and Furry (1946), Batchelor (1954), Ostroumov (1958) and Daniels (1985; Daniels & Wang 1994) on narrow cavities and of Mallinson and de Vahl Davis (1973, 1977; de Vahl Davis 1998) on three-dimensional effects deserves particular mention. Other references will be found in most sections of this thesis.

3.1 Free convection vapour transport

The transport of vapour between a surface and an unbounded gaseous phase has been studied by many investigators. Much of the theoretical work has focused on semi-infinite vertical plates and used similarity or Pohlhausen integral techniques (Somers 1956; Mathers, Madden & Piret 1957; Wilcox 1961; Acrivos 1962; Gill, W. N., del Casal & Zeh 1965, Adams & Lowell 1968; Saville & Churchill 1970; Taunton, Lightfoot and Stewart 1970; Gebhart & Pera 1971; Bottemanne 1972*a*; Schenk, Altmann & DeWit 1976; Nilson & Baer 1982; Boyadjiev & Halatchev 1998; Halatchev & Boyadjiev 1998). Numerical solutions of the 'boundary layer' equations were obtained by Callahan and Marner (1976), for the evolution problem for a semi-infinite plate subjected to a step change in temperature and vapour mass fraction, and Mahajan and Angirasa (1993), for combinations of the parameter values that did not allow similarity solutions. Bejan (1985; § 3.3.5) used scale analysis to obtain the functional forms of the Sherwood and Nusselt numbers for various limiting cases. Perhaps the earliest theoretical work is that of Schmidt (1929), who derived approximate results from those for the analogous single fluid heat transfer problem. Experiments have been performed by Schmidt (1929), Adams & McFadden (1966), Bottemanne (1972*b*) and Mathers et al. (1957).

In the problems considered in the present project, the domains of influence of the various surfaces of the enclosures overlap, so that the results of these studies of free convection are not directly applicable. Many of the difficulties of formulating the governing equations, however, are common.

Few of the above investigations included finite mass transfer rate effects ($\Phi \neq 0$). Somers (1956) and Adams and Lowell (1968) did include transpiration, but not interdiffusion, which is not a generally appropriate approximation (§§ 2.3.2, 4.4, 6.3). W. N. Gill et al. (1966) included both transpiration and interdiffusion, but only allowed variation of the mixture specific heat capacity in some problems. This is inconsistent (see p. 20).

Another common problem of free convection and convection in enclosures is how to combine the buoyancy forces in correlating the results. Schmidt (1929) assumed that they were simply additive, i.e. he used a combined Grashof number similar to $Gr(1+N)$, and demonstrated the appropriateness of this for the special case $\Phi = 0, Pr_r = Sc$. Somers (1956) predicted a more complicated relation in which the buoyancy ratio, N, should be multiplied by $(Pr_r/Sc)^{1/2}$. Neither of these two approaches is generally correct. Their relative merits were much debated in the cited literature (see especially Gebhart & Pera 1971). Schmidt's idea is implicit in the velocity scale employed in (2.27), but it is not relied upon to remove N as an independent parameter. I did find, however, that N could be neglected for plane vertical square cavities for $10^4 \leq Gr(1+N) \leq 2 \times 10^5$ and properties appropriate for air–water vapour mixtures (McBain 1995, 1997*b*; § 3.3.16). Difficulties do occur, however, for other Schmidt and Prandtl numbers (§ 3.3.15).

Free convection vapour transport has been reviewed in more detail by Ostrach (1980) and Gebhart et al. (1988, ch. 6).

3.2 The Stefan diffusion tube

In order to measure the diffusivity of a gas–vapour mixture, vapour transport must be set up in a configuration for which the governing equations admit an exact solution. Unfortunately, no such configurations are known. A popular configuration is the Stefan diffusion tube, in which a small amount of volatile liquid is placed in an open vertical cylinder and a gas stream of known vapour content is blown across the top. If the vapour transport is assumed to be isothermal, one-dimensional and quasistationary, and the gas stream is assumed not to disturb the gas–vapour mixture in the tube, the governing equations are soluble (Bird et al. 1960, pp. 522–7; § 4.4).

Ampoules similar to Stefan diffusion tubes have also been used for the growth of crystals from their vapours (Markham & Rosenberger 1980).

3.2.1 The no-slip condition

Unfortunately, the one-dimensional assumption violates the no-slip condition at the cylinder walls if $\Phi \neq 0$ (Lee, C. Y. & Wilke 1954).

C. Y. Lee and Wilke (1954) suggested that the flow would be unidirectional with a parabolic profile, as for fully developed pressure-driven flow (§ 7.5.1). This assumption was adopted by Heinzelmann, Wasan & Wilke (1965) and S. S. Rao and Bennett (1966) in their attempts to establish whether m and Sh varied radially.

While the velocity profile is probably parabolic for much of the length of the tube if $\Phi << 1$ (Markham & Rosenberger 1980; § 3.2.3), this procedure is somewhat problematic. If the velocity field is regarded as given, the species equation (2.53) can be solved independently, but the problem is overconstrained. The vapour mass fraction is known or assumed at both ends of the tube, but the normal component of the vapour mass fraction gradient there can be calculated from the transpiration boundary condition (2.59). The species equation is second order in each spatial direction, including the axial direction of the tube, but four boundary conditions have been imposed on the vapour mass fraction. If no boundary conditions at the mouth were assumed, the problem would not be overconstrained but it would be ill-posed. The species equation is elliptic and therefore its solution would not depend continuously on the given value of the function and its normal gradient at the liquid interface (Courant & Hilbert 1962, pp. 216, 227; Garabedian 1964, p. 484). An arbitrarily small variation in the given data would change the solution greatly. Such data only lead to correctly set problems for hyperbolic equations (Hadamard 1952, pp. 37–9). While ill-posed problems are not necessarily devoid of physical meaning (Courant & Hilbert 1962, pp. 230–1; see the papers in the collection edited by Hämmerlin & Hoffmann 1983 for counterexamples), this is the case for the present problem. The physical interpretation is simple: it would be impossible to simultaneously fix both the velocity and the vapour mass fraction at the interface; even if a gas–vapour mixture from a source

of known composition were injected through a surface, the composition at the interface would be affected by diffusion. In conclusion, though the transpiration condition relates the normal component of velocity and the normal component of the gradient of the mass fraction field, it must be regarded as a boundary condition on the velocity if the vapour mass fraction is independently known, e.g. by the requirement of thermodynamic equilibrium with the neighbouring condensed phase. The interfacial velocity must be determined as part of the solution.

Whitaker (1967) attempted to dispel the entire problem by asserting that 'the traditional no-slip condition is not valid for that motion occurring because of concentration gradients'. S. S. Rao and Bennett (1967) countered this by citing independent experimental evidence that slip only occurs in diffusion-induced flows at lower pressures and in smaller tubes than those relevant to the Stefan diffusion tube (or the present project). Wasan (1967) responded to Whitaker by stating that the assumption of no-slip did indeed violate the conservation of species but that the flow rate in the tube was almost identical for the two extreme cases of plug and parabolic flow profiles. Wasan's first contention is incorrect: the no-slip condition is only inconsistent with the conservation of species and a finite mass transfer rate if the gas is assumed to be stationary; a simple assumption, but one with no physical basis.

The effect of the no-slip condition in the Stefan diffusion tube was later studied in more detail by Meyer and Kostin (1975), Markham and Rosenberger (1980), and Greenwell, Markham and Rosenberger (1981), as reviewed in §§ 3.2.2 – 3.2.4.

3.2.2 Meyer and Kostin (1975)

Meyer and Kostin (1975) considered a system similar to the Stefan diffusion tube, except that it was two-dimensional (planar). They formulated an approximate model and solved the resulting equations numerically.

Their model omits the inertial terms from the equation of motion, which is inconsistent with the inclusion of the advective terms in the species equation, since

the ratio of the magnitudes of these is obviously the reciprocal of the Schmidt number, which is of order unity for most gas–vapour mixtures.

The correct approach would have been an asymptotic expansion for small values of Φ. The velocity vanishes in the limit $\Phi \to 0$. The zeroth order approximation for the species would then be Laplace's equation, with the simple solution that m would be a linear function of the height above the liquid surface. This could then be used to calculate the boundary conditions for the first order velocity correction, leading to a Stokes problem with uniform inflow and outflow at the vapour source and sink. The resulting velocity field can be used in an advection–diffusion equation for the first order correction to the vapour mass fraction field, and so forth. At each stage the velocity and vapour mass fraction fields are uncoupled. Each correction to the vapour mass fraction influences the boundary conditions for the next correction to the velocity field, and each correction to the velocity field enters into the advection terms in the equation for the next correction to the vapour mass fraction.

Nevertheless, their conclusion that nonzero values of the mass transfer rate factor, Φ, must lead to circulation of the gas is correct: in 1967, Whitaker showed that a stagnant gas (i.e. $\rho\mathbf{u}_* \equiv \mathbf{n}_*$) is not consistent with the presence of nonslip boundaries joining the vapour source and sink. The circulation was confirmed by the rigorous numerical solutions of Markham and Rosenberger (1980; reviewed in § 3.2.3).

There is also some confusion in Meyer and Kostin's use of both mass and molar quantities. Their expressions for the molar fluxes contain the mass average velocity, whereas they should use the molar average velocity (see Bird et al. 1960, pp. 496–502 for consistent formulations). Gross error is avoided, however, since both the total density and the total molar concentration are assumed uniform. This is equivalent to an assumption of equal molar masses. If the molar masses of the stagnant and diffusing species are equal, mass fractions and mole fractions are identical and very little is gained from this mixed formulation.

It would seem that in any vapour transport problem except for the most hydrodynamically trivial, such as one-dimensional Stefan diffusion (Bird et al. 1960, pp. 522–7), a momentum equation must be solved, which must be formulated in terms of a mass average velocity, as Newton's Law of Viscosity is (Bird et al. 1960, pp. 79–80, 565). The molar fluxes involve the molar average velocity, which can only be simply expressed in terms of the mass average velocity in the special case of equal molar masses. Indeed, 'if the molecular weights... are significantly different, the problem takes on an appalling complexity'; the two average velocities not even being parallel in general (Rao, S. S. & Bennett 1967). It was for these reasons that a consistently mass-based formulation was used in chapter 2. A mass-based formulation was also adopted by Markham and Rosenberger (1980) and Greenwell et al. (1981) who fully accounted for differing molar masses; i.e. did not use the Boussinesq approximation.

3.2.3 Markham and Rosenberger (1980)

Markham and Rosenberger (1980) numerically solved the non-Boussinesq equations for a Stefan diffusion tube with a length equal to five times its diameter, for $\Phi = 0.3, 1$ and 5. For the two lower mass transfer rates, the mass average velocity was found to have an 'entrance length' of 0.5 and 1 tube diameters, respectively. No fully developed region was predicted at the highest mass transfer rate.

Markham and Rosenberger's results confirmed that the gas must circulate in the Stefan diffusion tube; up (parallel to the primary direction of the vapour) along the axis and down near the walls. In their study, the vapour was heavier than the gas, and gravity was included. Although the one-dimensional 'Rayleigh–Bénard' problem is convectively stable, the radial composition variations did lead to buoyancy forces affecting the flow field: the mass average velocity was reduced, most markedly along the axis.

They also pointed out that the greatest deviations from the one-dimensional solution must be expected at intermediate values of the mass transfer rate fac-

tor, a quantity which they called the 'Peclet number' (which is an appropriate name for it in this problem). At low mass transfer rates, diffusion reduces radial concentration gradients, while at very high mass transfer rates, viscous effects should be confined to thin layers near the walls. The same conclusion applies to buoyancy-effects, except that these could also be more important for shorter or wider tubes.

As far as overall vapour transfer rates are concerned, the error of the one-dimensional prediction was zero to within the accuracy of the numerical solutions (1%).

3.2.4 Greenwell, Markham and Rosenberger (1981)

An interesting and relevant (in the context of § 6.1.3) result from the numerical study by Greenwell et al. (1981) at $\Phi = 0.944$ is that while viscous interaction of the transpiration-induced flow with the nonslip connecting walls was found to cause radial variations in the vapour mass fraction field, the overall mass transfer rate still agreed with the one-dimensional prediction to within the limits of computational accuracy ($\pm 0.5\%$). The Boussinesq assumption was not made. The cylinders considered had lengths from 0.5 to 10 times the radius. Surprisingly, the nonslip connecting walls caused the greatest departures from the one-dimensional behaviour not for long cylinders, but when the length was nearly equal to the radius, or when 'the "redistributing walls" are not too remote from the core of the fluid'.

3.2.5 Buoyancy effects

Bird et al. (1960, p. 527) assumed that buoyancy forces would only be important if the vapour was lighter than the gas ($\zeta > 0$). This follows from the one-dimensional assumption (§ 2.6.2). If, however, the no-slip condition gives rise to radial concentration gradients at finite mass transfer rates, then buoyancy forces will always affect the velocity and vapour flux fields (Markham & Rosenberger

1980; § 3.2.3).

For a light vapour, questions of convective stability are foremost. C. Y. Lee and Wilke (1954) pointed out that convection could be eliminated by making the tube thin enough. Sparrow and coworkers (Sparrow, Nunez & Prata 1985; Nũnez-Testa 1986; Nunez and Sparrow 1988; Sparrow and Nunez 1988) studied the postcritical flow under the assumption of axisymmetry. Suehrcke and Harris (1995; Suehrcke, Harris & McBain 1996) investigated the transition criterion under the same restriction. It has recently been shown that the least stable modes for such a system are not axisymmetric, and that the assumption of axisymmetry leads to an estimate of the critical density gradient (Rayleigh number) that is seven times too high (McBain, Suehrcke and Harris, in press).

3.2.6 Conclusions

The transpiration boundary condition (2.59) is essential to the analysis of the Stefan diffusion tube, and is used in all the cited studies; several of them also give derivations.

Although many questions have been raised about the validity of the use of the Stefan diffusion tube for the determination of diffusivity coefficients, the results obtained are probably of acceptable accuracy, since, as is easily shown, the evaporation rate predicted by the one-dimensional analysis is asymptotically correct to $O(1)$ as $\Phi \to 0$, and most experiments occur with very low values of Φ. To the best of my knowledge, no upper bound has been placed on the errors caused by finite values of Φ, though given the symmetry property derived in § 2.6.3, it should be at most $O(\Phi^2)$ for the overall Sherwood number.

The Stefan diffusion tube is a classical vapour transport problem, and embodies many of the physical phenomena of the present problem. As such, the literature surrounding it has been very useful.

3.3 Gas-filled enclosures

While the Stefan diffusion tube can be regarded as a special case of a gas-filled enclosure, here I consider works involving horizontal vapour transport in a gravitational field.

3.3.1 Klosse and Ullersma (1973)

Klosse and Ullersma (1973) were the first to attempt an analytical description of the nonisothermal vapour transport across a gas-filled enclosure. They considered the limit $\mathcal{A} \to 0$ for plane ($\mathcal{S} \to 0$) vertical rectangular cavities. Their method was somewhat irrational, however, and was thoroughly criticized by Jhaveri and Rosenberger (1982; § 3.3.4). For example, they assumed that the temperature would depend only on x, on account of the small value of $\mathcal{A}$. This is correct (Cormack, Leal & Imberger 1974), but would equally imply $m \sim x$, so that only a trivial mass transfer result would be obtained. Further, like Meyer and Kostin (1975; see comments in § 3.2.2), they omitted the inertial terms from the equation of motion but retained the advective component of the vapour flux.

3.3.2 Hu and El-Wakil (1974)

Hu and El-Wakil (1974) performed a series of experiments on the nonisothermal vapour transport across cuboids. In order to create a uniform vapour mass fraction at the hot wall, they forced liquid through a slot cut in the top of it. This caused two deviations from ideality. First, the liquified vapour streaming down the hot and cold walls meant that there was a nonzero tangential velocity at the boundary of the vapour phase. Second, the vapour was saturated at these boundaries.

They did account for the slip velocity at the hot and cold walls in their numerical simulations. They demonstrated that it: 'strongly influences flow, temperature and concentration, causing strong asymmetry in them'; 'may also cause

transition from unicellular to tricellular motion'; and 'enhances the convective contributions, thus the heat and mass transfer rates'.

While the saturated boundary conditions would have meant that the vapour was saturated in at least part of the interior (Close & Sheridan 1989, fig. 1*b*; McBain 1995, fig. 18; McBain, Harris, Close & Suehrcke 1998, fig. 4), they ignored the possibility of internal condensation in their numerical solutions. That the vapour was indeed supersaturated can be concluded from the fact that they had to heat the transparent front and back walls in order to be able to see through them—otherwise they were obscured by condensate!

Their two-dimensional numerical model included transpiration ($\Phi \neq 0$) but excluded interdiffusion ($Pr_I = 0$). This is common to many of the studies reviewed here, but is inconsistent (§§ 2.3.2, 4.4, 6.3).

3.3.3 Jhaveri, Markham and Rosenberger (1981)

A feature of the model derived in chapter 2 is that the velocity boundary condition is singular at the edges where the vapour source or sink meet the nonslip connecting walls. This was the focus of the numerical study of Jhaveri et al. (1981). They studied isothermal systems (i.e. $Gr = 0, N \to \infty$, but $Gr(1+N)$ finite at $100\mathcal{A}^{-3}$) in plane cavities ($\mathcal{S} \to \infty$) ranging from $\mathcal{A} = 0.1$ to $\mathcal{A} = 4$. The Schmidt number was taken as unity.

They investigated the effect of the singularity at the corner by obtaining pairs of solutions, treating the corners as part of either the interface or the solid wall. They found that this had no effect on the vapour mass fraction field or the local Sherwood number, but did influence the velocity field in the vicinity of the corners.

The singularity at the corners is analogous to that found in a lid-driven cavity—see, for example, Mills (1965), Nallasamy and Krishna Prasad (1977), or the *Fastflo* Tutorial Guide (CSIRO 1997, p. 114) for a description of this problem. One problem can be locally converted to the other by the addition to the velocity of a suitable uniform transverse field. The pressure cannot be expected

to be regular near such a corner, even in the viscous limit (Cahouet & Chabard 1988). This difficulty was not discussed by Jhaveri et al., as they reformulated the equation of motion in terms of vorticity and a stream-function, but will become apparent in the numerical solutions of chapter 5.

Of great interest is the run at $\Phi = -0.4$ in the cavity of height $\mathcal{A} = 4$, for which they report, 'the flow is basically one-dimensional except adjacent to the walls'. This is the only prior evidence at finite mass transfer rates of the existence of the *conduction–diffusion regime*, defined and discussed in chapter 5.

3.3.4 Jhaveri and Rosenberger (1982)

Jhaveri and Rosenberger (1982) gave an extensive critique of Klosse and Ullersma's (1973; § 3.3.1) model by comparing it with two-dimensional numerical solutions. Jhaveri and Rosenberger's numerical model is somewhat simplified in that it neglects the contribution of compositional variation to buoyancy ($N = 0$) and omits interdiffusion ($Pr_I = 0$); this is not completely unphysical, in so far as it would occur if the gas and vapour had equal molar masses and partial specific heat capacities, but is generally an inconsistent approximation. As only very shallow cavities were considered ($\mathcal{A} = 1/10, \mathcal{S} = \infty$)—this being one of Klosse and Ullersma's basic assumptions—the results are not directly applicable to any of the specific problems treated in this project.

One relevant feature of the paper is the use of a Sherwood number equivalent to (2.60). Jhaveri and Rosenberger arrived at this normalization of the vapour transport by considering one-dimensional solutions. The same reasoning will be applied here in chapter 4.

3.3.5 Bejan (1985)

Bejan (1985) extended the time-independent part of the scale analysis of Patterson and Imberger (1980) for the analogous single fluid heat transfer problem to binary mixtures. The finite mass transfer rate effects of transpiration and

interdiffusion were neglected ($\Phi \to 0$). The scales for the mean Sherwood and Nusselt numbers are deduced from a simple model of the semi-infinite vertical plate boundary layer. The six possible permutations of Pr_r, Sc and unity in the relation $a \ll b \ll c$ are examined for $N \to 0$ and $N^{-1} \to 0$. Since ν, $\lambda/\rho c_{pr}$ and D are typically of a similar magnitude for gas–vapour mixtures; so that $Pr_r \approx Sc \approx 1$; none of these limiting cases are applicable. They are, however, of theoretical interest, and are important for amalgams and brines, for which $Pr_r \ll 1 \ll Sc$ (Bergman & Hyun 1996) and $1 \ll Pr_r \ll Sc$ (Hyun & Lee 1990), respectively.

Bejan verified his predictions by comparison with numerical solutions for the limiting case $N = 0$ and $Gr \to 0$ with $Pr_r \sim O(1)$ and $Sc^{-1} \sim O(Gr)$ in two-dimensional vertical cavities of height $\mathcal{A} = 1, 2$ and 4. Further tests of the predicted scales were undertaken by Béghein et al. (1992; § 3.3.15).

A result relevant to the consideration of the conduction regime in chapters 4–5 is that the vertical velocity profile at midheight ($y = \mathcal{A}/2$) depended only weakly on $\mathcal{A}$ for $\mathcal{A} \geq 2$.

3.3.6 Keey and Wee (1985)

Keey and Wee (1985) designed an apparatus to test precisely the problem of interest in the present project. Such an apparatus was used in their later experiments (Wee, Keey & Cunningham 1989; § 3.3.10).

The greatest difficulty is the provision of steady uniform vapour mass fractions on the hot and cold walls. Their idea was to construct these walls from sintered nonhygroscopic polymer (high density polythene) beads. The outsides of these walls would be exposed to air vigorously stirred in the presence of saturated salt solutions (the use of saturated salt solutions to control humidity is well known—see, for example, Leopold & Johnston 1927 or Stokes & Robinson 1949). Their preliminary tests showed that the mass transfer 'resistance' of the porous walls was about five times that of the same thickness of stagnant air or about half that

of the quiescent test cavity, although it varied with the imposed mass fraction difference. The humidity boundary conditions so imposed on the cavity would not be known with much accuracy. This turned out to be the case (see § 3.3.10).

The apparatus of Keey and Wee is incapable of measuring the energy transfer associated with condensation and evaporation of the vapour, since the hot and cold walls allow the vapour to pass through without condensing. This is unfortunate, since this may often be the dominant energy transfer mechanism (McBain 1995; McBain, Harris, Close & Suehrcke 1998; Suehrcke & McBain 1998; § 4.5).

3.3.7 Trevisan and Bejan (1987)

Trevisan and Bejan (1987) considered vapour transport across a plane vertical rectangular cavity at low mass transfer rates ($\Phi \to 0$). Uniform flux boundary conditions were imposed at the hot and cold walls. Exact solutions were reported for infinitely tall cavities ($\mathcal{A} \to \infty$) at large combined Grashof numbers, $Gr(1 + N)$, for three limiting cases: $Sc = Pr$; $N = 0$, $Sc \gg Pr$; and $|N| \to \infty$, $Sc \ll Pr$. The first of these is actually not quite exact, in that it assumes that there exists a stagnant stratified core between the boundary layers on the walls, so that the transverse length scale of the flow near the hot and cold walls is much smaller than the breadth of the cavity; it is therefore equivalent to Prandtl's (1952, p. 422; Elder 1965; Gill 1966) solution for heat transfer from a single wall to an unbounded pure fluid. A solution valid across the breadth of the cavity was given independently by Vest and Arpaci (1969) and Aung (1972). The paper also contains numerical solutions for $\mathcal{S} \to 0, 1 \leq \mathcal{A} \leq 4$, $3.5 \times 10^5 \leq GrPr \leq 7 \times 10^6$, $-11 \leq N \leq 9$, $1 \leq (Sc/Pr) \leq 40$ and $Pr = 0.7, 7$.

Trevisan and Bejan offered a simple scaling argument to determine when transpiration could be neglected for $N = 0$ and $Sc \gg Pr \gg 1$. Their result was that this is safe when

$$\Delta m_{*r} \left(\frac{Pr}{Sc}\right)^{1/3} \ll 1. \tag{3.1}$$

This is more or less in agreement with the criterion obtained in chapter 6:

$$\Phi \ll 1, \tag{3.2}$$

since Φ approaches zero as the vapour mass fraction difference does. The inclusion of the Prandtl and Schmidt numbers in the criterion is incorrect, however, since although the transpiration-induced velocities decrease as the Schmidt number increases (2.59), this is balanced by the factor Sc in the advective flux (2.35). The influence of the Prandtl number is complicated by the associated effects of interdiffusion and the variability of the mixture specific heat. This matter is dealt with in more detail in chapter 6, in the light of the solutions including the effects of transpiration generated in chapters 4–5.

3.3.8 Ranganathan and Viskanta (1988)

Ranganathan and Viskanta (1988) reported numerical solutions for plane vertical square cavities. The interdiffusion Prandtl number was set to zero and the Schmidt number was taken equal to the (reference) Prandtl number. The problem is therefore completely analogous to the isothermal mass transfer problem.

There is also some analysis of the effect of transpiration. Solutions for the vapour mass fraction and temperature profiles formally similar to those derived here in the narrow cavity limit ($\mathcal{A} \to \infty$, see § 4.4) are given for two somewhat inappropriate cases, both with $N = -1$: when $Pr_r = Sc$ so that the distributions of temperature and vapour mass fraction are identical (if the boundary conditions are analogous) and the density is uniform; and $\Phi \to -\infty$ for which buoyancy forces are supposed to be overwhelmed by the transpiration-induced flow. The latter is inconsistent with the nonslip boundary conditions at the floor and the ceiling of the cavity, although the Reynolds number would be infinite in this case; $\Phi \to -\infty$ is a singular perturbation problem, with the regions of nonuniformity being the floor and ceiling (see Van Dyke 1964, ch. 7, for a discussion of viscous flow at large Reynolds numbers). They did not present any numerical solutions for large negative mass transfer rate factors to compare with the analysis.

Transpiration is included but the interdiffusion energy flux is neglected which is not particularly consistent (§ 6.3). Since the first requires $\Phi \neq 0$, the second implies $Pr_I \approx 0$. The latter would only make sense if the partial specific heat of the vapour were approximately equal to that of the gas, which is usually not the case (see § 2.3.2). The neglect of interdiffusion led to the absurd result of the one-dimensional energy transfer rate depending on the partial specific heat capacity of the gas (§ 4.4).

3.3.9 Nelson and Wood (1989)

In a brief note, Nelson and Wood (1989) derived the fully developed vapour mass fraction, velocity, pressure and temperature fields for an inclined plane parallel-plate duct. They considered only low mass transfer rates ($\Phi = 0$). Their result is a simple extension of Aung's (1972) for the analogous single fluid heat transfer problem. Their result is extended in chapter 4 to include the effects of transpiration, interdiffusion and the variability of the mixture specific heat.

They also considered constant flux conditions, but only obtained an exact result for $Sc = Pr$, for which the problem is identical to that for a pure fluid. This conclusion was also reached by Trevisan and Bejan (1987; § 3.3.7), whose work they appear to have been unaware of.

3.3.10 Wee, Keey and Cunningham (1989)

The sole experimental study of the unsaturated cavity that I was able to identify is that of Wee et al. (1989)—other studies (Hu & El-Wakil 1974; Weaver & Viskanta 1991*c*; Rosenberger et al. 1997; reviewed in §§ 3.3.2, 3.3.14, 3.3.18) used saturated boundary conditions. Wee et al. dealt with very dilute concentrations of the vapour (less than 750 Pa partial pressure, or 0.5% by mass at 1 atm). In tropical climates, the water vapour mass fraction can be an order of magnitude higher so that the finite mass transfer rate effects of wall interfacial velocity and species interdiffusion may become appreciable. This is because, as evident from

the basic equations of chapter 2 or the narrow cavity limiting solution of chapter 4, these effects depend on the mass transfer rate factor, Φ, which (for fixed vapour mass fraction difference, Δm_*) is an increasing function of the reference vapour mass fraction (see the definition: equation 2.33). Of course, higher temperatures also make larger mass fraction differences possible.

Wee et al. attempted to impose the type of boundary conditions considered in § 2.5: uniform temperature and vapour mass fraction on the hot and cold walls, but had great difficulty with the mass transfer boundary conditions. This was a result of the apparatus they used (Keey & Wee 1985; § 3.3.6). They estimated that, although they were able to measure the vapour transfer rate to within $\pm 1.5\%$, the uncertainty of the mean Sherwood number was up to $\pm 34\%$. As well as the uncertainty of the value of the vapour mass fraction at the hot and cold walls, there was no way of determining its uniformity. An alternative idea for controlling the humidity at the boundary, using semipermeable membranes has been discussed elsewhere (McBain, Close, Suehrcke, Harris & Brandemuehl 1998; Hill 1998).

They also simulated their experiments with plane numerical solutions. The measured quantities were the overall transfer rates. They used Schmidt's (1929; § 3.1) idea of correlating the results with a combined Grashof number based on a simple addition of buoyancy forces, $Gr(1 + N)$. This worked well for both vapour and energy transfer rates; the agreement between experiment and numerical solution being well within the experimental uncertainty. This is another reason for the use of this combined Grashof number in the present work.

Wee et al. also studied cavities with horizontal hot and cold walls.

The vertical cavities considered had $\mathcal{A} = 7$, and so are taller than many of those studied in chapter 5, for which a fully developed region is to be expected sufficiently far from the floor and ceiling, but the combined Grashof numbers employed, $Gr(1 + N) \geq 6 \times 10^4$ were such that $\mathcal{A} = 7$ could not be considered narrow; thus, no runs pertained to the conduction–diffusion regime, as defined in

chapter 5. Instead, thermal and solutal boundary layers formed on the hot and cold walls, and the core was stratified.

Since Wee et al. did not consider the conduction–diffusion regime, high mass transfer rates or three-dimensional effects, their results are not directly comparable with those obtained here. Of course, the test cavity must have had a finite span, $\mathcal{S}b$, but it is not mentioned by Wee et al. or Keey and Wee (1985). The only measured quantities were the overall transfer rates, so it is difficult to say what role the third dimension may have played; the spanwise aspect ratio may well have been sufficiently large for $\mathcal{S}$ not to have affected $\overline{Nu}$ or $\overline{Sh}$. This topic is discussed in more detail in § 7.1.

3.3.11 Lin, Huang and Chang (1990)

Lin, Huang and Chang (1990) reported numerical solutions for the vapour transport analog of the problem posed for a pure fluid by Patterson and Imberger (1980): the evolution of an initially isothermal uniform gas–vapour mixture in a plane vertical rectangular cavity subjected to a step change in the temperature and vapour mass fraction at the hot and/or cold walls. These step changes were not imposed symmetrically, however. Only square cavities were considered ($\mathcal{S} \to 0, \mathcal{A} = 1$). The Schmidt and Prandtl numbers were fixed at 0.6 and 0.7, respectively.

None of the solutions displayed the oscillatory approach to steady-state discussed by Patterson (1984). Patterson's analysis was predicated on the relation $Pr \gg 1 \gg \mathcal{A}$, so it is only marginally applicable to the the problem of Lin et al. Other differences in the problems were the lack of symmetry, noted above, and the introduction of a second species. One of the conditions for the oscillation—the broadening of the intrusion layer as it approaches the other vertical wall and consequent tilting of the isotherms beyond the horizontal—is apparent in the numerical solutions. Unfortunately, the numerical scheme of Lin et al. was only first order accurate in time, and no tests of the independence of the results on the time

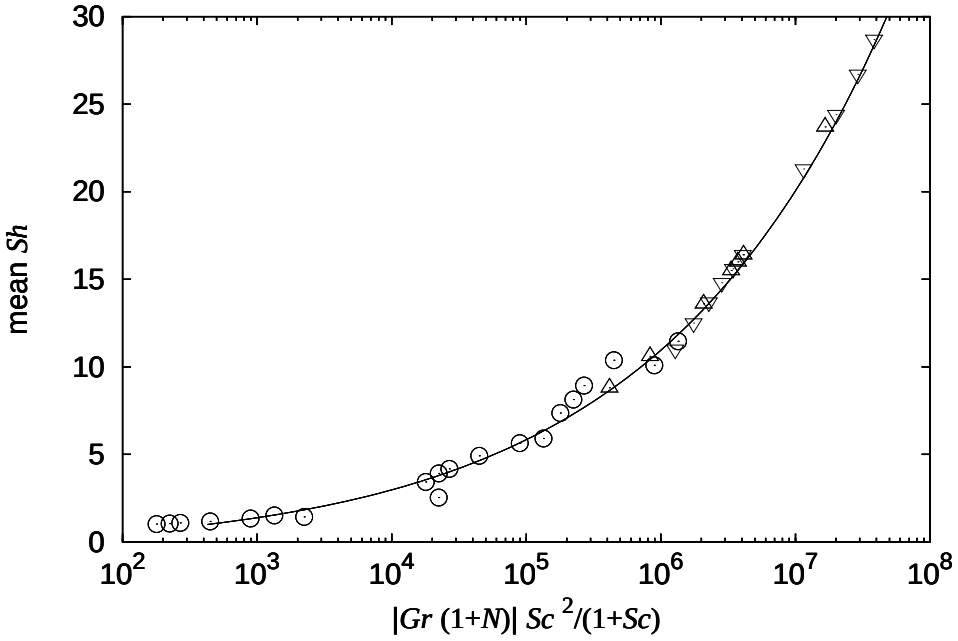

Figure 3.1: Vapour transfer ($\overline{Sh}$) in a plane vertical square cavity. Comparison of (3.3), —, and the results of Lin et al. (1990), $\odot$, and Béghein et al. (1992, table 3, $\triangle$; table 4, $\triangledown$).

step were reported, so it may be that the solutions simply do not accurately reflect the evolution of the system—that they were unable to resolve complex transient behaviour like decaying internal gravity waves. I must leave this question open, however, as the response of a gas–vapour mixture to a shock as violent as a step change in boundary conditions is beyond the scope of this study.

Like Ranganathan and Viskanta (1988; reviewed in § 3.3.8), Lin et al. included transpiration, with Φ fixed at $\ln(20/19)$, but neglected the interdiffusion energy flux; the comments in § 3.3.8 apply.

The solutions were carried to steady-state. The asymptotic mean Sherwood and (sensible) Nusselt numbers were reported and are compared with other numerical results and my formulae (McBain 1997*b*; § 3.3.16, equations 3.3 and 3.4) in figures 3.1 and 3.2.

The agreement is reasonable over most of the range but the data of Lin et

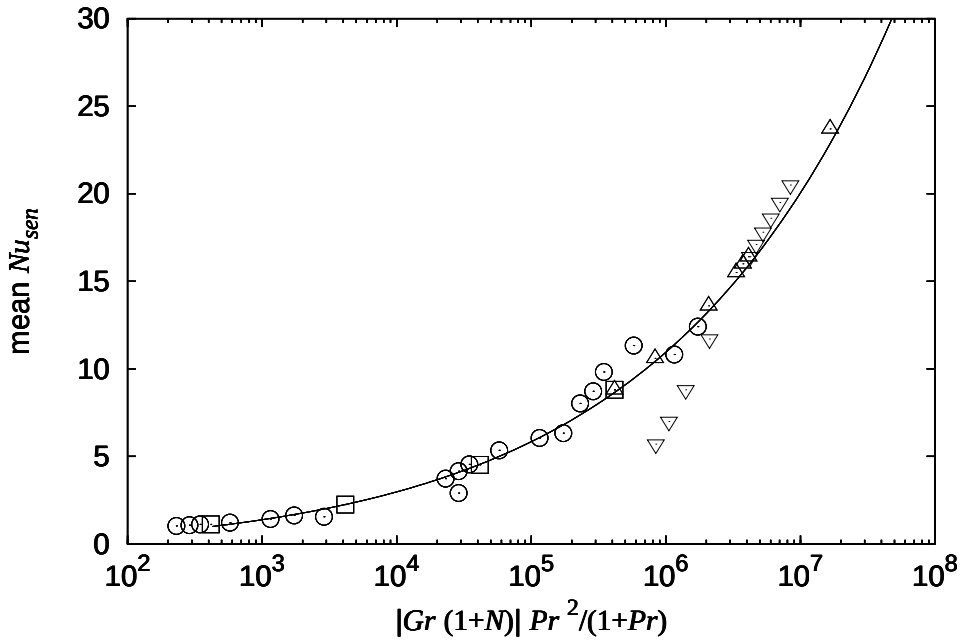

Figure 3.2: Energy transfer ($\overline{Nu_{sen}}$) in a plane vertical square cavity. Comparison of: (3.4), —, and data from Lin et al. (1990), ⊙, Béghein et al. (1992, table 3, △; table 5, ▽), and de Vahl Davis (1983), ⊡.

al. show an (as yet unexplained) peak for values of the abscissae around 5×10^5 before returning to the curve at the highest values. The correlations proposed by Lin et al. involved a combined Grashof number of the form $Gr(1+N)^{0.77}$, which is difficult to justify theoretically, does not remove the peculiar maximum and increases the scatter of the data points relative to figures 3.1 and 3.2, particularly at $N = -0.9$, as admitted by Lin et al. Their correlations do not involve Pr_r, Sc or Φ.

A difficulty with the quoted Sherwood and Nusselt numbers is that they are only based on the gradients of the vapour mass fraction and temperature, which means that they would not be the same at the hot and cold walls; cf. the expressions derived in § 2.3.4; and so do not really reflect the vapour and energy transfer rates. Lin et al. did not specify which wall the gradients were calculated at, so it has not been possible to correct their figures for the finite value of Φ. The point

here is that when $\Phi \neq 0$, vapour and energy cross the boundaries of the cavity by advection as well as diffusion and conduction.

3.3.12 Weaver and Viskanta (1991*a*)

Weaver and Viskanta (1991*a*) reported numerical solutions for plane vertical square cavities. Their principal intention was to demonstrate the effects of spatial variations in the thermophysical properties due to temperature and vapour mass fraction gradients.

There is a serious inconsistency in the energy equation (their equation 5), which was formulated with the mixture specific enthalpy as the dependent variable rather than temperature. Fourier's Law was employed for the conduction flux, but in writing this in terms of the gradient of the mixture enthalpy, h was taken as a function only of temperature. When they calculated the temperature field from the mixture specific enthalpy field, however (their equation 18), h was taken as a function of both temperature and vapour mass fraction. Consistency would have required the temperature gradient in the conduction term to have been replaced by the weighted sum of mixture specific enthalpy and vapour mass fraction gradients. While possible, this would certainly have been inconvenient.

A consistent formulation of the energy equation in terms of temperature was derived in § 2.1.3 (see also Bird et al. 1960, pp. 560–6). The general difficulty encountered both here and by Weaver and Viskanta is that the energy equation contains advection terms, which are naturally expressed in terms of enthalpy, and a conduction term, which must be expressed in terms of temperature. Since temperature is a measurable quantity whereas enthalpy is not, and since expressing the conduction in terms of enthalpy would require two sets of second order derivatives (as noted above), temperature seems the natural choice for the dependent variable of the energy equation. This was also the choice in the detailed and rigorous numerical model of Rosenberger et al. (1997; § 3.3.18).

Note that the formulation for the mixture enthalpy used in § 2.1.3 is identical

with Weaver and Viskanta's (their equation 18), except that in § 2.1.3, the partial specific heats are taken to be independent of temperature. This difference in no way affects the consistency or otherwise of the equations.

The inconsistency of their treatment of the mixture enthalpy led Weaver and Viskanta to a gross error. In one of their numerical solutions, a strong interior relative minimum appeared in temperature field. This is impossible: it contradicts Theorem 1 (p. 35).

3.3.13 Weaver and Viskanta (1991*b*)

In the second part of their paper, Weaver and Viskanta (1991*b*) aimed to demonstrate the effects of the interdiffusion and Dufour energy fluxes and the Soret vapour flux. As in the first part of the paper (1991*a*), the vehicle was a series of numerical solutions for plane vertical square cavities.

As explained in § 3.3.12, the treatment of interdiffusion was fundamentally flawed. Further results (neglecting the Soret and Dufour effects; their inclusion would violate the hypotheses of Theorem 1) showing strong relative extrema of temperature were presented. This phenomena was erroneously ascribed to interdiffusion (its occurrence in the solutions of 1991*a* was supposedly due to the inclusion of interdiffusion at the boundaries).

The treatment of the Dufour effect was marred by the fact that the expression presented for the diffusion-thermo flux did not have the same dimensions as the other energy fluxes (conduction, interdiffusion and bulk advection).

Lacking experimental data and doubting the accuracy of theoretical predictions, Weaver and Viskanta assigned arbitrary values to the thermal diffusion factor. This detracts from the usefulness of the study. Bizarrely, in some runs the thermal diffusion factor was assigned different values in the thermal diffusion and diffusion-thermo fluxes; this contradicts Onsager's reciprocal relation (Bird et al. 1960, p. 564).

The conclusions drawn by Weaver and Viskanta (1991*a*, *b*) are vague, quali-

tative and often erroneous.

3.3.14 Weaver and Viskanta (1991*c*)

Weaver and Viskanta (1991*c*) performed experiments similar to those of Hu and El-Wakil (1974; reviewed in § 3.3.2). The test cavity had $\mathcal{A} = 1$. They also simulated the experiments numerically.

The experimental study suffers from the same flaw as that of Hu and El-Wakil: liquid is present on the opposing vertical walls ($x = 0, 1$). This may give rise to two quite different problems:

- condensation in the flow field, or on the connecting walls; and
- nonzero tangential velocity (slip) at the hot and cold walls.

Like Hu and El-Wakil (1974), Weaver and Viskanta were forced to resort to heating the connecting walls to prevent condensation, thus destroying the intended thermal boundary condition (linear variation).

Unlike Hu and El-Wakil (1974), they did not account for the slip velocity at the hot and cold walls due to the falling liquid film.

The agreement between the numerical and experimental results was generally poor, probably for the reasons listed. No attempt was made to compare the results with their other sets of numerical solutions (Weaver & Viskanta 1991*a*, *b*). The vapour and energy transfer rates were not reported.

3.3.15 Béghein, Haghighat and Allard (1992)

Béghein et al. (1992) performed an extensive series of numerical solutions to test the two-dimensional scale analysis of Bejan (1985; § 3.3.5). They neglected three-dimensional ($\mathcal{S} \to \infty$) and finite mass transfer rate effects ($\Phi = 0$) and considered square cavities ($\mathcal{A} = 1$) for a Prandtl number appropriate to air ($Pr_r = 0.7$).

The first part of the paper is rather redundant since the Schmidt number was set equal to the Prandtl number, so that the problem becomes mathematically

identical to the analogous single fluid heat transfer problem (§ 2.4). Nevertheless, the results, gathered from their table 3, are plotted as upright triangles in figures 3.1 and 3.2.

Further series of runs were carried out with $Pr_r = 0.71$ and Schmidt numbers ranging from 0.21 to 3.5 for purely thermal or compositional buoyancy forces ($N = 0, \infty$). The finite vertical aspect ratio of the cavity was found to cause a discrepancy between the results and Bejan's (1985) predictions. The simple one-dimensional scale analysis is incapable of fully describing two-dimensional vapour transport. The difficulties are most pronounced for Schmidt numbers in the range [0.35,0.7], which is unfortunate, as this includes many vapours of interest, such as water vapour ($Sc = 0.61$). A modification of Bejan's analysis to take account of Prandtl and Schmidt numbers of near unit magnitude and the finite height of enclosures is discussed in § 3.3.16.

Béghein et al. reported the mean Sherwood number of the results at $N = 0$ (table 4) and the mean Nusselt number for $N = \infty$ (table 5); these are plotted as inverted triangles in figures 3.1 and 3.2, respectively. The four lowest of these points in figure 3.2 are not at all well represented by (3.4). These are the points corresponding to Schmidt numbers larger than unity ($Sc = 3.5, 2.8, 2.1$ and 1.4). The other six values, corresponding to $0.35 < Sc < 0.7$, lie quite close to the curve. This behaviour is not unexpected (§ 3.3.16).

3.3.16 McBain (1995, 1997*b*)

Béghein et al. (1992; § 3.3.15) found that Bejan's (1985) scale analysis did not work well in square cavities for Schmidt numbers in the range [0.35, 0.7]. This is understandable, as the analysis is really one-dimensional. In particular, the vertical length scale is taken to be equal to the height of the cavity, $\mathcal{A}b$. The vertical boundary layers, assuming the parameter values are such that they exist, do not extend over the full height of the walls.

Consider, for definiteness, the hot wall boundary layer when $N > 0$. The

boundary layer does not begin at the floor, since this region is rather stagnant and the flow there is dominated by viscosity (Luchini 1986). Instead, the 'intrusion flow' rises from the floor before being entrained (Patterson 1984). A region of increased pressure exists at the top of the hot wall, which is what causes the flow to turn and flow along the ceiling. This turning does not occur right at the corner, but rather over a finite length of the wall. These considerations indicate that the correct vertical length scale in the vertical boundary layers will generally be slightly less than the cavity height.

In my B.E. thesis (McBain 1995), I suggested that the correction could be made by deducting the length of the corner regions; a rough estimate for these being obtained from the nominal boundary layer thickness. An expression for the speed scale was obtained in terms of the 'diffusion thickness' or 'conduction thickness' from the usual balance of vertical advection and horizontal diffusion or conduction in the vertical compositional or thermal boundary layer (Gill 1966; Bejan 1995, p. 223). A second expression, in terms of the velocity boundary layer thickness, was obtained from a balance of inertia and buoyancy in the momentum equation; the friction–buoyancy balance recommended by Bejan (1995, p. 223) as 'marginally valid for gases ($Pr \sim 1$)' being rejected in favour of a balance appropriate for low Prandtl and Schmidt numbers. By assuming that the nominal boundary layer thickness was given by the diffusion thickness when calculating mass transfer or the two-dimensional conduction thickness when calculating heat transfer, the speed scale could be eliminated between these two expressions to give a relation between the mean Sherwood or Nusselt number and the boundary conditions (Gr, N, Sc and Pr).

The final relations were contaminated by algebraic errors, which were detected by Dr Harry Suehrcke (pers. comm., Dec. 1995). Dr Suehrcke also suggested modifying the analysis by including friction in the momentum balance (pers. comm., 10 Feb. 1996). This had the effect of giving the heat transfer result the same asymptotic behaviour at large and small Prandtl numbers as the formulae of

LeFevre (1957), and Berkovsky and Polevikov (1977). The corrected and modified results, published in 1997 (McBain 1997*b*), were:

$$53.5\ \overline{Sh}(\overline{Sh}+\mathcal{A}^{-1})^3 = \frac{Gr(1+N)Sc^2}{\mathcal{A}(1+Sc)}; \quad \text{and} \tag{3.3}$$

$$53.5\ \overline{Nu_{sen}}(\overline{Nu_{sen}}+\mathcal{A}^{-1})^3 = \frac{Gr(1+N)Pr^2}{\mathcal{A}(1+Pr)}. \tag{3.4}$$

The constant of proportionality, 53.5, in (3.4) and (3.3) was determined by fitting the results of numerical solutions for the mean Nusselt number in the range $1.7 < Nu < 6$, or values of the abscissa between 3000 and 87 000.

The formulae are compared with the numerical results of Lin et al. (1990; § 3.3.11) and Béghein et al. (1992; § 3.3.15) in figures 3.1 and 3.2. The abscissae of these results lie in a much wider range than those on which the proportionality constant was based, so that the curves pictured represent a considerable extrapolation.

The formulae give meaningless results (< 1) for values of the abscissae below 435 and are not plotted in this range. At such low combined Grashof numbers, there are no distinct boundary layers or diffusion or conduction layers, so that the analysis is invalid.

Mean Nusselt numbers from de Vahl Davis's (1983) bench-mark numerical solutions for the analogous single fluid heat transfer problem ($Pr = 0.71, \mathcal{A} = 1$) are also included as squares in figure 3.2.

In the above formulae, the mean Sherwood number does not depend on Pr, and $\overline{Nu_{sen}}$ does not depend on Sc. This follows from the assumption that for mass (/heat) transfer, the velocity boundary layer is equal in thickness to the diffusion (/conduction) layer. This is a reasonable approximation only when the Prandtl and Schmidt numbers are comparable and both are less than unity. It is particularly poor, for the heat transfer, for example, if the Schmidt number is larger than unity and the velocity boundary layer is primarily driven by compositional buoyancy. This explains the deviation in figure 3.2 of the four points taken from table 5 of Béghein et al. They correspond to solutions with $Sc > 1$ and $N = \infty$.

This deviation makes it clear that the combined Grashof number, $Gr(1+N)$, is generally not sufficient to remove the dependence of the overall transfer rates on N.

The numerical solutions used to validate the scale analysis did not use the Boussinesq approximation. Solutions were generated for cavities 50 mm wide with a 5 K temperature difference. The material properties used were those for air–water vapour. The mean temperature took on the values 10(10)50°C and the hot and cold wall relative humidities were set at 0(50)100% relative humidity at 1 atm; this gave 45 combinations. Since the results were successfully correlated by the Boussinesq scale analysis summarized above, it was concluded that non-Boussinesq effects are unlikely to be important in building wall cavities. This is one of the reasons for the use of the approximation in the present project.

Amongst the variable properties was the mixture specific heat capacity. This is inconsistent with the neglect of the interdiffusion energy flux, as noted on p. 20. Unlike in the solutions of Weaver and Viskanta (1991*a*, *b*; §§ 3.3.12 – 3.3.13) though, the parameter values were such that neither the variability of the mixture specific heat nor interdiffusion would have had much effect. Thus, this error probably does not invalidate the results; a conclusion which could also be obtained by inspection of figures 3.1 and 3.2.

3.3.17 Costa (1997)

Costa (1997) presented numerical solutions for the steady-state heat and mass transfer in a vertical stack of plane vertical square cavities separated by solid layers one-tenth the height of the cavities. This configuration was supposed to represent a building construction element. The temperature and concentration fields were assumed to be harmonic in these layers; i.e. Fourier's and Fick's Laws were assumed to hold there. Although this would be a reasonable approach for a pure heat transfer problem, it is probably too simplistic for the porous media envisaged by Costa.

According to Künzel and Kiessl (1997), the vapour flux in such materials is driven by gradients in both partial pressure (for effusion and Fickian diffusion) and relative humidity (for the transport of liquefied vapour in sorbed layers or capillaries). The energy flux is due to gradients in temperature (for conduction) and vapour pressure (for the enthalpy flux by vapour diffusion with phase changes). This leads to a nonlinear strongly coupled pair of field equations in the porous solid layers, even when advection is neglected.

Studies of the conjugate heat and mass transfer problem, such as Costa's, are necessary but they are only of value if realistic constitutive laws are employed in both phases. In addition to the oversimplified expressions for the fluxes, Costa did not use realistic values for the conductivity or diffusivity in the porous layers, only arbitrary ones. References to methods for the experimental determination of the required transport properties may be found in Künzel and Kiessl's article.

3.3.18 Rosenberger et al. (1997)

Rosenberger et al. (1997) studied the transport of iodine vapour along a horizontal cylinder (length$\approx$4.5 diameters$\approx$100 mm) filled with octofluorocyclobutane between vertical plane crystalline source and sink walls. Experiments and numerical simulations were performed. Their work is remarkable for a number of reasons.

The first is the extreme verisimilitude of the numerical modelling. The time-accurate solutions of the non-Boussinesq three-dimensional evolution equations were obtained. All fluid properties were taken as functions of composition (though not temperature, except for D). Very few simplifying assumptions were made; the only serious ones being that the property variations were independent of temperature (except D) and given by standard formulae from the kinetic theory of gaseous mixtures, and that the iodine vapour only condensed at the sink wall. The importance of the latter problem was mentioned on p. 14. This assumption was not a source of error, however, as explained in the next point.

The second is the approach to the prevention of supersaturation and nucleation. The axial variation of the azimuthally uniform wall temperature in the experimental cavity was adjusted until no condensation occurred on the wall connecting the hot and cold walls. This is to be contrasted with the evident supersaturation in the experiments of Hu and El-Wakil (1974; § 3.3.2) and Weaver and Viskanta (1991*c*; § 3.3.14).

The third is the novel and local nature of the comparison between the numerical solutions and the experiments. Overall vapour transport rates were measured, and were in reasonable agreement with the numerical predictions, but as demonstrated here in chapters 5 and 6, this global measure can be insensitive to the local details of the solution. As suggested on p. 16, given the numerical solution for the temperature and mass fraction (and total pressure in the case of a non-Boussinesq model), it is possible to calculate the degree of saturation that would obtain in the absence of secondary condensation. Rosenberger et al. did this by comparing calculated and saturation partial pressure curves for the lines running along the top and bottom of the cylinder, and found that calculated curves mostly lay beneath the saturation curves, while approaching very close to them in the region near the cold wall. For mixtures with constant properties, supersaturation is more likely near the cold wall for gas-vapour mixtures for which $Sc > Pr$, since this imparts a reverse-sigmoid shape (negative curvature near the cold wall and positive curvature near the hot wall) to the mass fraction–temperature curve (McBain 1995, fig. 18; McBain, Harris, Close & Suehrcke 1998, fig. 4; Close & Sheridan 1989, fig. 1*b*).* Since the thermal boundary conditions applied in the numerical solutions were obtained from the profiles found experimentally to be just sufficient to prevent secondary condensation, the proximity of the calculated partial pressure curves to saturation is a striking confirmation of the fidelity of the model.

While the work of Rosenberger et al. (1997) represents the state-of-the-art in

*Note that the keys in the legend to Close and Sheridan's (1989) figure 1 (*b*) are incorrectly assigned.

detailed numerical modelling of vapour transport, it also exemplifies the limitation of this approach: the modelling is so detailed and specific that it is difficult to draw any general conclusions from the results. This means that to predict the outcome of a future experiment with different given data another numerical solution of equal complexity would be required. It is submitted that the natural complement to this approach is provided by a much simpler level of modelling and the use of analytical methods. It is hoped that the reader will find examples of this in the present work.

Another limitation of the 'high fidelity' approach is that while it was very successful in modelling a small enclosure, representative of a PVT ampoule, it would become very demanding of time and computational resources if applied to large enclosures, such as building wall cavities. The reason for this is the sensitive dependence of the combined Grashof number, and thus the nonlinearity of the problem, on the length scale, b. This restriction is likely to be eased in the future, however, as the speed of computers and efficiency of algorithms continue to increase. The combined Grashof number is also comparatively low in PVT ampoules due to the reduced total pressure (this increases the kinematic viscosity by reducing the density).

Rosenberger et al. did form one general, rather stern, conclusion which is relevant to the consideration of three-dimensional effects in chapters 7–8: 'agreement between the results of laboratory experiments and two-dimensional transport models should be met with reservation'.

3.3.19 Conclusions

In conclusion, the study by Rosenberger et al. (1997) has shown that it is now possible to realistically model vapour transport in real (three-dimensional) enclosures, at least at low combined Grashof numbers.

There have been several numerical studies of plane vertical square cavities. The predicted overall transport rates, with some real exceptions, are reasonably

correlated by simple scale analysis. Results for taller cavities are much scarcer; the largest value of $\mathcal{A}$ uncovered in the literature is 7 (Wee et al. 1989; § 3.3.10). I have not found any results for three-dimensional transport in cuboids. Experimental confirmation of the results for squares, rectangles or cuboids is also notably lacking.

The available theoretical results for horizontal nonisothermal vapour transport in a gravitational field are restricted to two-dimensional geometries and cases where the mass transfer rate factor is vanishingly small. The present work supplies some results for finite mass transfer rates (ch. 4) and three-dimensional geometries (chapters 7–8).

Many of the studies reviewed did not consistently treat the related mass transfer effects of transpiration, interdiffusion and a variable mixture specific heat. This is treated in great detail in chapters 2, 4 and 6. It is shown that, in general, these should either all be included or all be neglected.

Chapter 4

The Narrow Cavity Limit

CLOSED form expressions for the velocity, temperature and vapour mass fraction fields in the space bounded by two parallel vertical walls are found by solving the equations for a cuboid in the limit as the vertical and spanwise aspect ratios tend to infinity. The flow length scales are assumed to correspond to those of the cavity in the same direction; thus ruling out multicellular flows. The vertical walls are held at different constant temperatures and vapour mass fractions and are impermeable to the gas and nonslip.

This constitutes an exact solution of the system of equations derived in chapter 2, including the finite mass transfer effects of interfacial velocity and enthalpy interdiffusion.

4.1 Introduction

In 1954, Batchelor investigated heat transfer across cavities filled with a single fluid. He realized that if the cavity is narrow enough, i.e. $\mathcal{A}$ and $\mathcal{S}$ are large enough, a fully developed regime could exist in the region sufficiently far from the floor and ceiling, and the front and back walls. Here the temperature would vary linearly across the cavity while the purely vertical velocity would have a symmetric cubic profile. This is identical to the solution for a cavity bounded only

by two vertical walls, reported in 1946 by Jones and Furry and in many textbooks (Bird et al. 1960, pp. 297–300; Rohsenhow & Choi 1961, pp. 143–6; Gebhart et al. 1988, pp. 728–30; Kakaç & Yener 1994, pp. 342–6). Various attempts (Batchelor 1954; Eckert & Carlson 1961; Dixon & Probert 1975; Daniels & Wang 1994) to find the minimum vertical aspect ratio for which this regime exists (in the single fluid case), will be treated in chapter 5.

In 1972, Aung found exact solutions for the fully developed temperature and velocity profiles in vertical channels open at the top and bottom to a uniform environment. The temperature variation is unchanged, but the velocity profile contains an additional constant governing the influence of the ambient temperature and hence the net vertical mass flux and the deviation of the velocity profile from odd symmetry. Aung also solved the problem for constant wall heat fluxes.

While the most familiar fully developed flows, e.g. axisymmetric and plane Poiseuille flow, and those of Jones and Furry (1946) and Aung (1972), are unidirectional, exact solutions have been published for the plane flow of a pure fluid between vertical (Rao, A. K. 1962) and horizontal (Gill, W. N., del Casal & Zeh 1966) parallel plates with uniform normal interfacial velocity and buoyancy effects due to heat transfer.

In the first treatment of the effect of a diffusing species, Nelson and Wood (1989) showed that Aung's (1972) results for the constant wall temperature case may be simply extended to include constant wall vapour mass fraction provided that the vapour flux is small enough for the interfacial velocity and the interdiffusion of enthalpy to be neglected. The question of when these effects may be neglected is discussed in detail in the present chapter, and chapter 6.

In the study by T. S. Lee et al. (1982) of heat and mass transfer across finite vertical channels, the high mass transfer rate effects of interfacial velocity and the interdiffusion of enthalpy are included but the mass transfer boundary conditions (constant and zero flux at the two opposing vertical walls) prevent the establishment of a fully developed regime, although at the lower mass transfer

rates the results indicate invariant axial velocity profiles over much of the channel height if one or other of the buoyancy forces is dominant; i.e. for very large or very small $|N|$. It is shown here that a fully developed regime can exist with nonzero transverse velocity, but only if it is constant.

Recent numerical work on heat and mass transfer in vertical cavities (McBain 1995; McBain, Harris, Close & Suehrcke 1998) and plane (Yan, Tsay & Lin 1989; Yan & Lin 1990) and axisymmetric (Chang, Lin & Yan 1986; Lin, Chang & Yan 1988; Lee, K. T., Tsai & Yan 1997) conduits filled with gas–vapour mixtures has suggested that mass transfer can significantly change both the flow field and the overall energy transfer rate—a conclusion supported by the present analysis. Indeed, the narrow cavity limit is an excellent example for the study of the effect of a diffusing vapour since analytic expressions for the velocity and temperature fields, as well as the steady energy transfer rate, are available for both the dry gas (Batchelor 1954) and gas–vapour mixture cases (§ 4.4).

4.2 The two-dimensional equations

In terms of the Cartesian components of velocity and the normalized coordinates (2.74), the conservation equations for the gas–vapour mixture (2.52)–(2.55) are

$$\frac{\partial u}{\partial X} + \frac{1}{\mathcal{A}}\frac{\partial v}{\partial Y} + \frac{1}{\mathcal{S}}\frac{\partial w}{\partial Z} = 0, \tag{4.1}$$

$$Gr(1+N)Sc\left(u\frac{\partial m}{\partial X} + \frac{v}{\mathcal{A}}\frac{\partial m}{\partial Y} + \frac{w}{\mathcal{S}}\frac{\partial m}{\partial Z}\right) = \frac{\partial^2 m}{\partial X^2} + \frac{1}{\mathcal{A}^2}\frac{\partial^2 m}{\partial Y^2} + \frac{1}{\mathcal{S}^2}\frac{\partial^2 m}{\partial Z^2}, \tag{4.2}$$

$$Gr(1+N)\left(u\frac{\partial u}{\partial X} + \frac{v}{\mathcal{A}}\frac{\partial u}{\partial Y} + \frac{w}{\mathcal{S}}\frac{\partial u}{\partial Z}\right) = -\mathcal{A}\frac{\partial p}{\partial X} + \frac{\partial^2 u}{\partial X^2} + \frac{1}{\mathcal{A}^2}\frac{\partial^2 u}{\partial Y^2} + \frac{1}{\mathcal{S}^2}\frac{\partial^2 u}{\partial Z^2}, \tag{4.3}$$

$$Gr(1+N)\left(u\frac{\partial v}{\partial X} + \frac{v}{\mathcal{A}}\frac{\partial v}{\partial Y} + \frac{w}{\mathcal{S}}\frac{\partial v}{\partial Z}\right) = -\frac{\partial p}{\partial Y} + \frac{T+Nm}{1+N} + \frac{\partial^2 v}{\partial X^2} + \frac{1}{\mathcal{A}^2}\frac{\partial^2 v}{\partial Y^2} + \frac{1}{\mathcal{S}^2}\frac{\partial^2 v}{\partial Z^2}, \tag{4.4}$$

$$Gr(1+N)\left(u\frac{\partial w}{\partial X}+\frac{v}{\mathcal{A}}\frac{\partial w}{\partial Y}+\frac{w}{\mathcal{S}}\frac{\partial w}{\partial Z}\right)= -\frac{\mathcal{A}}{\mathcal{S}}\frac{\partial p}{\partial Z}+\frac{\partial^2 w}{\partial X^2}+\frac{1}{\mathcal{A}^2}\frac{\partial^2 w}{\partial Y^2}+\frac{1}{\mathcal{S}^2}\frac{\partial^2 w}{\partial Z^2}, \tag{4.5}$$

and

$$Gr(1+N)\left[Pr_r+Pr_I\left(1-\mathrm{e}^{-\Phi}\right)m\right]\left(u\frac{\partial T}{\partial X}+\frac{v}{\mathcal{A}}\frac{\partial T}{\partial Y}+\frac{w}{\mathcal{S}}\frac{\partial T}{\partial Z}\right) -\frac{Pr_I}{Sc}\left(1-\mathrm{e}^{-\Phi}\right)\left(\frac{\partial m}{\partial X}\frac{\partial T}{\partial X}+\frac{1}{\mathcal{A}^2}\frac{\partial m}{\partial Y}\frac{\partial T}{\partial Y}+\frac{1}{\mathcal{S}^2}\frac{\partial m}{\partial Z}\frac{\partial T}{\partial Z}\right)= \frac{\partial^2 T}{\partial X^2}+\frac{1}{\mathcal{A}^2}\frac{\partial^2 T}{\partial Y^2}+\frac{1}{\mathcal{S}^2}\frac{\partial^2 T}{\partial Z^2}. \tag{4.6}$$

Restricting attention for the moment (until chapter 7) to two dimensions by considering only cavities very extensive in the spanwise direction, in the limit $\mathcal{S}\to\infty$; the above equations (4.1)–(4.6) become

$$\frac{\partial u}{\partial X}+\frac{1}{\mathcal{A}}\frac{\partial v}{\partial Y} = 0, \tag{4.7}$$

$$Gr(1+N)Sc\left(u\frac{\partial m}{\partial X}+\frac{v}{\mathcal{A}}\frac{\partial m}{\partial Y}\right) = \frac{\partial^2 m}{\partial X^2}+\frac{1}{\mathcal{A}^2}\frac{\partial^2 m}{\partial Y^2}, \tag{4.8}$$

$$Gr(1+N)\left(u\frac{\partial u}{\partial X}+\frac{v}{\mathcal{A}}\frac{\partial u}{\partial Y}\right) = -\mathcal{A}\frac{\partial p}{\partial X} +\frac{\partial^2 u}{\partial X^2}+\frac{1}{\mathcal{A}^2}\frac{\partial^2 u}{\partial Y^2}, \tag{4.9}$$

$$Gr(1+N)\left(u\frac{\partial v}{\partial X}+\frac{v}{\mathcal{A}}\frac{\partial v}{\partial Y}\right) = -\frac{\partial p}{\partial Y}+\frac{T+Nm}{1+N} +\frac{\partial^2 v}{\partial X^2}+\frac{1}{\mathcal{A}^2}\frac{\partial^2 v}{\partial Y^2}, \tag{4.10}$$

$$Gr(1+N)\left(u\frac{\partial w}{\partial X}+\frac{v}{\mathcal{A}}\frac{\partial w}{\partial Y}\right) = \frac{\partial^2 w}{\partial X^2}+\frac{1}{\mathcal{A}^2}\frac{\partial^2 w}{\partial Y^2}, \tag{4.11}$$

and

$$Gr(1+N)\left[Pr_r+Pr_I\left(1-\mathrm{e}^{-\Phi}\right)m\right]\left(u\frac{\partial T}{\partial X}+\frac{v}{\mathcal{A}}\frac{\partial T}{\partial Y}\right)= \frac{Pr_I}{Sc}\left(1-\mathrm{e}^{-\Phi}\right)\left(\frac{\partial m}{\partial X}\frac{\partial T}{\partial X}+\frac{1}{\mathcal{A}^2}\frac{\partial m}{\partial Y}\frac{\partial T}{\partial Y}\right) + \frac{\partial^2 T}{\partial X^2}+\frac{1}{\mathcal{A}^2}\frac{\partial^2 T}{\partial Y^2}. \tag{4.12}$$

It is seen that apart from (4.11), none of the equations depend on w, so that it may be ignored and (4.11) dropped; note that $w = 0$ is a solution of the large $\mathcal{S}$ limit of the spanwise component of the momentum equation (4.11). It may then be assumed that m, u, v, p and T are independent of Z, so long as this is consistent with the boundary conditions on all walls with the possible exception of the front and back walls, since these are now ($\mathcal{S} \to \infty$) infinitely removed.

4.3 The narrow cavity limit

We seek an asymptotic solution of this problem for large vertical aspect ratio. In the limit $\mathcal{A} \to \infty$, equations (4.7)–(4.10) and (4.12) become

$$\frac{\partial u}{\partial X} = 0, \tag{4.13}$$

$$Gr(1+N)Sc\ u\frac{\partial m}{\partial X} = \frac{\partial^2 m}{\partial X^2}, \tag{4.14}$$

$$0 = \frac{\partial p}{\partial X}, \tag{4.15}$$

$$Gr(1+N)\ u\frac{\partial v}{\partial X} + \frac{\partial p}{\partial Y} - \frac{T+Nm}{1+N} = \frac{\partial^2 v}{\partial X^2}, \tag{4.16}$$

and

$$Gr(1+N)\left[Pr_r + Pr_I\left(1-\mathrm{e}^{-\Phi}\right)m\right]u\frac{\partial T}{\partial X} = \frac{Pr_I}{Sc}\left(1-\mathrm{e}^{-\Phi}\right)\frac{\partial m}{\partial X}\frac{\partial T}{\partial X} + \frac{\partial^2 T}{\partial X^2}, \tag{4.17}$$

provided the other parameters are fixed and finite.

The vertical and spanwise derivatives of m, u, v and T have dropped out of the elliptic field equations (4.14)–(4.17). This means that the boundary conditions at the floor and ceiling and front and back walls must be abandoned. This is entirely analogous to the situation for the tangential velocity component in slightly viscous flow over a nonslip surface (Van Dyke 1964, ch. 7). It means that unless the solution fortuitously matches these conditions (without their being enforced) there will be regions of nonuniformity in the neighbourhoods of $Y = 0, 1$ and $Z = \pm 1/2$.

At the remaining boundaries; the vertical walls $X = 0, 1$; apply constant temperatures and vapour mass fractions and the transpiration (2.59) and no-slip boundary conditions:

$$T = m = X, \qquad \text{on } X = 0, 1 \tag{4.18}$$

$$u = -\frac{1 - \mathrm{e}^{-\Phi}}{Gr(1+N)Sc}\frac{\partial m}{\partial X}, \qquad \text{on } X = 0 \tag{4.19}$$

$$u = -\frac{\mathrm{e}^{\Phi} - 1}{Gr(1+N)Sc}\frac{\partial m}{\partial X}, \qquad \text{on } X = 1 \tag{4.20}$$

$$v = 0, \qquad \text{on } X = 0, 1. \tag{4.21}$$

The equation set above, (4.13)–(4.17), subject to (4.18)–(4.21), will apply for the mid-section of the cavity, sufficiently far away from the floor and ceiling and front and back walls. The precise meaning of this statement must await the solution of the ceiling and floor problems in chapter 5, and the front and back wall problems in chapter 7.

4.4 The fully developed solution

Being linear and only weakly coupled, these equations are easily solved.

The equation of continuity of the mixture (4.13) can be immediately integrated to give $u = u_\infty$, a constant.

This may be substituted into the equation of continuity of vapour (4.14), which can then be integrated twice to give:

$$m = \frac{1 - \exp[Gr(1+N)Sc\ u_\infty X]}{1 - \exp[Gr(1+N)Sc\ u_\infty]}, \tag{4.22}$$

once the vapour mass fraction boundary conditions (4.18) have been satisfied. Differentiating this expression with respect to X and substituting into either of the transpiration boundary conditions, (4.19) or (4.20), leads to:

$$u = \frac{-\Phi}{Gr(1+N)Sc} \tag{4.23}$$

and

$$m = \frac{1 - \mathrm{e}^{-\Phi X}}{1 - \mathrm{e}^{-\Phi}}. \tag{4.24}$$

The other transpiration boundary condition is automatically satisfied, which is to be expected since the formulation of the equations in § 2.1.1 guarantees that mass is conserved.

Now that u and m are known, the energy equation simplifies to:

$$-\Phi_T \frac{\partial T}{\partial X} = \frac{\partial^2 T}{\partial X^2}. \tag{4.25}$$

Equation (4.25) is of the same form as the species equation (4.14), so that the solution satisfying the boundary conditions (4.18) is

$$T = \frac{1 - \exp(-\Phi_T X)}{1 - \exp(-\Phi_T)}. \tag{4.26}$$

The solutions for the pressure gradient and vertical component of velocity are;

$$\begin{aligned} v &= \frac{Sc}{1+N}\left\{\frac{(\sigma - T)}{\Phi\Phi_T(Pr_r + Pr_I - 1)} + \frac{N(\sigma - m)}{\Phi^2(Sc-1)}\right. \\ &\quad \left. + \frac{\sigma - X}{\Phi}\left[\frac{1}{\Phi_T} + \frac{N}{\Phi} - c(1+N)\right]\right\} \end{aligned} \tag{4.27}$$

and

$$\frac{\mathrm{d}p}{\mathrm{d}Y} = \frac{\overline{T} + N\overline{m}}{1+N} + c, \tag{4.28}$$

where c is indeterminate, as discussed in § 4.4.2,

$$\sigma = \frac{1 - \exp[-\Phi X/Sc]}{1 - \exp[-\Phi/Sc]}, \tag{4.29}$$

and the quantities with overbars are averages across the cavity, given by

$$\begin{aligned} \overline{m} &\equiv \int_0^1 m \ \mathrm{d}X \\ &= \frac{1}{1 - \mathrm{e}^{-\Phi}} - \frac{1}{\Phi} \end{aligned} \tag{4.30}$$

$$\begin{aligned} \overline{T} &\equiv \int_0^1 T \ \mathrm{d}X \\ &= \frac{1}{1 - \exp(-\Phi_T)} - \frac{1}{\Phi_T} \end{aligned} \tag{4.31}$$

The vapour mass fraction and temperature profiles are illustrated in figure 4.1, and the velocity profile in figures 4.2 – 4.4.

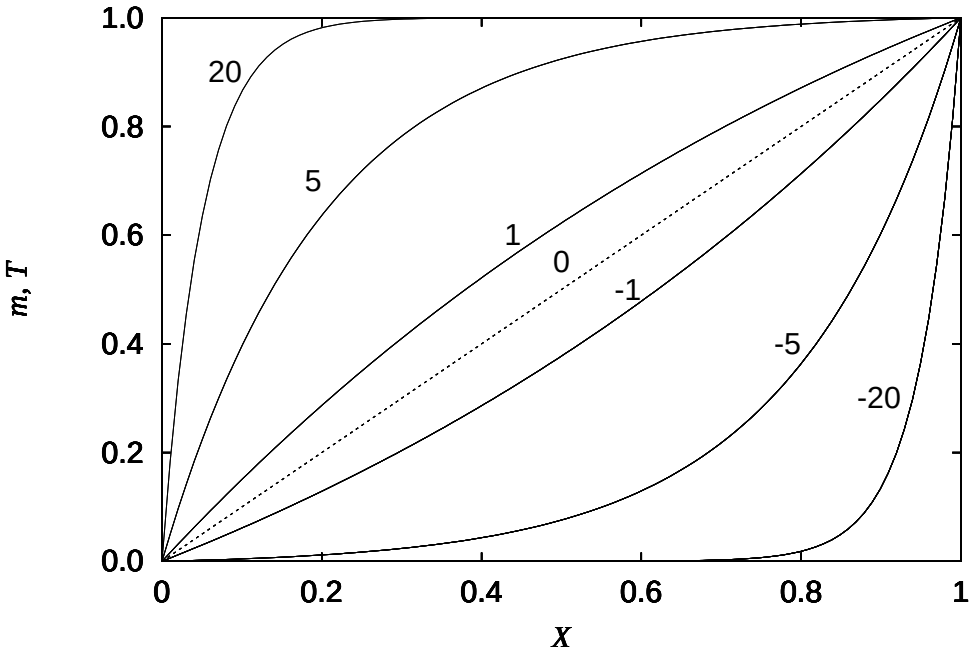

Figure 4.1: Profiles of the vapour mass fraction (4.24), with parameter Φ, and temperature (4.26), with parameter Φ_T, in the narrow cavity limit.

As in the heat transfer only solution of Aung (1972), the temperature (and here also mass fraction) distribution is unaffected by the vertical velocity; this can be seen from the fact that the combined Grashof number, $Gr(1+N)$, does not appear in the solutions (4.26) or (4.24).

With the substitution of mole fractions for mass fractions (because of the assumption of constant density rather than constant total molar concentration), the distributions of vapour mass fraction (4.24) and temperature (4.26) are identical to those given by Bird et al. (1960, pp. 572–4) for simultaneous heat and mass transfer across a stagnant film of noncondensable gas (see also Bird et al. 1960, pp. 522–6; Rohsenhow & Choi 1961, pp. 398–400; Greenwell et al. 1981 for derivations of the same mass fraction profile in other configurations).

A temperature distribution with the same form as equation (4.26) was suggested by Ranganathan and Viskanta (1988; reviewed in § 3.3.8) for a square cavity ($\mathcal{A} = 1, \mathcal{S} \to \infty$) with $Pr_I = 0$ and $N = -1$ in the special cases $Sc = Pr_r$, for

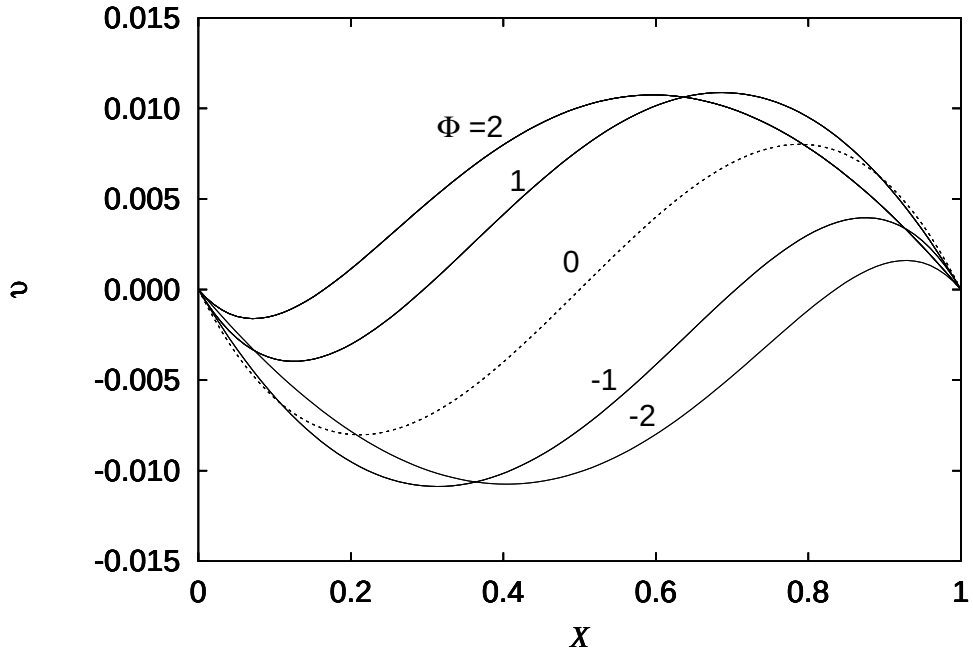

Figure 4.2: Profiles of the vertical component of velocity (4.27), with parameter Φ, in the narrow cavity limit, for $N = 1$, $Sc = 0.6$, $Pr_r = 0.7$, $Pr_I = 1$ and $c = 0$.

which net buoyancy effects vanish everywhere, and $\Phi \to -\infty$, for which the mass transfer–induced horizontal velocities are assumed to overwhelm the buoyancy-induced vertical velocities. Neither of these conclusions is quite correct.

In the first case, $Sc = Pr_r$, it results that the temperature distribution depends on the specific heat capacity of the mixture, whereas it is evident on expressing equation (4.26) in terms of primitive quantities that it only depends on the partial specific heat of the vapour, since

$$\begin{aligned} \Phi_T &\equiv \frac{(\nu\rho c_{pr}/\lambda) + [\nu\rho(c_{pA} - c_{pB})(1 - m_{*r})/\lambda]}{\nu/D}\Phi \\ &= \frac{\rho D c_{pA}}{\lambda}\Phi; \end{aligned} \tag{4.32}$$

the reciprocal of the quantity multiplying Φ being called the *vapour Lewis number* by McBain (1998), and McBain and Harris (1998). Thus, in the narrow cavity limit, the temperature distribution is independent of the partial specific heat capacity of the gas. The error of Ranganathan and Viskanta (1988) arose from

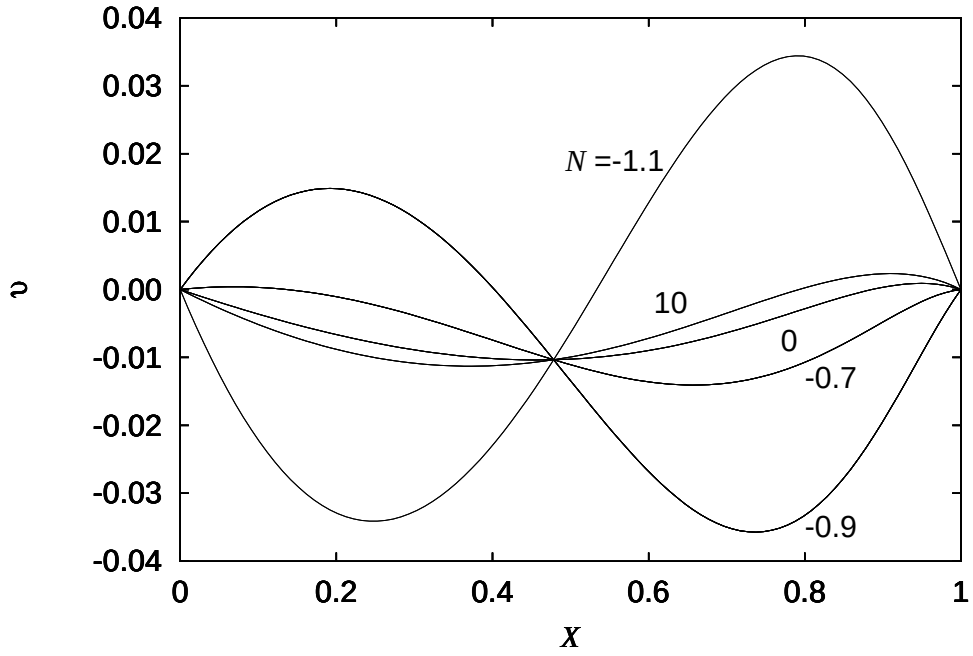

Figure 4.3: Profiles of the vertical component of velocity (4.27), with parameter N, in the narrow cavity limit, for $\Phi = 2$, $Sc = 0.6$, $Pr_r = 0.7$, $Pr_I = 1$ and $c = 0$.

their neglect of the interdiffusion term (and variation of mixture specific heat capacity) in the energy equation and so vanishes only if the gas and vapour partial specific heat capacities are equal, i.e. $Pr_I = 0$, an unlikely situation due to the fact that partial specific heat capacity of vapours is in general much higher than that of gases, as pointed out in § 2.3.2. From this one can deduce that the mass transfer effects of transpiration and enthalpy interdiffusion (including variable mixture specific heat capacity) should be included together: one should only be included in a model without the other in the rare circumstance that the interdiffusion Prandtl number, Pr_I, is numerically either very small or large.

In the second case, $\Phi \to -\infty$, their solution is inconsistent with the no-slip boundary conditions at the floor and ceiling. These will affect a large proportion of the cavity, since this is not narrow ($\mathcal{A} = 1$) in their study. As shown by Meyer and Kostin (1975; reviewed in § 3.2.2), the nonslip walls give rise to a circulation of the gas.

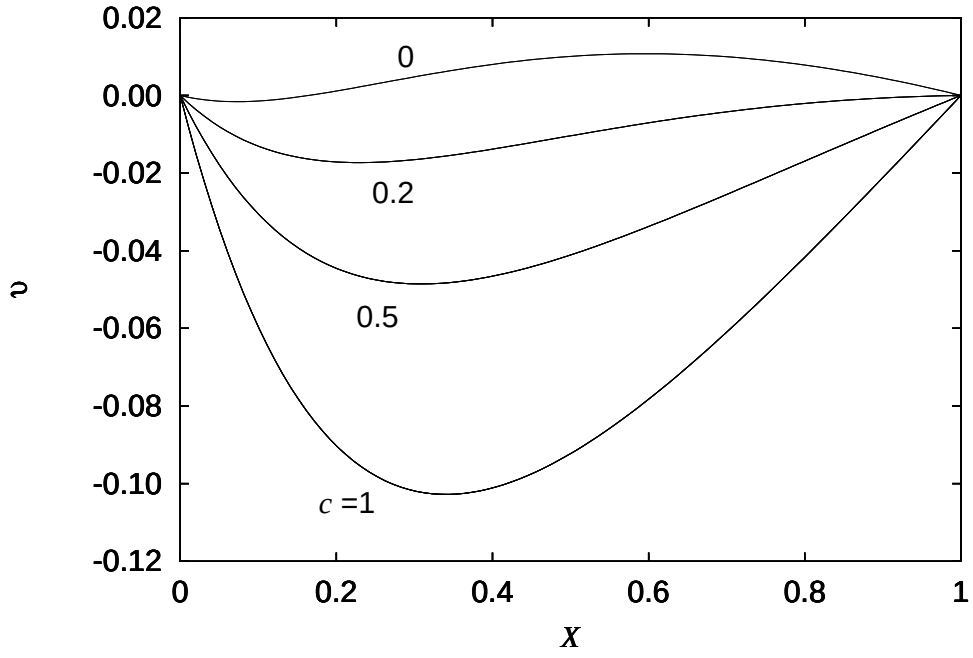

Figure 4.4: Profiles of the vertical component of velocity (4.27), with parameter c, in the narrow cavity limit, for $N = 1$, $Sc = 0.6$, $Pr_r = 0.7$, $Pr_I = 1$ and $\Phi = 2$.

A concentration profile similar to equation (4.24) also occurs as the exact solution of the general one-dimensional advection–diffusion equation discussed by Patankar (1980, p. 86) in connection with upwinding in finite volume numerical schemes. There, the parameter Φ of equation (4.24) plays the role of a cell Peclet number. Recall (§ 3.2.3) that Markham and Rosenberger (1980) called Φ the Peclet number of a Stefan diffusion tube.

The velocity profile (4.27), illustrated in figures 4.2 – 4.4 is a new result, differing from the single fluid heat transfer cubic profile because of the horizontal advection of vertical momentum due to the vapour migration and the curved buoyancy distribution; the temperature and mass fraction varying differently and nonlinearly across the cavity.

The vapour mass fraction (4.24), temperature (4.26) and velocity (4.27) solutions all have singularities at $\Phi = 0$, but these are removable. This can be seen

from the Maclaurin series in Φ for σ, for example:

$$\sigma = X - \frac{X(X-1)}{2Sc}\Phi + \frac{X(X-1)(2X-1)}{12Sc^2}\Phi^2 - \frac{X^2(X-1)^2}{24Sc^3}\Phi^3 + O(\Phi^4) \quad (4.33)$$

Note the σ has the same functional form as m and T—with 1 and $Sc/(Pr_r + Pr_I)$ replacing Sc, respectively. Thus, the solutions are made analytic for $-\infty < \Phi < \infty$ by setting

$$m = X \quad (4.34)$$

$$u = 0 \quad (4.35)$$

$$v = \frac{X(X-1)}{2}\left(\frac{1-2X}{6} + c\right) \quad (4.36)$$

$$\frac{dp}{dY} = \frac{1}{2} + c \quad (4.37)$$

$$T = X \quad (4.38)$$

for $\Phi = 0$, which is equivalent to the solution of Nelson and Wood (1989).

The dashed line in figure 4.2, drawn from equation (4.36), also represents the solution for the analogous single fluid heat transfer problem; i.e. Aung's (1972) solution, since then the buoyancy ratio, N, enters only through the speed scale in the definition of v (2.27).

There are also removable singularities at $Sc = 1$ and $Pr_r + Pr_I = 1$ which are less important. The nondimensionalization breaks down in the vicinity of $N = -1$, as discussed in § 2.6.2. Note the dramatic difference between the velocity profiles in figure 4.3 for $N = -0.9$ and -1.1.

4.4.1 Mass and energy fluxes at the vertical walls

In the narrow cavity limit, sufficiently far from the horizontal surfaces, the dimensionless mass transfer rates, at the hot and cold walls are obtained by substituting the horizontal velocity (4.23) into (2.62)

$$Sh_0 = Sh_1 = -\frac{Gr(1+N)Sc}{\Phi} \times \frac{-\Phi}{Gr(1+N)Sc} = 1 \quad (4.39)$$

or the mass fraction field (4.24) into (2.63)

$$Sh_0 = \frac{1-\mathrm{e}^{-\Phi}}{\Phi} \times \frac{\Phi}{1-\mathrm{e}^{-\Phi}} = 1 \tag{4.40}$$

$$Sh_1 = \frac{1-\mathrm{e}^{-\Phi}}{\Phi \mathrm{e}^{-\Phi}} \times \frac{\Phi \mathrm{e}^{-\Phi}}{1-\mathrm{e}^{-\Phi}} = 1. \tag{4.41}$$

The two methods of calculating the mass transfer rate—from the transpiration velocity or the mass fraction gradient—are in agreement, as expected. That the Sherwood numbers at the hot and cold walls are equal means that the rates of evaporation and condensation are equal, so that no net mass enters the cavity at any level where the fully developed solution applies.

The Nusselt number is also a constant (independent of position on the wall, and the same for each wall) but does depend on a fixed combination of Φ_T and Λ. It is given by equations (2.66) and (4.26) as

$$Nu = 1 + [1 - \exp(-\Phi_T)]\Lambda. \tag{4.42}$$

4.4.2 The vertical pressure gradient

A more general solution that still satisfies equations (4.13)–(4.17) and boundary conditions (4.18)–(4.21) is one where c varies with Y, but this must be rejected on physical grounds as it leads to a net vertical mass flux that varies with height. This violates the conservation of mass, as by equation (4.39) the cold and hot wall Sherwood numbers are equal, so that there is no net addition of mass to the cavity through the hot and cold walls at any horizontal section for which this fully developed solution applies.

The value of the constant c remains indeterminate. It is clearly related to the net vertical mass flux, which is proportional to the integral of v across the cavity. This integral depends on c.

In the small mass transfer rate factor limit, the integral from $X = 0$ to 1 of v (4.36) is $-c/12$. For the cavity, the net vertical mass flux in this limiting case must be zero (assuming3 there is no mass flux at the floor or ceiling, or front or

back walls) so that $c = 0$. For an open channel, c is determined by the pressure boundary conditions at the inlet and outlet.

No such simple treatment is possible for a cavity with $\Phi \neq 0$. An inspection of figures 4.2 or 4.3, for which $c = 0$ in all the plotted profiles, reveals that the condition of the pressure gradient balancing the mean density perturbation (i.e. $c = 0$, from equation 4.28); does not imply a net zero vertical mass flux. Further, if $Gr(1 + N) \neq 0$, a recirculating flow would be expected, which would certainly cause the net mass added to the cavity through the hot and cold walls to be different in the top and bottom end regions. This difference cannot be determined without the solutions valid for these regions. These are obtained numerically in chapter 5.

4.5 A numerical example

If the vapour condenses at one of the walls, the vapour base enthalpy, h_{A_r}, is naturally taken as the enthalpy of the vapour at T_{*r} relative to that of the condensed state at the same temperature. This can easily make $[1 - \exp(-\Phi_T)]\Lambda$ (the dimensionless 'latent heat transfer') the dominant component of the overall energy transfer (4.42). This is the same conclusion as reached by Yan et al. (1989), from their numerical studies of the finite length channel. For points well up the channel from the entrance, their results are well described by the above formula.

For example, in their Case II ($T_{*r} = 30°\mathrm{C}$, $\Delta T_* = 20\,\mathrm{K}$) with both walls saturated with water vapour and the total pressure about 1 atm), the dimensionless parameters take on the values $\Lambda = 66.0$ and $\Phi_T = 0.118$. Equation (4.42) gives $Nu = 8.349$. For a point 560 channel widths up from the entrance, Yan et al. (1989) give $Nu = 8.347$, which is excellent agreement. With saturated boundary conditions such as these, the vapour will certainly be supersaturated in the channel, so that gas-phase condensation is possible, but this was neglected in the cited work. Equation (4.42) is therefore applicable.

It is obvious from this example that the humidity difference has a large effect on the energy transfer, as will often be the case.

Numerous further numerical examples, due to Dr Harry Suehrcke, supporting this conclusion can be found in our recent joint paper (Suehrcke & McBain 1998).

4.6 Limitations of the narrow cavity limit

4.6.1 The ceiling and floor regions

In the solution for the flow near a nonslip surface at high Reynolds numbers, the next stage after finding the basic inviscid flow is to expand the coordinate perpendicular to the surface where the boundary condition was dropped. Here the coordinate is Y and the obvious choice for the expansion factor is $\mathcal{A}$, so that the full equations have to be solved in these regions. This will be the subject of chapter 5. Once solutions are found for these regions, a composite solution can be constructed for a cavity with $\mathcal{A}$ arbitrary above a minimum determined by the size of the end regions.

Similarly, to obtain solutions valid near the front and back walls, the coordinate Z must be expanded by the factor $\mathcal{S}$. This is treated analytically in chapter 7 for the low mass transfer rate limit.

4.6.2 Stability

It is well known (Gebhart et al. 1988, pp. 728–30; Vest & Arpaci 1969) that the narrow cavity limit flow in the analogous single fluid problem; i.e. that reported by Jones & Furry (1946); is susceptible to both stationary and travelling instabilities. Thus, while the studies projected in § 4.6.1 will define the aspect ratios for which the present solution is valid, a stability analysis must still be performed to determine the applicable range of Gr and the other parameters. This lies beyond the scope of the present project.

4.7 Conclusions

In this chapter I have presented the fully developed profiles of temperature, mass fraction and velocity, and the consequent mass and energy fluxes at the vertical walls, in the space between two parallel walls at different but constant conditions for a perfect Boussinesq mixture of a gas and a vapour with constant properties except for the mixture specific heat. The finite mass transfer effects of interfacial velocity and the interdiffusion of enthalpy were included.

The governing equations were obtained from those for a cuboid by taking the limit as the vertical and spanwise aspect ratios tended to infinity. In this process, the vertical and spanwise gradients of all dependent variables dropped out of the field equations (apart from a uniform vertical pressure gradient). As a consequence, the boundary conditions at the other surfaces had to be abandoned. The solutions presented thus apply equally well to flow in open channels as well as cavities, but only sufficiently far from the ends. The question of how far is sufficiently far must await the solution for the flow in the end regions, which will be treated in chapters 5 and 7.

In the zero mass transfer limit, the temperature and mass fraction vary linearly across the cavity while the horizontal velocity is zero and the vertical velocity is described by a cubic (odd symmetric for a cavity, and tending toward an even symmetric parabola as the imposed pressure gradient becomes large compared to the density perturbation for an open channel). For finite mass transfer, the horizontal velocity is nonzero, but must be constant. This horizontal advection profoundly alters the transport of vapour, energy and momentum across the cavity, so that while their profiles can still be expressed in closed form, this involves exponential functions rather than polynomials. The expression derived for the wall energy flux shows that the overall cavity energy transfer can be very much higher if a vapour condenses at the walls.

Chapter 5

The Floor and the Ceiling

In chapter 4, the equations of gas–vapour transport were solved for one of the simplest geometries possible: the infinite vertical channel. The usefulness of this solution is limited, of course, by the fact that real cavities are not infinitely tall; they have floors and ceilings. The question here is whether the narrow cavity limiting solution can in fact describe the behaviour of a gas–vapour mixture in a finitely tall cavity, sufficiently far from the floor or ceiling, and in particular, how narrow the cavity must be for this description to be adequate. In this chapter, numerical methods and solutions for the floor and ceiling problems are explained. The assumption of two-dimensionality is retained. The two-dimensional domain is illustrated in figure 5.1.

As pointed out in § 4.6.1, the full equations—or at least those of § 4.2—must be solved in the floor and ceiling regions; the terms inversely proportional to positive integral powers of the vertical length scale, $\mathcal{A}$, can no longer be ignored. This greatly increases the difficulty of the problem—in particular, the equations are now nonlinear and strongly coupled—so necessitating a numerical approach. A significant hydrodynamical difficulty in solving these equations is that the boundary condition on the velocity at a mass transfer interface (2.59) depends on the unknown composition gradient. The flexibility of the finite element package *Fastflo* (CSIRO 1997) makes it well suited to the solution of this class of problems.

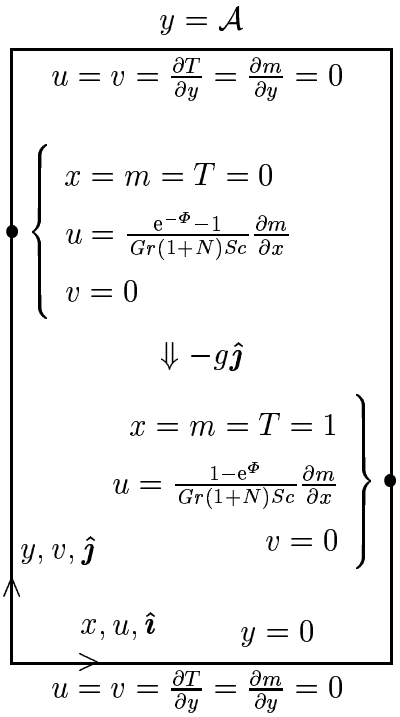

Figure 5.1: Geometry and boundary conditions for the *Fastflo* solutions.

The first part of this chapter (§§ 5.1 – 5.3) is devoted to the development of a numerical method for solving the basic equations of vapour transport, after which it is used used to investigate the problem raised in § 4.6.1: the floor and ceiling regions.

5.1 Vapour transport in *Fastflo*

In this section, numerical methods using the finite element package *Fastflo* for solving the basic equations of vapour transport (ch. 2) are presented, including transpiration, the transport of enthalpy by interdiffusion, and buoyancy forces due to temperature and vapour mass fraction differences. The penalty method fails for this problem, so an alternative algorithm is described. A simple modification of the automatic square mesh generator provided with *Fastflo*, `unit.c`, creates a mesh of smoothly varying fineness. The results of a single simulation are presented in some detail to illustrate the variety of postprocessing procedures possible with

Fastflo (§ 5.2.2).

5.1.1 Continuum model

The continuum equations to be solved here are (2.52)–(2.55). At the vertical walls, the boundary conditions are the same as used for the narrow cavity limit: (4.18)–(4.21). Assume the floor and ceiling to be solid surfaces, so that they are nonslip

$$u = 0 \qquad \text{on } y = 0, \mathcal{A}; \tag{5.1}$$

and impermeable to the mixture

$$v = 0 \qquad \text{on } y = 0, \mathcal{A}; \tag{5.2}$$

and vapour

$$\frac{\partial m}{\partial y} = 0 \qquad \text{on } y = 0, \mathcal{A}. \tag{5.3}$$

The thermal boundary conditions on the floor and ceiling are not unimportant, since they are known in the analogous single fluid heat transfer problem to influence the penetration of convective effects into the core (Daniels & Wang 1994). For the purposes of the present problem, however, it is adequate to consider the simple adiabatic condition (cf. equation 2.25):

$$\frac{\partial T}{\partial y} = 0 \qquad \text{on } y = 0, \mathcal{A}. \tag{5.4}$$

The boundary conditions are summarized in figure 5.1.

The speed scale in these equations is $\nu Gr(1+N)/b$ which expresses a balance between buoyancy and viscosity in the momentum equation, if diffusion and conduction dominate the species and energy equations. In narrow cavities (large $\mathcal{A}$) there may occur a region sufficiently far from the horizontal surfaces in which the fluid does not accelerate vertically. It was shown in chapter 4 that the nondimensional velocity based on this speed scale is independent of the Grashof number (see especially equation 4.27). Thus, if a solution at one Grashof number is used as an initial guess for one at a different number, for which there is also a fully

developed region, no change should be required from the guess to the new solution in the intersection of the two regions. This scale, and the numerical method presented in the following section, would not be appropriate for highly convective flows. When vertical velocity boundary layers occur, the speed varies more as the square root of the Grashof number (McBain 1995, fig. 12; 1997*b*, fig. 2), reflecting the steepened density gradients near the hot and cold walls. The range of parameters for which a fully developed region may be expected is discussed later in this chapter (§ 5.5).

5.1.2 The interfacial velocity

The transpiration boundary condition (2.59) associated with the semipermeable interfaces significantly increases the difficulty of the hydrodynamical problem as it introduces an extra coupling between the momentum (2.54) and species (2.53) equations. Unless the net influx to the cavity is zero, the problem for the velocity field is ill-posed and has no solution (Gresho 1988). Thus the species equation is coupled to the momentum equation both by the Dirichlet condition and the continuity constraint, as well as the buoyancy force term. This requires special treatment, as described in the following section.

5.1.3 Augmented Lagrangian algorithm

The system of equations (2.52)–(2.55) has the usual difficulties of viscous incompressible fluid dynamics: the continuity constraint and the nonlinearity of the advection terms. In many cases these can be handled by the simple penalty method (Gresho 1988), but this gives poor results for this problem for nonzero mass transfer ($\Phi \neq 0$) because of the transpiration boundary condition as described in the previous section. Further, the penalty method does not provide an accurate solution for the pressure field, which is important here since the unknown constant, c, of the fully developed solution occurs in the expressions for the vertical component of velocity and the pressure (4.27)–(4.28).

One of the next simplest algorithms is the augmented Lagrangian technique (Thomasset 1984). This differs slightly from the augmented Lagrangian technique presented in the *Fastflo* Tutorial Guide (CSIRO 1997, p. 117) in that the set of equations for momentum, temperature and mass fraction are solved by under-relaxtion of the advection—including interdiffusion—terms before each pressure update. A relaxation factor of 0.5 was used, with a convergence tolerance of 5×10^{-4} in the relative change in the solution variables. The penalty factor for the divergence was 500; no relaxation was employed for the pressure updates. The outer (pressure) loop was continued until the divergence of the calculated velocity field (normalized by the maximum nodal velocity component) was less than 10^{-3}, thus ensuring an accurate pressure solution, as required for the determination of the unknown constant, c.

This approach was found to be more robust with respect to the continuity difficulties mentioned in the previous section than that described in the *Fastflo* Tutorial Guide, where the pressure is updated between each iteration of the momentum equation. The method employed here differed from Thomasset's only in that the basis functions for the unknowns were conforming quadratics, except for pressure for which they were linear.

The first run through the outer loop of the augmented Lagrangian algorithm is identical to the simple penalty method. With the penalty factor employed here, typically 10–20 pressure updates were required for satisfaction of the continuity constraint to the prescribed level. The (normalized) divergence at the end of the first loop was usually extreme, with values of several hundred percent not uncommon. The use of a larger penalty parameter, which would usually enforce continuity more strongly, here resulted in spurious pressure gradients normal to the mass transfer interfaces, $x = 0, 1$.

The algorithm was by no means fast, runs taking typically in excess of t-wo hours on a 150 MHz Silicon Graphics Indy R5000, but did provide accurate solutions. Algorithms more sophisticated than the penalty and augmented La-

grangian methods, such as the *Fastflo* operator splitting technique (CSIRO 1997, pp. 180–203) certainly exist and should be investigated for further research into this class of flows.

5.1.4 Implementation of unusual terms

The mathematical description of vapour transport through a confined gas developed in chapter 2 involves two terms not usually encountered in computational fluid dynamics: the interdiffusion term in the energy equation (2.55); and the interfacial velocity boundary condition (2.59). Implementing these with a 'black-box' package, though possible (Suehrcke & Harris 1995; McBain & Harris 1998), is not nearly so straightforward as with *Fastflo*.

Since the gradient of the mass fraction, $\boldsymbol{\nabla} m$, is required both in the interior of the domain, for the interdiffusion term of the energy equation, and on the boundary, for the interfacial velocity boundary condition, it is conveniently calculated at each node and placed on the 'local vector stack' by a command of the form

```
e v300 = [grad] {v104}
```

inside the problem for the inner (mass fraction, temperature and momentum) loop, where it is understood that `v104` holds the values of the mass fraction from the last inner iteration. The intermediate solution vector `v300` is then available for use in statements defining both the field equations and boundary conditions.

The old values are used in the interdiffusion term, as this is analogous to the treatment of the other advective terms, where the advecting velocity is that from the last iteration. The interdiffusion term is a type of advection term, as it represents the incremental energy advected by the diffusive flux of vapour. Thus, a Picard linearization is used for all the nonlinear terms in the inner loop.

Though the interfacial velocity boundary condition (2.59) is linear in the unknowns $\mathbf{u}$ and m, convergence was only obtainable by using old values for $\boldsymbol{\nabla} m$, perhaps because the condition must be a condition on $\boldsymbol{\nabla} m$ and not on $\mathbf{u}$ (§ 3.2.1).

Since these were already required for the interdiffusion term, no extra computational cost was incurred evaluating it.

A sample *Fasttalk* file can be found in appendix A.

5.1.5 The finite element mesh

Fastflo has two mesh generators for rectangular domains. The first, a C program called `unit.c`, uses a square grid (thereby limiting the domain aspect ratio to the quotient of two integers) and the second, a built-in, creates an unstructured grid from triangular elements. Neither of these is particularly satisfactory since a graded structured quadrilateral mesh is preferred for rectangular cavity flows (Cleary 1995*b*). The square mesh generator is easily adapted though, by simple stretching of the nodal coordinates while preserving connectivity. This could be achieved in *Fasttalk*, the language of *Fastflo*, or, as the mesh data file consists of simply formatted ascii, with a short C program. Here, `unit.c` was modified to include the stretching function recommended (originally for finite difference grids) by Vinokur (1983):

$$x = \frac{1}{2}\left\{1 + \frac{\tanh\left[s\left(\frac{x'}{l'} - \frac{1}{2}\right)\right]}{\tanh\frac{s}{2}}\right\}, \tag{5.5}$$

where x' and l' are the nodal coordinate and domain dimension of the unstretched mesh and s is the stretching factor. The function can be applied with different values of s to each of the coordinates, x and y (the values of y being afterwards multiplied by $\mathcal{A}$). The function is plotted for various values of s in figure 5.2. The advantage of a nonuniform grid in this problem is that the mass fraction gradients near the vertical walls can be calculated more accurately with smaller elements, while a lesser number of elements overall is obtained by using larger elements in the core. Further, a very fine mesh can be used near the corners, where the velocity boundary conditions are singular—a problem first described by Jhaveri et al. (1981; § 3.3.3), who also prescribed this remedy. An example of a mesh created by such a procedure is shown in figure 5.3.

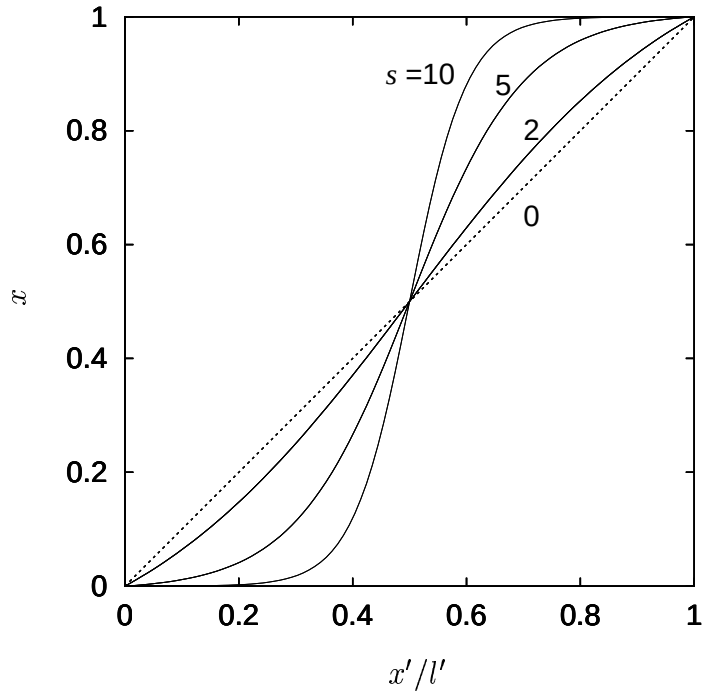

Figure 5.2: Vinokur's (1983) symmetric stretching function.

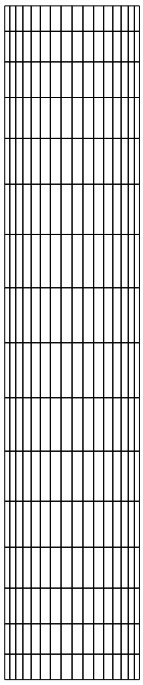

Figure 5.3: A 16×16 mesh for a domain of aspect ratio $\mathcal{A} = 5$ with stretching factor $s = 2$ in both directions.

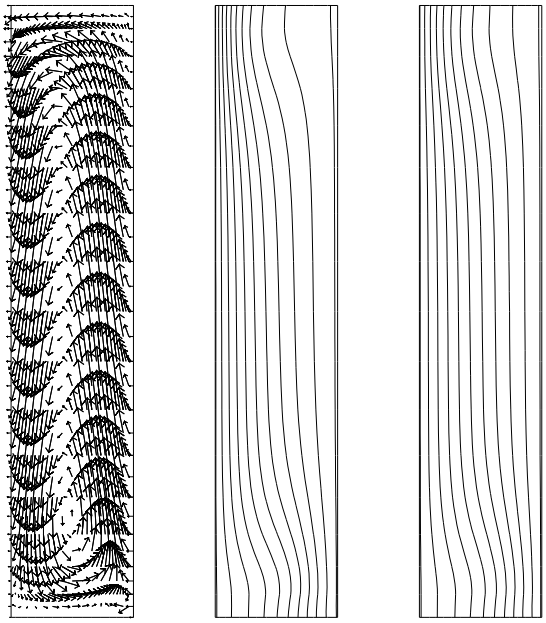

Figure 5.4: Solution variables from a sample *Fastflo* run: (a) velocity, $\mathbf{u}$; (b) temperature, T; and (c) vapour mass fraction, m for $\Phi = 0.69$, $Gr(1+N)Pr_r = 10^3$, $Pr_r = 0.71$, $Pr_I = Sc = 0.61$, $N = 0.5$, and $\mathcal{A} = 5$.

5.2 Results

The variety of phenomena possible in the seven parameter system defined by equations (2.52)–(2.55) and the geometry (fig. 5.1) is far too diverse to be adequately addressed here. Instead, a single case is presented in some detail. The parameters are: $\Phi = 0.69$, $Gr(1+N)Pr_r = 10^3$, $Pr_r = 0.71$, $Pr_I = Sc = 0.61$, $N = 0.5$ and $\mathcal{A} = 5$, and the mesh used is that shown in figure 5.3. Figure 5.4 shows the solution variables.

5.2.1 Grid independence

Grid independence was tested by obtaining solutions with the 16×16 mesh of 8-noded quadrilateral elements shown in figure 5.3 and on one of half the resolution: 8×8 elements, with the same stretching factor, $s = 2$. The independence criteria

CRITERION	8×8	16×16	% CHANGE
$\int_0^{\mathcal{A}} u\|_{x=0}\,\mathrm{d}y$	-0.004232	-0.004251	+0.45
$\int_0^{\mathcal{A}} u\|_{x=1}\,\mathrm{d}y$	-0.004211	-0.004254	+1.02
$\int_0^{\mathcal{A}}\int_0^1 u\,\mathrm{d}x\,\mathrm{d}y$	-0.004221	-0.004252	+0.73

Table 5.1: Tests of grid independence and overall conservation of mass.

chosen were those related to the mass transfer rate: the vertical integrals of the horizontal velocity component. Three integrals were taken for each grid: on the left wall, the right wall and the entire domain; and the results reported in Table 5.1. The spread of the figures in each set is another measure of the error since by overall conservation of mass and the impermeability of the horizontal boundaries they should be equal.

5.2.2 Postprocessing

The solution variables are not always those most suitable for presentation, and they may not be the ones of interest. The velocity vector plot (fig. 5.4 *a*), for example, is very cluttered. The temperature contour plot (fig. 5.4 *b*) suggests that the heat transfer is practically one-dimensional throughout much of the height of the cavity, with deviations only near the horizontal surfaces. It is difficult, though, to quantify this from the figure.

The flow field is more readily envisaged with stream-lines. These are easily generated in *Fasttalk* (CSIRO 1997, p. 121) and are plotted in figure 5.5 (*a*).

The question of whether or not the temperature profiles are fully developed is easily answered by subtracting the finite element solution from the analytic solution, for a cavity of infinite vertical aspect ratio, equation (4.26), and contouring the result, T'. Figure 5.5 (*b*) clearly displays the range of influence of the horizontal surfaces into the cavity core. This question is taken up in more detail in § 5.5.

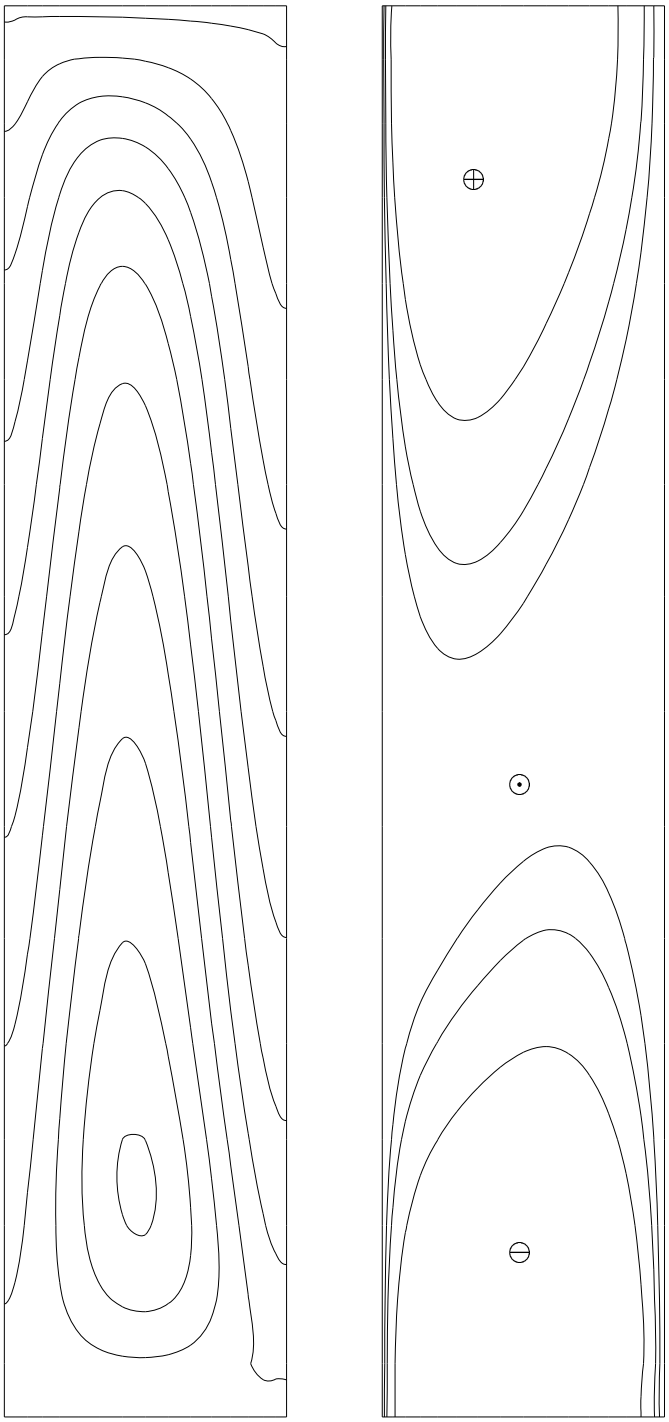

Figure 5.5: Processed solution variables from the same run as figure 5.4: (a) stream-function, with contours at $1, 10, 20, \ldots, 90, 99\%$; (b) temperature discrepancy, T', with contours at $\pm 1, 2$ and 5%, with signs as shown.

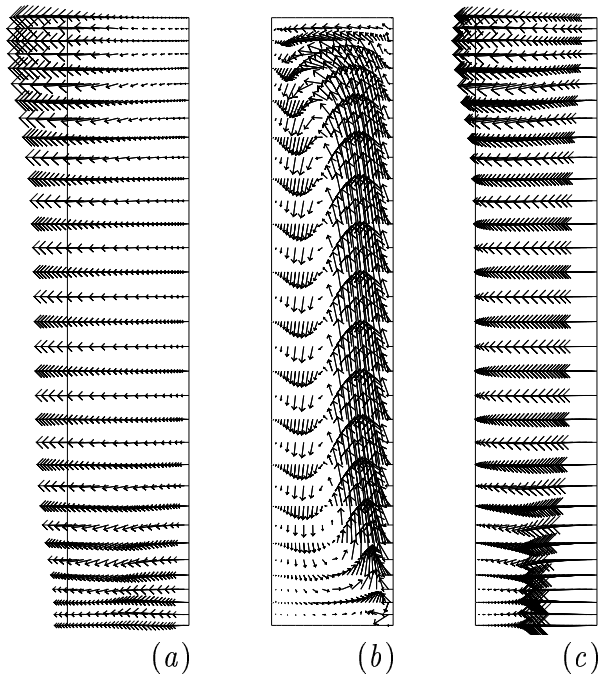

Figure 5.6: Energy flux components: (a) conduction, $\mathbf{e}_{cond}$; (b) bulk advection, $\mathbf{e}_{adv}$; and (c) interdiffusion, $\mathbf{e}_{int}$. Arrows scaled to the maximum magnitude of each component.

Further insight into the energy transfer can be obtained from vector plots of each of the component energy fluxes, defined by (2.48)–(2.51). It must be noted that this separation of $\mathbf{e}$ into its component parts is not unique, since it suffers from the same arbitrariness (an additive constant without physical significance) as the thermodynamic internal energy (Guggenheim 1959, p. 11). The present choice is convenient as it means that both the advective, $\mathbf{e}_{adv}$ (2.49), and interdiffusive, $\mathbf{e}_{int}$ (2.50), fluxes vanish at the left wall, since these are proportional to the reduced temperature, T. This simplifies calculation of the overall energy transfer rate, which thus can be accomplished by integrating just the conduction, $\mathbf{e}_{cond}$ (2.48), and latent, $\mathbf{e}_{lat}$ (2.51), parts over the cold wall. Alternatively, the total energy flux can be integrated over the domain. The conductive, advective and interdiffusive fluxes are plotted in figure 5.6. The component fluxes, $\mathbf{e}_{cond}$, $\mathbf{e}_{adv}$ and $\mathbf{e}_{int}$, unlike their sum, $\mathbf{e}$, are not solenoidal. Figure 5.6 shows how the energy

is transported into the cavity from the right wall by advection and interdiffusion, how these fluxes are converted to the conduction flux, and finally how energy is conducted out of the cavity into the left wall. The arrows in figure 5.6 (*c*) which seem to be leaving the cavity in fact are not; this is another example of the cluttered nature of vector plots which is treated by the 'heat-lines' introduced below.

The total energy flux is obtained from the component fluxes and (2.47) and is plotted in figure 5.7 (*a*). Since the energy flux vector, **e**, like the velocity, **u**, is plane and solenoidal, a 'heat-function' can be formed by analogy with the stream-function (Trevisan & Bejan 1987), and is easily implemented in *Fasttalk*. In fact, the same *Fastflo* 'problem' can be used for the stream-function as the heat-function; it is merely a matter of passing either the velocity field, **u**, or the energy flux field, **e**. The heat-lines, the contours of the heat-function (fig. 5.7 *b*), show the paths that energy follows through the cavity, though it is affected by the arbitrariness of the energy flux vector. Since an equal amount of energy flows between each of the heat-lines, it is clear from figure 5.7 (*b*) that the local flux through the left wall is strongest nearer the top, and decreases down the wall. This comes about because hot vapour-rich air is convected across the top of the cavity by the counterclockwise rotating cell visible in the stream-line plot (fig. 5.5 *a*).

5.2.3 Overall transfer rates

The overall energy transfer rates may be calculated from (2.66) or by averaging the horizontal component of the total energy flux (2.47) over any vertical line segment joining the floor and the ceiling (since these boundaries are adiabatic). The latter is chosen here as a test of the overall conservation of energy and the accuracy of the postprocessing operations involved in the calculation of $\boldsymbol{e}$. Results are presented for averages over the left wall, the right wall and the total domain in Table 5.2. As can be seen, the estimates of the overall energy transfer rate

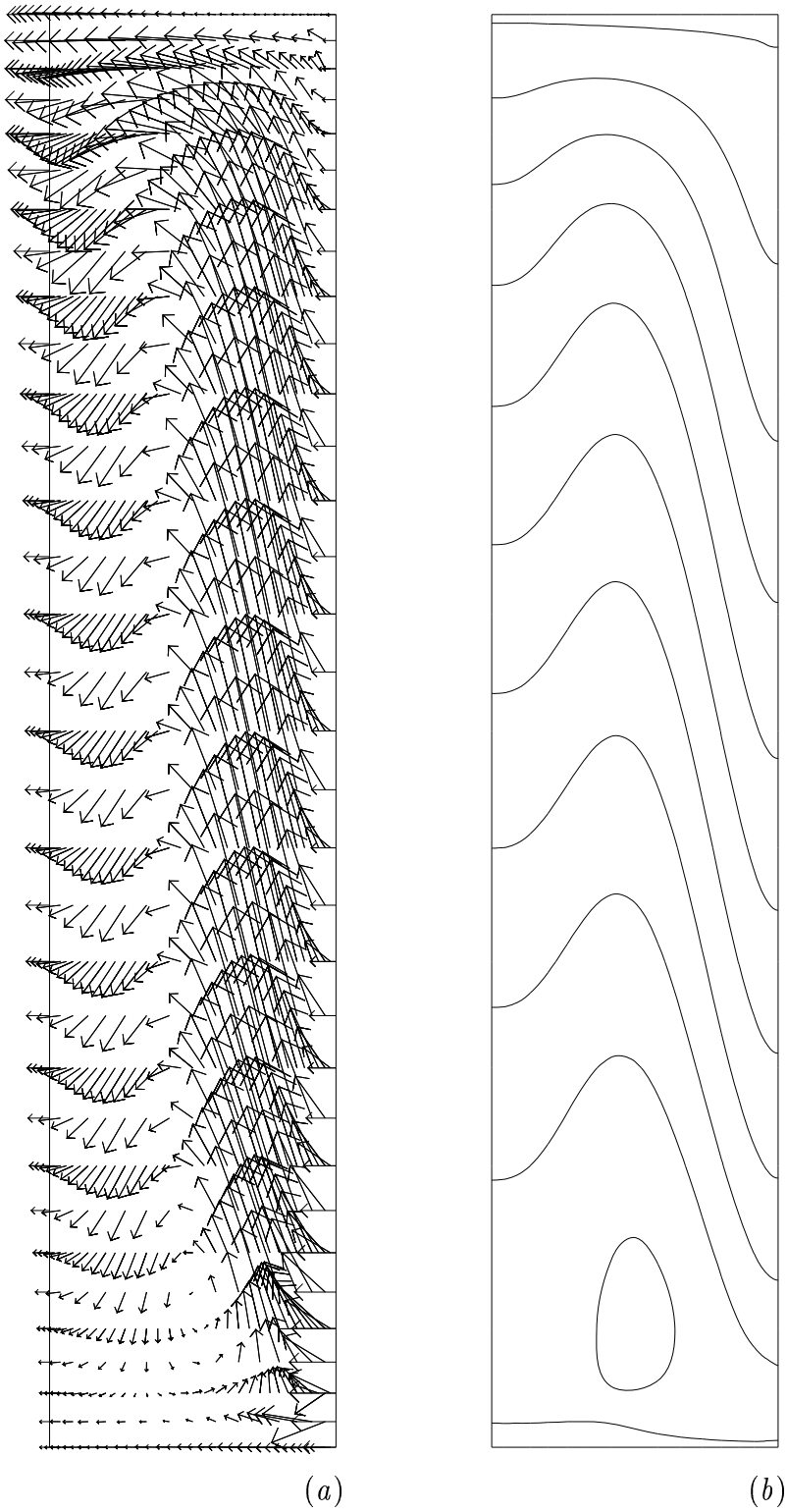

Figure 5.7: Energy transfer in the cavity: (a) energy flux vector, $\mathbf{e}$, and (b) 'heat-lines'.

$\mathcal{A}^{-1}\int_0^{\mathcal{A}} e\|_{x=0}\,\mathrm{d}y$	1.0788
$\mathcal{A}^{-1}\int_0^{\mathcal{A}} e\|_{x=1}\,\mathrm{d}y$	1.0800
$\mathcal{A}^{-1}\int_0^{\mathcal{A}}\int_0^1 e\;\mathrm{d}x\;\mathrm{d}y$	1.0843

Table 5.2: Overall energy transfer rate and test of conservation of energy.

agree with each other to within 0.5%.

The postprocessing for the mass transfer is similar to that for the energy transfer. The details are omitted, though the overall transfer rate can be inferred from equation (2.62) and table 5.1:

$$\begin{aligned}\overline{Sh} &= -\frac{Gr(1+N)Sc}{\Phi}\times\frac{\int_0^{\mathcal{A}}\int_0^1 u\,\mathrm{d}x\,\mathrm{d}y}{\mathcal{A}}\\ &= -\frac{938.7(1+0.5)0.61}{0.69}\times\frac{-0.004252}{5}=1.06.\end{aligned}\tag{5.6}$$

The closeness of the average transfer rates to unity is indicative of both the aptness of the scales chosen in § 2.3.4 and the low degree of convective enhancement with the present parameter values.

5.3 Conclusions on the use of *Fastflo*

The principal advantages of *Fastflo* for this problem are:

- It handles the unusual terms arising from the mass transfer effects.
- It allows the use of alternative solution algorithms.
- The simplicity and generality of the postprocessing procedures allows easy investigation and presentation of the results, including unusual transformations of the results, such as the 'heat-function'.

5.4 The floor and ceiling problems

In the remainder of this chapter, the solution and postprocessing method just developed is used to investigate the floor and ceiling problems.

The understanding of vapour transport across gas-filled enclosures has been hampered by the large number of dimensionless parameters and possible flow regimes. Here, a conduction–diffusion regime is defined by the existence of a fully developed region, for which an analytic solution is available (ch. 4). Numerical solutions demonstrating the existence of the regime for a cavity of finite vertical aspect ratio are presented. The agreement between the numerical and analytic solutions gives mutual validation. The range of parameters over which the regime applies is investigated, with emphasis on the penetration of end-effects into the core. The functional dependence of the overall transfer rates on the vertical aspect ratio is also presented.

First, let us review the relevant literature.

There have been several previous investigations of vapour transport across gas-filled enclosures, as summarized in chapter 3. These studies have produced various formulae for the heat and mass transfer rates, but it is difficult to assess their domain of validity, given the large number of dimensionless governing parameters and the range of possible flow regimes, the principal divisions amongst which arise from the existence of turbulence, multiple cells and/or boundary layers.

A demarcation of regimes for strongly convective flows driven either by heat ($N = 0$) or mass ($N^{-1} = 0$) transfer with vanishingly dilute vapours ($\Phi = 0$) according to the relative magnitudes of the Schmidt, Sc, and (reference) Prandtl, Pr_r, numbers was made by Bejan (1985; § 3.3.5). These results were verified by Béghein et al. (1992; § 3.3.15), but only for values of Sc and Pr_r much larger or smaller than unity. Unfortunately, for gas–vapour mixtures, the diffusivities of momentum, temperature and species are all of similar order of magnitude. Theoretically based formulae for the heat and mass transfer rates have been developed that are valid for Prandtl and Schmidt numbers near, but not necessarily equal

to, unity (McBain 1997*b*; § 3.3.16). These latter formulae are based on a scale analysis appropriate for boundary layer regimes, and so perform poorly for flows where diffusive effects penetrate across the width of the cavity.

In chapter 4, an analytic solution of the system of governing equations was presented that is valid in the narrow cavity limit, $\mathcal{A}$, $\mathcal{S} \to \infty$. This solution is analogous to that of Jones and Furry (1946); i.e. equations (4.35)–(4.38) with $c = 0$; for the single fluid heat transfer problem (defined in § 2.4). Thus, this new solution can be taken to define a 'conduction–diffusion regime' for the nonisothermal vapour transport problem, in the same way that Batchelor (1954) and Eckert and Carlson (1961) defined a conduction regime for the heat transfer problem, as that in which the one-dimensional profiles occur over at least some section of the height of the cavity.

One of the present purposes is to demonstrate numerically that the conduction–diffusion regime can exist in a two-dimensional cavity of finite vertical aspect ratio. Previously the only evidence was the qualitative assertion of Jhaveri et al. (1981) for a case of isothermal mass transfer; $N = \infty$, $Gr = 0$, $Gr(1 + N) = 1.6$, $Sc = 1$, $\Phi = -0.4$ and $\mathcal{A} = 4$; that the flow was essentially one-dimensional, except adjacent to the horizontal walls. Demonstrating the existence of the regime also simultaneously validates the former analytic and present finite element solutions.

A second desirable purpose would be to determine the range of the dimensionless parameters for which the regime exists, but this is difficult for two reasons. Firstly, the large number of governing parameters makes an exhaustive set of numerical experiments prohibitively expensive; there are seven parameters in the present model compared with three for the pure fluid problem: Gr, Pr and $\mathcal{A}$. Secondly, there may be several mechanisms which can lead to the destruction of the regime. According to Daniels (1985), the pure fluid conduction regime can break down in three ways:

- travelling wave instability;
- stationary spanwise roll instability with vertical periodicity; or

- a gradual penetration of convective effects into the core from the ends as the Grashof number increases.

The travelling wave instability, in the pure fluid case, occurs only for large Prandtl numbers so that it should not be relevant for gas–vapour mixtures. The minimum Prandtl number is given as 11.4 by Gershuni and Zhukhovitskii (1976, p. 276), and 12.7 by Bergholz (1978).

A proper consideration of the second mechanism would require reference to the unsteady equations (Cleary 1995*a*); the numerical model developed in §§ 5.1 – 5.3 treats only the stationary forms of the equations. Linear stability analysis of the pure fluid problem predicts the appearance multiple rolls if the Grashof number exceeds a critical value weakly dependent on the Prandtl number. It decreases from its zero Prandtl number limit of 7932 (Korpela, Gözüm & Baxi 1973) to 7349.516 at $Pr = 0.1$, then increases to 8093.723 at $Pr = 0.5$, decreases again to 7848.831 at $Pr = 2.3$ and slowly increases thereafter, the value at $Pr = 10$ being 7870.43 (Ruth 1979). The discrepancy between the theoretical value, 8038, at $Pr = 0.71$ (Korpela et al. 1973) and Hollands and Konicek's (1973) experimental value of 11 000 for air was ascribed by Lee and Korpela (1983) to the stabilizing effect of the slight positive vertical temperature gradient resulting from the finite vertical aspect ratio of the physical cavity. In the absence of knowledge of the effect of Φ, N, Pr_I or Sc on the critical Grashof number, the parameters for this study were chosen so that the combined Grashof number, $Gr(1 + N)$, was considerably less than 8000.

Even if consideration is restricted to the third mechanism, the problem has not yet been solved conclusively even for pure heat transfer. Some authors have asserted that the conduction regime exists below a certain fixed Rayleigh number, giving values between 1500 and 3000 (Vest & Arpaci 1969; Dixon & Probert 1975; Gebhart et al. 1988, p. 730). The analyses of Batchelor (1954), Patterson and Imberger (1980), and Daniels (1985), on the other hand, suggest that the maximum Rayleigh number is proportional to the vertical aspect ratio. The

boundary drawn on the Ra–$\mathcal{A}$ plane by Eckert and Carlson (1961), based on their experimental results, gives a one-third power dependence on $\mathcal{A}$. Though intermediate, this conclusion must be treated with some caution, since the sparsity of the experimental data points allowed Dixon and Probert to draw, just as plausibly, their vertical line.

5.4.1 The fully developed solution

A solution satisfying all of the above equations and conditions (see § 5.1.1) except the velocity boundary conditions on the horizontal surfaces (5.1)–(5.2) and which, if stable, can be expected to apply sufficiently far from these surfaces, is the narrow cavity limiting solution derived in chapter 4, equations (4.23)–(4.24), (4.26)–(4.27).

In two dimensions (x and y), the conduction–diffusion regime is defined as a state of the system in which the limiting solution applies for some values of y.

The constant c depends on the net vertical mass flow rate through the fully developed region, arising from the transversely asymmetric convective mass transfer in the end-zones. In the analogous single fluid heat transfer problem, the net vertical mass flow rate is known (§ 4.4.2) so that there are no undetermined constants in the fully developed solution of Jones and Furry (1946).

The well-known (Gill 1966) centrosymmetry of the analogous single fluid heat transfer problem allows a considerable simplification: an end-zone can be treated as a semi-infinite rectangular strip, with the Jones–Furry solution as a boundary condition at infinity (Batchelor 1954; Daniels 1985; Daniels & Wang 1994). With finite mass transfer rates ($\Phi \neq 0$), the solutions are no longer centrosymmetric so that the advantage of this approach is lost and the domain is here taken as the full cavity. This also avoids the difficulty of truncating an unbounded domain. The *a priori* indeterminacy of c and the loss of centrosymmetry are discussed further once the numerical solutions are presented in the next section.

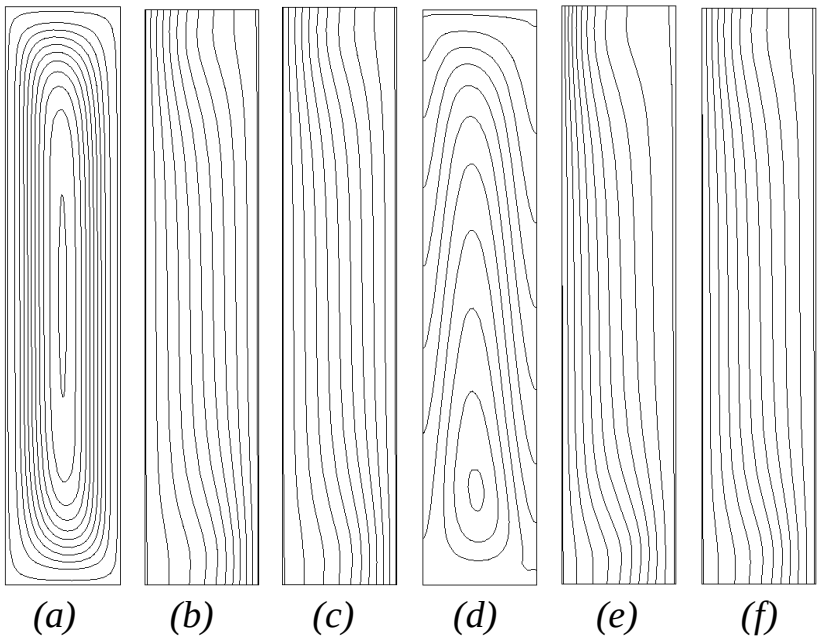

Figure 5.8: Contours of stream-function (a, d), T (b, e) and m (c, f) from two *Fastflo* runs: $\Phi = N = 0$ in $(a$–$c)$ and $\Phi = 0.69$, $N = 0.5$ in $(d$–$f)$. In both runs, $\mathcal{A} = 5$, $Gr(1 + N)Pr_r = 10^3$, $Pr_I = Sc = 0.61$ and $Pr_r = 0.71$.

5.4.2 Numerical solutions

Solutions were obtained by the means described above (§ 5.1). The mesh was that of § 5.1.5 and figure 5.3, except that for the narrowest cavity ($\mathcal{A} = 10$; see fig. 5.10 below), the number of elements in the vertical direction was doubled to 32. The results of two sample runs are plotted in figure 5.8. The first is for the zero mass transfer limit ($\Phi = N = 0$), for which the interfacial velocity (2.59) and interdiffusion energy flux (2.50) vanish. The second uses a rather large value of Φ, 0.69, to vividly illustrate the effects of a finite mass transfer rate.

That the mesh is sufficiently fine was demonstrated by the grid independence tests of § 5.2.1. Further confidence can be derived from the agreement between the finite element and analytic solutions in the fully developed regions (§ 5.5; figs 5.9 – 5.11).

A third check on the accuracy of the solutions was obtained by comparing

the results for several cases with those of the parallel FIDAP (Fluid Dynamics International 1996) solutions of Dr Jonathan Harris (McBain & Harris 1998). The solutions generated by FIDAP and *Fastflo* were found to agree closely. For example, for $\mathcal{A} = 1$, $N = 0.1$, $Pr_r = 0.71$, $Pr_I = Sc = 0.61$, $\Phi = 0.105$ and $Gr(1+N)Pr_r = 10^3$, using similar 12×12 nonuniform meshes of quadratic elements, the integrated mass and energy transfer rates agreed to within 0.6% and 0.02%, respectively.

That Gill's centrosymmetry properties do not apply when transpiration is introduced ($\Phi \neq 0$) is readily apparent in figure 5.8. Compare, for example, the stream-lines (figs 5.8 *a, d*) in the 'departure corners' (top-right and bottom-left). The most pronounced effect of the interfacial velocity in the temperature (e) and mass fraction (f) distributions is the reduction of the gradients normal to the hot wall (right) with a corresponding increase at the cold wall (left). The combined influence of the interdiffusion effect and the variation of specific heat (remembering that these cannot be separated—see § 2.1.3) is most obvious in the dissimilarity of the temperature and mass fraction profiles across the fully developed region (temperature is more curved, since $\Phi_T = 1.49 > \Phi = 0.69$) and the extreme stretching of the isotherms in the top-right corner of figure 5.8 (e): in this region, the mixture is rich in vapour (m large), so that, since $Pr_I > 0$, the effective Prandtl number,

$$Pr_r + Pr_I[1 - \exp(-\Phi)]m,$$

is comparatively high.

One of the most obvious features of figure 5.8 is that in (a), the entire boundary is a stream-line, whereas in (d), stream-lines intersect the vertical walls. Since, in general, a stream-line originating on the right wall does not intersect the left wall at the same height, y, there is a net vertical mass flow through the central portion of the cavity. The horizontal surfaces are impermeable, though, so that in the end-zones the net contribution of mass from the vertical walls at a particular level must be nonzero (positive in the lower portion, and negative above). The

contribution in the fully developed portion vanishes since the horizontal component of velocity there is uniform, by (4.39). The reason for the departure in the end-zones is the shifting of the concentration isopleths by the convection cell. For example, the gradients are clearly steeper in the 'starting corners' (bottom-right and top-left) in figure 5.8 (f). Because the net vertical mass flow rate depends on the turning flow near the ends, no information about it can be gained from the fully developed solution; therefore, c can only be evaluated *a posteriori*.

5.5 The conduction–diffusion regime

That the temperature and mass fraction are practically independent of height near $y = \mathcal{A}/2$ in the examples of figure 5.8 is qualitatively evident. To quantify the extent of the fully developed region, and hence the existence or otherwise of the conduction–diffusion regime, the discrepancies between the finite element solution and the fully developed profiles (4.24)–(4.26), now subscripted with ∞, are introduced:

$$m' = m - m_\infty; \tag{5.7}$$

$$u' = \frac{u - u_\infty}{\max|u|}; \tag{5.8}$$

$$v' = \frac{v - v_\infty}{\max|v|}; \tag{5.9}$$

$$\frac{\partial p'}{\partial y} = \frac{\frac{\partial p}{\partial y} - \frac{\mathrm{d}p_\infty}{\mathrm{d}y}}{\frac{\mathrm{d}p_\infty}{\mathrm{d}y}}; \tag{5.10}$$

$$T' = T - T_\infty. \tag{5.11}$$

$$\tag{5.12}$$

The maxima in the definitions of the velocity component discrepancies, u' (5.8) and v' (5.9) are taken over the nodal values of the *Fastflo* solution.

Determination of the velocity profile, v_∞, from (4.27), requires evaluation of the integration constant c. Here, c was chosen so as to minimize the root-mean-square discrepancy on the mid-height line, $y = \mathcal{A}/2$, using the 32 nodal

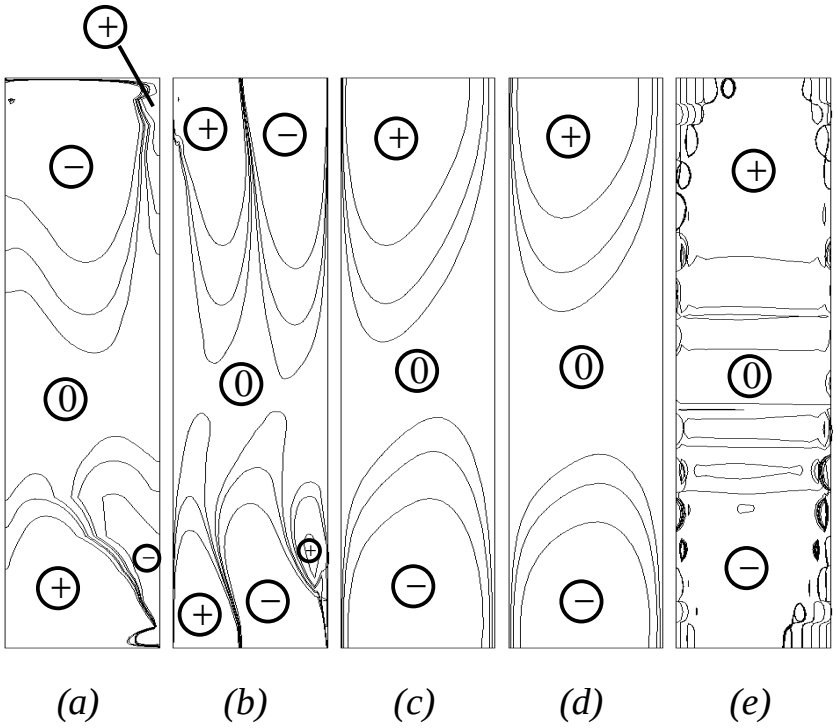

Figure 5.9: Discrepancies between the *Fastflo* and analytic solutions: (a) u', (b) v', (c) T', (d) m' and (e) $\partial p'/\partial y$. Same run as figures 5.8 $(d$–$f)$. Contours shown at $\pm 1, 2$ and 5%, with signs marked by circled symbols.

values. This value of c can then be checked against the numerical vertical pressure gradient via (4.28) and (5.10). Figure 5.9 plots the discrepancies for the same run as figures 5.8 $(d$–$f)$.

The obvious irregularity of the pressure field in figure 5.9 (e) is not unexpected, nor is it necessarily of purely numerical origin. Pressure singularities were anticipated in the corners due to the multivalued boundary condition on u (§ 3.3.3). They do appear to have deleteriously affected large regions of the pressure solution, but the result in the fully developed zone accords with the analytic solution of chapter 4.

Since the discrepancies (5.7)–(5.11) are less than 1% for some continuous horizontal lines in each of figures 5.9 $(a$–$e)$, this set of parameters pertains to the conduction–diffusion regime. The proportion of the height of the cavity between

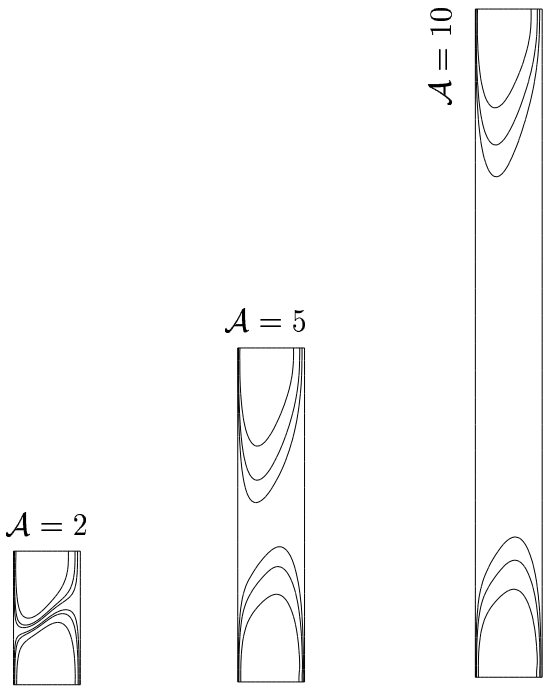

Figure 5.10: The effect of $\mathcal{A}$ on the existence of the conduction-diffusion regime. Temperature discrepancy levels as in figure 5.9 (*c*). Gr, Sc, Pr_r, Pr_I, N and Φ as in figures 5.8 (*d–f*).

the end-zones is small, so that this case is near the limit of the regime. To investigate this, *Fastflo* solutions were obtained for the same set of parameters except for the vertical aspect ratio, $\mathcal{A}$, which was varied. The temperature discrepancy, T', is plotted in figure 5.10. These plots clearly reveal that the conduction–diffusion regime can be destroyed simply by decreasing the vertical aspect ratio—the critical aspect ratio here being somewhere between 2 and 5. The idea, then, that the boundary of the regime could depend simply on a critical combined Grashof or Rayleigh number (based on the cavity width) is false. Another interesting feature of figure 5.10 is the similarity of the end-zones in the cavities of vertical aspect ratio 5 and 10. This suggests that it may be possible to correlate the overall energy transfer rates in a form analogous to that proposed by Batchelor (1954; see also Lee & Korpela 1983) for the conduction regime in the pure fluid problem:

$$\mathcal{A}\overline{Nu} = \mathcal{A}Nu_\infty + f(Gr, Sc, Pr_r, Pr_I, N, \Phi) \tag{5.13}$$

	$\mathcal{A}$		
$Gr(1+N)Pr_r$	2	5	10
100	1.00	1.00	1.00
1000	1.17	1.08	1.04
2000	—	1.08	1.11
5000	—	—	1.32

Table 5.3: Sensible Nusselt numbers, Nu_{sen}, from *Fastflo* runs for $\Phi = 0.69, N = 0.5, Pr_r = 0.71, Pr_I = Sc = 0.61$.

where Nu is a dimensionless energy transfer rate and the overbar denotes an average over $0 < y < \mathcal{A}$. The complete set of average sensible Nusselt numbers from the *Fastflo* runs is given in table 5.3. This validity of this approach was demonstrated in an earlier joint paper (McBain & Harris 1998, fig. 6), using the data of table 5.3 and Dr Harris's FIDAP solutions.

A similar result may be expected to hold for the overall mass transfer rate.

The other principal parameter involved in the determination of the conduction–diffusion regime is the combined Grashof number, $Gr(1+N)$. Figure 5.11 shows how the regime can be destroyed by increasing Gr with all other parameters fixed.

5.6 A possible analytical approach

Daniels's (1985) treatment of the destruction of the conduction regime in the analogous single fluid heat transfer problem focused on the large Prandtl number limit; nevertheless, he outlined, in passing, an approach that might be of value to the present problem: an expansion of the solution in powers of Ra.

This had in fact already been attempted by Batchelor in 1954, though, unfortunately, that analysis is flawed and should be repeated. Batchelor employed 'Grashof's formula' for the approximation of the solution of the biharmonic equation, which the first order stream-function satisfies, and also appears in the

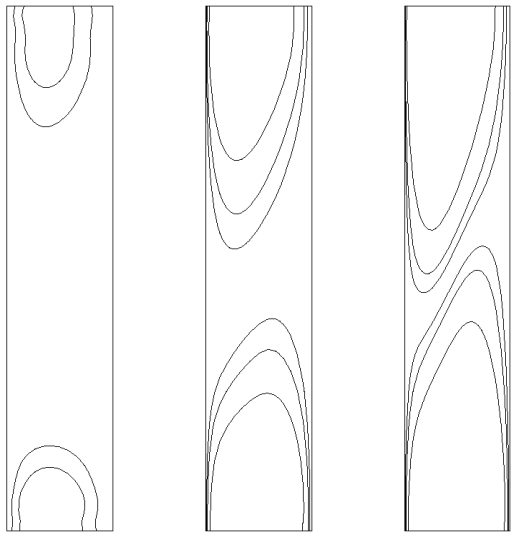

Figure 5.11: Destruction of the conduction-diffusion regime by a gradual penetration of convective effects into the core as the Grashof number increases. $Gr(1+N)Pr_r = (a)$ 100, (b) 1000 and (c) 2000. Temperature discrepancy contours, levels as in figure 5.9 (c). $Sc, Pr_r, Pr_I, N, \mathcal{A}$ and Φ as in figures 5.8 $(d$–$f)$.

theory of elasticity. He adduces Love (1944) for this, saying that it is applicable for $\mathcal{A}$ 'not too different from unity'. Love (1944, p. 495), however, writes that 'the formula, though devoid of theoretical foundation, has often been treated with respect... it will be seen that Grashof's formula leads to a serious over-estimate of the strength of a plate which is at all nearly square'. Since it is possible to obtain solutions for this equation to any desired degree of accuracy (see Love 1944, or the references given by Daniels 1985), there would not seem to be any need to persist with Grashof's approximation.

A very similar problem was solved by Cormack, Leal and Imberger (1974): the single fluid heat transfer problem at low vertical aspect ratio and Rayleigh number. The techniques applied there would require hardly any modification to be used for the large $\mathcal{A}$ problem.

The extension to the nonisothermal vapour transport problem would entail a double expansion in powers of Ra; or, equivalently Gr or $Gr(1+N)$; and the

mass transfer rate factor, Φ. Note that the first order approximations will be independent (i.e. simply additive) whereas cross-effects will enter at higher orders (Van Dyke 1964, p. 35). I certainly recommend this approach to the problem as worthy of future investigation.

5.7 Conclusions

The conduction–diffusion regime has been defined as a stationary state of the system for which the profiles of velocity, temperature, mass fraction and pressure gradient are one-dimensional over some section of the height. The existence of the regime in a two-dimensional cavity has been demonstrated, simultaneously validating the numerical and analytic solutions.

In the regime, the size of the end-zone relative to the cavity width appears to be independent of the aspect ratio, suggesting a simplification of the functional form of the overall heat and mass transfer rates. If the combined Grashof number is sufficiently large (the required value increasing with vertical aspect ratio) the regime is destroyed by penetration of convective effects from the end-zones into the core.

Chapter 6

A Rational Approximation for Low Mass Transfer Rates

IT MUST be stressed that the value of the mass transfer rate factor ($\Phi = 0.69$) employed in chapter 5 was much larger than those values likely to be encountered in air–water vapour systems at ordinary temperatures. It was chosen large so as to show more clearly the effects of mass transfer (enthalpy interdiffusion and transpiration); to show that the numerical method was capable of handling these; and to show that the narrow cavity limiting solution (ch. 4) could apply—and, therefore, the conduction–diffusion regime exist—at a high mass transfer rates.

Indeed, in the experiments of McBain, Suehrcke & Harris (unpub.) on the evaporation of free water into air at 20–40°C and 75% relative humidity, Φ did not exceed 0.012. Given the not inconsiderable difficulty added to the solution of vapour transport problems by the interdiffusion energy flux and the transpiration boundary condition (§ 5.1), and noting that both of these effects vanish with Φ, there is much motivation for constructing an approximation for low mass transfer rates. This is the task of the present chapter.

A rational approximation is one that is exact in some limit (Van Dyke 1964, pp 2–3). The limit considered here is, of course, small Φ. The superiority of this approach over the dropping, however intuitive or judicious, of 'negligible' terms

should be obvious; in particular, the accuracy of a rational approximation can always be investigated by examining more terms in the asymptotic expansion.

Several irrational approximations for vapour transport have already been uncovered in the literature:

- allowing the mixture specific heat capacity to vary with composition in the bulk advective energy flux, $\mathbf{e}_{adv}$, but neglecting the interdiffusion flux, $\mathbf{e}_{int}$, (§ 2.1.3);
- neglecting inertial terms in the momentum equation while retaining the advective flux of vapour, $\mathbf{n}_{adv}$, (§ 3.2.2);
- including transpiration but not interdiffusion (§ 3.3.8);

and it was shown what inconsistencies they can lead to. Actually even these approximations could be considered as rational, as each would become exact in the large Schmidt number limit. Since, however, this is not a physically appropriate approximation for gas–vapour mixtures, and since this was unlikely to have been the intention of the authors, the above distinction seems apt.

There are other possibilities for the small parameter with which to characterize low mass transfer rates, such as the maximum vapour mass fraction or Spalding's (1960) driving force for mass transfer,

$$B \equiv \mathrm{e}^{-\Phi} - 1 \equiv \frac{-\Delta m_*}{1 - m_{*r}}. \tag{6.1}$$

Although in many ways equivalent, the present choice possesses several advantages over these, as will be demonstrated.

6.1 Implications of the narrow cavity limit

The narrow cavity limiting solution (ch. 4) is used to investigate the effect of a finite mass transfer rate factor on the overall vapour and energy transport rates. A similarity in the form of the results to those of 'film theory' suggests an extension of the results to arbitrary aspect ratios.

6.1.1 Utility of the narrow cavity limit

The narrow cavity limit is useful here for two reasons.

Firstly, while some numerical studies (e.g. Weaver & Viskanta 1991*b*; Rosenberger et al. 1997) have included the transpiration boundary condition and the interdiffusion energy flux, there has been no attempt to quantify their influence on the overall transfer rates. This is not surprising, since even for plane laminar steady constant-property flow, the problem depends on eight dimensionless parameters. However, for the narrow cavity limit, the effects are precisely quantified.

Secondly, the concept of a narrow vertical air space is a very practical one. It has long been known (Batchelor 1954) that including an air cavity within a building wall is an economical means of reducing its thermal conductance, and the thickness of the air space is the parameter over which the designer has the most control. The importance of the narrowness of the space is that although the rate of radiative transfer is almost independent of it, if 'the product of the temperature difference (in degrees Fahrenheit) and the cube of the space thickness (in inches) is less than 3 [$3°\mathrm{F.in}^3 \approx 3 \times 10^{-5}\,\mathrm{K.m}^3$]... convection is practically suppressed' (ASHRAE 1993, p. 20.7). This equates to about 1 cm wall separation for a 30 K temperature difference, or with the properties of dry air at 20°C, a Grashof number, Gr, of about 4000—about half the critical Grashof number usually (§ 5.4) associated with the transition to multicellular convection. Given the strong dependency of Gr on the space thickness, b, though, the ASHRAE rule of thumb represents a reasonable margin of safety. The suppression of convection also depends on the height of the cavity (§ 5.5), and a proper assessment of the strength of convection should also take into account the buoyancy force due to gradients in humidity (Wee et al. 1989). The narrow cavity limit is useful as it provides an upper bound on the thermal resistivity.

6.1.2 The narrow cavity and 'film theory'

In the narrow cavity limit, the wall fluxes of vapour and sensible and latent energy are:

$$Sh_\infty = 1; \tag{6.2}$$

$$Nu_{sen,\infty} = 1; \tag{6.3}$$

$$Nu_{lat,\infty} = \left(1 - \mathrm{e}^{-\Phi_T}\right) \Lambda, \tag{6.4}$$

or, in dimensional terms:

$$\left.\begin{array}{rcccccc} -\hat{\boldsymbol{\imath}} \cdot \mathbf{n}_{*,\infty} & = & \rho & \frac{D}{b} & \left(1 - \mathrm{e}^{-\Phi}\right) & \frac{\Phi}{1-\mathrm{e}^{-\Phi}} \\ -\hat{\boldsymbol{\imath}} \cdot \mathbf{e}_{*,sen,\infty} & = & & \frac{\lambda}{b} & \Delta T_* & \frac{\Phi_T}{1-\mathrm{e}^{-\Phi_T}} \\ -\hat{\boldsymbol{\imath}} \cdot \mathbf{e}_{*,lat,\infty} & = & \rho h_{fg} & \frac{D}{b} & \left(1 - \mathrm{e}^{-\Phi}\right) & \frac{\Phi}{1-\mathrm{e}^{-\Phi}} \end{array}\right\}. \tag{6.5}$$

There is a striking similarity between these three fluxes: each being the product of a specific capacity, a conductance, a driving force and a mass transfer correction factor. The factor $[1 - \exp(-\Phi)]$ is Spalding's driving force for mass transfer, $-B$ (see equation 6.1). These expressions are formally identical to those arising from the 'film theory' of simultaneous heat and mass transfer between a bulk fluid and a surface developed by Colburn and Drew (1937) and refined by Bird et al. (1960, ch. 21), except that there the conductances are unknown functions of the flow field, considered to be the ratio of a conductivity (D or λ) and the 'film thickness'. Here, the fictitious film thickness is simply the width of the air-space, b. It is interesting to note that the associated mass fraction (4.24) and temperature (4.26) profiles are also generally fictitious, but that here they are exactly realized.

This formal similarity suggests a means of extending the range of validity of the analysis to cavities that are not narrow. The film theory approximately separates the effects of the bulk flow field and interfacial mass transfer. The former is lumped into the conductances, or film thicknesses, while the latter is given by corrections of the form

$$\frac{\Phi}{1 - \exp(-\Phi)} \equiv \frac{\Phi}{-B}. \tag{6.6}$$

The film theory has been used successfully in the study of both laminar boundary layers and fully turbulent systems with simultaneous heat and mass transfer (Sherwood & Pigford 1952, ch. 4). Thus, even if the conditions for the narrow cavity solution are not met, so that the film thickness differs from the cavity width, the relative effects of interfacial velocity and interdiffusion may still be assessable from the same mass transfer rate factors.

Rather than being continually encumbered with the mass transfer rate correction factors, however, it would seem to be much simpler to combine these into the driving forces; i.e. for the vapour transport, to use Φ instead of Spalding's B, and for energy transport, to use $\Delta T_* \Phi_T / [1 - \exp(-\Phi_T)]$, instead of the temperature difference, ΔT_*. This is precisely what was done in nondimensionalizing the vapour and energy fluxes in § 2.3.1.

The intended result is that the Sherwood and (sensible) Nusselt numbers should be much less dependent on Φ. This was perfectly achieved in the narrow cavity limit (§ 4.4.1).

6.1.3 Transport rate dependence on Φ

To test the dependence of the overall vapour and energy transport rates on the mass transfer rate factor, a series of *Fastflo* solutions were obtained for a square cavity ($\mathcal{A} = 1$) by the method described in chapter 5. The mass transfer rate factor was varied from 0.105 to 0.693. All other parameters were kept constant, except the buoyancy ratio, N, which, like B, is proportional to the mass fraction difference, Δm_*, for fixed reference mass fraction level, m_{*r}. The overall transport rates are listed in tables 6.1 – 6.2. The mass transfer rate correction factors are also listed in the second last column of each table.

It will be noticed that the mean Sherwood and Nusselt numbers vary by less than 0.8% and 1.3%, respectively, in spite of the fact that the mass transfer rate correction factors vary by 31% and 73%. The variability in the predicted Sherwood and Nusselt numbers is close to the limits of accuracy of the numerical

Φ	$\frac{\Phi}{1-\exp(-\Phi)}$	$\overline{Sh}$
0.105	1.054	1.088
0.223	1.116	1.087
0.693	1.386	1.080

Table 6.1: Dependence of overall vapour transport rate on Φ. Mean Sherwood numbers from *Fastflo* runs for $\mathcal{A} = 1, Pr_r = 0.71, Pr_I = Sc = 0.61, Gr(1 + N)Pr_r = 10^3, N = 1 - \exp(-\Phi)$.

Φ	Φ_T	$\frac{\Phi_T}{1-\exp(-\Phi_T)}$	$\overline{Nu}_{sen}$
0.105	0.228	1.118	1.122
0.223	0.483	1.261	1.124
0.693	1.500	1.931	1.11

Table 6.2: Dependence of overall energy transport rate on Φ. Mean sensible Nusselt numbers from same the *Fastflo* runs as table 6.1.

solutions and may also be affected by the changes in the buoyancy ratio, N, though this parameter generally has little effect on the transport rates at these Schmidt and Prandtl numbers if $Gr(1+N)$ is fixed (McBain 1995, 1997*b*; § 3.3.16).

The corresponding wide variation in the mass transfer rate correction factors is exactly reflected in the dimensional transport rates; thus, this series of runs strongly supports the contention (§ 6.1.2) that the present nondimensionalization of the vapour and energy fluxes accounts for the effect of the mass transfer rate factor, Φ.

The energy transfer results (table 6.2) may be compared with de Vahl Davis's (1983) bench-mark solution for the analogous single fluid heat transfer problem ($\Phi = N = 0, \mathcal{A} = 1, Pr_r \equiv Pr = 0.71, Gr(1 + N)Pr \equiv Ra = 10^3$). He estimated $Nu = 1.118 \pm 0.001$, which lies within 1% of each of the three present results for finite Φ.

Another example of the effect of Φ is provided by the numerical solutions of Markham and Rosenberger (1980; § 3.2.3) and Greenwell et al. (1981; § 3.2.4) for

isothermal vapour transport in cylinders. Both studies found that moderately large values of Φ (1.0 and 0.944) led to strong radial variations in the vapour transport, but had no discernible effect on the mean Sherwood number.

The results of this section suggest that in order to calculate the overall vapour and (sensible) energy transport rates it may be possible to use a solution with a different value of Φ; in particular, one with $\Phi = 0$. The latent energy transport rate can then be immediately calculated from the Sherwood number and (2.68). This, of course, has great computational advantages: the transpiration boundary condition (2.59) becomes trivially homogeneous, the mixture specific heat capacity in the advective energy flux (2.49) becomes constant, and the interdiffusion flux (2.50) vanishes. The last two changes greatly simplify the energy equation (2.55), which then takes on the form (2.70).

This procedure is not exact. The mass transfer rate factor, Φ, does appear in the governing equations and cannot be completely dismissed as a parameter. Deviations from the mass transfer rate correction factors predicted by film theory have been noted for the forced convection laminar boundary layer by Bird et al. (1960, pp. 672–6), Spalding (1963, pp. 148–51) and Rosner (1966). These errors are small, however, unless the mass transfer rate is high, and vanish as $\Phi \to 0$. The use of Φ as the driving force is certainly expected to be superior to its alternatives, but the primary purpose of the present chapter is the formulation of a simplifying approximation for small values of Φ; any degree of accuracy at high values should be regarded as a bonus.

If, as is the case in the growth of crystals from the vapour, the local values of Sh are important, rather than just their mean, solution of the full equations is certainly indicated. Even in this case, though, the low mass transfer rate approximation may be useful for understanding qualitative features of the flow, particularly those due to buoyancy, and as a good initial guess for iterative solution procedures. Being rational, it could also be taken as the zeroth term in an asymptotic expansion.

6.2 A rational approximation for low mass transfer rates

In the field equations, Φ enters only in the energy equation in the factor $[1 - \exp(-\Phi)]$, which has the Maclaurin series

$$1 - \mathrm{e}^{-\Phi} \equiv -B = \sum_{n=1}^{\infty} \frac{(-1)^{n+1}\Phi^n}{n!} \qquad (|\Phi| < \infty) \tag{6.7}$$

and vanishes like $O(\Phi)$.

From its definition (2.33), it is clear that for $m_{*r} < 1$, Φ only vanishes when the vapour mass fraction difference, Δm_*, does. If this difference were zero, the buoyancy ratio, N, would be too. Note that N can be expressed

$$N \equiv \frac{\zeta \Delta m_*}{\beta \Delta T_*} \tag{6.8}$$

$$= \frac{1 - \mathrm{e}^{-\Phi}}{[\beta/\zeta(1 - m_{*r})]\Delta T_*} \tag{6.9}$$

$$\sim \frac{\Phi}{[\beta/\zeta(1 - m_{*r})]\Delta T_*}[1 + O(\Phi)] \qquad (\Phi \to 0). \tag{6.10}$$

It would be inappropriate to require N to vanish in the low mass transfer rate limit, however, since it is inversely proportional to temperature difference, ΔT_*. In applying the Boussinesq approximation in chapter 2, $\beta \Delta T_*$ was assumed to be a small quantity. Moreover, in applications, there will often be a direct link between the temperature difference and the mass fraction difference, and so the mass transfer rate factor. In physical vapour transport, for example, the vapour mass fraction difference is created by differentially heating two opposing surfaces of pure solidified vapour (Jhaveri & Rosenberger 1982). Indeed, quite generally, the partial pressure of the vapour over the condensed phase will increase with temperature, as may be quantified by Clapeyron's relation (Guggenheim 1959, p. 148). Consider, for example, an ideal saturated mixture: the limiting value of the buoyancy ratio is (Close & Sheridan 1989)

$$\lim_{\Delta T_* \to 0} N = \frac{m_*(M_B - M_A)h_{fg}}{\Re T_*}, \tag{6.11}$$

where $\Re$ is the universal gas constant and M_A and M_B are the molar masses of the vapour and gas, respectively. This limit is finite; substituting in the properties of air and water vapour at 30°C, for example, gives a limiting value of N of 0.28, which is hardly negligible compared to unity.

In the unsaturated case there is no such general relation between Φ and ΔT_*. Nevertheless, the buoyancy ratio, and any other terms containing a similar ratio of Φ and ΔT_* should not be eliminated in the low mass transfer rate limit.

Another example is furnished by the product $\Lambda\Phi_T$, appearing in the expression for the latent Nusselt number (2.68). It can be expressed (cf. equation 4.32) as

$$\Lambda\Phi_T = \frac{\Phi}{(\lambda/\rho D h_{fg})\Delta T_*}, \tag{6.12}$$

or

$$\Lambda\Phi_T = \frac{Pr_r}{Sc}\frac{\Phi}{c_{pr}\Delta T_*/h_{fg}}, \tag{6.13}$$

which shows that, by the rule established above, Nu_{lat} should be retained in the low mass transfer rate limit. To take a numerical example, for humid air at 30°C, $h_{fg}/c_{pr} \approx 2400\,\mathrm{K}$, which will make the denominator of (6.13) small indeed.

In summary, the rational approximation for low mass transfer rates is obtained by taking the limit $\Phi \to 0$ with

$$\frac{\Delta T_*}{\zeta(1-m_{*r})/\beta} = O(\Phi) \tag{6.14}$$

$$\frac{\Delta T_*}{Pr_r\ h_{fg}/(Sc\ c_{pr})} = O(\Phi). \tag{6.15}$$

6.2.1 The low mass transfer rate equations

Under the approximation defined above, the system (2.52)–(2.55) becomes to order O(1)

$$\boldsymbol{\nabla}\cdot\mathbf{u} = 0 \tag{6.16}$$

$$Gr(1+N)Sc\ \mathbf{u}\cdot\boldsymbol{\nabla}m = \nabla^2 m \tag{6.17}$$

$$Gr(1+N)\mathbf{u}\cdot\boldsymbol{\nabla}\mathbf{u}+\mathcal{A}\boldsymbol{\nabla}p-\frac{T+Nm}{1+N}\hat{\boldsymbol{\jmath}} = \boldsymbol{\nabla}^2\mathbf{u} \tag{6.18}$$

$$Gr(1+N)Pr_r\mathbf{u}\cdot\boldsymbol{\nabla}T = \nabla^2 T, \tag{6.19}$$

the transpiration boundary condition (2.59) is replaced by

$$\hat{\boldsymbol{n}}\cdot\mathbf{u}=0 \tag{6.20}$$

at the interfaces, and the equations for the Sherwood and Nusselt numbers become:

$$Sh = \hat{\boldsymbol{\imath}}\cdot\boldsymbol{\nabla}m; \tag{6.21}$$

$$Nu_{sen} = \hat{\boldsymbol{\imath}}\cdot\boldsymbol{\nabla}T; \quad \text{and} \tag{6.22}$$

$$Nu_{lat} = [1-\exp(-\Phi_T)]\Lambda Sh. \tag{6.23}$$

To the order of the approximation, the factor in brackets in (6.23) can be replaced by Φ_T; here the stated form is retained, however, as it is exact.

Equation (6.21) is not quite the same as the one recommended in elementary mass transfer textbooks (e.g. Incropera & DeWitt 1990, p. 348). The right hand side is the same, and is also formally identical to the usual expression for the Nusselt number in single fluid heat transfer problems (Incropera & DeWitt 1990, p. 347; § 2.4), but the left hand side uses for the driving force not the mass fraction difference, Δm_*, but the mass transfer rate factor, Φ.

Similarly, the sensible Nusselt number retains its earlier definition (2.64), which incorporates the mass transfer rate correction factor. Note that

$$\lim_{\Phi\to 0}\frac{\Phi_T\Delta T_*}{1-\exp(-\Phi_T)}=\Delta T_*; \tag{6.24}$$

so that the low mass transfer rate Nusselt number (6.22) is correct for zero mass transfer rates; i.e. in homogeneous fluids.

The key to the success of the results of § 6.1.3 is that the definitions from chapter 2 of the Sherwood and Nusselt numbers are used for both general mass transfer rates (e.g. chapters 4 and 5) and low mass transfer rates.

6.2.2 Other low mass transfer rate limits

If, following Spalding (1960, 1963), B had been used as the small parameter in the low mass transfer rate limit, the set of governing equations (6.16)–(6.19) would have been identical, since $-B \sim \Phi + O(\Phi^2)$ as $\Phi \to 0$, by (6.7). The equations of chapter 2 could also have been written more compactly, since Φ more often appears there in the form (6.1). Then, however, B would have been the driving force in the definition of the Sherwood number (Spalding 1963, p. 38).

In either low mass transfer rate limit, the narrow cavity mass fraction profile would be given by (4.34), and so the Sherwood number (6.21) would have the value unity. If the dimensional vapour transport rate were to be calculated from this, with B as the driving force, the result would be

$$-\hat{\boldsymbol{\imath}} \cdot \mathbf{n}_{*,\infty} = -\frac{\rho D}{b} B. \tag{6.25}$$

Successive approximations would add further terms in the (absolutely convergent) asymptotic series

$$-\hat{\boldsymbol{\imath}} \cdot \mathbf{n}_{*,\infty} = \frac{\rho D}{b} \sum_{n=1}^{\infty} \frac{(-B)^n}{n}, \tag{6.26}$$

but this is simply (6.5), since the series is just the Maclaurin expansion for Φ in terms of B. Thus, using Φ instead of B leads to one of those happy instances of the telescoping of terms of an asymptotic series by transformation of the perturbation quantity (for other examples, see Van Dyke 1975, pp. 22–3, 244); in this case an infinity of terms becomes one. The practical benefit of the collapse of the series is that described in § 6.1.2: the first approximation, i.e. that obtained from the solution of the low mass transfer limit equations (6.16)–(6.19), is either exact, in the narrow cavity limit, or very close to it, for the square cavity cases considered in § 6.1.3. If B had been used, the first term would have differed by the mass transfer rate correction factor (6.6).

Another advantage of Φ over B is its symmetry properties. Recall the transformation of § 2.6.3. The condition for invariance on the mass transfer rate factor

was

$$\tilde{\Phi} = -\Phi \tag{6.27}$$

or

$$\tilde{B} = \frac{-B}{B+1}. \tag{6.28}$$

Since this transformation is merely that of looking at the cavity from behind rather than from in front, the simple odd parity of the mass transfer rate factor seems more satisfying than the more complicated (6.28). Associated with this is the fact that the physically significant range of B is $(-1, \infty)$, whereas $-\infty < \Phi < \infty$. In general, for equal but opposite values of Φ, similar but reversed behaviour can be expected; whereas positive and negative values of B must be compared with (6.28) in mind. Further, one would quite naturally expect the dimensional mass transfer rate to be an odd function of its driving force, and this is the case if Φ is used; however, inspection of (6.26) shows that B fails this test for the narrow cavity limit. The simplest function of B with the required parity properties is $\ln(1+B) \equiv -\Phi$.

The energy transfer rate is not an odd function of the driving force implicit in the definition of the Nusselt number (2.64), although it is an odd function of the temperature difference. The chosen form of the Nusselt number is preferred in spite of this because of its reduced dependence on Φ_T (§ 6.1.3).

In a brief remark on page 156 of his book, Spalding (1963) came close to questioning the utility of his driving force, B, noting in particular the fact that the ratio of the dimensional mass transfer rate to B, i.e. the 'conductance' or 'mass transfer coefficient', depended on B. On page 159, the use of Φ is mentioned as a simplifying alternative. This option has been wholly adopted in the present work.

If the mass fraction difference were employed instead of Φ or B, it would be very difficult to calculate the higher approximations, since the transpiration boundary condition cannot be written in terms of it alone; the reference mass fraction, m_{*r}, is also required. Consider, for example, (2.59) for the simple case

$m = 0$,

$$\hat{\boldsymbol{n}} \cdot \mathbf{u} = \frac{-\left(1 - \mathrm{e}^{-\Phi}\right)}{Gr(1+N)Sc} \hat{\boldsymbol{n}} \cdot \boldsymbol{\nabla} m = \frac{-\Delta m_*}{Gr(1+N)Sc(1-m_{*r})} \hat{\boldsymbol{n}} \cdot \boldsymbol{\nabla} m. \tag{6.29}$$

The mass transfer rate factor, Φ, can be developed in a double power series:

$$\Phi = \Delta m_* + m_{*r} \Delta m_* + (\Delta m_*)^2 + \text{h.o.t.}; \tag{6.30}$$

thus, if $\Delta m_* \to 0$ and $m_{*r} \to 0$, then $\Phi \sim \Delta m_* + O((\Delta m_*)^2 + m_{*r} \Delta m_*)$. In other words, the mass fraction difference is an acceptable approximation for the driving force only if it and the reference mass fraction level are small; i.e. if the vapour is everywhere dilute. Using Δm_* as driving force in the Sherwood number, the calculated dimensional vapour transport rate would vary by the factor,

$$\frac{\Phi}{(1 - m_{*r})\left(1 - \mathrm{e}^{-\Phi}\right)}, \tag{6.31}$$

or the same mass transfer correction factor encountered for B increased by the factor $(1 - m_{*r})^{-1}$. Further disadvantages of the use of the mass fraction difference are discussed by Spalding (1963, p. 66 f.). The most serious problem here is that in order to obtain higher approximations, the reference mass fraction level must be introduced as a extra parameter.

These fairly obvious considerations notwithstanding, many authors have employed the mass fraction difference as the driving force for mass transfer (e.g. Rohsenhow & Choi 1961, p. 385; Bejan 1985; Prata & Sparrow 1985; Nunez & Sparrow 1988; McBain 1995, 1997*b*).

6.3 Conclusions

In this chapter, I have presented a limiting form of the basic equations of vapour transport that should accurately model the full system for low mass transfer rates. The degree of approximation is quantified by the parameter Φ. The system is considerably simplified, which will allow us to tackle much more difficult problems in the following chapters.

While the reduced system is only designed for use with low mass transfer rates, in the two examples considered—the narrow cavity limit and mild convection in a square cavity—the overall vapour and energy transport rates predicted are in exact and excellent agreement, respectively, with the results of the full model.

It will be noticed that in passing from the full equations to the present limiting form, the interfacial velocity, the variability of the specific heat capacity in the bulk advective energy flux, and the interdiffusive energy flux all vanish together, provided Sc, Pr_r and Pr_I are of order unity, as is typical for gas–vapour mixtures.

Chapter 7

Tall Cavities with Bounded Sections

EXACT solutions of the low mass transfer rate equations are obtained for the fully developed vapour mass fraction, temperature, velocity and pressure gradient in a vertical cavity subject to horizontal heat and mass transfer. The solutions for rectangular sections are in terms of Fourier series, while for elliptic sections a simple polynomial describes the vertical velocity. Uniqueness of the solutions is demonstrated under the restriction that the mass fraction, velocity and temperature fields are independent of height. For a cavity of rectangular section, it is predicted and verified that the flow in the plane of spanwise symmetry is practically independent of the span if this exceeds 1.7 times the width.

7.1 Introduction

In the investigations of vapour transport across cuboids described in previous chapters, it has been assumed that all dependent variables were independent of z (see fig. 2.1 *a* for the geometry and axes), but since the confining walls cannot physically be of infinite horizontal extent, the flow in such a geometry is inherently three-dimensional. This assumption is common to the vast majority of previous

studies of both the present and the analogous single fluid heat transfer problems. This is true not only of analytical (Batchelor 1954) and numerical (Elder 1966) investigations, but also many experimental studies. The two main questions about this assumption are whether or not the flow at any particular location is affected by the presence of the end-walls, and what effect the finite spanwise aspect ratio, $\mathcal{S}$, has on global parameters, such as the overall flow and vapour and energy transport rates.

Nonintrusive techniques for visualizing the density disturbance field, such as the shadowgraph method (Schöpf, Patterson & Brooker 1996), schlieren method (Han & Kuehn 1991) and Mach–Zehnder (Eckert & Carlson 1961) and schlieren (Sernas & Fletcher 1970) interferometry, all involve an integration through the fluid along the path of a light ray. With rare exceptions (Schöpf & Stiller 1997), these rays have been directed horizontally and parallel to the hot and cold walls, leading to images more or less comparable with the results of planar analyses. The problem with this methodology is that such images provide no information on variations along the line of sight, whereas this information is required for their interpretation, e.g. for the back-calculation of the temperature field. The typical remedy is the assumption of uniformity, consistent with the two-dimensional hypothesis.

Some common methods of investigating the flow field, such as thermocouple probes and laser-Doppler and hot wire anemometry do not have this intrinsic planarity, since the measurements are strictly local. Nevertheless, experiments are often set up with large $\mathcal{S}$ and measurements restricted to the plane of spanwise symmetry ($z = 0$). An example of this is the work of Aung, Fletcher and Sernas (1972) on flow in vertical ducts, where $8 < \mathcal{S} < 32$. Though these figures are doubtless large enough for the midplane flow to be independent of $\mathcal{S}$, it is necessary to know the minimum value of $\mathcal{S}$ for which this is true in order to apply the results. Further, at the lower values of $\mathcal{S}$ employed, the end-walls would certainly have reduced the net vertical flow rate. In their study of a fully enclosed flow,

Ozoe et al. (1983) did vary the spanwise location of the point of intersection of the Doppler laser beams, but only within a restricted range about the centre: sufficient to demonstrate local two-dimensionality of the flow, but providing only an upper bound on the domain of influence of the end-walls.

Early investigations of the analogous single fluid heat transfer problem, such as those of Mull and Reiher (described by Jakob 1949, p. 537), focused on measurements of the overall heat transfer rate rather than the flow or temperature fields. After a test in which $\mathcal{S}$ was halved from 25.7 while the other parameters were kept constant resulted in only a 1.3% reduction in the heat transfer coefficient, $\mathcal{S}$ was dropped as a governing dimensionless group. For the laminar boundary layer regime, however, $\mathcal{S}$ must become increasingly important as it decreases, as demonstrated by ElSherniby, Hollands and Raithby (1982) who on halving $\mathcal{S}$ from 15 found a 3% change in the heat transfer coefficient. In the *Handbook of Heat Transfer Fundamentals*, Raithby and Hollands (1985) state that very little information exists on the effect of $\mathcal{S}$ on the overall heat transfer rate for moderate to high $\mathcal{A}$.

No single approach can lead to the complete solution of this problem, since there are several possible flow regimes; depending on the existence of multiple cells, boundary layers and/or turbulence; all of which will interact differently with the end-walls. The purpose of the present chapter is to provide exact answers to these questions for the conduction–diffusion regime; defined in chapter 5, and here generalized to three-dimensions for the low mass transfer rate limit.

There have been several three-dimensional numerical treatments of the analogous single fluid heat transfer problem; the special case of the cube ($\mathcal{A} = \mathcal{S} = 1$) being recently proposed as a bench-mark computational fluid dynamics problem (Leong, Hollands & Brunger 1998, 1999). Most studies have dealt with values of $\mathcal{A}$ near unity (e.g. Viskanta, Kim & Gau 1986; Mallinson 1987; Fusegi, Hyun & Kuwahara 1993). This is probably because the greatest accuracy for a given number of grid points is achieved if the solution domain is a cube, according to

Mallinson and de Vahl Davis (1977), who did treat cases with $\mathcal{A} = 5$, but only for a very few values of the Rayleigh number, Ra, the least value being 10 000. Batchelor's (1954) two-dimensional criterion ($Ra < 500\mathcal{A}$) indicates that a fully developed flow could only be expected in a cavity of this height if the Rayleigh number were less than about 2500, and, indeed, the effects of the horizontal surfaces were felt throughout the height of the cavity.

The only treatment, then, of the effects of the end-walls on a fully developed buoyant flow uncovered in my search of the literature was the recent theoretical study of Bühler (1998). There, however, the fluid is almost ideally thermally and electrically conducting and is subjected to a strong magnetic field, so that the buoyancy force and pressure gradient are mostly balanced by the Lorentz force. Since, under these conditions, viscous effects are only important in boundary layers near the walls, there is little connection between Bühler's work and the present problem.

In this chapter, unique analytic solutions of the governing equations are derived for the fully developed mass fraction, temperature and velocity profiles which satisfy the boundary conditions at the vertical walls, for cavities and ducts of rectangular or elliptic section. These solutions are then analysed to reveal how large $\mathcal{S}$ must be for the plane-flow assumption to be accurate for the central region and to quantify the retarding effect of the end-walls on the vertical flow.

7.1.1 Boundaries of the conduction regime

The boundaries of the conduction regime for plane cavities were discussed in §5.4. Here, the possible effects of a finite spanwise aspect ratio are considered.

An investigation of the three-dimensional stability of the conduction regime flow is beyond the scope of the present project, but since the vorticity in the plane of transverse odd-symmetry—the plane of shear between the rising and falling fluid streams—only decreases with decreasing $\mathcal{S}$ (see §7.6.1), it is expected that the critical Grashof number for instability in any cavity of bounded section

would be larger. This would be analogous with the linear stability analysis of finite rectangular boxes heated from below; Davis (1967) found that as the length of the rolls (i.e. the span of the box) decreased from infinity, the critical Rayleigh number increased. Thus while the conduction regime is somewhat restrictive—Gill and Davey (1969) calculated that the critical temperature difference for a 1 cm air gap is around 40 K, but only 5 K for a 2 cm gap—it may be less so once the third dimension is taken into account.

The importance of treating tall cavities as three-dimensional has been stressed by Chait and Korpela (1989) for another reason. They showed that for air in the $\mathcal{A}, \mathcal{S} \to \infty$ case, the secondary two-dimensional multiple cells are only stable up to $Gr = 8550$, beyond which the flow is no longer restricted to vertical–transverse planes.

7.2 General model

In the low mass transfer rate limit, the field equations are (6.16)–(6.19), and the velocity vanishes on all walls (cf. equation 6.20):

$$\mathbf{u} = \mathbf{0}. \tag{7.1}$$

Since Gill's (1966) centrosymmetry properties are regained in the low mass transfer rate limit, it is convenient to translate the origin of the coordinates to the centroid of the cuboid, and, as in chapter 4, use normalized coordinates (see equation 2.74, fig. 7.1 *b*).

A general thermal boundary condition is:

$$C(T - X) + I\hat{\boldsymbol{n}} \cdot (\boldsymbol{\nabla}_\perp T - \hat{\boldsymbol{\imath}}) = 0 \tag{7.2}$$

where $\hat{\boldsymbol{n}}$ is the unit outward normal, $\hat{\boldsymbol{\imath}}$ is the unit vector in the X-direction and

$$\boldsymbol{\nabla}_\perp \equiv \frac{\partial}{\partial X}\hat{\boldsymbol{\imath}} + \frac{1}{\mathcal{S}}\frac{\partial}{\partial Z}\hat{\boldsymbol{k}} \tag{7.3}$$

is a horizontal gradient operator. C and I are dimensionless scalars defined on the walls, which may vary with position so long as C and I do not both vanish

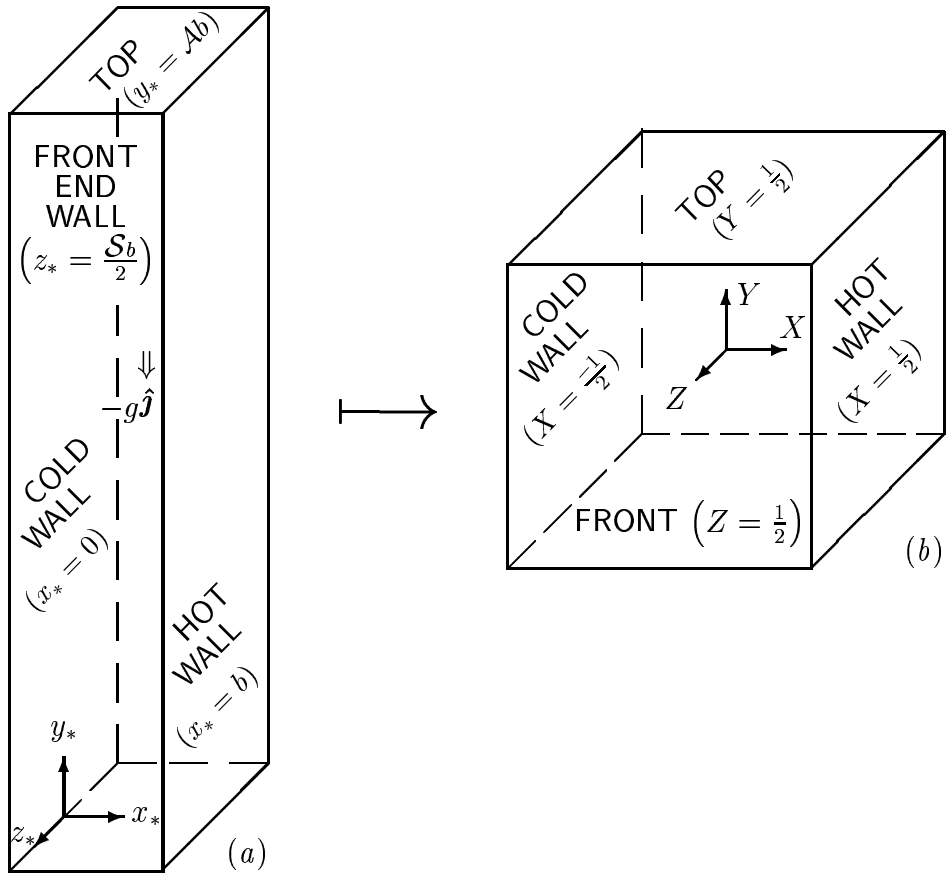

Figure 7.1: Geometry for cavities and ducts of rectangular section, in (a) primitive and (b) central normalized coordinates.

at any point. If $C = 0$ everywhere, the temperature is rendered determinate by the further condition

$$\iiint T \, \mathrm{d}X \, \mathcal{A} \mathrm{d}Y \, \mathcal{S} \, \mathrm{d}Z = 0 \tag{7.4}$$

where the integral extends over the entire domain.

On the end-walls, $I = 0$ leads to a linear temperature variation, while $C = 0$ gives an adiabatic condition. On the hot and cold walls, $C = 0$ implies a uniform heat flux while $I = 0$ gives an isothermal condition. If the solid presumed to be surrounding the fluid has a higher thermal conductivity, $I = 0$ everywhere is a simple and consistent idealization (Batchelor 1954; Leong et al. 1998) , although the condition $I = 0$ on the heated and cooled walls and $C = 0$ on the connecting

walls appears frequently in the literature (Mallinson & de Vahl Davis 1973, 1977; Schladow, Patterson & Street 1989; Fusegi, Hyun & Kuwahara 1991).

A boundary condition for m analogous to (7.2) is:

$$C_m(m - X) + I_m \hat{\boldsymbol{n}} \cdot (\boldsymbol{\nabla}_\perp m - \hat{\boldsymbol{\imath}}) = 0. \tag{7.5}$$

It will be noticed that the reference levels, m_{*r} and T_{*r} are no longer evaluated at the cold wall, but are rather taken as the means.

7.3 Narrow cavities with bounded sections

A solution is sought for the limit $\mathcal{A} \to \infty$; the method is essentially similar to that used in chapter 4 for the narrow cavity limit ($\mathcal{A}, \mathcal{S} \to \infty$), but here $\mathcal{S}$ is allowed to remain arbitrary.

It is convenient to decompose the velocity into horizontal and vertical components:

$$\mathbf{u} \equiv \mathbf{u}_\perp + v\hat{\boldsymbol{\jmath}}. \tag{7.6}$$

In the limit $\mathcal{A} \to \infty$, with Gr, N, Pr, Sc and $\mathcal{S}$ fixed and finite, the equations reduce to:

$$\boldsymbol{\nabla}_\perp \cdot \mathbf{u}_\perp = 0 \tag{7.7}$$

$$Gr(1+N)Sc\ \mathbf{u}_\perp \cdot \boldsymbol{\nabla}_\perp m = \nabla_\perp^2 m \tag{7.8}$$

$$0 = -\frac{\partial p}{\partial X} \tag{7.9}$$

$$Gr(1+N)\ \mathbf{u}_\perp \cdot \boldsymbol{\nabla}_\perp v = -\frac{\partial p}{\partial Y} + \frac{T + Nm}{1+N} + \nabla_\perp^2 v \tag{7.10}$$

$$0 = -\frac{\partial p}{\partial Z} \tag{7.11}$$

$$Gr(1+N)Pr\ \mathbf{u}_\perp \cdot \boldsymbol{\nabla}_\perp T = \nabla_\perp^2 T \tag{7.12}$$

in $\Omega^\square \equiv \{\mathbf{X} : |X| < 1/2, |Z| < 1/2\}$, subject to (7.1), (7.5) and (7.2) on $\partial\Omega^\square$, the boundary of $\Omega^\square$.

There should also be boundary conditions at $Y = \pm 1/2$, corresponding to the floor and ceiling of the cavity, but these cannot be met by the solution of equations

(7.7)–(7.12). As in the narrow cavity limit (ch. 4), the problem is singular in the sense of perturbation theory; the basic solution cannot be uniformly valid over the domain. For very large $\mathcal{A}$, however, the region of nonuniformity should be limited to thin layers near $Y = \pm 1/2$, corresponding to a small proportion of the unscaled cavity in terms of y. The full set of equations (2.52)–(2.55) would have to be solved to obtain the flow in these regions. This restriction is an advantage for the present work, though, as it means that the same fully developed solution will apply to both ducts and cavities. Some distinction between these will be made in § 7.3.3.

Since the horizontal components of the momentum equation (2.54) have degenerated to a statement of the horizontal uniformity of the pressure (equations 7.9 and 7.11), u and w are determined only by the continuity equation (7.7) and the boundary conditions (7.1). An obvious solution is

$$u = w = 0. \tag{7.13}$$

Accepting this solution (uniqueness follows from Theorem 2, p. 164, if the velocity is assumed to be independent of Y), the species (7.8) and energy (7.12) equations reduce to:

$$\nabla_\perp^2 m = 0; \quad \text{and} \tag{7.14}$$

$$\nabla_\perp^2 T = 0. \tag{7.15}$$

The unique solution satisfying these and the boundary conditions (7.2), for all values of C, I, C_m and I_m is

$$m = T = X. \tag{7.16}$$

Substituting this into the vertical momentum equation (7.10) leads to:

$$\nabla_\perp^2 v = \frac{\mathrm{d}p}{\mathrm{d}Y} - X, \tag{7.17}$$

subject to (7.1) on $X = \pm 1/2$ and $Z = \pm 1/2$. This is conveniently decomposed into two simpler Poisson equations by defining the forced and natural contribu-

tions, v_f and v_n, satisfying

$$v_f + v_n = v \tag{7.18}$$

$$\nabla_\perp^2 v_f = \frac{\mathrm{d}p}{\mathrm{d}Y} \tag{7.19}$$

$$\nabla_\perp^2 v_n = -X \tag{7.20}$$

in $\Omega^\square$ and

$$v_f = v_n = 0 \qquad \text{on} \quad \partial\Omega^\square. \tag{7.21}$$

7.3.1 Forced flow

The equation (7.19) for v_f is simply that for fully developed laminar flow in a duct of rectangular section, the solution for which is well known (Dryden, Murnaghan & Bateman 1956, p. 197):

$$\begin{aligned} \frac{v_f}{-\,\mathrm{d}p/\,\mathrm{d}Y} &= \frac{v_f^{\parallel}}{-\,\mathrm{d}p/\,\mathrm{d}Y} \\ &- 4\sum_{k=0}^{\infty} \frac{(-1)^k}{[(2k+1)\pi]^3} \cos[(2k+1)\pi X] \frac{\cosh[(2k+1)\pi\mathcal{S}Z]}{\cosh[(2k+1)\pi\mathcal{S}/2]}, \end{aligned} \tag{7.22}$$

where $v_f^{\parallel}$ is the solution valid for $\mathcal{S} \to \infty$ (Lamb 1932, p. 582):

$$\frac{v_f^{\parallel}}{-\,\mathrm{d}p/\,\mathrm{d}Y} = \frac{1 - 4X^2}{8}. \tag{7.23}$$

7.3.2 Natural flow

Solution of (7.20) requires a particular integral. Two rational choices for this integral can be obtained by considering the asymptotic solutions for large and small $\mathcal{S}$.

The solution valid in the limit $\mathcal{S} \to \infty$ is (cf. equation 4.36):

$$v_n^{\parallel} = \frac{X(1 - 4X^2)}{24}. \tag{7.24}$$

This result, due to Jones and Furry (1946), and used by Batchelor (1954) and many others (Vest & Arpaci 1969; Hart 1971; Gershuni & Zhukhovitskii 1976,

ch. 10; Nagata & Busse 1983; Daniels 1985; Chait & Korpela 1989) in the analysis of narrow cavities, describes the flow between infinite parallel plane vertical walls. It satisfies (7.21) at $X = \pm 1/2$ but not at $Z = \pm 1/2$. The combination $v_f^{\shortparallel} + v_n^{\shortparallel}$ was noted by Aung (1972) as the solution for the transversely heated duct problem with $\mathcal{S} \to \infty$.

The solution of equation (7.20) matching the boundary conditions (7.21) then follows readily from Fourier's method:

$$v_n = v_n^{\shortparallel} + \frac{1}{4\pi^3} \sum_{k=1}^{\infty} \frac{(-1)^k}{k^3} \sin(2k\pi X) \frac{\cosh(2k\pi \mathcal{S} Z)}{\cosh(k\pi \mathcal{S})}. \tag{7.25}$$

The difference $v_n - v_n^{\shortparallel}$ quantifies the effect of the end-walls.

For small $\mathcal{S}$, the geometry approaches that of the flow in the experiments of Hele-Shaw (1898, 1899)—the dominant effect on the flow being from the viscous damping of the end-walls. These experiments were analysed by Stokes (1899) who showed that the general form for the vertical velocity component is:

$$v_n(X, Z) = \mathcal{S}^2 v_n(X, 0) \frac{1 - 4Z^2}{8} \tag{7.26}$$

The function of this form satisfying (7.20) is

$$v_n^{=} = \mathcal{S}^2 \frac{X(1 - 4Z^2)}{8}. \tag{7.27}$$

This function satisfies the boundary conditions (7.21) at $Z = \pm 1/2$, but not those at $X = \pm 1/2$. The corresponding full solution is:

$$v_n = v_n^{=} - \frac{2S^2}{\pi^3} \sum_{k=0}^{\infty} \frac{(-1)^k}{(2k+1)^3} \frac{\sinh[(2k+1)\pi X/\mathcal{S}]}{\sinh[(2k+1)\pi/2\mathcal{S}]} \cos[(2k+1)\pi Z], \tag{7.28}$$

which clearly tends to (7.27) as $\mathcal{S} \to 0$, for fixed X, $|X| < 1/2$. The difference $v_n - v_n^{=}$ quantifies the effect of the hot and cold walls on the Hele-Shaw flow.

Both (7.25) and (7.28) are exact solutions of (7.20) and (7.21), and also; when combined with (7.16), (7.13) and (7.22); the full equation of motion (2.54), for all values of $\mathcal{S} \in (0, \infty)$.

7.3.3 Completely enclosed flows

Since v_n is odd in X, its integral over the section is zero and the only contribution to a net vertical flow rate comes from v_f. If the physical system of finite $\mathcal{A}$, modelled by equations (7.7)–(7.12) when $\mathcal{A}$ is large, has solid surfaces at $y_* = \pm b\mathcal{A}/2$, the net vertical flow rate must vanish to satisfy conservation of mass (2.52) so that:

$$\frac{\mathrm{d}p}{\mathrm{d}Y} = 0; \tag{7.29}$$

$$v_f(X,Z) = 0; \tag{7.30}$$

$$v(X,Z) = v_n(X,Z). \tag{7.31}$$

A similar line of reasoning leads to the conclusion that $\mathrm{d}p/\,\mathrm{d}Y$ is uniform in the case of a duct, where the planes $Y = \pm 1/2$ now represent orifices. Indeed, $\mathrm{d}p/\,\mathrm{d}Y$ is proportional to the net vertical flow rate (Dryden et al. 1956, p. 197).

7.3.4 Numerical evaluation of the solution

Though the solutions (7.22), (7.25) and (7.28) are exact, the ratios of hyperbolic functions appearing in the terms of the infinite series impose a limit on the accuracy of a numerical evaluation. The absolute value of the ratio is bounded by unity but the magnitude of the numerator and *a fortiori* the denominator increase rapidly, so that their values will cause an overflow error if evaluated by a machine with finite floating point arithmetic.

The problem is compounded by the relatively slow convergence of the series. By applying basic inequalities to the terms and using the well-known relation between series and improper integrals (Ramanujan & Thomas 1970, p. 110), the truncation error for v_n using the series (7.25),

$$E_K \equiv v_n - v_n^{\parallel} - \frac{1}{4\pi^3}\sum_{k=1}^{K}\frac{(-1)^k}{k^3}\sin(2k\pi X)\frac{\cosh(2k\pi\mathcal{S}Z)}{\cosh(k\pi\mathcal{S})}, \tag{7.32}$$

can be bounded by:

$$\frac{|E_K|}{\max|v_n^{\parallel}|} \leq \frac{27}{\sqrt{3}\pi^3 K^2}. \tag{7.33}$$

The analyses for equations (7.22) and (7.28) are entirely analogous, and so are omitted.

For example, the ANSI C library function `double cosh(double x)` is only guaranteed not to overflow for `x`< 85.8 (Kernighan & Ritchie 1988, p. 258). For a duct with $\mathcal{S} = 4$, this would limit the number of calculable terms of (7.25) to six, so that, by equation (7.33), the relative error may be as high as 1.4%.

This less than satisfactory situation can be remedied by replacing the ratio of hyperbolic cosines by its asymptotic expansion for large values of the argument in the denominator:

$$\frac{\cosh(2k\pi\mathcal{S}Z)}{\cosh(k\pi\mathcal{S})} \sim \exp[k\pi\mathcal{S}(2|Z|-1)] \qquad (k\pi\mathcal{S} \to \infty) \tag{7.34}$$

but this is not uniform in Z, failing for $Z = O([k\mathcal{S}]^{-1})$, a thin strip about the plane of spanwise symmetry. Thus, this expansion is not useful for automatic computation, but is of physical significance as will become apparent in § 7.4.2.

To overcome the nonuniformity, the exact correction can be added. This gives the identity:

$$\frac{\cosh(2k\pi\mathcal{S}Z)}{\cosh(k\pi\mathcal{S})} \equiv \exp[k\pi\mathcal{S}(2|Z|-1)] + \frac{\mathrm{e}^{-k\pi\mathcal{S}}[\mathrm{e}^{-2k\pi\mathcal{S}|Z|} - \mathrm{e}^{2k\pi\mathcal{S}(|Z|-1)}]}{1+\mathrm{e}^{-2k\pi\mathcal{S}}}. \tag{7.35}$$

Since the absolute value of Z has been used (noting that the hyperbolic cosine ratio is even in Z), the only possible finite floating point arithmetic problem is underflow, which is unlikely to cause problems as the default behaviour of the ANSI C library function `double exp(double x)` is to return zero on underflow (Kernighan & Ritchie 1988, p. 250).

7.3.5 Results for rectangular sections

Contours of the vertical component of velocity due to buoyancy, v_n, calculated using (7.25) and (7.35) are shown in figure 7.2, in the unnormalized coordinates x and z. The curves can be interpreted as either contours of v_n or vortex-lines, since the gradient of velocity in the y-direction is zero (see Theorem 3, p. 166).

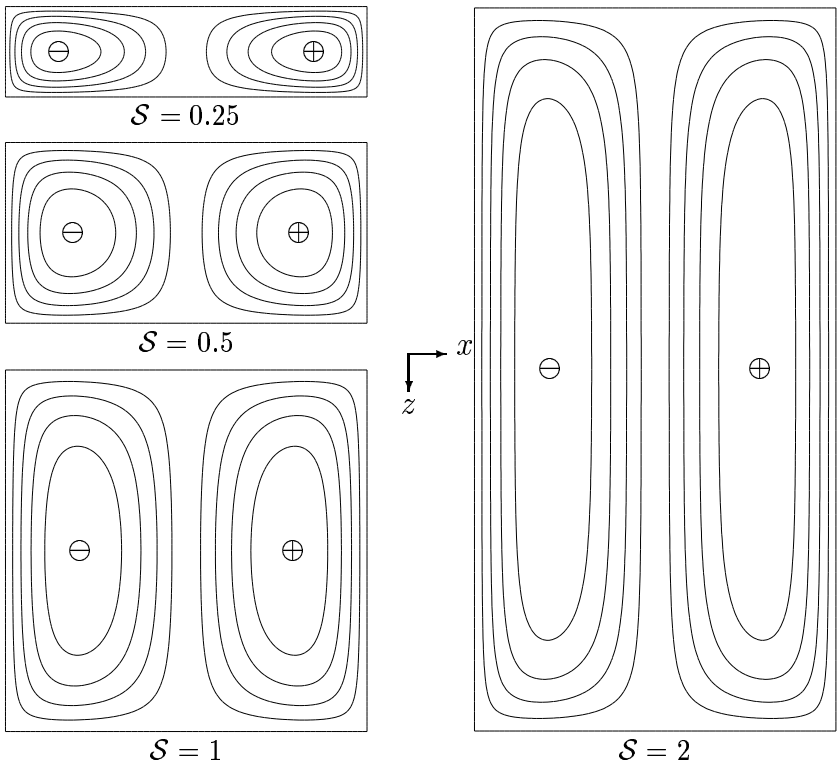

Figure 7.2: Fully developed buoyancy-induced flow in various rectangular sections. Curves can be interpreted as either vortex-lines or contours of the vertical component of velocity with levels at $\pm 20, 40, 60$ and 80% of maximum. $\oplus$ and $\ominus$ mark extrema of v_n (points of zero vorticity).

7.4 Extreme spanwise aspect ratios

While (7.25) and (7.28) are exact solutions of the equations of motion, both are difficult to evaluate numerically for very large or small values of $\mathcal{S}$. There is a physical reason for this which may be explained by analogy with the theory of elasticity.

Consider (7.25) for large $\mathcal{S}$. The problem solved by $v_n - v_n^{\parallel}$ is formally identical to that for the sum of the bending moments about two perpendicular axes in a uniform elastic plate subjected to a distributed bending moment about the edge proportional to $-v_n^{\parallel}$ (Timoshenko & Woinowsky-Krieger 1959, p. 93). The applied moment vanishes along the edges $X = \pm 1/2$ and is odd-symmetric on the edges

$Z = \pm 1/2$. Thus, by Saint-Venant's principle (Love 1944, p. 131), the effects of the applied moment are of negligible magnitude at distances which are large compared with the width of the edges $Z = \pm 1/2$: $1/\mathcal{S}$ in terms of Z. For $\mathcal{S} \gg 2$, then, each end-wall should be sensibly independent of the other's presence. The exact solution (7.25), however, combines the effects of the two.

For small $\mathcal{S}$, Stokes (1899) has pointed out that, for the general Hele-Shaw problem, the velocity field will only differ from the limiting form (7.26) over a distance from obstacles or walls comparable with the wall separation.

In this section, solutions are derived which account for the effect of the nearest short wall first. The basic solutions to be perturbed are (7.24) and (7.27) for large and small $\mathcal{S}$, respectively. Since neither of the basic solutions satisfy the condition (7.21) at all parts of the boundary, both the large and small $\mathcal{S}$ asymptotic expansions are singular perturbation problems.

7.4.1 Small spanwise aspect ratios

For small spanwise aspect ratios,

$$v_n \sim v_n^{=} \qquad (\mathcal{S} \to 0) \tag{7.36}$$

but not uniformly. The region of nonuniformity adjacent to the hot wall, $X = 1/2$, may be treated by the method of matched asymptotic expansions (Van Dyke 1964, ch. 5); i.e. introducing a coordinate there stretched by the factor suggested by Stokes's (1899) estimate of the length scale for the influence of the short walls:

$$\xi = \frac{\frac{1}{2} - X}{\mathcal{S}} = \frac{\frac{b}{2} - x}{\mathcal{S}b}, \tag{7.37}$$

(as illustrated in figure 7.3 *a*) and assuming an asymptotic expansion there of the form:

$$v_n(\xi, Z; \mathcal{S}) \sim \sum_i \Delta_i(\mathcal{S}) \mathcal{V}_i(\xi, Z) \qquad (\mathcal{S} \to 0), \quad (\xi, Z) \quad \text{fixed.} \tag{7.38}$$

The Δ_i form an asymptotic sequence to be determined along with the $\mathcal{V}_i$ in the course of the solution. The series (7.38) is called the *inner* solution.

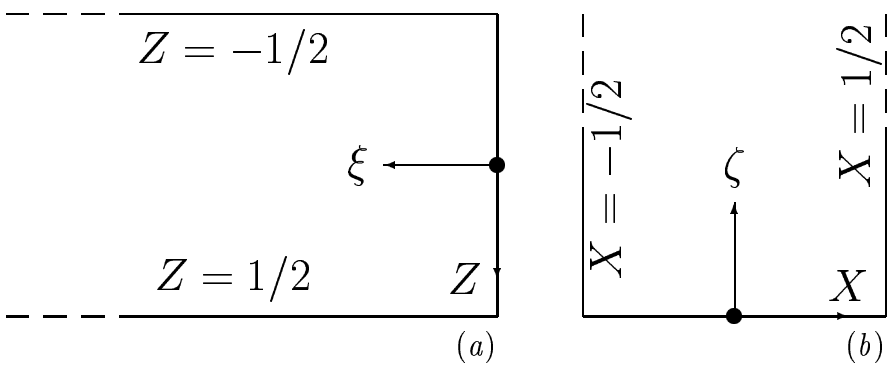

Figure 7.3: The stretched coordinates (a) (ξ, Z) and (b) (X, ζ) for the viscous layers adjacent to the hot wall for small $\mathcal{S}$ and the front wall for large $\mathcal{S}$, respectively.

Any attempt to extend the basic solution, $v_n^=$, in terms of X and Z, to form an *outer* solution with a series

$$v_n(X, Z; \mathcal{S}) \sim v_n^= + \sum_i \delta_i(\mathcal{S}) v_i(X, Z) \tag{7.39}$$

leads to the homogeneous problems

$$\frac{\partial^2 v_i}{\partial Z^2} = 0 \tag{7.40}$$

for which the unique solution satisfying the no-slip conditions at $Z = \pm 1/2$ is

$$v_i = 0 \tag{7.41}$$

regardless of the choice of δ_i. Thus

$$v_n = v_n^= + o(\mathcal{S}^K) \qquad (\mathcal{S} \to 0), \quad (X, Z) \text{ fixed}, \quad \forall K \in \{0, 1, 2, \ldots\}. \tag{7.42}$$

For nondegenerate $\mathcal{V}_1$, choose

$$\Delta_1 = \mathcal{S}^2 \tag{7.43}$$

whence $\mathcal{V}_1$ satisfies

$$\frac{\partial^2 \mathcal{V}_1}{\partial \xi^2} + \frac{\partial^2 \mathcal{V}_1}{\partial Z^2} = -\frac{1}{2} \tag{7.44}$$

subject to

$$\mathcal{V}_1 = 0 \qquad \text{at} \quad \xi = 0 \tag{7.45}$$

$$\mathcal{V}_1 = 0 \qquad \text{at} \quad Z = \pm 1/2 \tag{7.46}$$

and a condition arising from the asymptotic matching process:

$$\mathcal{V}_1 \sim \frac{1-4Z^2}{16} + o(\xi) \qquad (\xi \to \infty). \tag{7.47}$$

Noticing that the limiting form (7.47) satisfies the field equation (7.44) and the boundary conditions at the end-walls (7.46), take it as a particular integral and solve by Fourier's method to obtain:

$$\begin{aligned} \mathcal{V}_1(\xi, Z) &= \frac{1-4Z^2}{16} \\ &- \frac{2}{\pi^3} \sum_{k=0}^{\infty} \frac{(-1)^k}{(2k+1)^3} \exp[-(2k+1)\pi\xi] \cos[(2k+1)\pi Z]. \end{aligned} \tag{7.48}$$

For $\Delta_2 = S^3$, $\mathcal{V}_2$ satisfies

$$\frac{\partial^2 \mathcal{V}_2}{\partial \xi^2} + \frac{\partial^2 \mathcal{V}_2}{\partial Z^2} = \xi \tag{7.49}$$

subject to

$$\mathcal{V}_2 = 0 \qquad \text{at} \quad \xi = 0 \tag{7.50}$$

$$\mathcal{V}_2 = 0 \qquad \text{at} \quad Z = \pm 1/2 \tag{7.51}$$

and a condition arising from the asymptotic matching process:

$$\mathcal{V}_2 \sim -\frac{\xi(1-4Z^2)}{8} + o(\xi) \qquad (\xi \to \infty). \tag{7.52}$$

Here the limiting form (7.52) satisfies the field equation (7.49) and all the boundary conditions; (7.50), (7.51) and (7.52); it must itself, therefore, be the solution.

Further terms in the series (7.39) lead only to trivial solutions, so that the inner asymptotic expansion to any order is:

$$
\begin{aligned}
v_n(\xi, Z; \mathcal{S}) \quad &\sim \quad \mathcal{S}^2 \left\{ \frac{1-4Z^2}{16} \right. \\
&+ \quad \left. \frac{2}{\pi^3} \sum_{k=0}^{\infty} \frac{(-1)^k}{(2k+1)^3} \exp[-(2k+1)\pi\xi] \cos[(2k+1)\pi Z] \right\} \\
&- \quad \mathcal{S}^3 \frac{\xi(1-4Z^2)}{8} + o(\mathcal{S}^K), \\
&\qquad (\mathcal{S} \to 0), \quad (\xi, Z) \text{ fixed}, \quad \forall K \in \{0, 1, 2, \ldots\}.
\end{aligned} \tag{7.53}
$$

Rewriting the inner solution (7.53) in terms of (X, Z) coordinates gives:

$$
\begin{aligned}
v_n(X, Z; \mathcal{S}) &\sim v_n^{=} \\
-\mathcal{S}^2 \frac{2}{\pi^3} \sum_{k=0}^{\infty} \frac{(-1)^k}{(2k+1)^3} &\exp\left[\frac{-(2k+1)\pi(\frac{1}{2} - X)}{\mathcal{S}} \right] \cos[(2k+1)\pi Z]
\end{aligned} \tag{7.54}
$$

which satisfies the full field equation (7.20) for all values of $\mathcal{S} \in (0, \infty)$, and all the boundary conditions except $v_n = 0$ at the cold wall ($X = -1/2$).

To convert the inner solution (7.54) into a full solution the effect of the cold wall msut be incorporated. A simple way to do this is to subtract the difference between itself and the known full solution (7.28).

The same solution can also be used near the cold wall by taking advantage of the odd symmetry of v_n with respect to X.

7.4.2 Large spanwise aspect ratios

The procedure for large $\mathcal{S}$ is similar. The solution of (7.20) as $\mathcal{S} \to \infty$ is (7.24) but not uniformly in space. The neglected boundary conditions are at the end-walls. Near the front end-wall, a coordinate, ζ, stretched by the factor suggested by Saint-Venant's principle, is introduced:

$$
\zeta = \mathcal{S}\left(\frac{1}{2} - Z\right) = \frac{1}{b}\left(\frac{\mathcal{S}b}{2} - z\right), \tag{7.55}
$$

as illustrated in figure 7.3 (b).

The outer expansion is:

$$
\begin{aligned}
v_n(X, Z; \mathcal{S}) \quad &\sim \quad v_n^{\shortparallel} + o(\mathcal{S}^K) \\
&\qquad (\mathcal{S} \to \infty), \quad (X, Z) \text{ fixed}, \quad \forall K \in \{0, 1, 2 \ldots\}.
\end{aligned} \tag{7.56}
$$

The inner expansion valid near the front end-wall, $(Z = 1/2)$, is:

$$\begin{aligned} v_n(X,\zeta;\mathcal{S}) &\sim v_n^{\parallel} \\ &+ \frac{1}{4\pi^3}\sum_{k=1}^{\infty}\frac{(-1)^k}{k^3}\sin[(2k+1)\pi X]\mathrm{e}^{-2k\pi\zeta} + o(\mathcal{S}^K), \\ &\qquad (\mathcal{S}\to\infty), \quad (X,\zeta)\text{ fixed}, \quad \forall K\in\{0,1,2,\ldots\}, \end{aligned} \tag{7.57}$$

or, in terms of (X, Z),

$$\begin{aligned} v_n(X,Z;\mathcal{S}) &\sim v_n^{\parallel} + \\ &\frac{1}{4\pi^3}\sum_{k=1}^{\infty}\frac{(-1)^k}{k^3}\sin(2k\pi X)\exp[-k\pi\mathcal{S}(1-2Z)]. \end{aligned} \tag{7.58}$$

This is a solution of the partial differential equation (7.20) and the boundary conditions at $X = \pm 1/2$ and $Z = 1/2$. It is converted to a full solution by subtracting the difference between it and the full solution (7.25):

$$\begin{aligned} v_n &= v_n^{\parallel} \\ &+ \frac{1}{4\pi^3}\sum_{k=1}^{\infty}\frac{(-1)^k}{k^3}\sin(2k\pi X)\exp[-k\pi\mathcal{S}(1-2Z)] \\ &+ \frac{1}{4\pi^3}\sum_{k=1}^{\infty}\frac{(-1)^k}{k^3}\sin(2k\pi X)\frac{\mathrm{e}^{-k\pi\mathcal{S}}[\mathrm{e}^{-2k\pi\mathcal{S}Z} - \mathrm{e}^{-2k\pi\mathcal{S}(1-Z)}]}{1-\mathrm{e}^{-2k\pi\mathcal{S}}} \end{aligned} \tag{7.59}$$

This is now a full solution that is practical for large $\mathcal{S}$ in the vicinity of the front end-wall. A solution useful near the back end-wall is easily constructed by exploiting the even symmetry of v_n with respect to Z. The first term of (7.59) is the Jones–Furry solution, the second gives the effect of the front end-wall and the third the effect of the back end-wall. In the earlier representation for v_n using the Jones–Furry solution as a particular integral (7.25), the effects of the two end-walls are entangled, whereas in (7.59), they are separated.

This representation (7.59) of v_n, arrived at by physical reasoning, is identical to that suggested in § 7.3.4 on purely numerical grounds.

7.4.3 Extent of the effect of the end-walls

The representation (7.59) of v_n suggests a means of finding a simple approximate answer to one of the principal questions of this chapter: how large $\mathcal{S}$ must be

for the flow in the spanwise plane of symmetry to be essentially described by the Jones–Furry solution (7.24).

Near the front end-wall ($Z = 1/2$) it is clear that the second series can be neglected in comparison to the Jones–Furry solution and the first series if $\mathcal{S}$ is sufficiently large. In the first series, the effect of the k^{th} term has reduced in magnitude by a factor of e after a distance from the front end-wall of $\zeta = 1/(2k\pi)$. Thus the first term, which also has the largest magnitude due to the pre-exponential factor with k^{-3} dependence, acts over the longest distance. It has reduced to less than 0.5% of its influence at $\zeta = 0$ for $\zeta \geq \ln(200)/2\pi$. Since the location of the plane of spanwise symmetry is $\zeta = \mathcal{S}/2$, the flow there may be expected to be sensibly independent of the presence of the end-walls for $\mathcal{S} \geq \ln(200)/\pi \doteq 1.7$. This is a refinement of the prediction $\mathcal{S} \gg 2$ based on Saint-Venant's principle given at the start of this section. Applying a similar procedure to v_f leads to $\mathcal{S} \geq 2\ln(200)/\pi \doteq 3.4$.

To investigate this approximation, plots of the difference between the actual solution for v_n, calculated from (7.59) for each half of the section, and the Jones–Furry solution (7.24) are given in figure 7.4 for values of $\mathcal{S}$ spanning the estimate $\mathcal{S} = 1.7$. The figure shows that the departure from the two-dimensional Jones–Furry limit is indeed less than 1% for $\mathcal{S} \geq 1.7$.

7.5 Sections other than rectangular

In deriving the solutions for the horizontal velocity components (7.13) and vapour mass fraction and temperature (7.16), no reference was made to the shape of the section, since the solutions satisfy the boundary conditions (7.1), (7.2) and (7.5) for all X and Z. Thus the problem for a general section can be written:

> *Find $v = v_f + v_n$ in Ω, the domain, where v_f and v_n satisfy (7.19) and (7.20), respectively, in Ω and (7.21) on $\partial\Omega$, its boundary.*

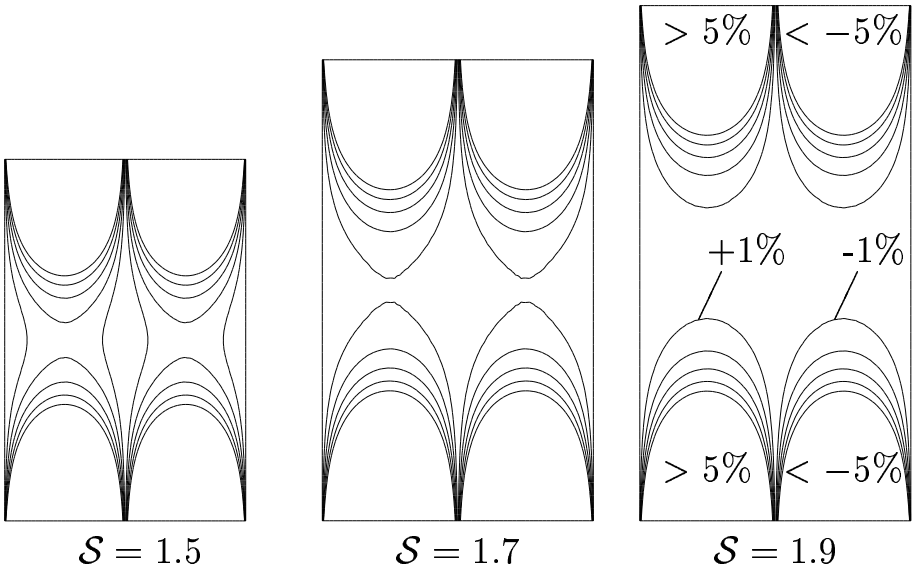

Figure 7.4: The effect of the end-walls. Contours of the difference between the full solution (7.59) and the Jones–Furry limiting form (7.24). Contours at $\pm 1(1)5\%$ of the maximum ($= \max v_n^{\parallel} = \sqrt{3}/216$), as labelled in the rightmost plot.

7.5.1 Circular section

For a circular section of diameter b, $\mathcal{S}$=1 and the domain is given by

$$\Omega^{\circ} = \{\mathbf{X} : X^2 + Z^2 < 1/4\}. \tag{7.60}$$

The forced flow solution is (Stokes 1845; Lamb 1932, p. 585; Bird et al. 1960, p. 46):

$$\frac{v_f^{\circ}}{-\,\mathrm{d}p/\,\mathrm{d}Y} = \frac{1 - 4(X^2 + Z^2)}{16}. \tag{7.61}$$

A solution to equation (7.20) can be obtained in closed form by transforming the independent variables (X, Z) to (X, R), where

$$R = (X^2 + Z^2)^{1/2} \tag{7.62}$$

whence it becomes apparent that (7.20) admits solutions of the form $v_n^{\circ} = X f(R)$ provided

$$f''(R) - \frac{3}{R} f'(R) + 1 = 0. \tag{7.63}$$

For $f(1/2) = 0$ and f bounded as $R \to 0$, the solution of this is:

$$f(R) = \frac{1 - 4R^2}{32} \tag{7.64}$$

$$\text{whence} \qquad v_n^{\circ} = \frac{X[1 - 4(X^2 + Z^2)]}{32}. \tag{7.65}$$

This solution was reported by Ostroumov (1958) for the analogous single fluid heat transfer problem. It is also similar to the fully developed horizontal flow in a long axially heated cylinder (Klosse & Ullersma 1973; Bejan & Tien 1978).

7.5.2 Elliptic section

For elliptic sections, with one axis of length b parallel to the x-axis and the other of length $\mathcal{S}b$ parallel to the z-axis, the domain is again given by (7.60) (see fig. 7.5).

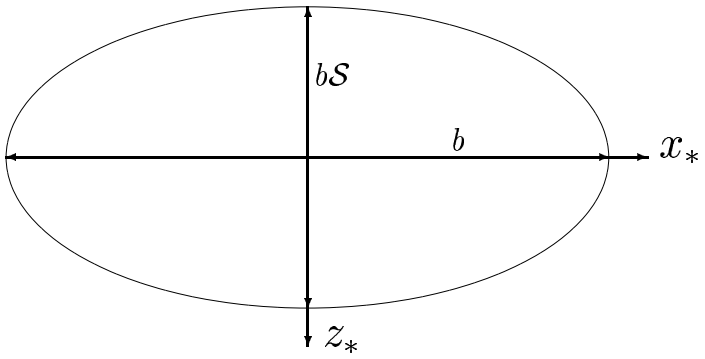

Figure 7.5: Geometry for elliptic sections.

The forced flow solution (Lamb 1932, p. 587), is

$$\frac{v_f^{\circ}(X, Z)}{-\,\mathrm{d}P/\,\mathrm{d}Y} = \frac{1 - 4(X^2 + Z^2)}{8(1 + \mathcal{S}^{-2})} \tag{7.66}$$

Although equation (7.20) could be solved for Ω° by using the Jones–Furry solution (7.24) as a particular integral and the inverse hyperbolic cosine conformal mapping (Carslaw & Jaeger 1959, pp. 439–40), a possible form for the solution is

suggested by those in $\Omega^{\parallel} = \{\mathbf{X} : X^2 < 1/4\}$, equation (7.24), and Ω°, equation (7.65):

$$v_n^{\circ}(X,Z) \stackrel{?}{=} \frac{X[1-4(X^2+Z^2)]}{g(\mathcal{S})}. \tag{7.67}$$

This certainly satisfies the boundary condition (7.1) on $\partial\Omega^{\circ}$, and it also satisfies (7.20) on Ω° if $g(\mathcal{S}) = 8(3+\mathcal{S}^{-2})$. Thus

$$v_n^{\circ}(X,Z) = \frac{X[1-4(X^2+Z^2)]}{8(3+\mathcal{S}^{-2})}. \tag{7.68}$$

Contours of the vertical component of velocity due to buoyancy, v_n°, are displayed for elliptic sections of various spanwise aspect ratio in figure 7.6. Again,

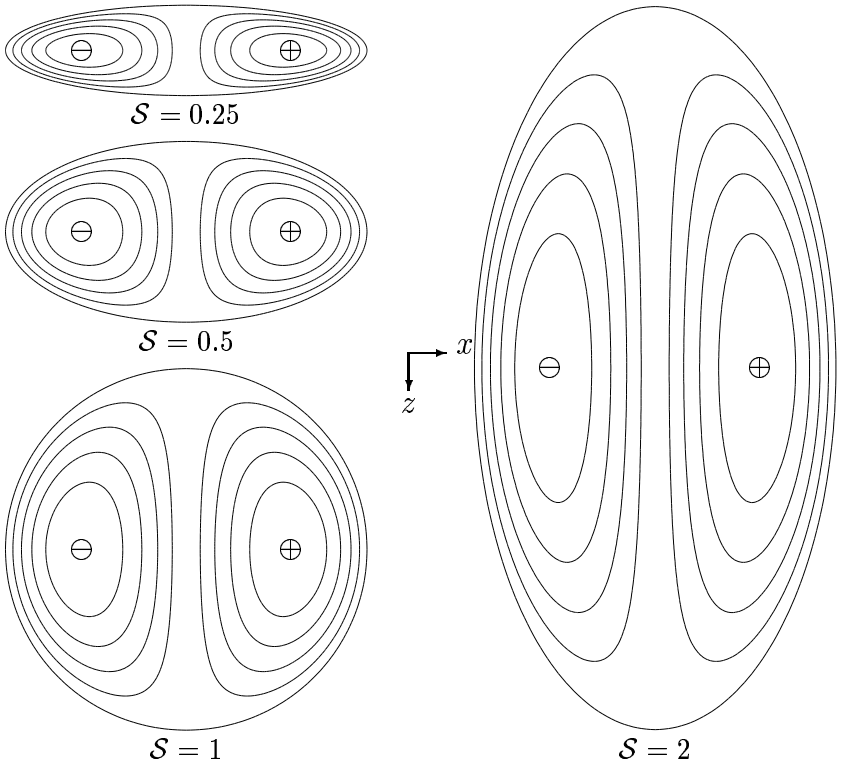

Figure 7.6: Fully developed buoyancy-induced flow in various elliptic sections. Curves can be interpreted as either vortex-lines or contours of the vertical component of velocity with levels at $\pm 20, 40, 60$ and 80% of maximum. $\oplus$ and $\ominus$ mark extrema of v_n (points of zero vorticity).

the curves can alternatively be interpreted as vortex-lines.

Notice that the solution for the circular cylinder (7.65) is regained for $\mathcal{S} = 1$, while

$$v_n^{\circ} \sim \frac{X(1-4X^2)}{24} + O(Z^2) = v_n^{\parallel} + O(Z^2) \qquad (\mathcal{S} \to \infty, Z \to 0) \tag{7.69}$$

and

$$v_n^{\circ} \sim v_n^{=} + O(X^2) \qquad (\mathcal{S} \to 0, X \to 0). \tag{7.70}$$

Thus, v_n° includes the Jones–Furry (7.24) and Hele-Shaw (7.27) limits as special cases, as does the solution for the rectangular domain.

Apart from the simplicity of the result (7.68), the elliptic section is remarkable for two reasons. First, the velocity profile in the plane $Z = 0$ has the same odd-symmetric cubic shape as the Jones–Furry flow (7.24) for all values of $\mathcal{S}$; only the amplitude varies. The second is the comparative ease with which the thermal boundary conditions (7.2) may be imposed. Consider the cavity or duct to be surrounded by a highly conducting solid in which, at large distances, the temperature gradient is uniform and parallel to the x-axis. The problem of the temperature distribution in the solid is analogous to that for potential flow relative to an elliptic cylinder moving uniformly along the axis. From the solution to the latter problem (Lamb 1932, p. 84), it can be seen that the temperature at the section boundary varies linearly with x; i.e. (7.2) applies with $I = 0$. If the vapour mass fraction exerted by the boundaries is a function of temperature, and ΔT_* is small enough for this to be linearized, then the same applies to the boundary conditions on m (7.5).

7.6 Flow in the spanwise symmetry plane

If the assumption of two-dimensionality is to be at all applicable to a three-dimensional flow in a tall cavity or duct, it is most likely to be so at the plane of spanwise symmetry ($Z = 0$), since this is furthest from the end-walls. The flow in this plane is investigated here via the magnitude of the spanwise component of vorticity at the centre line $X = Z = 0$ (the other components vanish there,

by symmetry, for the sections considered in this chapter) and the profile of the vertical component of velocity along the line formed by the intersection of the plane and an arbitrary horizontal section $\{\mathbf{X} : -\frac{1}{2} < X < \frac{1}{2}, Z = 0\}$.

7.6.1 Vorticity at the section centre

A convenient single scalar quantifying the effect of the end-walls on the flow in the plane of spanwise symmetry is the magnitude of the vorticity there. If $\boldsymbol{\omega}$ is defined as the dimensionless vorticity, with scale $g(\beta\Delta T_* + \zeta\Delta m_*)b/\nu$, then for purely vertical flows,

$$\boldsymbol{\omega} = -\frac{1}{\mathcal{S}}\frac{\partial v}{\partial Z}\hat{\boldsymbol{\imath}} + \frac{\partial v}{\partial X}\hat{\boldsymbol{k}}. \tag{7.71}$$

At the centre ($X = Z = 0$) of an elliptic or rectangular section, the transverse (X-direction) component must vanish, since both v_f and v_n are even in Z. Thus, the vorticity at the centre is:

$$\omega_0 \equiv |\boldsymbol{\omega}(0,0)| = \hat{\boldsymbol{k}} \cdot \boldsymbol{\omega}(0,0) = \left.\frac{\partial v}{\partial X}\right|_{(0,0)}. \tag{7.72}$$

For elliptic sections, and considering only the buoyancy-induced part of the flow, v_n°,

$$\omega_{n0}^{\circ} = \frac{1}{8(3+\mathcal{S}^{-2})}. \tag{7.73}$$

For rectangular sections, using the series representation (7.25) for $v_n^{\square}$, the vorticity at the section centre is:

$$\omega_{n0}^{\square} = \omega_{n0}^{\parallel} + \frac{1}{2\pi^2}\sum_{k=1}^{\infty}\frac{(-1)^k}{k^2}\mathrm{sech}k\pi\mathcal{S} \tag{7.74}$$

where

$$\omega_{n0}^{\parallel} = \frac{1}{24} \tag{7.75}$$

is the asymptotic value for large $\mathcal{S}$. Series (7.74) is rapidly convergent and practical for all but extremely small values of $\mathcal{S}$. For these, the Hele-Shaw limit can be obtained from the limiting velocity profile for $\mathcal{S} \to 0$, equation (7.27):

$$\omega_{n0}^{\square} \sim \frac{\mathcal{S}^2}{8} \qquad (\mathcal{S} \to 0) \tag{7.76}$$

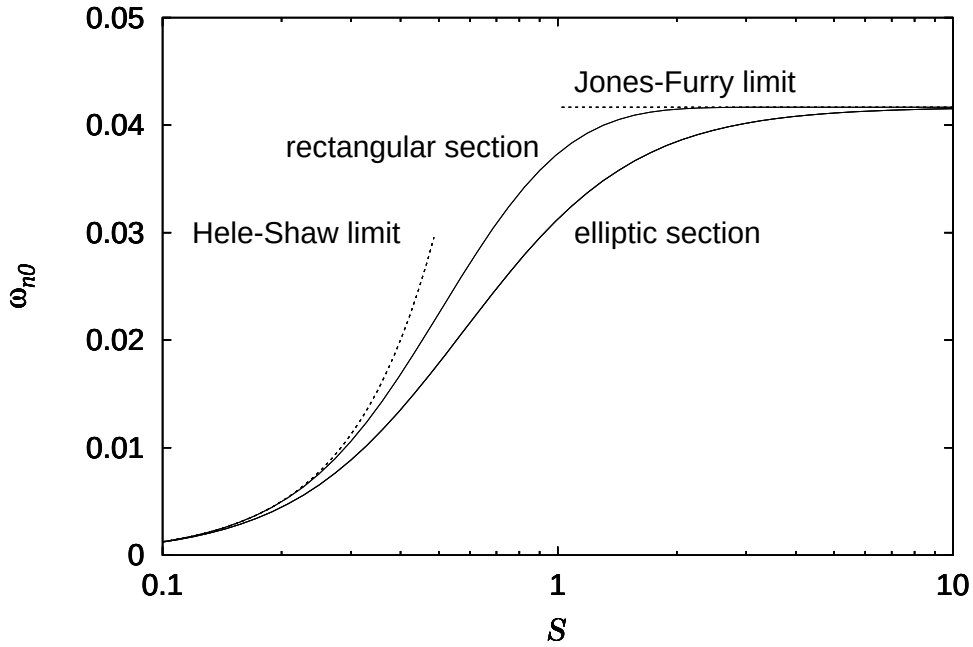

Figure 7.7: Vorticity due to buoyancy at the section centre. The Hele-Shaw limit is given by (7.76), and the Jones–Furry limit by (7.75).

The vorticity at the section centre is plotted from equations (7.73), (7.74), (7.75) and (7.76) in figure 7.7.

Figure 7.7 shows that the vorticity in the central vertical line of a cavity or duct of elliptic section is always less than that in a rectangular duct of the same aspect ratio. This is because the 'end-walls' are closer, on average, to the plane of spanwise symmetry in the elliptic section than in the rectangular section. Their viscous damping of the vertical flow is therefore greater.

For rectangular cavities, figure 7.7 confirms the validity of the estimate made in § 7.4.3 that for $\mathcal{S} > 1.7$ the flow in the plane $Z = 0$ would be essentially the same as for $\mathcal{S} \to \infty$. The equivalent figure for the elliptic section is $\mathcal{S} > 33^{1/2} \doteq 5.7$, the value being larger because of the stronger viscous damping from the 'end-walls'.

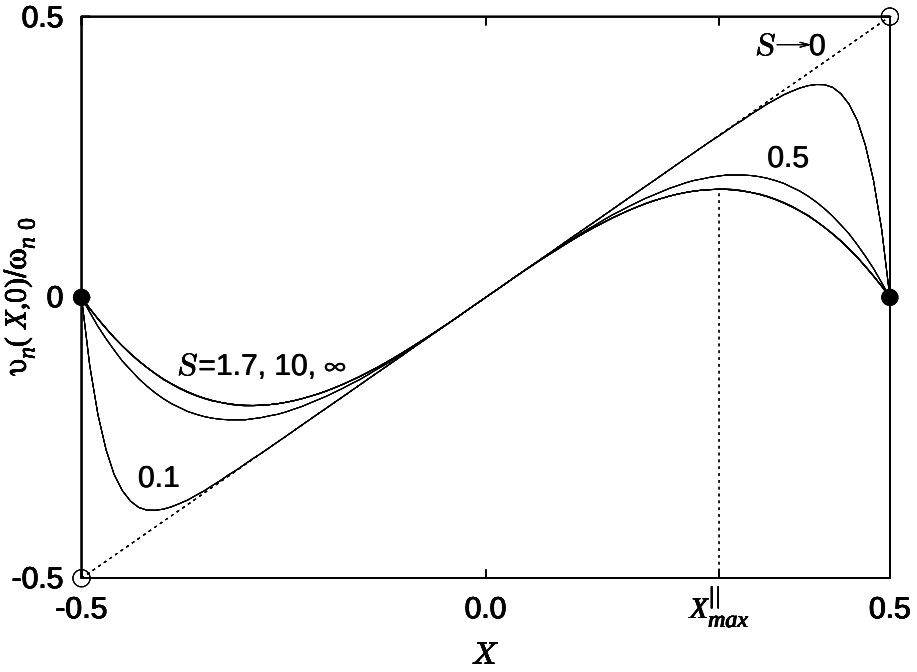

Figure 7.8: Buoyancy-induced velocity, v_n, in the plane of spanwise symmetry, $Z = 0$, of a duct or cavity of rectangular section.

7.6.2 Velocity in the plane of spanwise symmetry

For elliptic sections, by equation (7.68), the profile of the vertical component of velocity in the plane of spanwise symmetry,

$$v_n^{\circ}(X,0) = \frac{X(1-4X^2)}{8(3+\mathcal{S}^{-2})}, \tag{7.77}$$

is independent of $\mathcal{S}$; only the magnitude changes, as can be described by the magnitude of the vorticity at $X = Z = 0$ (see § 7.6.1). This is not so for rectangular sections, as is clear by inspection of figures 7.2 and 7.8. In figure 7.8, (7.25) is used, rather than (7.28) or (7.59), since it accounts equally for the effect of the two end-walls, as appropriate on the plane of spanwise symmetry. The figure also confirms that the flow in the spanwise plane of symmetry is practically independent of $\mathcal{S}$ for $\mathcal{S} \geq 1.7$. The location of the maximum is closer to the hot wall for smaller values of $\mathcal{S}$. This location is a simple scalar measure of the effect of $\mathcal{S}$ on the velocity profile in the plane of spanwise symmetry.

According to Theorem 3 (p. 166), if a flow has zero gradient in some direction, then the component of velocity in that direction is constant along vortex-lines. The flow given by $v_n^{\square}$, (7.25) or (7.28), falls under the hypothesis of this theorem, having no gradient in the vertical direction. If there exists an isolated maximum, then, of $v_n^{\square}$ in a section, there can be no projection in the section of a vortex-line through this point, otherwise the other points on the projection of the vortex-line would have the same velocity as at the maximum and the maximum would not be isolated. Thus, isolated maxima of $v_n^{\square}$ can only occur at points where the horizontal components of vorticity vanish.

The buoyancy-induced vorticity in a rectangular section is, from (7.28) and (7.71):

$$\begin{aligned}\boldsymbol{\omega}_n^{\square} = & \qquad (7.78)\\ &\left\{ X\mathcal{S}Z - \frac{2\mathcal{S}}{\pi^2}\sum_{k=0}^{\infty}\frac{(-1)^k}{(2k+1)^2}\frac{\sinh[(2k+1)\pi X/\mathcal{S}]}{\sinh[(2k+1)\pi/2\mathcal{S}]}\sin[(2k+1)\pi Z]\right\}\hat{\boldsymbol{\imath}}\\ &+\left\{\frac{\mathcal{S}^2(1-4Z^2)}{8} - \frac{2\mathcal{S}}{\pi^2}\sum_{k=0}^{\infty}\frac{(-1)^k\cosh[(2k+1)\pi X/\mathcal{S}]\cos[(2k+1)\pi Z]}{(2k+1)^2\sinh[(2k+1)\pi/2\mathcal{S}]}\right\}\hat{\boldsymbol{k}}\end{aligned}$$

from which it is clear that $\hat{\boldsymbol{\imath}}\cdot\boldsymbol{\omega}_n^{\square} = 0$ if $Z = 0$, so that the maximum of $v_n^{\square}$ must lie in the plane of spanwise symmetry. Thus, the problem of finding the maximum reduces to finding X_{max} such that

$$\hat{\boldsymbol{k}}\cdot\boldsymbol{\omega}_n^{\square}(X_{max},0) = 0, \qquad \text{and} \quad X_{max}\in(0,\tfrac{1}{2}). \qquad (7.79)$$

The limiting behaviour of X_{max} for large and small values of $\mathcal{S}$ can be obtained from the Jones–Furry (7.24) and Hele-Shaw (7.27) limiting vorticity profiles as:

$$\lim_{\mathcal{S}\to\infty} X_{max} \equiv X_{max}^{\parallel} = \frac{\sqrt{3}}{6} \qquad (7.80)$$

$$\lim_{\mathcal{S}\to 0} X_{max} \equiv X_{max}^{=} = \tfrac{1}{2}. \qquad (7.81)$$

For general $\mathcal{S}$, X_{max} may be found by bisection (Kahaner, Moler & Nash 1989, p. 240) on the line interval $\{\mathbf{X} : X\in[X_{max}^{\parallel}, X_{max}^{=}], Z = 0\}$; higher order methods, such as Newton–Raphson, being unsuitable since the vorticity is almost independent of X except near the hot wall if $\mathcal{S}$ is small. For very small $\mathcal{S}$ the

representation (7.54) of the velocity profile developed in § 7.4.1 is more appropriate; so much more so, in fact, that only the Hele-Shaw form and the first term of the series are required to give three figure accuracy in X_{max} for $\mathcal{S} < 0.4$. This leads to the approximation for the vorticity field:

$$\hat{\boldsymbol{k}} \cdot \boldsymbol{\omega}_n^{\square} \sim \frac{\mathcal{S}^2}{8} - \frac{2\mathcal{S}}{\pi^2} \exp\left[\frac{-\pi(\frac{1}{2} - X)}{\mathcal{S}}\right] \qquad (\mathcal{S} \to 0, X \text{ near } \tfrac{1}{2}), \tag{7.82}$$

from which the asymptotic relation (7.81) may be extended to:

$$X_{max} \sim \frac{1}{2} + \frac{\mathcal{S}}{\pi} \ln \frac{\mathcal{S}\pi^2}{16} \qquad (\mathcal{S} \to 0). \tag{7.83}$$

For large $\mathcal{S}$, (7.80) may be extended by taking the Jones–Furry form and the first term of the series in (7.25). The approximate spanwise vorticity in the plane $Z = 0$ is then:

$$\hat{\boldsymbol{k}} \cdot \boldsymbol{\omega}_n^{\square} \sim \frac{1 - 12X^2}{24} - \frac{\cos(2\pi X)}{2\pi^2 \cosh(\pi\mathcal{S})} \qquad (\mathcal{S} \to \infty). \tag{7.84}$$

By expanding the cosine in a second order Taylor series about $X = \sqrt{3}/6$, and finding the root of the resulting quadratic equation in X, an explicit approximation for X_{max} is obtained:

$$\begin{aligned} X_{max} \;\sim\; & \frac{\sqrt{3}}{6} + \left\{ \frac{\pi^2}{3} \cosh \pi\mathcal{S} - 2\pi \sin \frac{\pi}{\sqrt{3}} \right. \\ & + \left[\left(2\pi \sin \frac{\pi}{\sqrt{3}} - \frac{\pi^2}{3} \cosh \pi\mathcal{S} \right)^2 \right. \\ & - \left. \left. 4 \cos \frac{\pi}{\sqrt{3}} \left(2\pi^2 \cos \frac{\pi}{\sqrt{3}} - \pi^2 \cosh \pi\mathcal{S} \right) \right]^{1/2} \right\} \\ & \div 2 \left[2\pi^2 \cos \frac{\pi}{\sqrt{3}} - \pi^2 \cosh \pi\mathcal{S} \right] \qquad (\mathcal{S} \to \infty) \end{aligned} \tag{7.85}$$

The various estimates; (7.80), (7.81), (7.83) and (7.85); of X_{max}, along with the root found by bisection of (7.78), are plotted in figure 7.9 where it can be seen that there is only a narrow transition region, $0.4 < \mathcal{S} < 0.9$, inside which neither the large (7.85) or small (7.83) $\mathcal{S}$ asymptotic relations are accurate. The maximum error in X_{max} in using the more appropriate of these relations is less than 0.5% of the cavity width, and occurs near $\mathcal{S} = 0.57$.

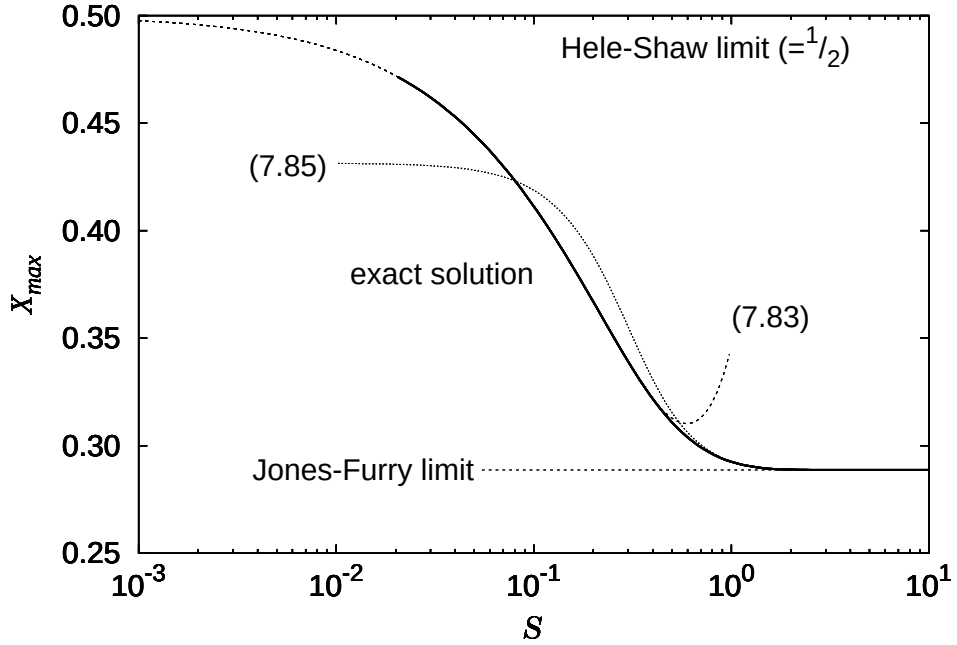

Figure 7.9: Velocity maximum (or zero of vorticity) in a fully developed buoyant flow in a rectangular section.

Figure 7.9 again confirms that for $\mathcal{S} > 1.7$, the flow in the plane of spanwise symmetry is essentially two-dimensional.

The behaviour of the location of the point of maximum vertical velocity is similar to that of the point of maximum deflection in a vertical elastic plate subjected to a hydrostatic pressure variation (Timoshenko & Woinowsky-Krieger 1959, p. 125): the point moves further from the centre as the aspect ratio (height to width, in this case) increases. These two problems are not exactly analogous, however, as the plate deflection satisfies a fourth order equation, rather than the Poisson equation (7.20). The problems become identical if the plate has no resistance to bending, and so is a uniformly stretched membrane.

7.7 Finite mass transfer rates

The problem becomes far more complicated if finite mass transfer rates are included. Although the plane solution of Nelson & Wood (1989) can be generalized to include these effects, as was done in chapter 4, the infinite plane parallel channel is the only geometry for which this is possible. In the narrow cavity limiting solution, there is a uniform transverse velocity which would be incompatible with the no-slip condition on any wall not normal to the x-axis. The question of how diffusion-induced velocities interact with no-slip boundaries has been raised several times in the literature (§§ 3.2, 3.2.3, 3.3.3) but the difficulties caused by the coupling of the momentum and species equations via the interfacial velocity boundary condition have hindered theoretical progress. It seems certain, though, that some spanwise velocity must be present.

7.8 Conclusions

Vapour transport across a vertical cavity or duct of bounded horizontal section was considered in the limit as the vertical length scale tends to infinity. Exact solutions were presented for rectangular and elliptic sections at low mass transfer rates.

The mass fraction and temperature in all cases vary linearly with the transverse coordinate. The unique exact solutions for the purely vertical velocity for rectangular and elliptic sections are infinite hyperbolic–trigonometric series and bivariate polynomials of degree 3, respectively. These match all the conditions of the full problem for vertical cavities or ducts of finite height except the boundary conditions at the top and bottom and are valid for all values of Gr, N, Pr, Sc and $\mathcal{S}$, though naturally their stability cannot be guaranteed for large Grashof numbers.

For large sectional spans, the flows approach the familiar odd cubic profile, which also exists in the plane of spanwise symmetry of an elliptic section of

arbitrary $\mathcal{S}$. In the rectangular section, the velocity profile for $Z = 0$ is distorted as $\mathcal{S}$ decreases, with the location of the extrema moving outward from $X = \pm\sqrt{3}/6$ toward the hot and cold walls; for $\mathcal{S} \geq 1.7$, however, the profile and magnitude are practically independent of $\mathcal{S}$.

The cavities found in the walls built from hollow concrete masonry blocks common in North Queensland are often characterized by a large vertical aspect ratio, $\mathcal{A}$, and a roughly rectangular section of spanwise aspect ratio $\mathcal{S} \approx 1.3$. Although the Grashof number in these cavities will often be too high for the unicellular flow described here to be stable, it is clear that a two-dimensional analysis would be inadequate. In particular, it would be necessary to consider the influence of the end-walls in predicting the critical Grashof number for the onset of multicellular convection.

Although this work deals with simultaneous heat and mass transfer, it may be pointed out that the corresponding results for the conduction regime in a cavity of bounded section in the analogous single fluid heat transfer problem (trivially obtained by setting the buoyancy ratio, N, to zero) are also new.

7.9 Two theorems on fully developed flow

Theorem 2 (Unidirectionality of fully developed flow) *Let* $\mathbf{u}$ *be a regular stationary solution of the incompressible Navier–Stokes equations with a purely vertical body force. If* $\mathbf{u}$ *vanishes on the boundary of a vertically prismatic domain and has zero vertical gradient then* $\mathbf{u}$ *is purely vertical.*[*]

Proof: Since $\hat{\boldsymbol{\jmath}} \cdot \boldsymbol{\nabla}\mathbf{u} = 0$, the equation of continuity reduces to

$$\boldsymbol{\nabla}_\perp \cdot \mathbf{u}_\perp = 0 \tag{7.86}$$

[*] *Note added in proof:* A slightly more general result, in which the body force is allowed horizontal components so long as they possess a potential, was known to Joseph & Tao (1963, *J. Appl. Mech.* **30**:147–148).

and the horizontal components of the equation of motion are

$$Re\ \mathbf{u}_\perp \cdot \boldsymbol{\nabla}_\perp \mathbf{u}_\perp = -\boldsymbol{\nabla} p + \boldsymbol{\nabla}_\perp^2 \mathbf{u}_\perp, \tag{7.87}$$

where Re is the Reynolds number.

The remnant of the equation of continuity (7.86) implies the existence of a scalar function, ψ (see Lamb 1932, pp. 62–3 for a construction) such that

$$u = -\frac{1}{\mathcal{S}}\frac{\partial \psi}{\partial Z} \tag{7.88}$$

$$w = \frac{\partial \psi}{\partial X}, \tag{7.89}$$

so that the horizontal momentum problem becomes

$$\frac{Re}{\mathcal{S}}\left(\frac{\partial \psi}{\partial Z}\frac{\partial}{\partial X} - \frac{\partial \psi}{\partial X}\frac{\partial}{\partial Z}\right)\nabla_\perp^2 \psi = -\nabla_\perp^4 \psi \tag{7.90}$$

subject to

$$\psi = \frac{\partial \psi}{\partial n} = 0 \qquad \text{on} \quad \partial\Omega, \tag{7.91}$$

where $\partial/\partial n$ is the outward normal derivative. On multiplying (7.90) through by φ, an arbitrary function also satisfying the boundary conditions (7.91), and integrating over the section, the variational form is obtained (Girault & Raviart 1979, p. 120):

$$\frac{Gr(1+N)}{\mathcal{S}} \iint\limits_\Omega \nabla_\perp^2 \psi \left[\frac{\partial \psi}{\partial Z}\frac{\partial \varphi}{\partial X} - \frac{\partial \psi}{\partial X}\frac{\partial \varphi}{\partial Z}\right] \mathrm{d}X\, \mathcal{S}\, \mathrm{d}Z = \iint\limits_\Omega (\nabla_\perp^2 \psi)(\nabla_\perp^2 \varphi)\, \mathrm{d}X\, \mathcal{S}\, \mathrm{d}Z. \tag{7.92}$$

If φ is then set equal to ψ, the integrand on the left hand side vanishes and the equation reduces to

$$\iint\limits_\Omega \left(\nabla_\perp^2 \psi\right)^2 \mathrm{d}X\, \mathcal{S}\, \mathrm{d}Z = 0 \tag{7.93}$$

which is only possible if $\nabla_\perp^2 \psi = 0$. With the boundary conditions (7.91), and the well-known uniqueness of harmonic functions in bounded domains (Lamb 1932, pp. 41, 64), we have $\psi = 0$ throughout Ω and so $u = w = 0$, uniquely. □

Note: The horizontal components of velocity satisfy a two-dimensional Navier–Stokes problem with no body force and homogeneous boundary conditions. The volume integral (7.93) is proportional to the net rate of viscous dissipation of energy by this horizontal flow per unit length in the vertical direction (Lamb 1932, p. 580). Since, under the hypothesis $\hat{\boldsymbol{\jmath}} \cdot \boldsymbol{\nabla}\mathbf{u} = 0$, the only available source for this power is the kinetic energy of the fluid, any existing horizontal motion would have to continually diminish in magnitude; thus, the entire proof is similar to that of the uniqueness of creeping flows with prescribed boundary velocities (Lamb 1932, pp. 617–8; Rayleigh 1913), even though the inertial terms of the equation of motion were not neglected here.

Theorem 3 (Vortex-lines in fully developed flow) *If a flow has zero gradient in some direction, the component of velocity in this direction is constant along vortex-lines.*

Proof: The hypothesis may be written

$$\hat{\boldsymbol{e}} \cdot \boldsymbol{\nabla}\mathbf{u} = 0,$$

where $\mathbf{e}$ is a unit vector. Adding three terms (the first and third of which are identically zero due to the uniformity of $\hat{\boldsymbol{e}}$) to each side of the hypothesis and forming the scalar product with the vorticity gives

$$(\boldsymbol{\nabla} \times \mathbf{u}) \cdot [\hat{\boldsymbol{e}} \cdot \boldsymbol{\nabla}\mathbf{u} + \mathbf{u} \cdot \boldsymbol{\nabla}\hat{\boldsymbol{e}} + \hat{\boldsymbol{e}} \times (\boldsymbol{\nabla} \times \mathbf{u}) + \mathbf{u} \times (\boldsymbol{\nabla} \times \hat{\boldsymbol{e}})] = (\boldsymbol{\nabla} \times \mathbf{u}) \cdot [\hat{\boldsymbol{e}} \times (\boldsymbol{\nabla} \times \mathbf{u})].$$

The triple scalar product on the right hand side vanishes, while the term in brackets on the left hand side is simply $\boldsymbol{\nabla}(\hat{\boldsymbol{e}} \cdot \mathbf{u})$; thus,

$$(\boldsymbol{\nabla} \times \mathbf{u}) \cdot \boldsymbol{\nabla}(\hat{\boldsymbol{e}} \cdot \mathbf{u}) = 0;$$

i.e. the component of velocity in the direction of zero gradient is constant along vortex-lines. □

Note: The hypothesis of the theorem includes all two-dimensional flows and all unidirectional solenoidal flows. The theorem is entirely kinematical; the only restriction placed on the velocity field is differentiability.

Chapter 8

Bounded Cavities

ALL the domains considered so far have been unbounded, either in the spanwise direction (ch. 5); the vertical direction (ch. 7); or both (ch. 4). This is, of course, a serious practical limitation, since real enclosures must be bounded. In this chapter, I present some results for the difficult problem of nonisothermal vapour transport across bounded gas-filled enclosures. Only the low mass transfer rate limit is considered.

8.1 The spanwise component of velocity

Apart from axisymmetric studies of cylinders—which cannot correctly account for buoyancy unless the imposed density gradient is antiparallel to the gravitational field (§ 3.2.5)—the only work on vapour transport across bounded gas-filled enclosures is the rather specific study by Rosenberger et al. (1997; § 3.3.18). The following discussion therefore reviews theoretical results for the analogous single fluid heat transfer problem.

The exact solutions for the cuboid in the limit $\mathcal{A} \to \infty$ derived in chapter 7 show a purely vertical flow, contradicting the general conclusion of de Vahl Davis (1998) that the end-walls necessarily give rise to a spanwise flow, even in the limit of zero Grashof number; i.e. $w = O(1)$ as $Gr \to 0$. Since this conclusion

was based on inspection of numerical solutions for $\mathcal{A} \leq 5$, it is submitted that the horizontal surfaces must play a role in the generation of nonzero w.

The spanwise flow in finite cuboids was first predicted by the numerical solutions of Mallinson and de Vahl Davis (1973, 1977) and later observed in the experiments of Morrison and Tran (1978) and Hiller, Koch and Kowalewski (1989). In 1973, Mallinson and de Vahl Davis explained the effect purely in terms of the reduction of the convective disturbance of the temperature field by the viscous damping of the end-walls, but in 1977 they postulated a second mechanism—the inertial interaction of a rotating mass of fluid and a stationary solid wall—by analogy with the work of Pao (1970) on the fluid confined in a rotating cylinder with one stationary end-wall. (This problem has been recently revisited by Lopez 1998.) Their explanation is merely by analogy, however, and does not involve the basic mechanism. The reason why an axial (spanwise in the case of the cavity) velocity is generated is immediately obvious from inspection of Pao's formulation of the governing equations—the axisymmetric Navier–Stokes equations in terms of azimuthal velocity and azimuthal vorticity and stream-function. The azimuthal velocity in Pao's problem is generated by the rotating boundary but the boundary conditions on the azimuthal stream-function are homogeneous; the vorticity, and hence the axial flow, is produced by the source term corresponding to the centrifugal force.

8.1.1 Inertial generation of spanwise flow

The inertial generation of a spanwise or axial flow by the viscous interaction of a rotating body of fluid and a perpendicular solid surface occurs in several areas of fluid mechanics, such as in curved rivers (Thomson 1876, 1877; Reynolds 1888; Falcón 1984; Johannesson & Parker 1989) and pipes (Thomson 1876; Eustice 1911; Dean, W. R. 1927; Patankar, Pratap and Spalding 1974; Jabbari, Burns & Goldstein 1998). The phenomenon is utilized in aquaculture to rid tanks of unwanted settleable solids (Timmons, Summerfelt & Vinci 1998; Peterson 1999).

Perhaps its most familiar manifestation is the gathering of tea leaves at the centre of the bottom of the cup on stirring.

This last quotidian example is quite instructive. One immediately notices that the tea leaves travel radially inward along the bottom and begin to rise along the axis regardless of whether the tea is stirred clockwise or anticlockwise; i.e. the secondary flow is independent of the sign of the rotational speed, Ω, of the stirring. This implies that the axial component of velocity at any point on the axis near the base must be an even function of Ω. Assuming that for sufficiently slow stirring, i.e. small Reynolds number $Re \equiv \Omega b^2/\nu$, the dimensional axial velocity, w_*, can be expanded in a power series, it will only contain the terms involving even powers of Ω:

$$\Omega^0, \Omega^2, \ldots, \Omega^{2n}, \ldots \tag{8.1}$$

It is obvious that the coefficient of Ω^0 must vanish, since there is no secondary flow without the primary flow, so that the first term is quadratic. The immediate conclusion is that there is no secondary flow in the creeping flow limit ($Re \to 0$). The corresponding dimensionless axial velocity, $w_*/\Omega b$, will be an odd function of Re.

The earliest scientific description of this general phenomenon seems to be Stokes's (1845). Of the motion of fluid between concentric coaxially rotating spheres (spherical Couette flow), he noted that motion in circular stream-lines about the axis of rotation was impossible unless the centrifugal force were neglected, whereas if it were included:

> it is easy to see that from the excess of centrifugal force in the neighbourhood of the equator of the [inner] revolving sphere the particles in that part will recede from the sphere, and approach it again in the neighbourhood of the poles, and this circulating motion will be combined with a motion about the axis. (Stokes 1845)

Spherical Couette flow was later studied by Lamb (1932, p. 588), who gave the creeping flow limiting solution, and Munson and Joseph (1971), who presented

results from an asymptotic expansion for low Reynolds number indicating the correctness of Stokes's and Lamb's predictions; in particular, the expansion for the motion in meridian planes involves only odd powers of the Reynolds number. There are also several recent numerical studies (Schwengels & Schulz 1989; Riad Mossad 1993; Ni & Nigro 1994; Nakabayashi & Tsuchida 1995; Zikanov 1996).

If the entire boundary of a fluid were rotating, the fluid, at steady state, would rotate as a solid body (Rayleigh 1913), in which case the effect of the centrifugal force would be to generate a pressure varying as the square of the azimuthal velocity (Lamb 1932, p. 28; Bird et al. 1960, pp. 96–8). With one end-wall fixed, the azimuthal velocity (and therefore the centrifugal force and consequent pressure) must vary axially. It is this axial variation in pressure which gives rise to the axial velocity. Now, the centrifugal force is inversely proportional to the radius of curvature of the azimuthal velocity. In the rotating cylinder this is simply equal to the distance from the axis, but if an analogy is drawn between Pao's problem and the buoyant flow in a cavity this need not be so. For a unicellular flow in a very tall cavity, the stream-lines sufficiently far from the horizontal surfaces will be practically straight, so that their radius of curvature is infinite and the centrifugal force vanishes. There is, therefore, no centrifugally generated pressure, no axial variation of centrifugally generated pressure and no force to cause axial/spanwise flow.

Of course, the temperature will also be independent of z in the fully developed region so that the first (thermal) mechanism is eliminated too.

The centrifugal force is proportional to the square of the azimuthal velocity, and therefore must vanish faster than the primary circulating flow as the speed scale, $\nu Gr(1+N)/b$, tends to zero. Thus, the second (inertial) mechanism for spanwise flow in a confined convective roll vanishes if either the stream-lines are straight or terms quadratic in the velocity vanish (creeping flow).

8.2 Spherical enclosures

The two mechanisms for producing spanwise flow proposed by Mallinson and de Vahl Davis (1973, 1977) are illuminated here by considering the flow in a spherical enclosure subject to horizontal vapour mass fraction and temperature gradients. Apart from the importance of spherical enclosures as part of closed porous materials, the results fully support the contentions of the previous section.

8.2.1 Previous work

To the best of my knowledge, there have been no studies of vapour transport across a spherical enclosure. The analogous single fluid heat transfer problem, however, has been studied independently by Lewis (1950) and Ostroumov (1958), in connection with gas bubbles in foam insulating materials and the geothermics of underground reservoirs, respectively. Both considered the asymptotic expansion for low Grashof numbers, as will I.

Unfortunately, both Lewis and Ostroumov assumed that the spanwise component of velocity would vanish in the sphere:

> In the case considered there are then two "privileged" directions [those of gravity and the imposed heating]. We expect therefore that the main circulating flow will be essentially plane, i.e. there will be only two components of velocity of reasonable order of magnitude. (Lewis 1950)

> Considering the conditions of symmetry, we assume that the streamlines lie in planes parallel to the plane determined by the directions $\mathbf{g}$ and [of the imposed heating]. (Ostroumov 1958)

For general Grashof numbers, this assumption is incorrect and their results are useless for the present purpose. They are correct, however, for creeping flow, as will be shown below: the dimensionless spanwise component of velocity is $O(Gr)$

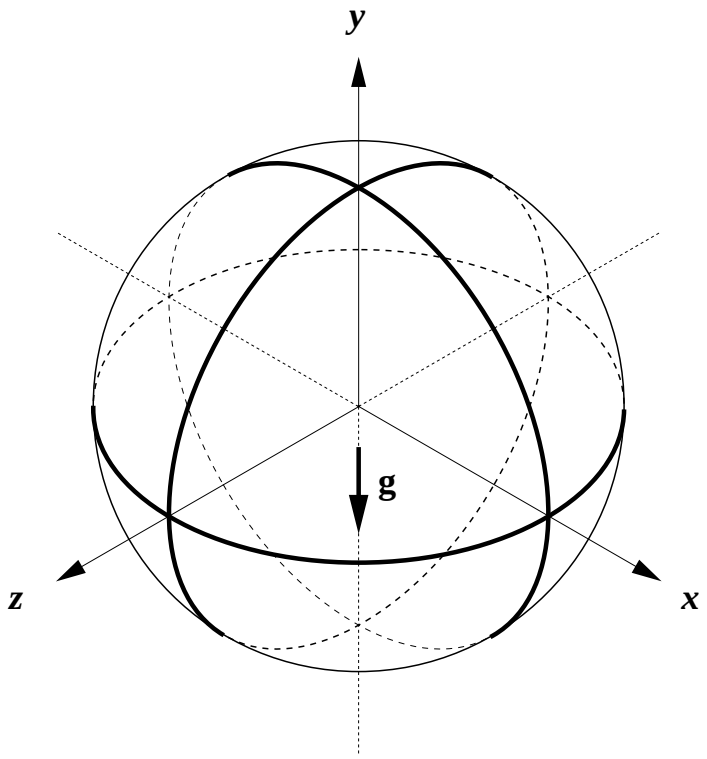

Figure 8.1: Cartesian axes for the spherical cavity subjected to a linear variation with x of vapour mass fraction and temperature at the boundary.

as $Gr \to 0$, whereas the other components are $O(1)$. The problem of the sphere seems not to have been returned to since these two early studies.

8.2.2 Geometry and boundary conditions

Take the diameter of the sphere as the length scale, b, and introduce spherical polar coordinates relative to the positive z-axis:

$$r \equiv \left(x^2 + y^2 + z^2\right)^{1/2}; \tag{8.2}$$

$$\theta \equiv \arctan \frac{\left(x^2 + y^2\right)^{1/2}}{z}; \tag{8.3}$$

$$\phi \equiv \arctan \frac{y}{x}. \tag{8.4}$$

The relation of the Cartesian axes to the directions of gravity and the imposed gradients, as illustrated in figure 8.1, is the same as for the cuboid.

Ostroumov's (1958) study is more general than mine in that it considers the finite conductivity of the surrounding solid. Since solids, in general, are much more conducting than gases, and since the primary purpose here is to illuminate confined convective flow, let us assume that the solid is infinitely conducting. If the temperature gradient in the solid far from the cavity is uniform and horizontal (parallel to the x-axis), the temperature at the boundary of the sphere is analogous to the flow potential on a solid sphere moving along the x-axis through a perfect fluid; i.e. it varies linearly with x (Lamb 1932, p. 123), though the gradient differs from that in the far solid. Explicitly, the temperature field

$$T = \frac{1}{3}\left(\frac{1}{8r^3} + 2\right) r \sin\theta \cos\phi \tag{8.5}$$

satisfies

$$\nabla^2 T = 0, \qquad (r > 1/2) \tag{8.6}$$

$$\frac{\partial T}{\partial r} = 0, \qquad (r = 1/2) \tag{8.7}$$

$$T \sim \frac{2}{3}x, \qquad (r \to \infty) \tag{8.8}$$

and leads to $T = x$ on the boundary of the cavity. The temperature field in the surrounding solid is shown in figure 8.2.

This point appears to have been missed by Lewis (1950) and Ostrach (1988), who thought that 'this temperature corresponds to that which would occur in the solid without gas bubbles' (Ostrach 1988), which is true but irrelevant.

As in § 7.5.2, it is assumed that the vapour mass fraction at the boundary is a linear function of temperature; thus,

$$m = T = x \qquad (r = \tfrac{1}{2}). \tag{8.9}$$

8.2.3 The low Grashof number expansion

It may be worthwhile at the outset to note that although low Reynolds number expansions for unbounded domains, e.g. viscous flow past a solid sphere (Lamb

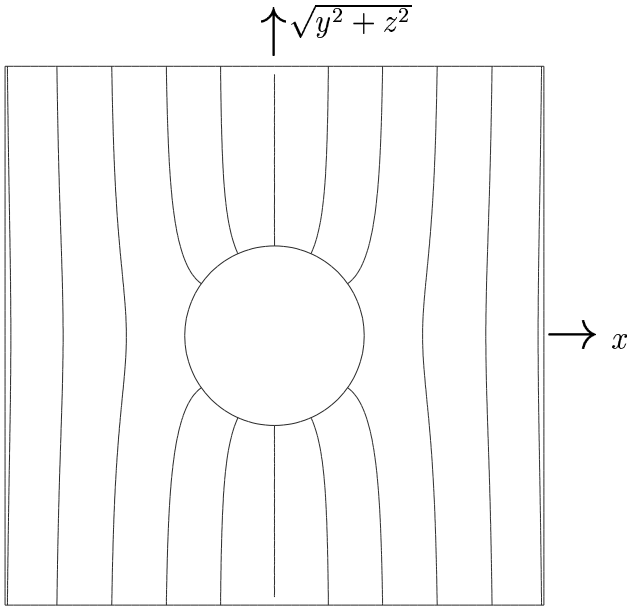

Figure 8.2: Temperature in the highly conducting solid surrounding a spherical cavity. The field is axisymmetric everywhere, and linear in the far field.

1932, p. 609; Van Dyke 1964, ch. 8), are singular perturbation problems, this is not the case for bounded domains (Munson & Joseph 1971). This makes sense: the region of nonuniformity in the former class of problems, where the neglected inertial terms are not negligible in comparison to the retained viscous terms, is typically a neighbourhood of the point at infinity.

Assume asymptotic expansions for the vapour mass fraction, velocity, pressure and temperature of the form:

$$m \sim m_0 + [Gr(1+N)]m_1 + [Gr(1+N)]^2 m_2 + \cdots \tag{8.10}$$

$$\mathbf{u} \sim \mathbf{u}_0 + [Gr(1+N)]\mathbf{u}_1 + [Gr(1+N)]^2 \mathbf{u}_2 + \cdots \tag{8.11}$$

$$p \sim p_0 + [Gr(1+N)]p_1 + [Gr(1+N)]^2 p_2 + \cdots \tag{8.12}$$

$$T \sim T_0 + [Gr(1+N)]T_1 + [Gr(1+N)]^2 T_2 + \cdots \tag{8.13}$$

as $Gr \to 0$, with $(1+N)$, Sc and Pr fixed and finite.

Substituting these in to the low mass transfer rate equations, (6.16)–(6.19), and taking the limit $Gr \to 0$ leads to a hierarchy of problems:

$$A_{mi} = \nabla^2 m_i; \tag{8.14}$$

$$A_{Ti} = \nabla^2 T_i; \tag{8.15}$$

$$m_i = T_i = \begin{cases} x, & (i=0) \\ 0, & (i=1,2,\ldots) \end{cases}, \quad (r=\tfrac{1}{2}), \tag{8.16}$$

where

$$A_{mi} \equiv Sc \sum_{k=0}^{i-1} \mathbf{u}_{i-1-k} \cdot \boldsymbol{\nabla} m_k \tag{8.17}$$

$$A_{Ti} \equiv Pr \sum_{k=0}^{i-1} \mathbf{u}_{i-1-k} \cdot \boldsymbol{\nabla} T_k \tag{8.18}$$

and

$$\boldsymbol{\nabla} \cdot \mathbf{u}_i = 0 \tag{8.19}$$

$$\mathbf{I}_i - \mathbf{B}_i = -\boldsymbol{\nabla} p_i + \nabla^2 \mathbf{u}_i \tag{8.20}$$

$$\mathbf{u}_i = \mathbf{0}, \quad (r=\tfrac{1}{2}) \tag{8.21}$$

where

$$\mathbf{I}_i \equiv \sum_{k=0}^{i-1} \mathbf{u}_{i-1-k} \cdot \boldsymbol{\nabla} \mathbf{u}_k \tag{8.22}$$

$$\mathbf{B}_i \equiv \frac{T_i + N m_i}{1+N} \hat{\boldsymbol{\jmath}}. \tag{8.23}$$

The series for A_{mi}, A_{Ti} and $\mathbf{I}_i$ are to be taken as zero if the lower index (zero) exceeds the upper; i.e. when $i = 0$. Each m_i and T_i satisfies a Laplace or Poisson equation, with source given in terms of previously calculated quantities. These are, in principle, all soluble by expanding the source term and the independent variable in spherical harmonics. For the equations of motion, however, the presence of the unknown pressure terms and the continuity constraints means that at each order a Stokes problem with known 'body force' must be solved. The Stokes problem in a sphere can be reduced to an uncoupled unconstrained set of scalar partial differential equations (Poisson and inhomogeneous biharmonic equations) by decomposing the velocity term into its poloidal and toroidal parts. This technique is summarized in appendix B.

The evaluation of $\mathbf{I}_i$ may be tedious, but can be simplified by noting that except for $k = (i-1)/2$ the terms of the series occur in pairs:

$$\mathbf{u}_{i-1-k} \cdot \boldsymbol{\nabla} \mathbf{u}_k + \mathbf{u}_k \cdot \boldsymbol{\nabla} \mathbf{u}_{i-1-k}, \tag{8.24}$$

which can be evaluated via the vector identity

$$\mathbf{u} \cdot \boldsymbol{\nabla} \mathbf{v} + \mathbf{v} \cdot \boldsymbol{\nabla} \mathbf{u} \equiv \boldsymbol{\nabla}(\mathbf{u} \cdot \mathbf{v}) + (\boldsymbol{\nabla} \times \mathbf{v}) \times \mathbf{u} + (\boldsymbol{\nabla} \times \mathbf{u}) \times \mathbf{v}. \tag{8.25}$$

The exceptional case, $k = (i-1)/2$, is expressed in spherical coordinates and components (u_r, u_θ, u_ϕ) as (Lamb 1932, p. 159):

$$\begin{aligned} \mathbf{u} \cdot \boldsymbol{\nabla} \mathbf{u} \;=\; & \left(u_r \frac{\partial u_r}{\partial r} + \frac{u_\theta}{r} \frac{\partial u_r}{\partial \theta} + \frac{u_\phi}{r \sin\theta} \frac{\partial u_r}{\partial \phi} - \frac{u_\theta^2 + u_\phi^2}{r} \right) \hat{\boldsymbol{r}} \\ & + \left(u_r \frac{\partial u_\theta}{\partial r} + \frac{u_\theta}{r} \frac{\partial u_\theta}{\partial \theta} + \frac{u_\phi}{r \sin\theta} \frac{\partial u_\theta}{\partial \phi} + \frac{u_r u_\theta - u_\phi^2 \cot\theta}{r} \right) \hat{\boldsymbol{\theta}} \\ & + \left(u_r \frac{\partial u_\phi}{\partial r} + \frac{u_\theta}{r} \frac{\partial u_\phi}{\partial \theta} + \frac{u_\phi}{r \sin\theta} \frac{\partial u_\phi}{\partial \phi} + \frac{u_r u_\phi + u_\theta u_\phi \cot\theta}{r} \right) \hat{\boldsymbol{\phi}}. \end{aligned} \tag{8.26}$$

8.2.4 Conduction–diffusion

The solution for the zeroth order mass fraction and temperature equations, (8.14) and (8.15) with $i = 0$, is obviously

$$m_0 = T_0 = x = r \sin\theta \cos\phi = r P_1^1(\cos\theta) \cos\phi. \tag{8.27}$$

The functions $P_n^m(\cos\theta)$ are defined and tabulated in appendix B.

8.2.5 Creeping flow

The solution for $\mathbf{u}_0$ and p_0 (creeping flow) is obtained by the method of § B.4.

Here the body force is

$$\mathbf{f}_0 = \mathbf{I}_0 - \mathbf{B}_0 \tag{8.28}$$

$$= \mathbf{0} - \frac{T_0 + N m_0}{1+N} \hat{\boldsymbol{\jmath}} = -x \hat{\boldsymbol{\jmath}} \tag{8.29}$$

$$= -r \sin^2\theta \sin\phi \cos\phi \, \hat{\boldsymbol{r}} - r \sin\theta \cos\theta \sin\phi \cos\phi \, \hat{\boldsymbol{\theta}} - r \sin\theta \cos^2\phi \, \hat{\boldsymbol{\phi}}. \tag{8.30}$$

The scalar defining its scaloidal part satisfies

$$\begin{aligned} \nabla^2 \mathcal{S}[\mathbf{f}_0] &= \boldsymbol{\nabla} \cdot \mathbf{f}_0 = 0 && (8.31) \\ \hat{\boldsymbol{r}} \cdot \boldsymbol{\nabla} \mathcal{S}[\mathbf{f}_0] &= \hat{\boldsymbol{r}} \cdot \mathbf{f}_0, \quad (r = \tfrac{1}{2}) \\ &= -\frac{1}{4} \sin^2\theta \sin\phi \cos\phi \\ &= -\frac{1}{24} P_2^2(\cos\theta) \sin 2\phi. && (8.32) \end{aligned}$$

This is

$$\mathcal{S}[\mathbf{f}_0] = -\frac{1}{4} r^2 \sin^2\theta \sin 2\phi, \tag{8.33}$$

so that

$$\begin{aligned} \mathbf{f}_0^{(S)} = \boldsymbol{\nabla} \mathcal{S}[\mathbf{f}_0] &= -\frac{1}{2}(r \sin^2\theta \sin 2\phi \, \hat{\boldsymbol{r}} + r \sin\theta \cos\theta \sin 2\phi \, \hat{\boldsymbol{\theta}} \\ &\quad + r \sin\theta \cos 2\phi \, \hat{\boldsymbol{\phi}}) && (8.34) \end{aligned}$$

and

$$\mathbf{f}_0 - \mathbf{f}_0^{(S)} = -\frac{1}{2} r \sin\theta \, \hat{\boldsymbol{\phi}}, \tag{8.35}$$

which is obviously solenoidal, as expected.

Clearly

$$\mathcal{P}[\mathbf{f}_0 - \mathbf{f}_0^{(S)}] = 0, \tag{8.36}$$

since

$$\hat{\boldsymbol{r}} \cdot (\mathbf{f}_0 - \mathbf{f}_0^{(S)}) = 0. \tag{8.37}$$

The problem for the scalar defining the toroidal part of the body force is:

$$\begin{aligned} \mathcal{L}^2 \mathcal{T}[\mathbf{f}_0 - \mathbf{f}_0^{(S)}] &= -\mathbf{r} \cdot \boldsymbol{\nabla} \times (\mathbf{f}_0 - \mathbf{f}_0^{(S)}) && (8.38) \\ &= r \cos\theta = r P_1^0(\cos\theta). && (8.39) \end{aligned}$$

The solution is

$$\mathcal{T}[\mathbf{f}_0 - \mathbf{f}_0^{(S)}] = -\frac{1}{2} r \cos\theta. \tag{8.40}$$

To illustrate the decomposition of the vector field here, the force-lines of $\mathbf{f}_0$, $\mathbf{f}_0^{(S)}$ and $\mathbf{f}_0^{(T)}$ in the plane $z = 0$ are plotted in figure 8.3. Since, in this case, all three

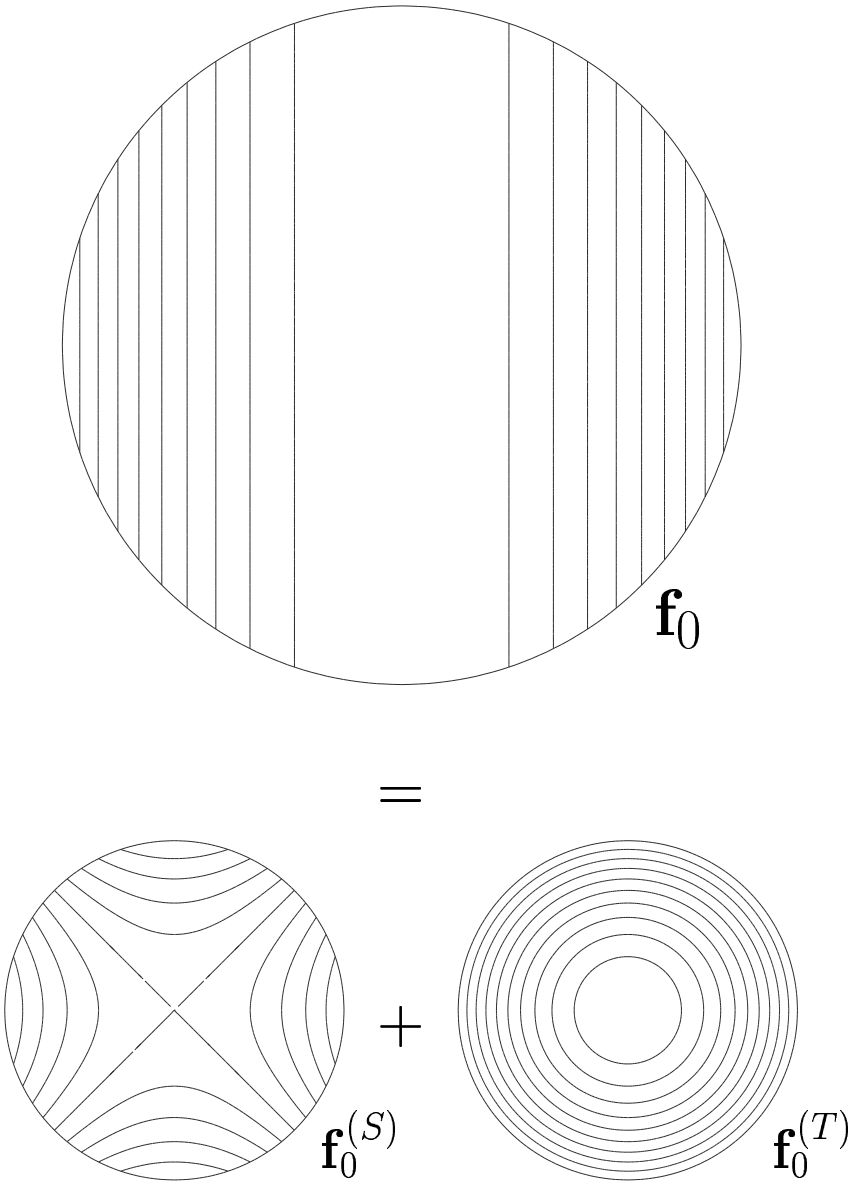

Figure 8.3: Decomposition of the vector field $\mathbf{f}_0$ into scaloidal, $\mathbf{f}_0^{(S)}$, and toroidal, $\mathbf{f}_0^{(T)}$, parts. The fields are represented by their force-lines in the plane $z = 0$, the contours of $x^2/2$, $(x^2 - y^2)/2$ and $(x^2 + y^2)/4$.

vector fields are plane and solenoidal, the force-lines can be represented as the contours of scalar functions. The functions are $x^2/2$, $(x^2-y^2)/4$ and $(x^2+y^2)/4$, respectively.

The problem for $\mathcal{T}[\mathbf{u}_0]$ is:

$$\nabla^2\mathcal{T}[\mathbf{u}_0] = \mathcal{T}[\mathbf{f}_0 - \mathbf{f}_0^{(S)}] = -\frac{r}{2}P_1^0(\cos\theta) \tag{8.41}$$

$$\mathcal{T}[\mathbf{u}_0] = 0, \quad (r = 1/2). \tag{8.42}$$

The solution is:

$$\mathcal{T}[\mathbf{u}_0] = \frac{r}{80}\left(1-4r^2\right)P_1^0(\cos\theta). \tag{8.43}$$

The other scalars, $\mathcal{P}[\mathbf{u}_0]$ and s, vanish.

Thus,

$$p_0 = -\mathcal{S}[\mathbf{f}_0] = \frac{r^2}{2}\sin^2\theta\sin\phi\cos\phi \tag{8.44}$$

$$\mathbf{u}_0 = \boldsymbol{\nabla}\times\mathcal{T}[\mathbf{u}_0]\mathbf{r} = \frac{r}{80}\left(1-4r^2\right)\sin\theta\hat{\boldsymbol{\phi}}. \tag{8.45}$$

The pressure is plotted in the plane of spanwise symmetry, $z = 0$, in figure 8.4. Since the velocity is purely toroidal, the pressure is due solely to the scaloidal part of the body force. The force-lines of $\mathbf{f}^{(S)}$ and the isobars, displayed in figures 8.3 and 8.4, are obviously related: they are mutually orthogonal.

The pressure is very simply expressed in terms of Cartesian coordinates:

$$p_0 = \frac{xy}{2}. \tag{8.46}$$

The fact that it is independent of z suggests—consider the spanwise component of the equation of motion (2.54)—that $w_0 = 0$. This is the case:

$$\mathbf{u}_0 = \frac{4r^2-1}{80}(y\hat{\boldsymbol{\imath}} - x\hat{\boldsymbol{\jmath}}). \tag{8.47}$$

Notice that in the horizontal plane through the centre ($\sin\phi = y = 0$) the velocity is purely vertical and identical to the fully developed flow in a cavity of circular horizontal section (7.65) except for a factor of $\frac{2}{5}$. Since $\mathbf{u}_0$ is independent of ϕ, the contours of v_n° for $\mathcal{S} = 1$ in figure 7.6 can also be interpreted as contours of the creeping speed in any plane passing through the z-axis of the sphere.

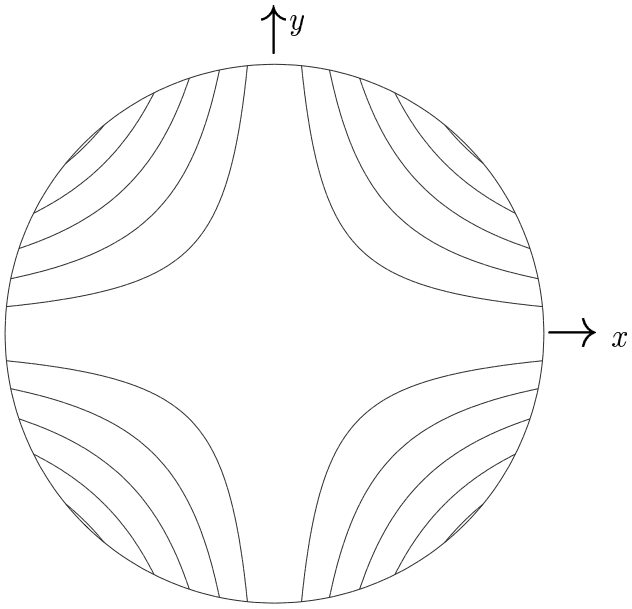

Figure 8.4: Zeroth order pressure, p_0, (8.46) in the plane $z = 0$. The maxima are in the upper-right and lower-left quadrants. Contour levels at 0.01, 0.1(0.1)0.4, 0.6(0.1)0.9, 0.99 of range.

8.2.6 First order mass fraction and temperature

From (8.17), (8.27) and (8.45),

$$\begin{aligned} A_{m1} &\equiv Sc\ \mathbf{u}_0 \cdot \boldsymbol{\nabla} m_0 \\ &= Sc\ \frac{r}{80}\left(1-4r^2\right)\sin\theta\,\hat{\boldsymbol{\phi}}\cdot\boldsymbol{\nabla}(r\sin\theta\cos\phi) \\ &= -Sc\ \frac{r}{80}\left(1-4r^2\right)\sin\theta\sin\phi \\ &= -Sc\ \frac{r}{80}\left(1-4r^2\right)P_1^1(\cos\theta)\sin\phi. \end{aligned} \tag{8.48}$$

The solution for (8.14) for $i = 1$ is then:

$$m_1 = \frac{Sc}{44\,800} r(1-4r^2)(9-20r^2)\sin\theta\sin\phi. \tag{8.49}$$

Similarly,

$$T_1 = \frac{Pr}{44\,800} r(1-4r^2)(9-20r^2)\sin\theta\sin\phi. \tag{8.50}$$

Noting that $y = r\sin\theta\sin\phi$, and $r^2 = x^2 + y^2 + z^2$, it can be seen that m_1 depends on the Cartesian coordinates only as $m_1 = m_1(y, x^2 + z^2)$, so that

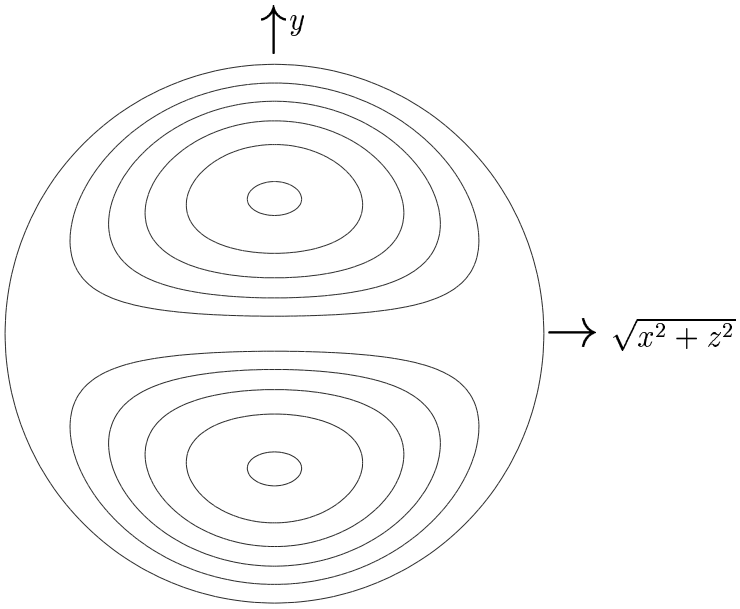

Figure 8.5: First order vapour mass fraction (8.49) or temperature (8.50) in any plane passing through the y-axis. m_1 and T_1 are nonnegative for $y \geq 0$. Contour levels at 0.01, 0.1(0.1)0.4, 0.6(0.1)0.9, 0.99 of range.

it is axisymmetric about the y-axis. Its contours in any plane passing through the y-axis are plotted in figure 8.5; it is nonnegative in the upper hemisphere, $0 \leq \phi \leq \pi$.

The vapour mass fraction field to first order, $m_0 + Gr(1+N)m_1$, is contoured for various values of $Gr(1+N)Sc$ in figure 8.6. The contours could also be interpreted as the temperature, $T_0 + Gr(1+N)$, for the corresponding value of $Gr(1+N)Pr$. By $Gr(1+N)Sc = 13\,000$, the mass fraction field has begun to exhibit internal extrema, which is impossible for the full solution, m, by Theorem 1. Since $m \sim m_0 + Gr(1+N)m_1$, the plots should be increasingly accurate for the lower values of $Gr(1+N)$; comparison with higher order approximations or full solutions would be required to quantify this. Some of the qualitative features of convection in plane vertical cavities, for example as seen in figure 5.8, are evident in figure 8.6, even at this low order: the stretching of the level curves at the departure 'corners', meaning the quadrants $xy > 0$; steepening of the horizontal gradients at the starting 'corners', $xy < 0$; and the beginnings of a stable vertical

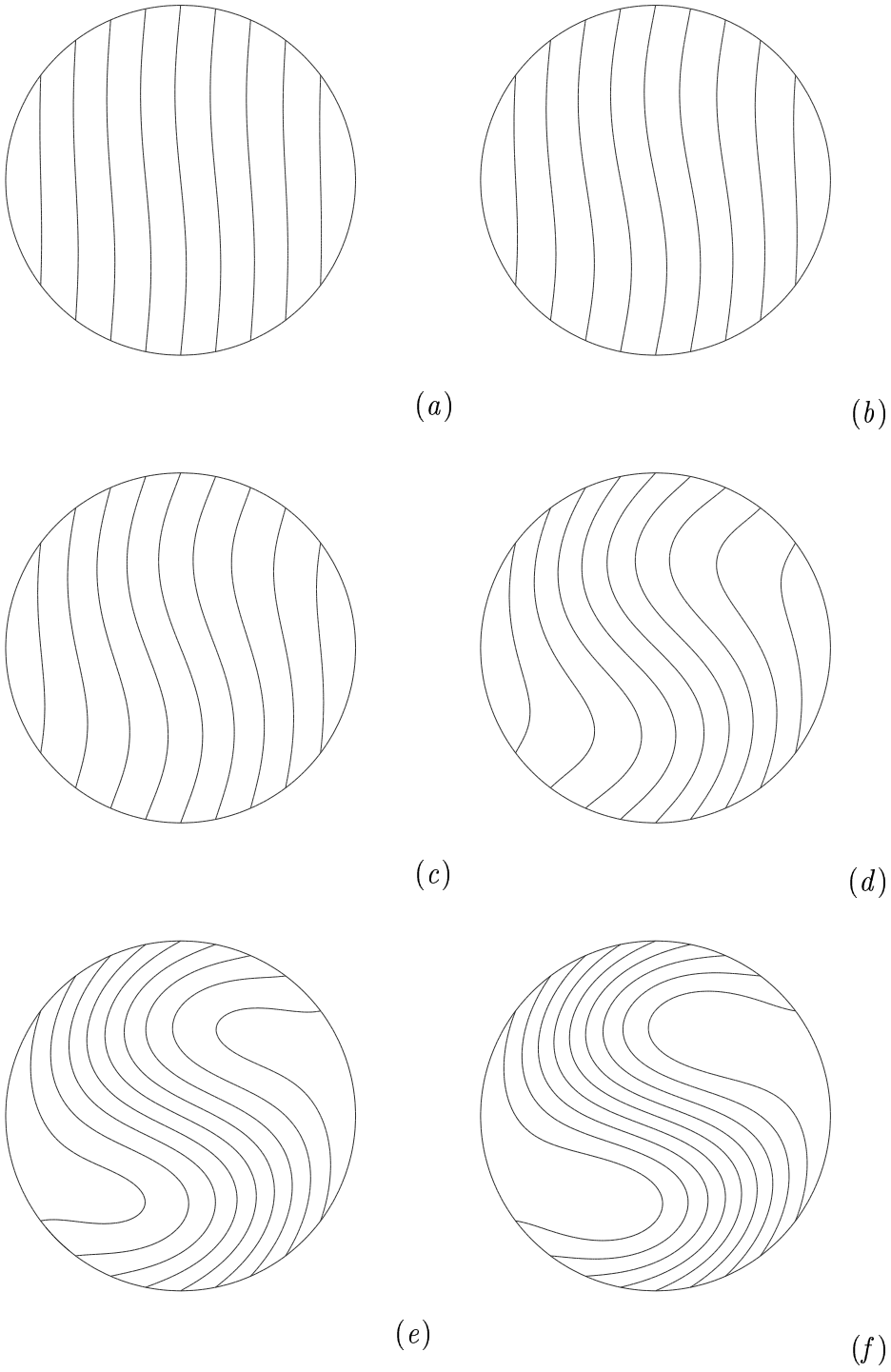

Figure 8.6: Vapour mass fraction in the plane $z = 0$ to first order, $m_0 + Gr(1 + N)m_1$, for $Gr(1 + N)Sc$ of (a) 500, (b) 1000, (c) 2000, (d) 5000, (e) 10 000, (f) 13 000. Contours at $m = -0.4(0.1)0.4$.

stratification in the core.

In comparing the present results with those for vertical plane rectangular cavities (ch. 5), it may be seen that the 'destruction of the conduction–diffusion regime by a gradual penetration of convective effects into the core' (p. 118) occurs at any finite value of $Gr(1+N)Sc$ or $Gr(1+N)Pr$ in the sphere. This is because the 'end-zones' of the spherical enclosure are simply the upper and lower hemispheres: nowhere is 'sufficiently far from the floor or ceiling' (p. 93).

The behaviour outside the plane $z = 0$ can easily be visualized by noting that to first order, $m \sim x + O(Gr^2)$ in the plane $y = 0$, while in the plane $x = 0$, $m_0 = 0$, so that $m \sim m_1 + O(Gr^2)$, which is pictured in figure 8.5.

8.2.7 First order flow correction for inertia

It is convenient to decompose the first order flow into the parts due to inertia and buoyancy:

$$\mathbf{u}_1 = \mathbf{u}_{1I} + \mathbf{u}_{1B}, \tag{8.51}$$

where the parts are both solenoidal and vanish at the boundary and satisfy

$$\mathbf{I}_1 = -\boldsymbol{\nabla} p_{1I} + \nabla^2 \mathbf{u}_{1I} \tag{8.52}$$

$$-\mathbf{B}_1 = -\boldsymbol{\nabla} p_{1B} + \nabla^2 \mathbf{u}_{1B}. \tag{8.53}$$

The inertia force, $\mathbf{I}_1$, contains the single term $\mathbf{u}_0 \cdot \boldsymbol{\nabla}\mathbf{u}_0$, which simplifies greatly from the general form (8.26). Since only the azimuthal component of $\mathbf{u}$ is nonzero, and since it is independent of ϕ, $\mathbf{I}_1$ reduces to

$$\mathbf{I}_1 = \mathbf{u}_0 \cdot \boldsymbol{\nabla}\mathbf{u}_0 = -\frac{(\hat{\boldsymbol{\phi}} \cdot \mathbf{u}_0)^2}{r}\,\hat{\boldsymbol{r}} - \frac{(\hat{\boldsymbol{\phi}} \cdot \mathbf{u}_0)^2 \cot\theta}{r}\,\hat{\boldsymbol{\theta}}. \tag{8.54}$$

These are precisely the terms of the equation of motion referred to in § 8.1.1: they are proportional to the square of the component of velocity about the axis and inversely proportional to the distance from the axis. Bird et al. (1960, p. 85) called them the 'centrifugal force'.

Again, $\mathbf{u}_{1I}$ is found by the method of § B.4. The inertia force, $\mathbf{I}_1$, is found to have no toroidal part; the scalars defining its decomposition are:

$$\begin{aligned}\mathcal{S}[\mathbf{I}_1] &= \frac{r^2(112r^4-72r^2+15)}{604\,800}P_2^0(\cos\theta) \\ &\quad -\frac{r^2(16r^4-12r^2+3)}{57\,600} \qquad (8.55)\\ \mathcal{P}[\mathbf{I}_1-\mathbf{I}_1^{(S)}] &= \frac{r^2(4r^2-1)(28r^2-11)}{1\,209\,600}P_2^0(\cos\theta) \qquad (8.56)\\ \mathcal{T}[\mathbf{I}_1-\mathbf{I}_1^{(S)}] &= 0. \qquad (8.57)\end{aligned}$$

As a result, the velocity is purely poloidal:

$$\begin{aligned}\mathcal{P}[\mathbf{u}_{1I}] &= \frac{r^2(1-4r^2)^2(28r^2-19)}{319\,334\,400}P_2^0(\cos\theta) \qquad (8.58)\\ \mathcal{T}[\mathbf{u}_{1I}] &= 0. \qquad (8.59)\end{aligned}$$

Its spherical components are:

$$\begin{aligned}\mathbf{u}_{1I} &= \frac{r(1-4r^2)^2(28r^2-19)(3\cos^2\theta-1)}{106\,444\,800}\,\hat{\boldsymbol{r}} \\ &\quad +\frac{r(1-4r^2)(336r^4-224r^2+19)\sin\theta\cos\theta}{35\,481\,600}\,\hat{\boldsymbol{\theta}}. \qquad (8.60)\end{aligned}$$

Since, in addition, $\mathcal{P}[\mathbf{u}_{1I}]$ is independent of ϕ, the flow field in any plane passing through the z-axis can be represented by a Stokes's stream-function (see § B.5):

$$\psi_{1I} = \frac{r^3(1-4r^2)^2(19-28r^2)\sin^2\theta\cos\theta}{106\,444\,800}, \qquad (8.61)$$

the contours of which are plotted in figure 8.7. The pressure,

$$p_{1I} = \frac{r^2[(3696r^4-2376r^2+567)\sin^2\theta+1232r^4-1188r^2+315]}{13\,305\,600}, \qquad (8.62)$$

is illustrated in figure 8.8.

Since the circulation is positive around maxima of the stream-function, the flow is radially inward along the z-axis and outward in the xy-plane, and so is analogous to secondary flow in curved pipes and rivers, circular aquaculture tanks and stirred tea cups, as discussed in § 8.1.1. The correction, $\mathbf{u}_{I1}$, is independent of all the parameters of the problem, but its effect on the velocity field vanishes with $Gr(1+N)$.

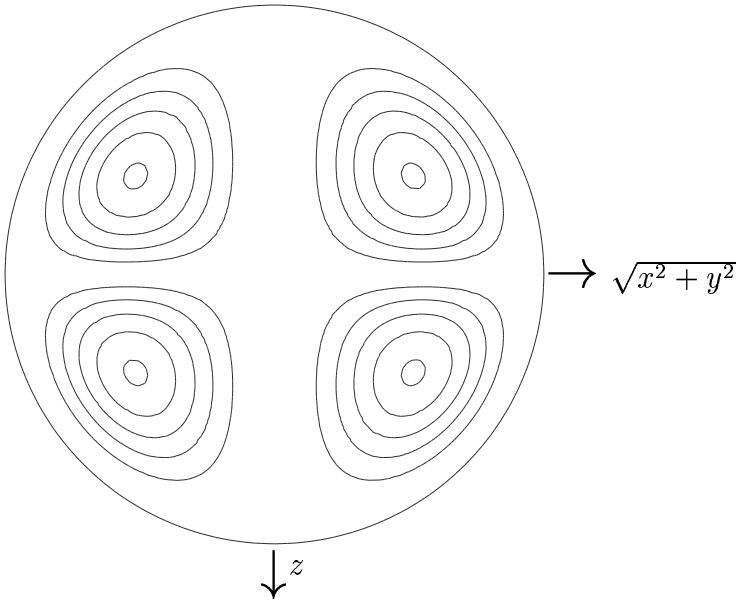

Figure 8.7: Stream-lines of the first order flow due to inertia (8.61) in any plane of constant ϕ. ψ_{1I} is nonnegative for $z \geq 0$. Contour levels at 0.01, 0.1(0.1)0.4, 0.6(0.1)0.9, 0.99 of range.

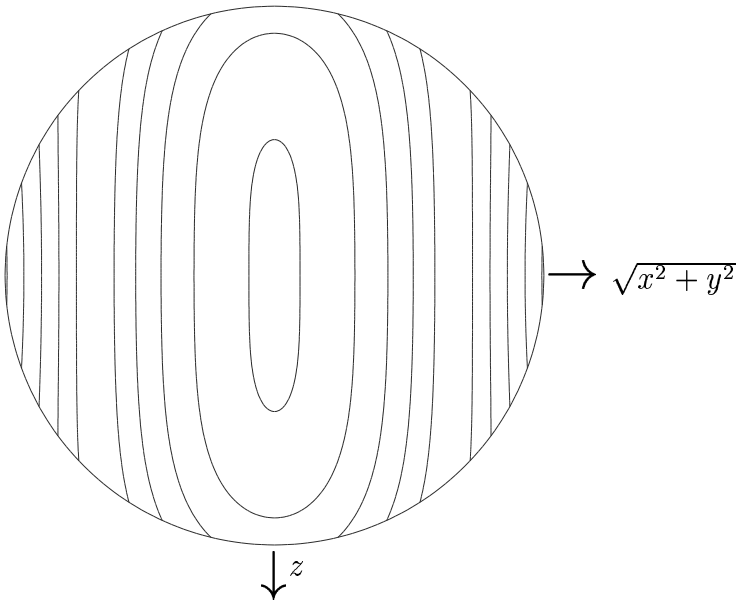

Figure 8.8: First order pressure due to inertia, p_{1I}, (8.62) in any plane of constant ϕ. The maxima occur in the circle $r = 1/2$, $\theta = \pi/2$. Contour levels at 0.01, 0.1(0.1)0.4, 0.6(0.1)0.9, 0.99 of range.

8.2.8 First order flow correction for buoyancy

Since the buoyancy force, $\mathbf{B}_1$, is purely vertical and axisymmetric about the y-axis, the analysis of the first order flow correction for buoyancy is considerably simplified by erecting a new set of spherical coordinates:

$$r \equiv \left(z^2+x^2+y^2\right)^{1/2} \tag{8.63}$$

$$\eta \equiv \arctan\frac{(z^2+x^2)^{1/2}}{y} \tag{8.64}$$

$$\upsilon \equiv \arctan\frac{x}{z}, \tag{8.65}$$

in terms of which the force is independent of the azimuth, υ:

$$\mathbf{B}_1 \equiv \frac{T_1+Nm_1}{1+N}\hat{\boldsymbol{j}} \tag{8.66}$$

$$= \frac{Pr+NSc}{1+N}r(1-4r^2)(9-20r^2)(\cos^2\eta\hat{\boldsymbol{r}}-\frac{\sin 2\eta}{2}\hat{\boldsymbol{\eta}}). \tag{8.67}$$

Note that the choice of polar axis for the spherical coordinates has no effect on the decomposition of vector fields described in appendix B; only the radial coordinate is used explicitly.

The scalars defining the decomposition of the force are:

$$\mathcal{S}[-\mathbf{B}_1] = -\frac{Pr+NSc}{2\,419\,200(1+N)}\left[3(80r^6-84r^4+27r^2)\right.$$
$$\left.+4(80r^6-72r^4+21r^2)P_2^0(\cos\eta)\right] \tag{8.68}$$

$$\mathcal{P}[-\mathbf{B}_1] = -\frac{Pr+NSc\;r^2(4r^2-1)(20r^2-13)P_2^0(\cos\eta)}{1\,209\,600(1+N)} \tag{8.69}$$

$$\mathcal{T}[-\mathbf{B}_1] = 0. \tag{8.70}$$

Again, the velocity is purely poloidal:

$$\mathcal{P}[\mathbf{u}_{1B}] = \frac{(Pr+NSc)r^2(1-4r^2)^2(23-20r^2)P_2^0(\cos\eta)}{319\,334\,400(1+N)} \tag{8.71}$$

$$\mathcal{T}[\mathbf{u}_{1B}] = 0. \tag{8.72}$$

Its spherical components are:

$$\mathbf{u}_{1B} = \frac{Pr+NSc}{106\,444\,800(1+N)}\left[r(1-4r^2)^2(23-20r^2)(3\cos^2\eta-1)\hat{\boldsymbol{r}}\right.$$
$$\left.-3r(1-4r^2)(240r^4-248r^2+23)\sin\eta\cos\eta\hat{\boldsymbol{\eta}}\right]. \tag{8.73}$$

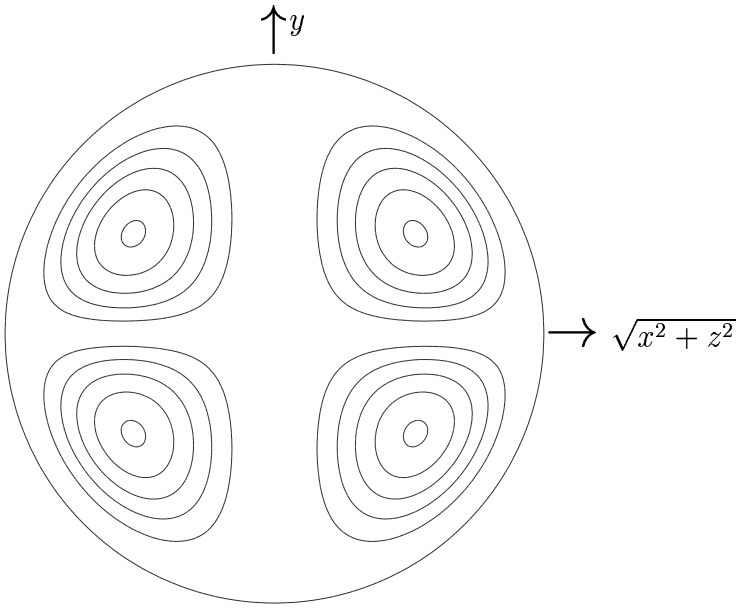

Figure 8.9: Stream-lines of the first order flow due to buoyancy (8.74) in any plane of constant υ. ψ_{1B} is nonnegative for $y \leq 0$. Contour levels at 0.01, 0.1(0.1)0.4, 0.6(0.1)0.9, 0.99 of range.

As $\mathcal{P}[\mathbf{u}_{1B}]$ is independent of the azimuthal angle, υ, the stream-lines of $\mathbf{u}_{1B}$ are confined to planes passing through the y-axis and can be represented by the contours of a Stokes's stream-function:

$$\psi_{1B} = \frac{Pr + NSc}{106\,444\,800(1+N)} r^3 (1-4r^2)^2 (20r^2 - 23) \sin^2\eta \cos\eta, \tag{8.74}$$

which is plotted in figure 8.9. The pressure,

$$\begin{aligned} p_{1B} \;=\; & \frac{Pr + NSc}{26\,611\,200(1+N)} r^2 \left[880r^4 - 1188r^2 + 357 \right. \\ & \left. +6(880r^4 - 792r^2 + 267)\cos^2\eta \right], \end{aligned} \tag{8.75}$$

is illustrated in figure 8.10.

Since the stream-function is nonnegative in the lower hemisphere, $\pi/2 \leq \eta \leq \pi$, the flow is radially outward along the y-axis and inward in the zx-plane, as might be expected from the distribution of vapour mass fraction and temperature given by m_1 and T_1 (fig. 8.5).

The first order correction to the flow field due to buoyancy is similar to that in a long axially heated horizontal tube (Bejan & Tien 1978). The cause is the

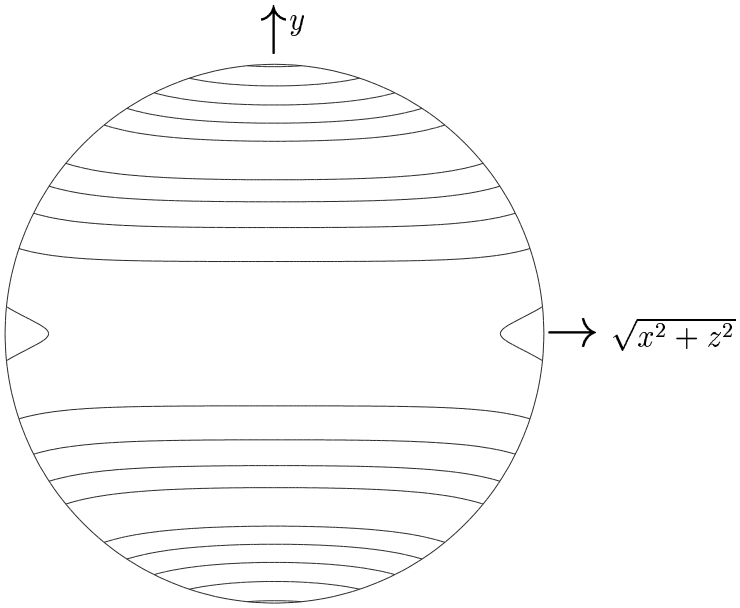

Figure 8.10: First order pressure due to buoyancy, p_{1B}, (8.75) in any plane of constant v. The maxima at the poles, $\sin\eta = 0$. Contour levels at 0.01, 0.1(0.1)0.4, 0.6(0.1)0.9, 0.99 of range.

same: the redistribution of buoyancy forces due to the primary flow leaves the lightest fluid directly above the centre of the sphere (see fig. 8.5) or tube axis. This leads to a vertical flow, which parts at the ceiling and moves outward and downward along the confining walls before returning inward along the horizontal mid-plane. The situation is the same in the lower half, but reversed.

The result of this section supports the conclusion of Mallinson and de Vahl Davis (1977) that (in the analogous pure fluid heat transfer problem) the thermal correction to the flow field depends only on the Grashof and Prandtl numbers in the combination, $GrPr = Ra$.

8.2.9 Flow structure to first order

The flow field correction due to buoyancy, $\mathbf{u}_{1B}$, is topologically equivalent to that due to inertia, $\mathbf{u}_{1I}$, though the sense is reversed.

Three-dimensional flow structures are conveniently discussed in terms of their *critical points* (Perry & Fairlie 1974; Perry & Chong 1987; Chong, Perry &

Cantwell 1990). Interior critical points are those at which the velocity vanishes. Critical points on the boundary are those at which the normal derivative of each component of velocity vanishes.

The two basic types of interior critical points are the *saddle–node* and the *focus*. A plane passes through each saddle–node which is tangential to the stream-lines at the point and in which the projections of the stream-lines converge to or diverge from the point—hence the 'node' part of the name. The node is referred to as stable or unstable, accordingly as the stream-lines converge or diverge. There are two other planes through the point which are also tangential to stream-lines. The projections of the stream-lines on these planes are separated into four regions by the lines corresponding to the other two planes. The flow is inward along the line corresponding to a stable node and outward along the other line—hence the 'saddle' part of the name; the situation is reversed for an unstable node.

A plane tangential to stream-lines also passes through each focus, in which the projections of the stream-lines spiral into or out of the focus accordingly as the focus is stable or unstable. The stream-lines outside this plane coil around the axis of the focus. A focus on the border between stability and instability is called a *centre*.

The three basic types of surface critical points are the saddle, node and focus.

For $\mathbf{u}_{1I}$ and $\mathbf{u}_{1B}$, the interior critical points consist of an axisymmetric *saddle–node* at $r = 0$ and two congruent circles about the axis of symmetry along which each point is a *centre* in its meridian plane; these may be called *vortex-rings*, since $\boldsymbol{\nabla} \times \mathbf{u}_{1I}$ and $\boldsymbol{\nabla} \times \mathbf{u}_{1B}$ are both purely azimuthal, having only a ϕ and a v component, respectively, so that the circles are indeed everywhere parallel to the vorticity. The boundary critical points are a separation point (stable node), for $\mathbf{u}_{1I}$, and a stagnation point (unstable node), for $\mathbf{u}_{1B}$, at each end of the axis of symmetry and a circle of stagnation points along $\theta = \pi/2$ for $\mathbf{u}_{I1}$ and separation points along $\eta = \pi/2$ for $\mathbf{u}_{1B}$.

Each point on the z-axis is a *centre* in the plane of constant z for the creeping

flow, $\mathbf{u}_0$. The boundary critical points of $\mathbf{u}_0$ are centres at $z = \pm 1/2$.

Since the three points $\{x = y = 0, z = \pm\frac{1}{2}, 0\}$ are critical for $\mathbf{u}_0$, $\mathbf{u}_{1I}$ and $\mathbf{u}_{1B}$, they are also critical points for the combined flow to first order in Gr, $\mathbf{u}_0 + Gr(1+N)\mathbf{u}_1$. The addition of the inertial correction to the creeping flow causes the centres at $z = \pm 1/2$ to become stable foci, meaning that the limiting surface stream-lines spiral in to the points. Similarly the centre in the plane $z = 0$ at $r = 0$ becomes an unstable focus. The addition of the buoyancy correction is not as obvious, since it is not orthogonal to the creeping flow, except in the plane $x = 0$, where it is very similar to the inertial correction.

It seems that at low Grashof numbers the basic structure of the flow is defined by the unstable focus in the xy-plane at $r = 0$ and the stable surface foci at $\sin\theta = 0$. The same conclusion was reached by Hiller et al. (1989) from their visualization studies of a cubic enclosure. This distribution of critical points over the boundary is consistent with the 'hairy-sphere theorem' (Perry & Chong 1987), which states that for surfaces topologically equivalent to the sphere, the number of nodes and foci must exceed the number of saddles by two, the *Euler number* of the surface (Hilbert & Cohn-Vossen 1952, p. 295). It will be noticed that the entire flow field can be seen as two nested families of (topological) tori, separated by the xy-plane and surrounding the z-axis, plus the line segments on each half of the z-axis. The Euler number of the torus is zero (Griffiths, H. B. 1976, p. 110), so that the surfaces need not have any critical points.

The three-dimensional nature of the flow is illustrated in figure 8.11 by the locus of a particle released into a steady flow at $Gr(1+N)Pr = 1000$, $Pr = 0.7$, $Sc = 0.6$ and $N = 0.0$. The release point, $r = 0.45, \theta = \phi = 0.05$, is marked with an $\times$. The subfigures are a sequence of snapshots. The particle traces out a stream-line (since the flow is steady) which clearly lies on one of the surfaces homeomorphic to a torus described above. The boundary of the sphere is not shown for clarity, but the Cartesian axes are only shown within the domain. The particle tracks were obtained by second order Runge–Kutta integration of the

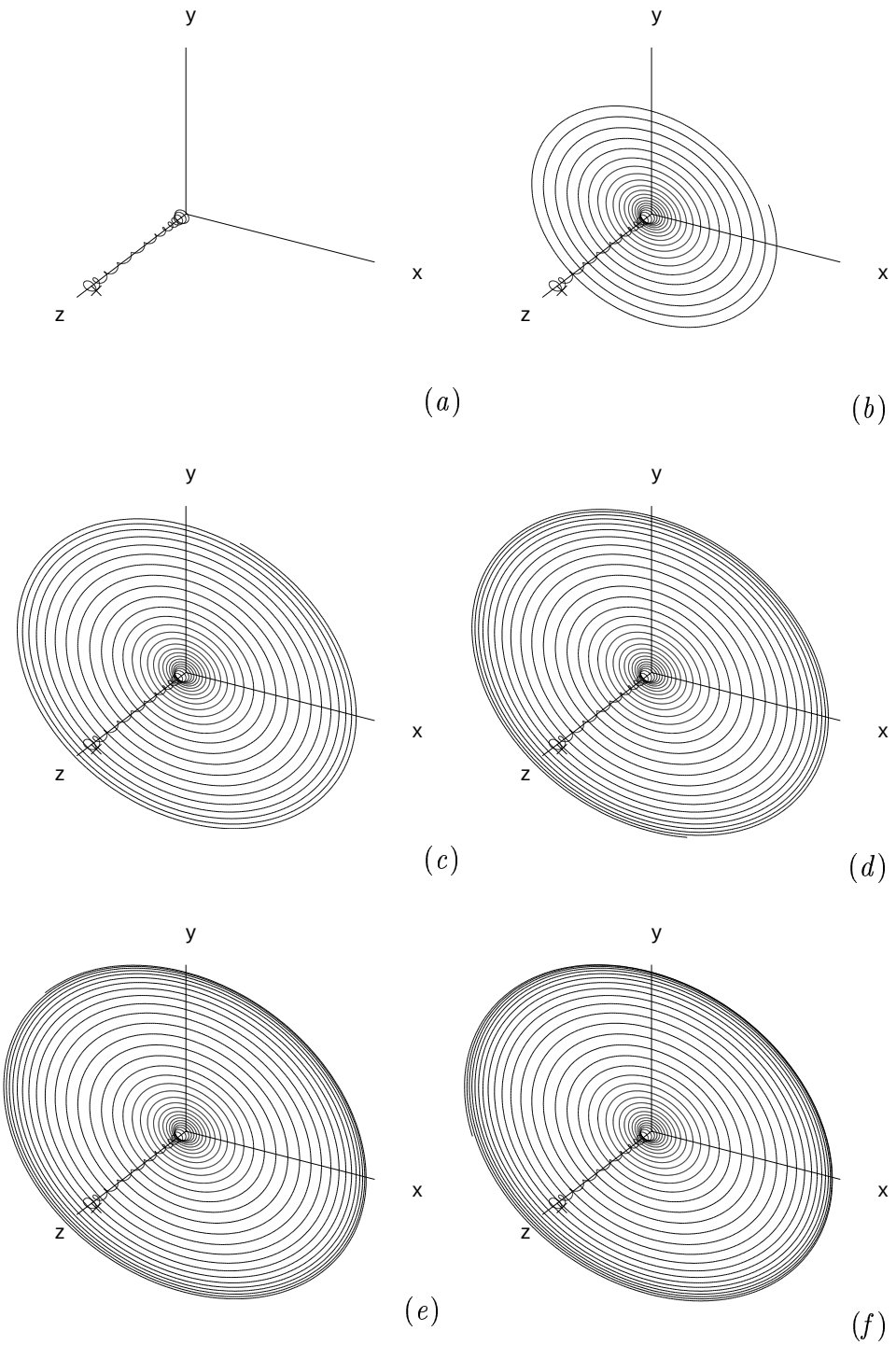

Figure 8.11: The trace of a particle released at the point $r = 0.45, \theta = \phi = 0.05$, marked with a $\times$, into the flow $\mathbf{u}_0 + Gr(1+N)\mathbf{u}_1$ with $Gr(1+N)Pr = 1000, Pr = 0.7, Sc = 0.6, N = 0$ after a dimensionless time interval (units of $b^2/\nu Gr(1+N)$) of (a) 1, (b) 2, (c) 3, (d) 4, (e) 5, (f) 6.

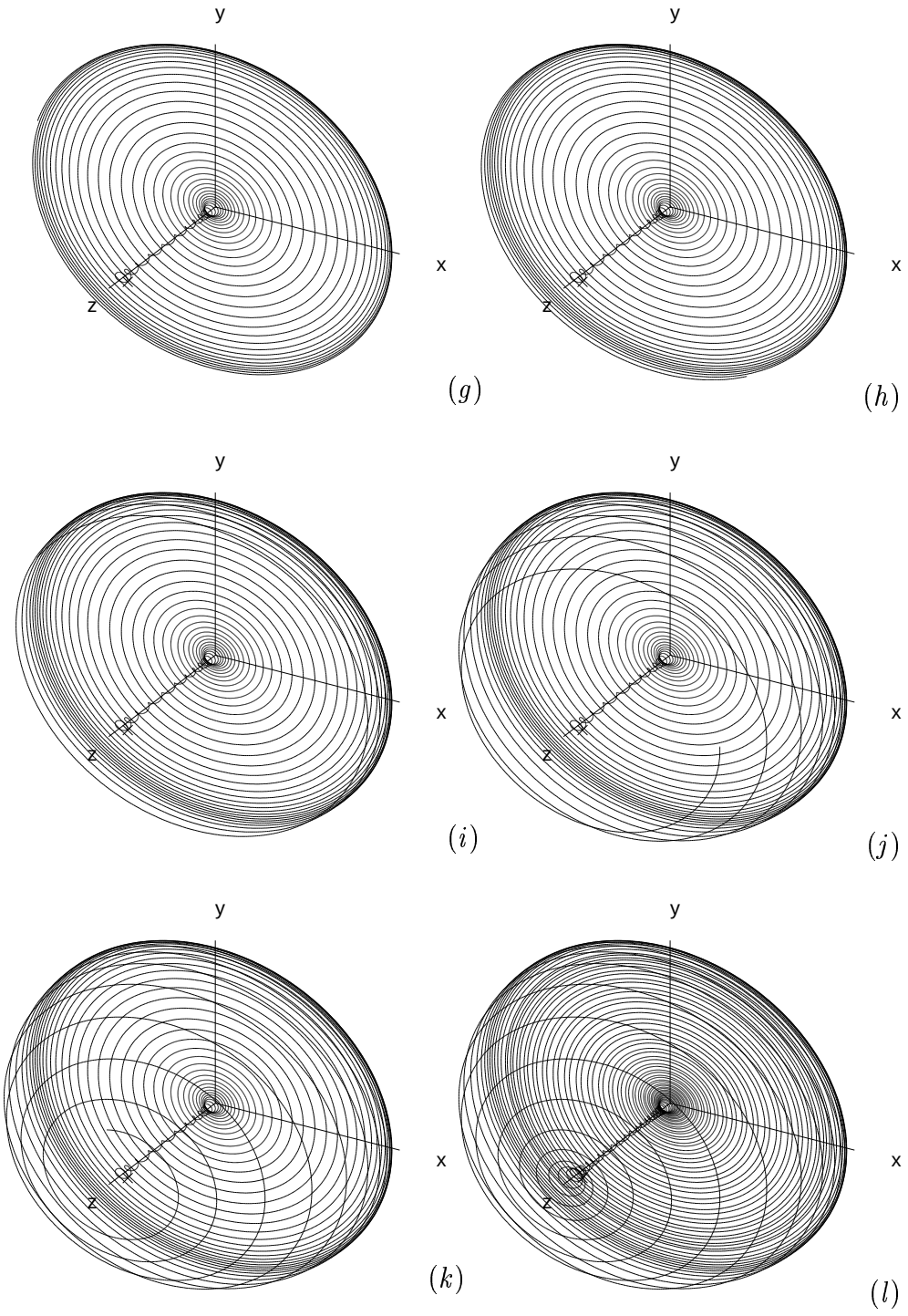

Figure 8.12: Continuation of previous figure. Elapsed times: of (g) 7, (h) 9, (i) 15, (j) 24, (k) 30, (l) 36.

velocity field. The resemblance of the tracks to those in a cuboid produced from the numerical solutions of the full Boussinesq equations of Mallinson and de Vahl Davis (1973, 1977) is startling. The reader is urged to compare figure 8.11 with their figures, some of which were reproduced by de Vahl Davis (1998) and Gebhart et al. (1988, p. 775).

The reason why the particle doesn't return to a starting point after a single 'traverse' of the stream-surface is not numerical error. In discussing their computed stream-lines in a cuboid, Mallinson and de Vahl Davis (1977), concluded that the stream-lines must be closed, but pointed out that 'multiple traverses on the same surface without streamline intersection are, however, possible and cannot be rejected *a priori*'. In fact, it may be demonstrated that it is entirely (kinematically and topologically) possible for a particle to travel an infinite distance in a steady flow field without returning to its starting point. Stream-lines can only cross at critical points, where their direction is undefined. It follows that stream-surfaces also only intersect at critical points. Consider the family of circles formed by the intersection of the surface of a torus and the family of cones coaxial with the torus and with its vertex at the torus's centre. This family of curves satisfies the kinematic and topological requirements of a set of stream-lines free from critical points; it is, for example, homeomorphic to the family of stream-lines on a typical stream-tube of the creeping flow, $\mathbf{u}_0$. Now cut the surface of the torus with a semi-plane bounded by its axis, twist one of its ends and then rejoin the surface and stream-lines. Unless a rational number of twists were applied to the end, the particle will never return to its starting point, even though it remains on the same finite surface (cf. the discussion of force-free magnetic field lines by Moffatt 1978, p. 30).

The addition of the correction for inertia to the creeping flow has a similar effect to the above cutting, twisting and rejoining operation.

8.2.10 Overall vapour and energy transfer rates

The definition of the Sherwood number for the cuboid, (6.21), is here modified for the sphere:

$$Sh = \operatorname{sgn} x \; \hat{\boldsymbol{r}} \cdot \boldsymbol{\nabla} m, \quad (r = \tfrac{1}{2}). \tag{8.76}$$

The net flux through the hemispherical surface $\{r = 1/2, \cos\phi > 0\}$ is

$$\left(\tfrac{1}{2}\right)^2 \int_{-\pi/2}^{\pi/2} \int_0^{\pi} Sh \sin\theta \, \mathrm{d}\theta \; \mathrm{d}\phi, \tag{8.77}$$

which is equal to the net flux through the disk, $\cos\phi = 0$ (i.e. the $x = 0$ plane) or the other hemispherical surface: $r = 1/2, \cos\phi < 0$. The Sherwood number is averaged by dividing the common net flux through these surfaces by the projection of their area in the yz-plane,

$$\left(\tfrac{1}{2}\right)^2 \int_{-\pi/2}^{\pi/2} \int_0^{\pi} (\hat{\boldsymbol{\imath}} \cdot \hat{\boldsymbol{r}}) \sin\theta \, \mathrm{d}\theta \; \mathrm{d}\phi = \frac{\pi}{4}; \tag{8.78}$$

thus

$$\overline{Sh} = \frac{1}{\pi} \int_{-\pi/2}^{\pi/2} \int_0^{\pi} Sh \sin\theta \, \mathrm{d}\theta \; \mathrm{d}\phi. \tag{8.79}$$

To first order in Gr,

$$\overline{Sh} \sim \overline{Sh_0} + Gr(1+N)\overline{Sh_1} + O(Gr^2) \tag{8.80}$$

$$\sim 1 + 0 + O(Gr^2). \tag{8.81}$$

The first order correction to the mean Sherwood number vanishes because m_1 is an odd function of ϕ. The increased diffusion in the quadrants $xy > 0$ is balanced by the lower rate in the other two quadrants. The first order correction to the Sherwood number may also have been expected to vanish from more general symmetry considerations: $\overline{Sh}$ should be an even function of Gr (§ 2.6.3).

The results for the energy transfer rate are completely analogous.

8.3 Conclusions

The flow to first order in the Grashof number in a spherical cavity subjected to horizontal gradients of vapour mass fraction and temperature is seen to embody

the two mechanisms adduced by Mallinson and de Vahl Davis (1973, 1977) for spanwise flow in a horizontally heated cuboid: the buoyancy effect, by which the end-walls retard the convective disturbance of the density field and so lead to spanwise density gradients; and the inertia effect. The terms in the governing equations responsible for these mechanisms are evident in the analytical derivation and expression of these corrections for the sphere. Although I have not been able to obtain equivalent solutions for the cuboid, the same terms would be active. The analysis has also made clear the conditions under which the corrections would not occur. The buoyancy effect vanishes with the Rayleigh number, or its equivalent for nonisothermal vapour transport, $Gr(Pr+NSc)$, and also if the flow is vertical, as in the tall cavity solutions of chapter 7, since there is then no disturbance of the temperature or vapour mass fraction fields. The inertia effect vanishes if the stream-lines are parallel, since the force is inversely proportional to their radius of curvature. It also vanishes with the Grashof number; in dimensional terms the force is proportional to the square of the primary velocity. The conclusion that

> for rolls adjacent to a solid boundary... as $Ra \to 0$, the axial flow asymptotes to a constant fraction of the cross-sectional flow, a fraction which is certainly not negligible, especially for $Pr \sim 1$ (de Vahl Davis 1998; paraphrasing Mallinson & de Vahl Davis 1977)

must be regarded as incorrect. Indeed, it is at variance with the results of Pao (1970), whence de Vahl Davis first derived the idea (Mallinson & de Vahl Davis 1977); thus, Davis's (1967; de Vahl Davis 1998) 'finite rolls', with only two nonzero Cartesian velocity components, for the linear stability analysis of a vertical cuboid heated from below are not rendered impossible by this argument (they are still, however, subject to the criticism levelled by Davies-Jones 1967).

The preceding analysis in no way precludes nonzero spanwise components of velocity at $Gr(1 + N) = 0$ in a cuboid, since there may be other mechanisms involved. The creeping flow in a cuboid, for example, must, unlike that in a sphere, have a poloidal part. The stream-lines of a toroidal flow are confined to

concentric spheres but infinitesimally close to a noncritical point of a solid wall, a solenoidal flow must be parallel to the wall.

Chapter 9

Conclusions

If the vapour transport rate is such that the normal interfacial velocity induced by diffusion cannot be ignored then the interdiffusion term should be included in the energy equation. The latter inclusion necessitates a composition-dependent mixture specific heat capacity if energy is to be conserved. A single parameter, the mass transfer rate factor, Φ, determines whether these three phenomena should be included or neglected.

When Φ is small, the governing equations may be considerably simplified, becoming more like those of the analogous single fluid heat transfer problem. The compositional contribution to buoyancy and the energy transport due to the evaporation and condensation of the vapour should be retained in the low mass transfer rate limit. Indeed, the latter may even then be the dominant mode of energy transport.

Definitions for the normalized vapour and energy transfer rates (Sherwood and Nusselt numbers) have been proposed which differ from those which would be derived by considering low mass transfer rates from the outset. It appears that these definitions account for much of the dependence of the overall transport rates on the mass transfer rate factor. This means that mean Sherwood or Nusselt numbers obtained (from experiments, or numerical or analytical solutions) at low mass transfer rates may be applicable at much higher mass transfer rates. This

fortuitous result has been previously reported for the Stefan diffusion tube. It does not apply to local fluxes.

Except possibly in the viscous limit, vapour transport in enclosures is likely to be strongly three-dimensional unless the enclosure is very tall and narrow. The latter restriction implies a small combined Grashof number. Future calculations of the onset of multicellular convection in tall cuboids should account for the finite span of the cavity, particularly if this does not exceed 1.7 times the breadth.

References

Abernathy, J. R. & Rosenberger, F. 1981 Soret diffusion and convective instability in a closed vertical cylinder. *Physics of Fluids* **24**, 377–381.

Acrivos, A. 1962 The asymptotic form of the laminar boundary-layer mass-transfer rate for large interfacial velocities. *Journal of Fluid Mechanics* **12**, 337–357.

Adams, J. A. & Lowell, R. L. 1968 Free convection organic sublimation on a vertical semi-infinite plate. *International Journal of Heat and Mass Transfer* **11**, 1215–1224.

Adams, J. A. & McFadden, P. W. 1966 Simultaneous heat and mass transfer in free convection with opposing body forces. *American Institute of Chemical Engineers Journal* **12**, 642–647.

Aris, R. 1989 *Vectors, Tensors, and the Basic Equations of Fluid Mechanics.* Dover.

ASHRAE 1993 *ASHRAE Handbook: Fundamentals*, I-P ed. American Society of Heating, Refrigerating and Air-Conditioning Engineers.

Aung, W. 1972 Fully developed laminar free convection between vertical plates heated asymmetrically. *International Journal of Heat and Mass Transfer* **15**, 1577–1580.

Aung, W., Fletcher, L. S. & Sernas, V. 1972 Developing laminar free

convection between vertical flat plates with asymmetric heating. *International Journal of Heat and Mass Transfer* **15**, 2293–2308.

Backus, G. 1986 Poloidal and toroidal fields in geomagnetic field modeling. *Reviews of Geophysics* **24**, 75–109.

Backus, G., Parker, R. & Constable, C. 1996 *Foundations of Geomagnetism.* Cambridge University Press.

Bajer, K. & Moffatt, H. K. 1990 On a class of steady confined Stokes flows with chaotic streamlines. *Journal of Fluid Mechanics* **212**, 337–363.

Batchelor, G. K. 1954 Heat transfer by free convection across a closed cavity between vertical boundaries at different temperatures. *Quarterly of Applied Mathematics* **12**, 209–233.

Béghein, C., Haghighat, F. & Allard, F. 1992 Numerical study of double-diffusive natural convection in a square cavity. *International Journal of Heat and Mass Transfer* **35**, 833–846.

Bejan, A. 1985 Mass and heat transfer by natural convection in a vertical cavity. *International Journal of Heat and Fluid Flow* **6**, 149–159.

Bejan, A. 1995 *Convection Heat Transfer*, 2nd ed. Wiley.

Bejan, A. & Tien, C. L. 1978 Fully developed natural counterflow in a long horizontal pipe with different end temperatures. *International Journal of Heat and Mass Transfer* **21**, 701–708.

Bergholz, R. F. 1978 Instability of steady natural convection in a vertical slot. *Journal of Fluid Mechanics* **84**, 743–768.

Bergman, T. L. & Hyun, M. T. 1996 Simulaton of two-dimensional thermosolutal convection in liquid metals induced by horizontal temperature and species gradients. *International Journal of Heat and Mass Transfer* **39**, 2883–2894.

Berkovsky, B. M. & Polevikov, V. K. 1977 Numerical study of problems of high-intensive free convection. In *Heat Transfer and Turbulent Buoyant Convection* (ed. D. B. Spalding & H. Afghan). Hemisphere.

Bird, R. B., Stewart, W. E. & Lightfoot, E. N. 1960 *Transport Phenomena*. Wiley.

Bottemanne, F. A. 1972*a* Experimental results of pure and simultaneous heat and mass transfer by free convection about a vertical cylinder for $Pr = 0.71$ and $Sc = 0.63$. *Applied Scientific Research* **25**, 372–382.

Bottemanne, F. A. 1972*b* Theoretical solution of simultaneous heat and mass transfer by free convection about a vertical flat plate. *Applied Scientific Research* **25**, 137–149.

Boyadjiev, Chr. & Halatchev, I. 1998 The mass transfer and stability in systems with large concentration gradients—I. mass transfer kinetics. *International Journal of Heat and Mass Transfer* **41**, 939–944.

Bühler, L. 1998 Laminar buoyant magnetohydrodynamic flow in vertical rectangular ducts. *Physics of Fluids* **10**, 223–236.

Busse, F. H. 1975 Patterns of convection in spherical shells. *Journal of Fluid Mechanics* **72**, 67–85.

Busse, F. H. 1978 Non-linear properties of thermal convection. *Reports on Progress in Physics* **41**, 1929–1967.

Cahouet, J. & Chabard, J.-P. 1988 Some fast 3D finite element solvers for the generalized Stokes problem. *International Journal for Numerical Methods in Fluids* **8**, 869–895.

Callahan, G. D. & Marner, W. J. 1976 Transient free convection with mass transfer on an isothermal vertical flat plate. *International Journal of Heat and Mass Transfer* **19**, 165–174.

Carslaw, H. S. & Jaeger, J. C. 1959 *Conduction of Heat in Solids*, 2nd ed. Clarendon.

Cement and Concrete Association of Australia 1976 *Australian Concrete Masonry,* by N. J. R. Christie & H. P. Isaacs. Concrete Masonry Association of Australia.

Chadwick, P. & Trowbridge, E. A. 1967 Elastic wave fields generated by scalar wave functions. *Proceedings of the Cambridge Philosophical Society* **63**, 1177–1187.

Chait, A. & Korpela, S. A. 1989 The secondary flow and its stability for natural convection in a tall vertical enclosure. *Journal of Fluid Mechanics* **200**, 189–216.

Chandrasekhar, S. 1981 *Hydrodynamic and Hydromagnetic Stability.* Dover.

Chang, C. J., Lin, T. F. & Yan, W. M. 1986 Natural convection flows in a vertical, open tube resulting from combined buoyancy effects of thermal and mass diffusion. *International Journal of Heat and Mass Transfer* **29**, 1543–1552.

Charlson, G. S. & Sani, R. L. 1970 Thermoconvective instability in a bounded cylindrical fluid layer. *International Journal of Heat and Mass Transfer* **13**, 1479–1496.

Charlson, G. S. & Sani, R. L. 1971 On thermoconvective instability in a bounded cylindrical fluid layer. *International Journal of Heat and Mass Transfer* **14**, 2157–2160.

Chenoweth, D. R. & Paolucci, S. 1986 Natural convection in an enclosed vertical air-layer with large horizontal temperature differences. *Journal of Fluid Mechanics* **169**, 173–210.

Chong, M. S., Perry, A. E. & Cantwell, B. J. 1990 A general classification of three-dimensional flow fields. *Physics of Fluids A* **2**, 765–777.

CLEARY, P. W. 1995*a* Multi-cell flow in differentially heated slots. In *Proceedings of the Twelfth Australasian Fluid Mechanics Conference* (ed. R. W. Bilger), vol. 1, pp. 57–60. The University of Sydney.

CLEARY, P. W. 1995*b* Numerical modelling of natural convection. *CSIRO Division of Mathematics and Statistics Technical Report* DMS - C 95/44.

CLOSE, D. J., PECK, M. K., WHITE, R. F. & MAHONEY, K. J. 1991 Buoyancy-driven heat transfer and flow between a wetted heat source and an isothermal cube. *ASME Journal of Heat Transfer* **113**, 371–376.

CLOSE, D. J. & SHERIDAN, J. 1989 Natural convection in enclosures filled with a vapour and a non-condensing gas. *International Journal of Heat and Mass Transfer* **32**, 855–862.

CLOSE, D. J., SUEHRCKE, H. & MASATTO, A. 1995 The effect of water vapour transfer on natural convection in building cavities. In *Proceedings Fourth International Building Simulation Conference* (ed. J. W. Mitchell & W. A. Beckman), pp. 1–6. International Building and Performance Simulation Association.

COLBURN, A. P. & DREW, T. B. 1937 The condensation of mixed vapors. *Transactions. American Institute of Chemical Engineers* **33**, 197–212.

CORMACK, D. E., LEAL, L. G. & IMBERGER, J. 1974 Natural convection in a shallow cavity with differentially heated end walls. part 1. asymptotic theory. *Journal of Fluid Mechanics* **65**, 209–229.

COSTA, V. A. F. 1997 Double diffusive natural convection in a square enclosure with heat and mass diffusive walls. *International Journal of Heat and Mass Transfer* **40**, 4061–4071.

COURANT, R. & HILBERT, D. 1962 *Methods of Mathematical Physics*, vol. 2. Interscience.

CSIRO (Commonwealth Scientific and Industrial Research Organisation) 1997 *Fastflo Tutorial Guide.* Numerical Algorithms Group. Jordan Hill Rd, Oxford, U.K. OX2 8DR.

Dahl, S. D., Kuehn, T. H., Ramsey, J. W. & Yang, C.-H. 1996 Moisture storage and non-isothermal transport properties of common building materials. *HVAC&R Research* **2**, 42–58.

Daniels, P. G. 1985 Transition to the convective regime in a vertical slot. *International Journal of Heat and Mass Transfer* **28**, 2071–2077.

Daniels, P. G. & Wang, P. 1994 Numerical study of thermal convection in tall laterally heated cavities. *International Journal of Heat and Mass Transfer* **37**, 375–386.

Davies-Jones, R. P. 1967 Thermal convection in an infinite channel with no-slip sidewalls. *Journal of Fluid Mechanics* **44**, 695–704.

Davis, S. H. 1967 Convection in a box: Linear theory. *Journal of Fluid Mechanics* **30**, 465–478.

de Vahl Davis, G. 1983 Natural convection of air in a square cavity: A bench mark numerical solution. *International Journal for Numerical Methods in Fluids* **3**, 249–264.

de Vahl Davis, G. 1998 Unnatural natural convection. In *Heat and Mass Transfer Australasia 1996* (ed. E. Leonardi & C. V. Madhusudana), pp. 1–16. Begell House.

Dean, J. A. 1992 *Lange's Handbook of Chemistry*, 14th ed. McGraw-Hill.

Dean, W. R. 1927 Note on the motion of fluid in a curved pipe. *The London, Edinburgh and Dublin Philosophical Magazine. Series 7.* **14**, 208–223.

DESCARTES, R. 1911 Rules for the direction of the mind. In *The Philosophical Works of Descartes* (trans. E. S. Haldane & G. R. T. Ross), v. 1, pp. 1–77. Cambridge University Press.

DIXON, M. & PROBERT, S. D. 1975 Heat transfer regimes in vertical, plane-walled air-filled cavities. *International Journal of Heat and Mass Transfer* **18**, 709–710.

DRYDEN, H. L., MURNAGHAN, F. D. & BATEMAN, H. 1956 *Hydrodynamics.* Dover.

ECKERT, E. R. G. & CARLSON, W. O. 1961 Natural convection in an air layer enclosed between two vertical plates with different temperatures. *International Journal of Heat and Mass Transfer* **2**, 106–120.

ELDER, J. W. 1965 Laminar free convection in a vertical slot. *Journal of Fluid Mechanics* **23**, 77–98.

ELDER, J. W. 1966 Numerical experiments with free convection in a vertical slot. *Journal of Fluid Mechanics* **24**, 823–843.

ELSASSER, W. M. 1946 Induction effects in terrestrial magnetism. I. theory. *Physical Review* **69**, 106–116.

ELSHERNIBY, S. M., RAITHBY, G. D. & HOLLANDS, K. G. T. 1982 Heat transfer by natural convection across vertical and inclined air layers. *ASME Journal of Heat Transfer* **104**, 96–102.

EUSTICE, J. 1911 Experiments on stream-line motion in curved pipes. *Royal Society of London: Proceedings. Series A (Mathematical and Physical Sciences)* **85**, 119–131.

EVANS, G. H. & GREIF, R. 1998 Transport and deposition in MOCVD for thin film fabrication of high temperature superconductors. In *Heat Transfer 1998* (ed. J. S. Lee), vol. 5, pp. 99–104. Korean Society of Mechanical Engineers.

FAKTOR, M. M. & GARRETT, I. 1974 *Growth of Crystals from the Vapour.* Chapman and Hall.

FALCÓN, M. 1984 Secondary flow in curved open channels. *Annual Review of Fluid Mechanics* **16**, 179–193.

FLETCHER, N. H. 1962 *The Physics of Rainclouds.* Cambridge University Press.

FLUID DYNAMICS INTERNATIONAL 1996 *FIDAP 7.6 Update Manual.* 500 Davis St, Suite 600, Evanston, IL 60201.

FORTE, A. M. & PELTIER, W. R. 1987 Plate techtonics and aspherical Earth structure: the importance of poloidal–toroidal coupling. *Journal of Geophysical Research* **92**, 3645–3679.

FUSEGI, T., HYUN, J. M. & KUWAHARA, K. 1991 Three-dimensional simulations of natural convection in a sidewall-heated cube. *International Journal for Numerical Methods in Fluids* **13**, 857–867.

FUSEGI, T., HYUN, J. M. & KUWAHARA, K. 1993 Three-dimensional natural convection in a cubical enclosure with walls of finite conductance. *International Journal of Heat and Mass Transfer* **36**, 1993–1997.

GADOIN, E. & LE QUÉRÉ, P. 1998 Characterization of unstable modes in partitioned cavities. In *Heat Transfer 1998* (ed. J. S. Lee), vol. 3, pp. 429–434. Korean Society of Mechanical Engineers.

GARABEDIAN, P. R. 1964 *Partial Differential Equations.* Wiley.

GEBHART, B., JALURIA, Y., MAHAJAN, R. L. & SAMMAKIA, B. 1988 *Buoyancy-Induced Flows and Transport*, textbook ed. Hemisphere.

GEBHART, B. & PERA, L. 1971 The nature of vertical natural convection flows resulting from the combined buoyancy effects of thermal and mass diffusion. *International Journal of Heat and Mass Transfer* **14**, 2025–2050.

GERSHUNI, G. Z. & ZHUKHOVITSKII, E. M. 1976 *Convective Stability of Incompressible Fluids* (trans. D. Louvish). Keter.

GILL, A. E. 1966 The boundary-layer regime for convection in a rectangular cavity. *Journal of Fluid Mechanics* **26**, 515–536.

GILL, A. E. & DAVEY, A. 1969 Instabilities of a buoyancy-driven system. *Journal of Fluid Mechanics* **35**, 775–798.

GILL, W. N., DEL CASAL, E. & ZEH, D. W. 1965 Binary diffusion and heat transfer in laminar free convection boundary layers on a vertical plate. *International Journal of Heat and Mass Transfer* **8**, 1135–1151.

GILL, W. N., DEL CASAL, E. & ZEH, D. W. 1966 Free and forced convection in conduits with asymmetric mass transfer. *American Institute of Chemical Engineers Journal* **12**, 266–271.

GIRAULT, V. & RAVIART, P.-A. 1979 *Finite Element Approximation of the Navier–Stokes Equations.* Springer.

GOBIN, D. & BENNACER, R. 1994 Double diffusion in a vertical fluid layer: Onset of the convective regime. *Physics of Fluids* **6**, 59–67.

GREENWELL, D. W., MARKHAM, B. L. & ROSENBERGER, F. 1981 Numerical modelling of diffusive physical vapor transport in cylindrical ampoules. *Journal of Crystal Growth* **51**, 413–425.

GRESHO, P. M. 1988 The finite element method in viscous incompressible flows. In *Recent Advances in Computational Fluid Dynamics* (ed. C. C. Chao, S. A. Orszag & W. Shyy), pp. 148–190. Springer.

GRIFFITHS, H. B. 1976 *Surfaces.* Cambridge University Press.

GRIFFITHS, R. W. 1979 The influence of a third diffusing component upon the onset of convection. *Journal of Fluid Mechanics* **92**, 659–670.

GUGGENHEIM, E. A. 1959 *Thermodynamics.* North-Holland.

HADAMARD, J. 1952 *Lectures on Cauchy's Problem in Linear Partial Differential Equations.* Dover.

HALATCHEV, I. & BOYADJIEV, CHR. 1998 The mass transfer and stability in systems with large concentration gradients—II. Hydrodynamic stability. *International Journal of Heat and Mass Transfer* **41**, 945–949.

HÄMMERLIN, G. & HOFFMANN, K.-H. (eds) 1983 *Improperly Posed Problems and Their Numerical Treatment.* Birkhäuser.

HAN, H. & KUEHN, T. H. 1991 Double diffusive natural convection in a vertical rectangular enclosure—I. Experimental study. *International Journal of Heat and Mass Transfer* **34**, 449–460.

HART, J. E. 1971 Stability of flow in a differentially heated inclined box. *Journal of Fluid Mechanics* **47**, 547–576.

HAYWARD, R. B. 1890 quoted in *The Oxford English Dictionary*, 2nd ed., Clarendon, 1989.

HEINZELMANN, F. J., WASAN, D. T. & WILKE, C. R. 1965 Concentration profiles in a Stefan diffusion tube. *Industrial and Engineering Chemistry Fundamentals* **4**, 55–61.

HELE-SHAW, H. S. 1898 The flow of water. *Nature* **58**, 34–36.

HELE-SHAW, H. S. 1899 Experimental investigation of the motion of a thin film of viscous fluid. *Report of the Sixty-Eighth Meeting of the British Association for the Advancement of Science*, 136–142.

HENS, H. 1996 Heat, air and moisture transfer in insulated envelope parts, final report, volume 1, task 1: Modelling. Tech. rep., Laboratorium Bouwfysica, Department Burgerlijke Bouwkunde, K.U.-Leuven.

Hilbert, D. & Cohn-Vossen, S. 1952 *Geometry and the Imagination*, (trans. P. Nemenyi). Chelsea.

Hill, B. 1998 Membrane materials. BE thesis, School of Engineering, James Cook University.

Hiller, W. J., Koch, S. & Kowalewski, T. A. 1989 Three-dimensional flow structures in laminar natural convection in a cubic enclosure. *Experiments in Thermal Fluid Science* **2**, 34–44.

Hollands, K. G. T. & Konicek, L. 1973 Experimental study of the stability of differentially heated included air layers. *International Journal of Heat and Mass Transfer* **16**, 1467–1476.

Hu, C. Y. & El-Wakil, M. M. 1974 Simultaneous heat and mass transfer in a rectangular cavity. In *Heat Transfer 1974* vol. 5, pp. 24–28. Japan Society of Mechanical Engineers and Society of Chemical Engineers, Japan.

Hyun, J. M. & Lee, J. W. 1990 Double-diffusive convection in a rectangle with cooperating horizontal gradients of temperature and concentration. *International Journal of Heat and Mass Transfer* **33**, 1605–1617.

Incropera, F. P. & DeWitt, D. P. 1990 *Fundamentals of Heat and Mass Transfer*, 3rd ed. John Wiley.

Ivey, G. N. 1984 Experiments on transient natural convection in a cavity. *Journal of Fluid Mechanics* **144**, 389–401.

Jabbari, M. Y., Burns, D. V. & Goldstein, R. J. 1998 Mass transfer downstream of a 90 degree bend in a square duct. In *Heat Transfer 1998* (ed. J. S. Lee), vol. 3, pp. 115–120. Korean Society of Mechanical Engineers.

Jakob, M. 1949 *Heat Transfer*. Wiley.

Jeans, J. 1940 *An Introduction to the Kinetic Theory of Gases*. Cambridge University Press.

Jhaveri, B. S., Markham, B. L. & Rosenberger, F. 1981 On singular boundary conditions in mass transfer across rectangular enclosures. *Chemical Engineering Communications* **13**, 65–75.

Jhaveri, B. S. & Rosenberger, F. 1982 Expansive convection in vapor transport across horizontal rectangular enclosures. *Journal of Crystal Growth* **57**, 57–64.

Johannesson, H. & Parker, G. 1989 Velocity distribution in meandering rivers. *Journal of Hydraulic Engineering* **115**, 1019–1039.

Jones, R. C. & Furry, W. H. 1946 The separation of isotopes by thermal diffusion. *Reviews of Modern Physics* **18**, 151–224.

Joseph, D. D. 1971 Stability of convection in containers of arbitrary shape. *Journal of Fluid Mechanics* **47**, 257–282.

Kahaner, D., Moler, C. & Nash, S. 1989 *Numerical Methods and Software.* Prentice-Hall.

Kakaç, S. & Yener, Y. 1994 *Convective Heat Transfer*, 2nd ed. CRC.

Keey, R. B. & Wee, H. K. 1985 Free convective heat and mass transfer in rectangular building cavities. In *Convective Flows in Porous Media* (ed. R. A. Wooding & I. White). DSIR.

Kernighan, B. W. & Ritchie, D. M. 1988 *The C Programming Language*, 2nd ed. Prentice-Hall.

Klosse, K. & Ullersma, P. 1973 Convection in a chemical vapor transport process. *Journal of Crystal Growth* **18**, 167–174.

Korpela, S. A., Gözüm, D. & Baxi, C. B. 1973 On the stability of the conduction regime of natural convection in a vertical slot. *International Journal of Heat and Mass Transfer* **16**, 1683–1690.

KÜNZEL, H. M. & KIESSL, K. 1997 Calculation of heat and moisture transfer in exposed building components. *International Journal of Heat and Mass Transfer* **40**, 159–167.

KWAK, H. S. & HYUN, J. M. 1998 Unsteady natural convection in an enclosure. In *Heat Transfer 1998* (ed. J. S. Lee), vol. 1, pp. 341–356. Korean Society of Mechanical Engineers.

LAMB, H. 1932 *Hydrodynamics*, 6th ed. Cambridge University Press.

LEE, C. Y. & WILKE, C. R. 1954 Measurements of gaseous diffusion co-efficients using the Stefan cell. *Industrial and Engineering Chemistry* **46**, 2381–2387.

LEE, K.-T., TSAI, H.-L. & YAN, W.-M. 1997 Mixed convection heat and mass transfer in vertical rectangular ducts. *International Journal of Heat and Mass Transfer* **40**, 1621–1631.

LEE, T. S., PARIKH, P. G., ACRIVOS, A. & BERSCHADER, D. 1982 Natural convection in a vertical channel with opposing buoyancy forces. *International Journal of Heat and Mass Transfer* **25**, 499–511.

LEE, Y. & KORPELA, S. A. 1983 Multicellular natural convection in a vertical slot. *Journal of Fluid Mechanics* **126**, 91–121.

LEFEVRE, E. J. 1957 Laminar free convection from a vertical plane surface. In *Proceedings of the Ninth International Congress of Applied Mechanics*, vol. 4, pp. 168–174.

LEONG, W. H., HOLLANDS, K. G. T. & BRUNGER, A. P. 1998 On a physically-realizable benchmark problem in internal natural convection. *International Journal of Heat and Mass Transfer* **41**, 3817–3828.

LEONG, W. H., HOLLANDS, K. G. T. & BRUNGER, A. P. 1999 Experimental Nusselt numbers for a cubical-cavity benchmark problem in natural convection convection. *International Journal of Heat and Mass Transfer* **42**, 1979–1989.

Leopold, H. G. & Johnston, J. 1927 The vapor pressure of the saturated aqueous solutions of certain salts. *Journal of the American Chemical Society* **49**, 1974–1988.

Lewis, J. A. 1950 Free convection in commerical insulating materials. PhD thesis, Brown University.

Lin, T. F., Chang, C. J. & Yan, W. M. 1988 Analysis of combined effects of thermal and mass diffusion on laminar forced convection heat transfer in a vertical tube. *ASME Journal of Heat Transfer* **110**, 337–344.

Lin, T. F., Huang, C. C. & Chang, T. S. 1990 Transient binary mixture natural convection in square enclosures. *International Journal of Heat and Mass Transfer* **33**, 287–299.

Lopez, J. M. 1998 Characteristics of endwall and sidewall boundary layers in a rotating cylinder with a differentially rotating endwall. *Journal of Fluid Mechanics* **359**, 49–79.

Love, A. E. H. 1944 *A Treatise on the Mathematical Theory of Elasticity*, 4th ed. Dover.

Luchini, P. 1986 Analytical and numerical solutions for natural convection in a corner. *AIAA Journal* **24**, 841–848.

Mahajan, R. L. & Angirasa, D. 1993 Combined heat and mass transfer by natural convection with opposing buoyancies. *ASME Journal of Heat Transfer* **115**, 606–612.

Mallinson, G. D. 1987 The effects of side-wall conduction on natural convection in a slot. *ASME Journal of Heat Transfer* **109**, 410–426.

Mallinson, G. D. & de Vahl Davis, G. 1973 The method of the false transient for the solution of coupled elliptic equations. *Journal of Computational Physics* **12**, 435–461.

Mallinson, G. D. & de Vahl Davis, G. 1977 Three-dimensional natural convection in a box: A numerical study. *Journal of Fluid Mechanics* **83**, 1–31.

Markham, B. L. & Rosenberger, F. 1980 Velocity and concentration distribution in a Stefan diffusion tube. *Chemical Engineering Communications* **5**, 287–298.

Mathers, W. G., Madden, A. J. & Piret, E. L. 1957 Simultaneous heat and mass transfer in free convection. *Industrial and Engineering Chemistry* **49**, 961–968.

McBain, G. D. 1995 The effect of humidity on natural convection in vertical air filled cavities. BE thesis, Department of Mechanical Engineering, James Cook University of North Queensland.

McBain, G. D. 1997*a* Modelling vapour diffusion across gas filled cavities with FASTFLO. In *Eleventh Australasian Users Conference Proceedings* (ed. A. Currie). Compumod.

McBain, G. D. 1997*b* Natural convection with unsaturated humid air in vertical cavities. *International Journal of Heat and Mass Transfer* **40**, 3005–3012.

McBain, G. D. 1998 Heat and mass transfer across tall cavities filled with gas–vapour mixtures: The fully developed regime. *International Journal of Heat and Mass Transfer* **41**, 1397–1403.

McBain, G. D., Close, D. J., Suehrcke, H., Harris, J. A. & Brandemuehl, M. 1998 Design of experimental apparatus for the measurement of overall heat transfer rates for internal natural convection in gas–vapour mixtures. In *Heat and Mass Transfer Australasia 1996* (ed. E. Leonardi & C. V. Madhusudana), pp. 25–32. Begell House.

McBain, G. D. & Harris, J. A. 1998 The conduction–diffusion regime for convection in rectangular cavities filled with gas–vapour mixtures. In *Heat Transfer*

1998 (ed. J. S. Lee), vol. 3, pp. 379–384. Korean Society of Mechanical Engineers.

McBain, G. D., Harris, J. A., Close, D. J. & Suehrcke, H. 1998 The effect of humidity on natural convection in vertical air filled cavities. In *Heat and Mass Transfer Australasia 1996* (ed. E. Leonardi & C. V. Madhusudana), pp. 49–56. Begell House.

McBain, G. D., Suehrcke, H. & Harris, J. A. (in press) Evaporation from an open cylinder, *International Journal of Heat and Mass Transfer*.

Meyer, J. P. & Kostin, M. D. 1975 Circulation phenomena in Stefan diffusion. *International Journal of Heat and Mass Transfer* **18**, 1293–1297.

Mills, R. D. 1965 On the closed motion of a fluid in a square cavity. *Journal of the Royal Aeronautical Society* **69**, 116–120.

Moffatt, H. K. 1978 *Magnetic Field Generation in Electrically Conducting Fluids.* Cambridge University Press.

Morrison, G. L. & Tran, V. Q. 1978 Laminar flow structure in vertical free convective cavities. *International Journal of Heat and Mass Transfer* **21**, 203–213.

Munson, B. R. & Joseph, D. D. 1971 Viscous incompressible flow between concentric rotating spheres. Part 1. Basic flow. *Journal of Fluid Mechanics* **49**, 289–303.

Munson, B. R. & Menguturk, M. 1975 Viscous incompressible flow between concentric rotating spheres. Part 3. Linear stability and experiments. *Journal of Fluid Mechanics*, **69**, 705-719.

Nagata, M. & Busse, F. H. 1983 Three-dimensional tertiary motions in a plane shear layer. *Journal of Fluid Mechanics* **135**, 1–26.

Nakabayashi, K. & Tsuchida, Y. 1995 Flow-history effect on higher modes in the spherical Couette system. *Journal of Fluid Mechanics* **295**, 43–60.

NALLASAMY, M. & KRISHNA PRASAD, K. 1977 On cavity flow at high Reynolds numbers. *Journal of Fluid Mechanics* **79**, 391–414.

NELSON, D. J. & WOOD, B. D. 1989 Fully developed combined heat and mass transfer natural convection between parallel plates with asymmetric boundary conditions. *International Journal of Heat and Mass Transfer* **32**, 1789–1792.

NI, W. & NIGRO, N. J. 1994 Finite element analysis of the axially symmetric motion of an incompressible viscous fluid in a spherical annulus. *International Journal for Numerical Methods in Fluids* **19** 207–236.

NILSON, R. H. & BAER, M. R. 1982 Double-diffusive counterbuoyant boundary layer in laminar natural convection. *International Journal of Heat and Mass Transfer* **25**, 285–287.

NUÑEZ-TESTA, G. A. 1986 Evaporation in the presence of isothermal and non-isothermal natural convection. PhD thesis, University of Minnesota.

NUNEZ, G. A. & SPARROW, E. M. 1988 Models and solutions for isothermal and non-isothermal evaporation from a partially filled tube. *International Journal of Heat and Mass Transfer* **31**, 461–477.

OLSON, J. M. & ROSENBERGER, F. 1979 Convective instabilities in a closed vertical cylinder heated from below. Part II. Binary gas mixtures. *Journal of Fluid Mechanics* **92**, 631–642.

OSTRACH, S. 1964 Laminar flow with body forces. In *Theory of Laminar Flows* (ed. F. K. Moore). High Speed Aerodynamics and Propulsion, vol. 4. Princeton University Press.

OSTRACH, S. 1980 Natural convection with combined driving forces. *PCH PhysicoChemical Hydrodynamics* **1**, 233–247.

OSTRACH, S. 1988 Natural convection in enclosures. *ASME Journal of Heat Transfer* **110**, 1175–1190.

Ostroumov, G. A. 1958 Free convection under the conditions of the internal problem (trans. S. Reiss). *NACA Tech. Rep.* TM 1407.

Ozoe, H., Ohmuro, M., Mouri, A., Mishima, S., Sayama, H. & Churchill, S. W. 1983 Laser-Doppler measurements of the velocity along a heated vertical wall of a rectangular enclosure. *ASME Journal of Heat Transfer* **105**, 782–788.

Padmavathi, B. S., Raja Sekhar, G. P. & Amaranth, T. 1998 A note on complete general solutions of Stokes equations. *The Quarterly Journal of Mechanics and Applied Mathematics* **51** 383–388.

Palaniappan, D., Nigam, S. D., Amaranth, T. & Usha, R. 1992 Lamb's solution of Stokes's equations: A sphere theorem. *The Quarterly Journal of Mechnanics and Applied Mathematics* **45**, 47–56.

Pao, H.-P. 1970 A numerical computation of a confined rotating flow. *Journal of Applied Mechanics* **37**, 480–487.

Patankar, S. V., Pratap, V. S. & Spalding, D. B. 1974 Prediction of laminar flow and heat transfer in helically coiled pipes. *Journal of Fluid Mechanics* **62**, 539–551.

Patterson, J. & Imberger, J. 1980 Unsteady natural convection in a rectangular cavity. *Journal of Fluid Mechanics* **100**, 65–86.

Patterson, J. C. 1984 On the existence of an oscillatory approach to steady natural convection in cavities. *ASME Journal of Heat Transfer* **106**, 104–108.

Pellew, A. & Southwell, R. V. 1940 On maintained convective motion in a fluid heated from below. *Royal Society of London: Proceedings. Series A (Mathematical and Physical Sciences)* **176**, 312–343.

Perez-Cordon, R. & Mengual, J. I. 1997 A straightforward approximation to the equations governing convective flows in multi-component fluids. *International Journal of Heat and Mass Transfer* **40**, 1427–1436.

Perry, A. E. & Chong, M. S. 1987 A description of eddying motions and flow patterns using critical point concepts. *Annual Review of Fluid Mechanics* **19**, 125–155.

Perry, A. E. & Fairlie, B. D. 1974 Critical points in flow patterns. *Advances in Geophysics* **18B**, 299–315.

Peterson, E. L. 1999 The effect of aerators on the benthic shear stress in a pond. PhD thesis, James Cook University.

Prandtl, L. 1952 *Essentials of Fluid Dynamics* (trans W. M. Deans). Blackie.

Prata, A. T. & Sparrow, E. M. 1985 Diffusion-driven nonisothermal evaporation. *ASME Journal of Heat Transfer* **107**, 239–242.

Raithby, G. D. & Hollands, K. G. T. 1985 Natural convection. In *Handbook of Heat Transfer Fundamentals* 2nd ed. (ed. W. M. Rohsenhow, J. P. Hartnett & E. N. Ganić), ch. 6. McGraw-Hill.

Ramanujan, M. S. & Thomas, E. S. 1970 *Intermediate Analysis.* Macmillan.

Ranganathan, P. & Viskanta, R. 1988 Natural convection in a square cavity due to combined driving forces. *Numerical Heat Transfer* **14**, 35–39.

Rao, A. K. 1962 Laminar natural convection flow with suction or injection. *Applied Scientific Research* **A11**, 1–9.

Rao, S. S. & Bennett, C. O. 1966 Radial effects in a Stefan diffusion tube. *Industrial and Engineering Chemistry Fundamentals* **5**, 573–575.

Rao, S. S. & Bennett, C. O. 1967 Velocity profile in the Stefan diffusion tube. *Industrial and Engineering Chemistry Fundamentals* **6**, 477.

RAYLEIGH, LORD 1913 On the motion of a viscous fluid. *Philosophical Magazine* **26**, 776–786.

REYNOLDS, O. 1888 On certain laws relating to the régime of rivers and estuaries, and on the possibility of experiments on a small scale. *Report of the Fifty-Seventh Meeting of the British Association for the Advancement of Science*, 555–562.

RIAD MOSSAD, R. 1993 Finite element solution of nonsteady incompressible viscous flow between two rotating concentric spheres. *Computers & Fluids* **22**, 697–711.

ROGERS, R. R. & YAU, M. K. 1989 *A Short Course in Cloud Physics*, 3rd ed. Pergamon.

ROHSENHOW, W. M. & CHOI, H. Y. 1961 *Heat, Mass and Momentum Transfer.* Prentice-Hall.

ROSENBERGER, F. & MÜLLER, G. 1983 Interfacial transport in crystal growth, a parametric comparison of convective effects. *Journal of Crystal Growth* **65**, 91–104.

ROSENBERGER, F., OUZZANI, J., VIOHL, I. & BUCHAN, N. 1997 Physical vapor transport revisited. *Journal of Crystal Growth* **171**, 270–287.

ROSNER, D. E. 1966 Effects of the Stefan–Nusselt flow on the apparent kinetics of heterogeneous chemical reactions in forced convection systems. *International Journal of Heat and Mass Transfer* **9**, 1233–1253.

RUTH, D. W. 1979 On the transition to transverse rolls in an infinite vertical fluid layer—a power series solution. *International Journal of Heat and Mass Transfer* **22**, 1199–1208.

SAVILLE, D. A. & CHURCHILL, S. W. 1970 Simultaneous heat and mass transfer in free convection boundary layers. *American Institute of Chemical Engineers Journal* **16**, 268–273.

SCHENK, J., ALTMANN, R. & DEWIT, J. P. 1976 Interaction between heat and mass transfer in simultaneous natural convection about an isothermal vertical flat plate. *Applied Scientific Research* **32**, 599–606.

SCHLADOW, S. G., PATTERSON, J. C. & STREET, R. L. 1989 Transient flow in a side-heated cavity at high Rayleigh number: a numerical study. *Journal of Fluid Mechanics* **200**, 121–148.

SCHMIDT, E. 1929 Verdunstung und Wärmeübergang (Evaporation and heat transfer). *Gesundheits-Ingenieur* **52**, 525–529.

SCHÖPF, W., PATTERSON, J. C. & BROOKER, A. M. H. 1996 Evaluation of the shadowgraph method for the convective flow in a side-heated cavity. *Experiments in Fluids* **21**, 331–340.

SCHÖPF, W. & STILLER, O. 1997 Three-dimensional patterns in a transient, stratified intrusion flow. *Physical Review Letters* **79**, 4373–4376.

SCHWENGELS, S. & SCHULZ, D. 1989 Second-order finite difference solutions for the flow between rotating concentric spheres. *International Journal for Numerical Methods in Fluids* **9** 1099–1111.

SERNAS, V. & FLETCHER, L. S. 1970 A schlieren interferometer method for heat transfer studies. *ASME Journal of Heat Transfer* **92**, 202–204.

SHERMAN, M. 1968 Toroidal and poloidal field representation for convective flow within a sphere. *Physics of Fluids* **11**, 1895–1900.

SHERWOOD, T. K. & PIGFORD, R. L. 1952 *Absorption and Extraction*, 2nd ed. McGraw-Hill.

SOMERS, E. V. 1956 Theoretical considerations of combined thermal and mass transfer from a vertical flat plate. *Journal of Applied Mechanics* **23**, 295–301.

SPALDING, D. B. 1960 A standard formulation of the steady convective mass transfer problem. *International Journal of Heat and Mass Transfer* **1**, 192–207.

Spalding, D. B. 1963 *Convective Mass Transfer.* Edward Arnold.

Sparrow, E. M. & Nunez, G. A. 1988 Experiments on isothermal and non-isothermal evaporation from partially filled, open-topped vertical tubes. *International Journal of Heat and Mass Transfer* **31**, 1345–1355.

Sparrow, E. M., Nunez, G. A. & Prata, A. T. 1985 Analysis of evaporation in the presence of composition-induced natural convection. *International Journal of Heat and Mass Transfer* **28**, 1451–1460.

Spiegel, E. A. & Veronis, G. 1960 On the Boussinesq approximation for a compressible fluid. *Astrophysical Journal* **131**, 442–447.

Stokes, R. H. & Robinson, R. A. 1949 Standard solutions for humidity control at 25°C. *Industrial and Engineering Chemistry* **41**, 2013.

Stokes, G. G. 1845 On the theories of the internal friction of fluids in motion, and of the equilibrium and motion of elastic solids. *Transactions of the Cambridge Philosophical Society* **8**, 287–319.

Stokes, G. G. 1899 Mathematical proof of the identity of the stream lines obtained by means of a viscous film with those of a perfect fluid moving in two dimensions. *Report of the Sixty-Eighth Meeting of the British Association for the Advancement of Science*, 143–144.

Suehrcke, H. & Harris, J. A. 1995 Enhancement of water evaporation from a cylindrical container due to concentration induced free convection. In *Proceedings of the Twelfth Australasian Fluid Mechanics Conference* (ed. R. W. Bilger), pp. 891–895. The University of Sydney.

Suehrcke, H., Harris, J. A. & McBain, G. D. 1996 Water evaporation from a cylindrical container: The Stefan problem revisited. In *Fifth Australasian Natural Convection Workshop*, (ed. S. Armfield). The University of Sydney.

SUEHRCKE, H. & MCBAIN, G. D. 1998 The effect of humidity on the heat and mass transfer across narrow vertical air spaces. In *Heat Transfer 1998* (ed. J. S. Lee), vol. 5, pp. 157–162. Korean Society of Mechanical Engineers.

TAUNTON, J. W., LIGHTFOOT, E. N. & STEWART, W. E. 1970 Simultaneous free-convection heat and mass transfer in laminar boundary layers. *Chemical Engineering Science* **25**, 1927–1937.

TENWOLDE, A. 1989 Moisture transfer through materials and systems in buildings. In *Water Vapor Transmission through Buildings Materials and Systems* (ed. H. R. Trechsel & M. Bomberg), pp. 11–18. American Society for Testing and Materials.

THOMASSET, F. 1984 Implementation of non-conforming linear finite elements. In *Navier-Stokes Equations* 3rd ed. (by R. Temam), pp. 472–492. North-Holland.

THOMSON, J. 1876 On the origin of windings of rivers in alluvial plains, with remarks on the flow of water round bends in pipes. *Royal Society of London. Proceedings* **25**, 5–8.

THOMSON, J. 1877 Experimental demonstration in respect to the origin of windings of rivers in alluvial plains, and to the mode of flow of water round bends of pipes. *Royal Society of London. Proceedings* **26**, 356–357.

TIMMONS, M. B., SUMMERFELT, S. T. & VINCI, B. J. 1998 Review of circular tank technology and management. *Aquacultural Engineering* **18**, 51–69.

TIMOSHENKO, S. & WOINOWSKY-KRIEGER, S. 1959 *Theory of Plates and Shells*, 2nd ed. McGraw-Hill.

TREVISAN, O. V. & BEJAN, A. 1987 Combined heat and mass transfer by natural convection in a vertical enclosure. *ASME Journal of Heat Transfer* **109**, 104–112.

TURNER, J. S. 1973 *Buoyancy Effects in Fluids.* Cambridge University Press.

TURNER, J. S. 1974 Double-diffusive phenomena. *Annual Review of Fluid Mechanics* **6**, 37–56.

TURNER, J. S. 1985 Multicomponent convection. *Annual Review of Fluid Mechanics* **17**, 11–44.

VAN DYKE, M. 1964 *Perturbation Methods in Fluid Mechanics.* Academic Press.

VAN DYKE, M. 1975 *Perturbation Methods in Fluid Mechanics*, annotated ed. Parabolic.

VEST, C. M. & ARPACI, V. S. 1969 Stability of natural convection in a vertical slot. *Journal of Fluid Mechanics* **36**, 1–15.

VINOKUR, M. 1983 On one-dimensional stretching functions for finite-difference calculations. *Journal of Computational Physics* **50**, 215–234.

VISKANTA, R., KIM, D. M. & GAU, C. 1986 Three-dimensional natural convection heat transfer of a liquid metal in a cavity. *International Journal of Heat and Mass Transfer* **29**, 475–485.

WASAN, D. T. 1967 Velocity profile in the Stefan diffusion tube. *Industrial and Engineering Chemistry Fundamentals* **6**, 477.

WEAVER, J. A. & VISKANTA, R. 1991*a* Natural convection due to horizontal temperature and concentration gradients. I. Variable thermophysical property effects. *International Journal of Heat and Mass Transfer* **34**, 3107–3120.

WEAVER, J. A. & VISKANTA, R. 1991*b* Natural convection due to horizontal temperature and concentration gradients. II. Species interdiffusion, Soret and Dufour effects. *International Journal of Heat and Mass Transfer* **34**, 3121–3133.

WEAVER, J. A. & VISKANTA, R. 1991*c* Natural convection in binary gases due to horizontal thermal and solutal gradients. *ASME Journal of Heat Transfer* **113**, 141–147.

Wee, H. K., Keey, R. B. & Cunningham, M. J. 1989 Heat and moisture transfer by natural convection in a rectangular cavity. *International Journal of Heat and Mass Transfer* **32**, 1765–1778.

Whitaker, S. 1967 Velocity profile in the Stefan diffusion tube. *Industrial and Engineering Chemistry Fundamentals* **6**, 476.

White, J. H. 1989 Moisture transport in walls: Canadian experience. In *Water Vapor Transmission through Building Materials and Systems* (ed. H. R. Trechsel & M. Bomberg), pp. 35–50. American Society for Testing and Materials.

Wilcox, W. R. 1961 Simultaneous heat and mass transfer in free convection. *Chemical Engineering Science* **13**, 113–119.

Yan, W. M. & Lin, T. F. 1990 Natural convection heat transfer enhancement through latent heat transfer in vertical parallel late channel flows. *The Canadian Journal of Chemical Engineering* **68**, 360–367.

Yan, W. M., Tsay, Y. L. & Lin, T. F. 1989 Simultaneous heat and mass transfer in laminar mixed convection flows between vertical parallel plates with asymmetric heating. *International Journal of Heat and Fluid Flow* **10**, 262–269.

Zikanov, O. Yu. 1996 Symmetry breaking bifurcations in spherical Couette flow. *Journal of Fluid Mechanics* **310**, 293–324.

Appendix A

Sample *Fasttalk* Code

A listing of a fully functioning sample *Fasttalk* file of the type described in § 5.1 follows. Note that the notation is that of the earlier works for which it was used (McBain 1997*a*; McBain & Harris 1998), rather than that of this thesis.

```
%humid.tal.prob
P Sc 0.61
P Le0 Sc/0.71
P GrSTAR 1000.0/(Sc/Le0)
P N 0.5
P B -0.5
P I 0.5
%
P LeA (B*Le0)/(B-(I*Le0))
P lnBp1 log(B+1.0)
P Lambda lnBp1/LeA
%
P Pen 5e2
P rvtol 1e-3
P rvtol2 5e-4
P rdiltol 1e-3
```

```
P Relx 0.5
%
F . ffFlib/cavbtag
%
A momentum
%
e D_i {-Pen} D_j U1_j + D_i {v201} - D_j D_j U1_i +\
  {v100*GrSTAR}_j D_j U1_i = {0.0, (1/(1.0+N))}_i U2 +\
  {0.0, (N/(1.0+N))}_i U3
e D_j D_j U2 + {v300 * I}_j D_j U2 =\
  {GrSTAR * Sc * ((I*v104)+(1.0/Le0)) * v100}_j D_j U2
e D_j D_j U3 =\
  {GrSTAR * Sc * v100}_j D_j U3
e v300 = [grad] {v104}
b floor U1 = {0.0, 0.0}
b rightwall U1 = {rightblow * v301, rightblow * v302}
b ceiling U1 = {0.0, 0.0}
b leftwall U1 = {leftblow * v301, leftblow * v302}
b rightwall U2 = {1.0}
b leftwall U2 = {0.0}
b rightwall U3 = {1.0}
b leftwall U3 = {0.0}
%
A [reduced] dilatation
e U1 = {1.0} D_j {v100}_j
%
F . ffFlib/myutes
%
A fickfluxp
```

```
e U1_i = {-1.0} D_i {v104}
%
A advvapflux
e v000={GrSTAR*Sc*v101*v104,GrSTAR*Sc*v102*v104}
%
A mflux
% bulk advective flux
e v500={GrSTAR*Sc*v101*v104,GrSTAR*Sc*v102*v104}
% Fickian diffusion flux
e v600=grad{-v104}
% total flux w.r.t. stationary coordinates
e v000={v500+v600}
%

< momloop
mtitno = 1
while rmaxchange>rvtol | mtitno<3
show mtitno
momentum
solv
v500=v200
if ((mtitno*bigitno)<2)
v200 = v100
endif
if ((mtitno*bigitno)>1)
v200 = (Relx*v100) + ((1.0-Relx)*v500)
endif
popp
clea
```

```
arro
cont 103
cont 104
v500 = v100 - v400
v500 = abs v500
v600 = abs v100
v601 = max v601
v602 = max v602
v603 = max v603
v604 = max v604
v500 = v500/v600
rmaxchange = max v500
show rmaxchange
mtitno = mtitno + 1
endwhile
>

< run
clock
prim
paras
leftblow =  B/(GrSTAR*Sc)
rightblow = leftblow/(B+1.0)
bigitno = 1
RelMaxDil=rdiltol+1
keeplooping=1
while keeplooping
show bigitno
momloop
```

```
rvtol=rvtol2
dilatation
solv
expand 1
v301 = v301 - (Pen * v101)
cont 301
v101=abs v101
MaxDil = max v101
show MaxDil
popp
oldrmd=RelMaxDil
uscal = max v601
vscal = max v602
uscal = uscal M vscal
RelMaxDil = MaxDil/uscal
show RelMaxDil

if RelMaxDil<rdiltol
keeplooping=0
endif

if RelMaxDil>rdiltol & RelMaxDil<oldrmd
keeplooping=1
endif

if RelMaxDil>oldrmd & bigitno>1
!#Divergence diverging!
keeplooping=keeplooping-0.2
endif
```

```
bigitno = bigitno + 1

endwhile
clock
name 100 velocity
name 103 temperature
name 104 mass fraction
name 201 pressure
>


< hhmark
!marknodes 2 1.0 # the second argument should be A/2
>

< eflux
% conduction flux
nostack
gradient 300 101 v103
solv 300
nostack -1
v300=-v300
name 301 conduction
name 302 conduction

% bulk advection flux
v401=GrSTAR*Sc*(I*v104 + (1.0/Le0))*v101*v103
v402=GrSTAR*Sc*(I*v104 + (1.0/Le0))*v102*v103
```

```
name 401 advection flux
name 402 advection flux

% interdiffusion flux
nostack
gradient 500 101 v104
solv 500
nostack -1
v501=-I*v501*v103
v502=-I*v502*v103
name 501 interdiffusion
name 502 interdiffusion

% total energy flux
v600 = v300 + v400 + v500
name 601 energy flux
name 602 energy flux
>

< heatlines
eflux
total_int 101 101 v601
ANubar=-Out
show ANubar
lscalint 101 101 v601
ANu0=-Out
Nuinfty=Lambda/(exp(Lambda)-1)
show ANu0
show Lambda
```

```
show Nuinfty
heatf 101 100 v600
solv
cont 101
popp
>

< b4c4
hhmark
mark 0
mark 102
show B
show Sc
show LeA
show N
>

< afterc4
push
push
limits -0.05 0.05
% calculate comparison with fully developed solution

% horizontal component of velocity, normalised by max u

uinf = lnBp1/(GrSTAR*Sc)
v101 = uinf
name 101 uinf
v201 = v301 - v101
```

```
umin = min v301
umax = max v301
umin = abs umin
uscal = umin M umax
v201 = v201/uscal
name 201 udefectnrmd

% temperature, not normalised (no need)

v103 = ((B+1.0)^(X1/LeA)-1.0)/((B+1.0)^(1.0/LeA)-1.0)
name 103 thetainf
v203 = v303 - v103
name 203 tdefect

% mass fraction, not normalised (no need)

v104 = ((B+1.0)^X1 - 1.0)/B
name 104 phiinf
v204 = v304 - v104
name 204 mdefect

% vertical component of velocity, normalised by max vinf

c1 = LeA*LeA/(Sc-LeA)/lnBp1/lnBp1
c2 = N/(Sc-1.0)/lnBp1/lnBp1
c3 = (((LeA+N)/lnBp1) + c4 * (N+1.0))/lnBp1
v102 = ((B+1.0)^(X1/Sc)-1.0)/((B+1.0)^(1.0/Sc)-1.0)
name 102 sigma
v102 = Sc*(c1*(v102-v103) + c2*(v102-v104) +\
```

```
 c3*(v102-X1))/(N+1.0)
name 102 vinf
vscal = max v102
v202 = v302 - v102
v202 = v202/vscal
name 202 vdefectnrmd

% vertical pressure gradient, normalised by dpdyinf

phibar = 1.0/lnBp1 - 1.0/B
thetabar = LeA/lnBp1 - 1.0/((B+1.0)^(1/LeA)-1.0)
denpertbar = (thetabar + N * phibar)/(1.0 + N)
nostack
gradient 501 101 v401
solv 501
nostack -1
name 501 pressure gradient
name 502 pressure gradient
dpdyinf = denpertbar + c4
v504 = v502 - dpdyinf
v504 = v504/dpdyinf
name 504 dpdydefectnrmd

hhmark
mark 0
mark 201
mark 202
mark 203
mark 204
```

```
mark 504
>

< paras
!#Problem Parameters:
show GrSTAR*Sc/Le0
show Sc/Le0
show Sc
show B
show I
show N
!#Solution Method Parameters:
show Pen
show Relx
show rvtol
show rvtol2
show rdiltol
>

< reading
open #1 r A5/a516sq._0.5.s.out
read #1
clos #1
v100=v100
open #2 r A5/a516sq._0.5.p.out
read #2
clos #2
v201=v201
>
```

The file inclusion commands, beginning with an `F`, include the contents of the files `ffFlib/cavbtag`:

```
D 1 floor
D 2 rightwall
D 3 ceiling
D 4 leftwall
```

and `ffFlib/myutes`:

```
A total_int
e [integrated] {v101}
%
A fscalint
b floor [integrated] {v101}
A rscalint
b rightwall [integrated] {v101}
A cscalint
b ceiling [integrated] {v101}
A lscalint
b leftwall [integrated] {v101}
%
A strf
e v101 = [curlv] {-v100}
e D_j D_j U1 = {v101}
b floor U1 = {0.0}
%
A heatf
e v101 = [curlv] {-v100}
e D_j D_j U1 = {v101}
b floor U1 = {0.0}
b ceiling U1 = {-ANubar}
```

```
A gradient
e U1_i = {1.0} D_i {v101}
%
```

The *Fasttalk* file calls a Bourne shell script, `marknodes`, which is listed below.

```
# marknodes coord_number coord_value:
# creates a mark.dat file from a mesh.dat
# Use coord_number = 1 for x, 2 for y
# Do not use on mesh.dat files invoking
# the triangular mesh generator

awk '
NF == 2 && $c == v { print }
' c=$1 v=$2 mesh.dat >mark.dat
```

Appendix B

Vector Fields in a Sphere

Originally developed for the representation of elastic and viscous vibrations (Love 1944, p. 280; Lamb 1932, pp. 632–7) and magnetic vector potentials (Elsasser 1946), the poloidal–toroidal decomposition has also been used occasionally for fluid velocity fields (Lamb 1932, pp. 594–602; Sherman 1968; Joseph 1971; Busse 1975; Munson & Menguturk 1975; Chandrasekhar 1981, pp. 225–6; Forte & Peltier 1987; Bajer & Moffatt 1990; Palaniappan et al. 1992; Padmavathi, Raja Sekhar & Amaranth 1998). The technique is analogous to the introduction of a stream-function in two-dimensional or axisymmetric flow (Moffatt 1978, pp. 20–1); if the flow is axisymmetric, the scalar defining the poloidal part is directly related to Stokes's stream-function (see § B.5). The essential properties of the decomposition are summarized here; further details can be found in the works of Chadwick and Trowbridge (1967), Moffatt (1978, pp. 17–22), Chandrasekhar (1981, pp. 622–6), Backus (1986) and Backus, Parker and Constable (1996, ch. 5). Basically, a toroidal field is a solenoidal field with no radial component and a poloidal field is a solenoidal field with a toroidal curl.

B.1 Solenoidal fields

The fundamental lemma is due to Chadwick and Trowbridge (1967).

Lemma 1 (Chadwick–Trowbridge) *Let* $\mathbf{v}$ *be a vector field possessing partial derivatives of order up to two which are Hölder continuous on* $S = \{(r, \theta, \phi) : 0 < r_1 \leq r \leq r_2 < \infty, 0 \leq \theta \leq \pi, 0 \leq \phi \leq 2\pi\}$. *Then if, in addition,* $\boldsymbol{\nabla} \cdot \mathbf{v} = 0$ *on* S, *there are scalars* $\mathcal{P}[\mathbf{v}]$ *and* $\mathcal{T}[\mathbf{v}]$ *such that* $\mathbf{v} = (\boldsymbol{\nabla}\times)^2(\mathcal{P}[\mathbf{v}]\mathbf{r}) + \boldsymbol{\nabla} \times (\mathcal{T}[\mathbf{v}]\mathbf{r})$ *on* S.

Vectors of the form $(\boldsymbol{\nabla}\times)^2\mathcal{P}\mathbf{r}$ and $\boldsymbol{\nabla} \times \mathcal{T}\mathbf{r}$ are called *poloidal* and *toroidal*, respectively. It has been shown by Backus (1986) that the lemma can be extended from spherical annuli to spheres. The scalars can be obtained as the regular solutions of

$$\mathcal{L}^2\mathcal{P}[\mathbf{u}] = -\mathbf{r} \cdot \mathbf{u} \tag{B.1}$$

$$\mathcal{L}^2\mathcal{T}[\mathbf{u}] = -\mathbf{r} \cdot (\boldsymbol{\nabla} \times \mathbf{u}), \tag{B.2}$$

where

$$\mathcal{L}^2 \equiv r^2\nabla^2 - \frac{\partial}{\partial r}r^2\frac{\partial}{\partial r} \equiv \frac{1}{\sin\theta}\frac{\partial}{\partial\theta}\sin\theta\frac{\partial}{\partial\theta} + \frac{1}{\sin^2\theta}\frac{\partial^2}{\partial\phi^2} \tag{B.3}$$

(Moffatt 1978, p. 18).

The operator $\mathcal{L}^2$ is the surface Laplacian for the unit sphere (Aris 1989, pp. 196–7, 222). Its eigenfunctions are the spherical harmonics:

$$\mathcal{L}^2 S_n = -n(n+1)S_n \tag{B.4}$$

$$S_n \equiv P_n^m(\cos\theta)\begin{Bmatrix}\sin m\phi \\ \cos m\phi\end{Bmatrix} \tag{B.5}$$

(Lamb 1932, pp. 112–117). The $P_n^m(\cos\theta)$ are given by

$$P_n^m(\cos\theta) \equiv \frac{\sin^m\theta}{2^n n!}\frac{\mathrm{d}^{(m+n)}}{\mathrm{d}(\cos\theta)^{(m+n)}}(-\sin^2\theta)^n, \quad (0 \leq m \leq n) \tag{B.6}$$

for integer m and n (Lamb 1932, pp. 114–7). The first few P_n^m are listed in table B.1.

An immediate and extremely useful consequence of (B.4) is

$$\nabla^2 r^m S_n = [m(m+1) - n(n+1)]r^{m-2}S_n. \tag{B.7}$$

	m				
n	0	1	2	3	4
0	1	—	—	—	—
1	c	s	—	—	—
2	$\frac{1}{2}(3c^2-1)$	$3cs$	$3s^2$	—	—
3	$\frac{1}{2}(5c^3-3c)$	$\frac{3}{2}s(5c^2-1)$	$15s^2c$	$15s^3$	—
4	$\frac{1}{8}(35c^4-30c^2+3)$	$\frac{5}{2}s(7c^3-3c)$	$\frac{15}{2}s^2(7c^2-1)$	$105s^3c$	$105s^4$

Table B.1: The first few $P_n^m(c)$. Note that $s^2 = 1-c^2$.

The spherical components of poloidal and toroidal fields are:

$$(\boldsymbol{\nabla}\times)^2\mathcal{P}\mathbf{r} = -\frac{1}{r}\mathcal{L}^2\mathcal{P}\hat{\boldsymbol{r}} + \frac{1}{r}\frac{\partial^2(r\mathcal{P})}{\partial r\partial\theta}\hat{\boldsymbol{\theta}} + \frac{1}{r\sin\theta}\frac{\partial^2(r\mathcal{P})}{\partial r\partial\phi}\hat{\boldsymbol{\phi}} \tag{B.8}$$

$$\boldsymbol{\nabla}\times\mathcal{T}\mathbf{r} = \frac{1}{\sin\theta}\frac{\partial\mathcal{T}}{\partial\phi}\hat{\boldsymbol{\theta}} - \frac{\partial\mathcal{T}}{\partial\theta}\hat{\boldsymbol{\phi}}. \tag{B.9}$$

Clearly, arbitrary functions of r may be added to $\mathcal{P}[\mathbf{v}]$ or $\mathcal{T}[\mathbf{v}]$ without affecting $\mathbf{v}^{(P)}$ or $\mathbf{v}^{(T)}$ (Moffatt 1978, p. 19).

B.2 Nonsolenoidal fields

While the velocity fields of interest here are all solenoidal, the inertia and buoyancy forces can have nonzero divergence. A general vector field (of sufficient smoothness) can be decomposed as follows. The treatment is specific to the domain $\{\mathbf{r} : 0 \le r < 1/2\}$, but it could easily be generalized to other spheres.

Lemma 2 (Decomposition of vector fields) *Any vector field,* $\mathbf{v}$*, with Hölder continuous second order partial derivatives in a sphere can be expressed:*

$$\mathbf{v} = \boldsymbol{\nabla}\mathcal{S}[\mathbf{v}] + (\boldsymbol{\nabla}\times)^2\left(\mathcal{P}[\mathbf{v}-\mathbf{v}^{(S)}]\mathbf{r}\right) + \boldsymbol{\nabla}\times\left(\mathcal{T}[\mathbf{v}-\mathbf{v}^{(S)}]\mathbf{r}\right). \tag{B.10}$$

Proof: Define $\mathcal{S}[\mathbf{v}]$ as the solution of the problem

$$\nabla^2 \mathcal{S}[\mathbf{v}] = \boldsymbol{\nabla} \cdot \mathbf{v}, \qquad (0 \leq r < \tfrac{1}{2}) \tag{B.11}$$

$$\hat{\boldsymbol{r}} \cdot \boldsymbol{\nabla} \mathcal{S}[\mathbf{v}] = \hat{\boldsymbol{r}} \cdot \mathbf{v}, \qquad (r = \tfrac{1}{2}), \tag{B.12}$$

and let

$$\mathbf{v}^{(S)} = \boldsymbol{\nabla} \mathcal{S}[\mathbf{v}]. \tag{B.13}$$

Then, $\mathbf{v} - \mathbf{v}^{(S)}$ is solenoidal and can be decomposed into poloidal and toroidal parts as before.* □

Following Elsasser (1946), $\mathbf{v}^{(S)}$ is called the *scaloidal* part of $\mathbf{v}$.

Note that if $\mathbf{v}$ is solenoidal but has a nonvanishing normal component at the surface of the sphere; i.e. is solenoidal but not purely toroidal; the poloidal part obtained by the present procedure,

$$\mathbf{v}^{(P)} \equiv \boldsymbol{\nabla} \times \boldsymbol{\nabla} \times \left(\mathcal{P}[\mathbf{v} - \mathbf{v}^{(S)}] \mathbf{r} \right) \tag{B.14}$$

will not necessarily equal that from (B.1). This is because some poloidal vector fields are irrotational and so can be alternatively represented as gradients. Only null toroidal fields are irrotational (Backus 1986).

It is advantageous here to apply the present procedure to all vector fields, whether or not they are solenoidal. This is because if a field is both irrotational and solenoidal, so that it has both scaloidal and poloidal representations, the scaloidal representation is usually easier to work with. In particular, in a momentum equation it can be combined with the pressure gradient term. The classic example of this is the integration of the Euler equations when the flow is both irrotational and incompressible (Lamb 1932, p. 19).

The toroidal part of a general vector field is then here defined as

$$\mathbf{v}^{(T)} \equiv \boldsymbol{\nabla} \times \left(\mathcal{T}[\mathbf{v} - \mathbf{v}^{(S)}] \mathbf{r} \right). \tag{B.15}$$

Note added in proof: The proof in incomplete since it has not been shown that $\mathbf{v} - \mathbf{v}^{(S)}$ inherits the smoothness of $\mathbf{v}$.

Note that the normal component at the spherical surface $r = 1/2$ of the poloidal part of a vector field (defined by Lemma 2) vanishes, since

$$\begin{aligned} \hat{\boldsymbol{r}} \cdot \mathbf{v}^{(P)} &= \hat{\boldsymbol{r}} \cdot \mathbf{v} - \hat{\boldsymbol{r}} \cdot \mathbf{v}^{(S)} - \hat{\boldsymbol{r}} \cdot \mathbf{v}^{(T)}, \quad (r = \tfrac{1}{2}) \\ &= 0 \end{aligned} \tag{B.16}$$

by (B.12) and (B.9).

B.3 Boundary conditions

For $\mathbf{v}^{(T)} = \mathbf{0}$ on a spherical surface, $\mathcal{T}[\mathbf{v}]$ must be uniform over the surface. Since any function of r can be subtracted from $\mathcal{T}[\mathbf{v}]$ without affecting $\mathbf{v}^{(T)}$, this constant can be taken as zero without loss of generality.

For $\hat{\boldsymbol{r}} \cdot \mathbf{v}^{(P)} = 0$ on a spherical surface,

$$\mathcal{L}^2 \mathcal{P}[\mathbf{v}] = 0, \qquad \text{on surface.} \tag{B.17}$$

Since the only regular solutions of this equation are functions only of r (Padmavathi et al. 1998, Lemma 2), and any such function can be subtracted from $\mathcal{P}[\mathbf{v}]$ without affecting $\mathbf{v}^{(P)}$, we can require $\mathcal{P}[\mathbf{v}] = 0$ on the surface.

For a poloidal velocity field to satisfy the no-slip condition, $\partial \mathcal{P}/\partial r$ must be uniform over the surface. Again, there is no loss of generality in requiring it to vanish.

B.4 The Stokes problem in the sphere

I present here a general solution of the inhomogeneous Stokes problem in the sphere with unit diameter.

The general solution for the case $\mathbf{f} = \mathbf{0}$, but with inhomogeneous boundary conditions has been discussed by Palaniappan et al. (1992) and Padmavathi et al. (1998).

An identity that will be used frequently is:

$$(\boldsymbol{\nabla}\times)^3(\mathbf{r}s) = -\boldsymbol{\nabla}\times(\mathbf{r}\nabla^2 s) \tag{B.18}$$

for any scalar s (Moffatt 1978, p. 19).

Lemma 3 (Zero vector fields) *If a vector field,* $\mathbf{v}$*, is both solenoidal and irrotational in a simply connected domain and has zero normal component over the surface, then* $\mathbf{v}$ *vanishes identically in the domain.*

Proof: The lemma is elementary; its proof is contained in most texts on vector analysis, potential theory or continuum mechanics—see, for example, Lamb (1932, pp. 37–41).

Basically, the irrotationality implies that the field may be expressed as the gradient of a scalar, the solenoidality implies that the scalar is harmonic and the boundary conditions imply that the scalar is uniform. □

Theorem 4 (Creeping flow in a sphere) *If* $\mathbf{f}$ *is a vector field with Hölder continuous second order partial derivatives in the sphere* $\{0 \le r \le \frac{1}{2}\}$*, then the solution of the inhomogeneous Stokes problem,*

$$\begin{aligned} \boldsymbol{\nabla}\cdot\mathbf{u} &= 0 \\ \mathbf{f} &= -\boldsymbol{\nabla}p + \nabla^2\mathbf{u} \\ \mathbf{u} &= \mathbf{0}, \quad (r = \tfrac{1}{2}) \end{aligned}$$

is

$$\begin{aligned} \mathbf{u} &= (\boldsymbol{\nabla}\times)^2(\mathcal{P}[\mathbf{u}]\mathbf{r}) + \boldsymbol{\nabla}\times\mathcal{T}[\mathbf{u}]\mathbf{r} \\ p &= -\mathcal{S}[\mathbf{f}] - s + \text{a constant} \end{aligned}$$

where $\mathcal{P}[\mathbf{u}]$*,* $\mathcal{T}[\mathbf{u}]$ *and* s *are scalar fields satisfying*

$$\nabla^4\mathcal{P}[\mathbf{u}] = \nabla^2\mathcal{P}[\mathbf{f} - \mathbf{f}^{(S)}], \quad (0 \le r < \tfrac{1}{2}) \tag{B.19}$$

$$\mathcal{P}[\mathbf{u}] = \hat{\boldsymbol{r}}\cdot\boldsymbol{\nabla}\mathcal{P}[\mathbf{u}] = 0, \quad (r = \tfrac{1}{2}), \tag{B.20}$$

$$\nabla^2\mathcal{T}[\mathbf{u}] = \mathcal{T}[\mathbf{f}-\mathbf{f}^{(S)}], \quad (0 \le r < \tfrac{1}{2}) \tag{B.21}$$

$$\mathcal{T}[\mathbf{u}] = 0, \quad (r = \tfrac{1}{2}), \tag{B.22}$$

(B.23)

$$\nabla^2 s = 0, \quad (0 \le r < \tfrac{1}{2}) \tag{B.24}$$

$$\hat{\boldsymbol{r}} \cdot \nabla s = \hat{\boldsymbol{r}} \cdot (\boldsymbol{\nabla}\times)^4(\mathcal{P}[\mathbf{u}]\mathbf{r}), \quad (r = \tfrac{1}{2}) \tag{B.25}$$

and $\mathcal{S}[\mathbf{f}]$, $\mathcal{P}[\mathbf{f}-\mathbf{f}^{(S)}]$ *and* $\mathcal{T}[\mathbf{f}-\mathbf{f}^{(S)}]$ *are scalars from the decomposition of* $\mathbf{f}$ *described by Lemma 2.*

Proof: The theorem is proved if it can be shown that the velocity field, $\mathbf{u}$, is solenoidal and vanishes on the boundary, and that the field equation is satisfied.

The divergence of $\mathbf{u}$ vanishes automatically since $\mathbf{u}$ is expressed as the sum of its poloidal and toroidal parts.

Both the poloidal and toroidal parts of $\mathbf{u}$ vanish on the surface, by the boundary conditions on $\mathcal{P}[\mathbf{u}]$ and $\mathcal{T}[\mathbf{u}]$ (§ B.3). Therefore the boundary condition on $\mathbf{u}$ is satisfied.

To show that the equation of motion is satisfied, let

$$\mathbf{v} \equiv \mathbf{f} + \boldsymbol{\nabla} p + (\boldsymbol{\nabla}\times)^2\mathbf{u}. \tag{B.26}$$

The required result follows from Lemma 3 if $\mathbf{v}$ is solenoidal and irrotational and has zero normal component on the surface $r = 1/2$.

The divergence of $\mathbf{v}$ is:

$$\begin{aligned} \boldsymbol{\nabla}\cdot\mathbf{v} &= \boldsymbol{\nabla}\cdot\mathbf{f} + \nabla^2 p \\ &= \nabla^2\mathcal{S}[\mathbf{f}] - \nabla^2\mathcal{S}[\mathbf{f}] - \nabla^2 s \\ &= 0 \end{aligned} \tag{B.27}$$

by (B.11) and (B.19).

The curl of $\mathbf{v}$ is:

$$\boldsymbol{\nabla}\times\mathbf{v} = \boldsymbol{\nabla}\times\mathbf{f} + (\boldsymbol{\nabla}\times)^3\mathbf{u}$$

$$\begin{aligned}
&= (\boldsymbol{\nabla}\times)^3\left(\mathcal{P}[\mathbf{f}-\mathbf{f}^{(S)}]\mathbf{r}\right)+(\boldsymbol{\nabla}\times)^2\left(\mathcal{T}[\mathbf{f}-\mathbf{f}^{(S)}]\mathbf{r}\right)\\
&\quad+(\boldsymbol{\nabla}\times)^5(\mathcal{P}[\mathbf{u}]\mathbf{r})+(\boldsymbol{\nabla}\times)^4(\mathcal{T}[\mathbf{u}]\mathbf{r})\\
&= \boldsymbol{\nabla}\times\left[\mathbf{r}\left(\nabla^4\mathcal{P}[\mathbf{u}]-\nabla^2\mathcal{P}[\mathbf{f}-\mathbf{f}^{(S)}]\right)\right]\\
&\quad+(\boldsymbol{\nabla}\times)^2\left[\mathbf{r}\left(\mathcal{T}[\mathbf{f}-\mathbf{f}^{(S)}]-\nabla^2\mathcal{T}[\mathbf{u}]\right)\right]\\
&= 0 \qquad\qquad (B.28)
\end{aligned}$$

by (B.1), (B.2), four applications of (B.18), and the fact that toroidal fields have zero radial components (B.9).

The normal component of $\mathbf{v}$ at $r=\frac{1}{2}$ is:

$$\begin{aligned}
\hat{\boldsymbol{n}}\cdot\mathbf{v} &= \hat{\boldsymbol{n}}\cdot\mathbf{f}+\hat{\boldsymbol{n}}\cdot\boldsymbol{\nabla}p+\hat{\boldsymbol{n}}\cdot(\boldsymbol{\nabla}\times)^4(\mathbf{r}\mathcal{P}[\mathbf{u}])+\hat{\boldsymbol{n}}\cdot(\boldsymbol{\nabla}\times)^3(\mathbf{r}\mathcal{T}[\mathbf{u}])\\
&= \hat{\boldsymbol{n}}\cdot\boldsymbol{\nabla}\mathcal{S}[\mathbf{f}]-\hat{\boldsymbol{n}}\cdot\boldsymbol{\nabla}\mathcal{S}[\mathbf{f}]-\hat{\boldsymbol{n}}\cdot\boldsymbol{\nabla}s\\
&\quad+\hat{\boldsymbol{n}}\cdot(\boldsymbol{\nabla}\times)^4(\mathcal{P}[\mathbf{u}]\mathbf{r})-\hat{\boldsymbol{n}}\cdot\boldsymbol{\nabla}\times(\mathbf{r}\nabla^2\mathcal{T}[\mathbf{u}])\\
&= 0; \qquad\qquad (B.29)
\end{aligned}$$

thus, $\mathbf{v}\equiv 0$ and the equation of motion is satisfied identically. □

Examples of the use of the method will be found in § 8.2.

No insurmountable difficulty would be added by the imposition of inhomogeneous boundary conditions on the velocity. The velocity field could be decomposed, due to the linearity of the Stokes problem, into parts induced by the body force and the boundary conditions. These would then be obtained by the methods of Theorem 4 and Palaniappan et al. (1992), respectively.

B.5 Axisymmetric poloidal fields

If a poloidal field, $(\boldsymbol{\nabla}\times)^2(\mathcal{P}[\mathbf{u}]\mathbf{r})$; or, equivalently, its defining scalar, $\mathcal{P}[\mathbf{u}]$; is independent of the azimuth, ϕ, the field-lines are confined to planes passing through the line $\sin\theta=0$ (the z-axis) and are identical in each such plane. Then,

$$(\boldsymbol{\nabla}\times)^2(\mathcal{P}[\mathbf{u}]\mathbf{r})=-\frac{1}{r^2\sin\theta}\frac{\partial\psi}{\partial\theta}\,\hat{\boldsymbol{r}}+\frac{1}{\sin\theta}\frac{\partial\psi}{\partial r}\,\hat{\boldsymbol{\theta}}, \qquad (B.30)$$

where

$$\psi \equiv r \sin\theta \frac{\partial \mathcal{P}[\mathbf{u}]}{\partial \theta} \tag{B.31}$$

is Stokes's stream-function which is constant along the field-lines (Lamb 1932, pp. 125–6). This connection between axisymmetric poloidal fields and Stokes's stream-function was pointed out by Moffatt (1978, p. 21), though he misprinted the relation.